THE MINOR PLANET BULLETIN

BULLETIN OF THE MINOR PLANETS SECTION OF THE ASSOCIATION OF LUNAR AND PLANETARY OBSERVERS

VOLUME 48, NUMBER 4, A.D. 2021 OCTOBER-DECEMBER 327.

LIGHTCURVE PHOTOMETRY OF ASTEROID (15989) 1998 XK39

Idris Abubakar Sani
NASRDA-Centre for Basic Space Science
Nsukka, Enugu State, NIGERIA
idrisabu4me@yahoo.com

Peter Offor
NASRDA-Centre for Basic Space Science

Nnaemeka Njoku-Achu
NASRDA-Centre for Basic Space Science

Raphael Okere
Department of Physics and Astronomy, University of Nigeria
Nsukka, Enugu State, Nigeria

Nnaemeka Onyeuwaoma
NASRDA-Centre for Basic Space Science

Ikechukwu Obi
NASRDA-Centre for Basic Space Science

Chukwujekwu Ofodum
NASRDA-Centre for Basic Space Science

Bonaventure Okere
NASRDA-Centre for Basic Space Science

(Received: 2021 June 4)

Lightcurve photometry of the main belt asteroid (15989) 1998 XK39 yielded an estimated period of 5.528 ± 0.006 h and an amplitude of 0.55 ± 0.04 mag.

CCD photometric observations of the main-belt asteroid (15989) 1998 XK39 was carried out in 2017 January at the Stone Edge Observatory, Sonoma, CA (G52). Data were obtained with a 0.5-m *f*/8.1 Ritchey-Chretien telescope and an FLI CG230 CCD camera using a clear filter. The pixel size was 1.55 arcseconds with binning set to 2×2. All exposures were 120 seconds.

Data processing and analysis were done with *MPO Canopus* (Warner, 2019). All images were calibrated with bias, dark, and flat field frames, and the instrumental magnitudes converted to R magnitudes using solar-colored field stars from the CMC-15 catalogue. Table I shows the observing circumstances and results.

(15989) 1998 XK39 was discovered on 1998 December 14 by the LINEAR Survey in Socorro, NM. It is a main-belt asteroid with an orbital period of 3.55 years, semi-major axis of 2.326 AU, eccentricity of 0.0997, and inclination of 5.708°. It has an absolute magnitude of 14.0. The WISE/NEOWISE survey (Masiero et al., 2011) reported a diameter of 3.727 ± 0.065 km and a visible albedo of 0.609 ± 0.113. Carvano et al. (2010) assigned a V-type taxonomic class (where V refers to the asteroid Vesta), but interestingly the asteroid's dynamical family is reported as Flora (Nesvorny, 2015). Researchers have theorized that such asteroids could be "fugitives" from the Vesta family (Roig et al., 2011) or alternatively the remaining traces of another differentiated parent body (Oszkiewicz et al., 2015).

Observations for 15989 were conducted over two nights and collected 347 data points. The lightcurve analysis shows a solution for the rotational period of P = 5.528 ± 0.006 h and with an amplitude A = 0.55 ± 0.04 mag, suggested by the strongest peak in the period spectrum.

A search through the asteroid lightcurve database (LCDB); Warner et al., 2009) and ADS indicate that our results may be the first reported lightcurve observations and results for this asteroid.

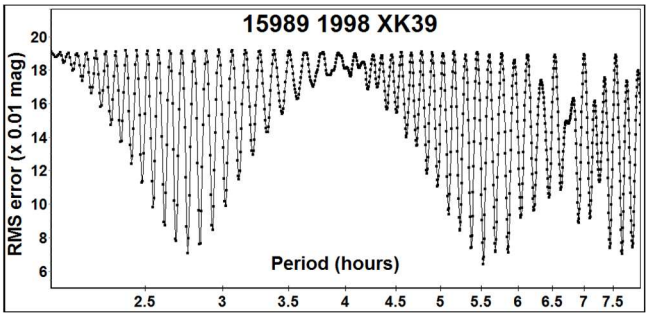

Number	Name	2017 mm/dd	Phase	L_{PAB}	B_{PAB}	Period(h)	P.E.	Amp	A.E.	Grp
15989	1998 XK39	01/25-01/29	4.04,3.87	127.7	6.4	5.528	0.006	0.55	0.04	Flora

Table I. Observing circumstances and results. The phase angle is given for the first and last date. If preceded by an asterisk, the phase angle reached an extrema during the period. L_{PAB} and B_{PAB} are the approximate phase angle bisector longitude/latitude at mid-date range (see Harris et al., 1984). Grp is the asteroid family/group (Warner et al., 2009).

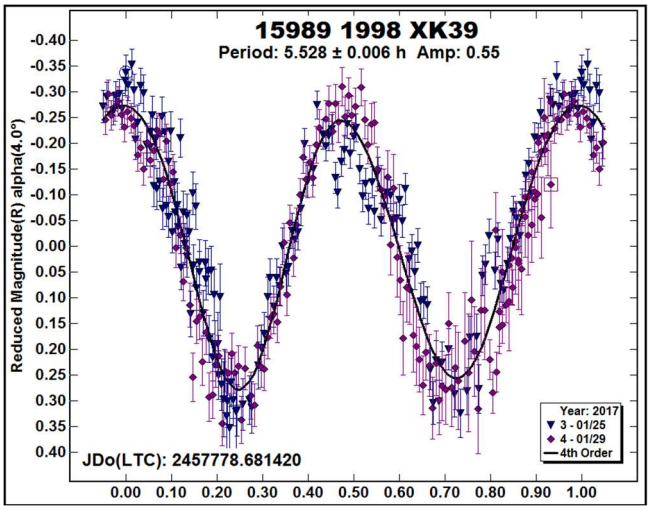

Acknowledgements

The authors would like to acknowledge the IAU ROAD offices, including NA-ROAD, WA-ROAD, and SA-ROAD; and Geneva Lake Astrophysics and STEAM (GLAS) Education, in Lake Geneva, Wisconsin. We would like to specially thank Matt Nowinski, Kate Meredith, Amanda Pagul, Adam McCulloch, and Katya Gozman. Our deepest appreciation is also extended to the McQuown Trust for financial support and access to the Stone Edge Observatory, Sonoma, CA.

References

Carvano, J.M.; Hasselmann, P.H.; Lazzaro, D.; Mothe-Diniz, T. (2010). "SDSS-based taxonomic classification and orbital distribution of main belt asteroids." *Astronomy and Astrophysics* **510**, 1-12.

Harris, A.W.; Young, J.W.; Scaltriti, F.; Zappala, V. (1984). "Lightcurves and phase relations of the asteroids 82 Alkmene and 444 Gyptis." *Icarus* **57**, 251-258.

Masiero, J.R.; Mainzer, A.K.; Grav, T.; Bauer, J.M.; Cutri, R.M.; Dailey, J.; Eisenhardt, P.R.M.; McMillan, R.S.; Spahr, T.B.; Skrutskie, M.F.; Tholen, D.; Walker, R.G.; Wright, E.L.; DeBaun, E.; Elsbury, D.; Gautier IV, T.; Gomillion, S.; Wilkins, A. (2011). "Main Belt Asteroids with WISE/NEOWISE. I. Preliminary Albedos and Diameters." *The Astrophysical Journal* **741**, 1-68.

Nesvorny, D. (2015) "Nesvorny HCM Asteroid Families V3.0." *EAR-A-VARGBDET-5-NESVORNYFAM-V3.0. NASA Planetary Data System.*

Oszkiewicz, D.; Kankiewicz, P.; Włodarczyk, I.; Kryszczyńska, A. (2015). "Differentiation signatures in the Flora region." *Astronomy and Astrophysics* **584**, 1-14.

Roig, F.; Folonier, H.; Beaugé, C.; Ribeiro, A.O. (2011). "Dynamical origin of V-type asteroids outside the Vesta family." *Workshop Series of the Asociacion Argentina de Astronomia 3*, 307-317.

Warner, B.D.; Harris, A.W.; Pravec, P. (2009). "The Asteroid Lightcurve Database." *Icarus* **202**, 134-146. Updated 2016 Sep. *http://www.minorplanet.info/lightcurvedatabase.html*

Warner, B.D. (2019). *MPO Canopus* Software, version 10.8.1.1. BDW Publishing. *http://www.bdwpublishing.com*

OBSERVATIONS OF 148 GALLIA

Neil B. Thomas
U.S. Air Force Academy
PO Box 978, Palmer Lake, CO 80133
neil.thomas@afacademy.af.edu

Patrick R. Lopez
U.S. Air Force Academy
Colorado Springs, CO, USA

(Received: 2021 May 3, Revised: 2021 August 5)

Photometric observations of 148 Gallia are reported as the asteroid approached opposition. We conducted 17 observing sessions between 2021 Feb 27 to 2021 Apr 9. This paper provides the full phase-folded lightcurve and reduced magnitude of this asteroid which has a spin period of slightly more than 20 h.

148 Gallia is a member of the MB-O group/family. It was discovered in 1875 by Prosper Henry. Its diameter is 98 km, and it has a relatively high inclination of 25.2°. We could not readily find an existing dense lightcurve covering the full phase of its rotation, although Warner (2007) covered it well enough to characterize its nature. No additional photometry was found in the Lightcurve Database (Warner et al., 2009). Considering its brightness, it is likely not heavily studied due to its period of slightly more than 20 h. This implies less than half of a phase being available each night and only about a 20% phase shift per day due to the earth's 24-hour day. Hence, a continuous campaign would require approximately five consecutive nights for full coverage.

The Lookout Observatory (LO) is primarily dedicated to the characterization of exoplanet transit lightcurves. As such, it typically attains a photometric precision of 1-2 thousands of a magnitude (mmag) for well exposed targets. The telescope is an 11-inch Celestron modified to f/1.9 with a HyperStar, providing a field of view of 114 × 86 arcmin (or 2.7 degrees^2) when coupled to an ASI 1600 CMOS camera. All photometry was unfiltered with exposures of 36 seconds.

We recently modified our exoplanet software to detect and track asteroids with the goal of obtaining lightcurves serendipitously during the ongoing exoplanet survey. Stars are subtracted from our reference image using Gaia catalog locations and magnitudes (Gaia Collab., 2018). Remaining objects are automatically compared to DSS imagery to eliminate galaxies. Remaining objects are examined over time to determine drift rate. If a consistent tracking solution is found, then this information is recorded and used to move the photometric aperture during the rest of the processing. We developed a test campaign targeting 148 Gallia since it was well-positioned and approaching opposition.

Gallia was the primary target from 2021 Feb 27 to 2021 Apr 9 (41-day span). This allowed for analysis of this moderate-period asteroid (20.66 h), to include a complete phase folded lightcurve. Most portions of the phase were observed on two or more occasions. All data is light time corrected (LTC) and approximately reduced to H. This is approximate since our software relies on Gaia DR2 for absolute magnitude calibration to the green (G) band. G-band is comparable to visual (V-band) but not precisely the same. After phase folding the 6,184 observations to our derived period, we bin data to simulate exposures of approximately two minutes for clarity and to reduce white noise. Six sessions required no

Number	Name	yyyy mm/dd	Phase	L_{PAB}	B_{PAB}	Period(h)	P.E.	Amp	A.E.	Grp
148	Gallia	2021 02/27-04/09	14.0,8.7	199	24	20.661	0.006	0.19	0.01	MB-O

Table I. Observing circumstances and results. The phase angle is given for the first and last date. L_{PAB} and B_{PAB} are the approximate phase angle bisector longitude/latitude at mid-date range (see Harris et al., 1984). Grp is the asteroid family/group (Warner et al., 2009).

magnitude adjustments in creating the phase curve while the other 11 were manually adjusted with offsets on the order of 0.03 magnitude or less.

A summary of the results is detailed in the table below along with the subsequent figures. Column 3 provides the date of the observation; column 4 provides the phase. Columns 5 and 6 provide the longitude and latitude of the Phase Angle Bisector (PAM), respectively. Columns 7 through 10 provide our derived periods and amplitudes, as well as their errors. The group or family is given in column 11.

The synodic period based on only our observations is 20.661 ± 0.006 h and agrees with Warner's of 20.666 ± 0.002 h (Warner, 2007). The amplitude agrees as well, with our result being 0.19 ± 0.01 mag and Warner's being 0.21 ± 0.02 mag. The features of the curve itself, however, are significantly different. This is not surprising because even though phase angles at the times of observation were similar, the PAM coordinates differed greatly. We observe a sharp drop in the first minimum and a flat bottom in the second. Additionally, the two minima are not separated by half of the period. The RMS between our 7th order trigonometric fit and our data is 7.5 mmag. This is not as good as our stellar photometry, but we expect degraded results with a moving target.

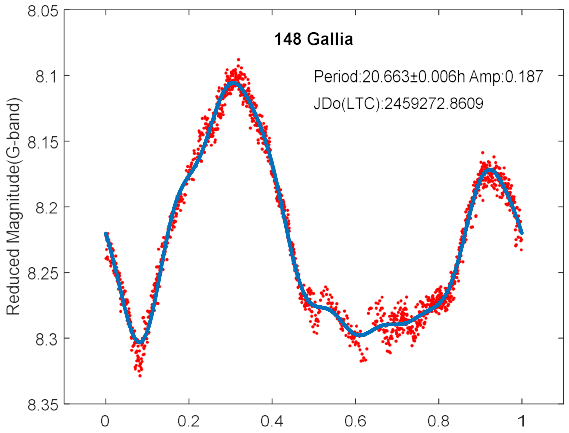

The reduced magnitude as the asteroid approached opposition from an initial phase of 14 degrees was then investigated. The expected linear brightening with reduced phase is observed. The minimum phase angle at opposition is slightly less than 9 degrees due to Gallia's large inclination. Thus, no opposition effect was noted. When this brightening is extrapolated to zero phase, we arrive at H=7.7, which agrees nicely with the accepted value of 7.72 (Warner, 2007).

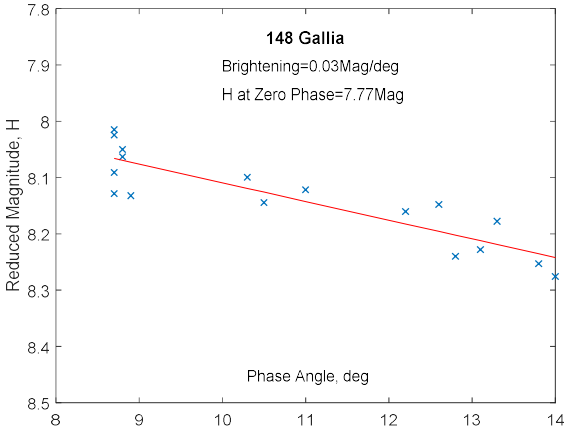

Acknowledgements

In addition to the support of the Astronautical Engineering Department at the US Air Force Academy (specifically Col Luke Sauter for the powerful gift of time), the authors would like to thank the LO construction team, Savannah Jane and P.P. This work presents results from the European Space Agency (ESA) space mission Gaia. Gaia data are being processed by the Gaia Data Processing and Analysis Consortium (DPAC). Funding for the DPAC is provided by national institutions, in particular the institutions participating in the Gaia MultiLateral Agreement (MLA). The Gaia mission website is https://www.cosmos.esa.int/gaia. The Gaia archive website is https://archives.esac.esa.int/gaia.

References

Gaia Collaboration (2018). "Gaia Data Release 2. Summary of the contents and survey properties" *AA*, **616A**.

Harris, A.W.; Young, J.W.; Scaltriti, F.; Zappala, V. (1984). "Lightcurves and phase relations of the asteroids 82 Alkmene and 444 Gyptis." *Icarus* **57**, 251-258.

Warner, B.D. (2007). "Asteroid Lightcurve Analysis at the Palmer Divide Observatory - March - May 2007." *Minor Planet Bulletin* **34**, 104-107.

Warner, B.D.; Harris, A.W.; Pravec, P. (2009). "The Asteroid Lightcurve Database." *Icarus* **202**, 134-146. Updated 2020 Oct. *http://www.minorplanet.info/lightcurvedatabase.html*

ROTATION PERIOD DETERMINATION FOR (13832) 1999 XR13

Alessandro Marchini, Leonardo Cavaglioni,
Chiara Angelica Privitera
Astronomical Observatory, DSFTA - University of Siena (K54)
Via Roma 56, 53100 - Siena, ITALY
marchini@unisi.it

Riccardo Papini, Fabio Salvaggio
Wild Boar Remote Observatory (K49)
San Casciano in Val di Pesa (FI), ITALY

(Received: 2021 July 14, Revised: 2021 July 31)

Photometric observations of the outer main belt asteroid (13832) 1999 XR13 were conducted in order to determine its synodic rotation period. It revealed to be a very slow rotator with P = 98.53 ± 0.04 h, A = 0.31 ± 0.03 mag.

CCD photometric observations of an outer main-belt asteroid were carried out in 2021 May - July at the Astronomical Observatory of the University of Siena (K54), a facility inside the Department of Physical Sciences, Earth and Environment (DSFTA, 2021). We used a 0.30-m *f*/5.6 Maksutov-Cassegrain telescope, SBIG STL-6303E NABG CCD camera, and clear filter; the pixel scale was 2.30 arcsec when binned at 2×2 pixels and all exposures were 300 seconds.

Data processing and analysis were done with *MPO Canopus* (Warner, 2018). All images were calibrated with dark and flat-field frames and the instrumental magnitudes converted to R magnitudes using solar-colored field stars from a version of the CMC-15 catalogue distributed with *MPO Canopus*. Table I shows the observing circumstances and results.

A search through the asteroid lightcurve database (LCDB; Warner et al., 2009) indicates that our results may be the first reported lightcurve observations and results for this asteroid.

(13832) 1999 XR13 was discovered on 1999 December 5 by LINEAR at Socorro. It is an outer main-belt asteroid with a semi-major axis of 3.365 AU, eccentricity 0.112, inclination 16.301°, and an orbital period of 6.17 years. Its absolute magnitude is H = 10.8 (JPL, 2021). The WISE/NEOWISE satellite infrared radiometry survey (Masiero et al., 2014) found a diameter D = 37.54 ± 0.34 km using an absolute magnitude H = 10.5.

Observations were conducted over sixteen nights and collected 312 data points. The observation of this asteroid was a challenging task: period is quite long and therefore time demanding; nights were very short at the end of the spring and the brightness was quickly fading after the opposition. Despite the collected data points cover less than full coverage, they seem sufficient to stabilize the period spectrum and the model fit is quite good. The period analysis shows a possible solution for the rotational period of P = 98.53 ± 0.04 h with an amplitude A = 0.31 ± 0.03 mag as the most likely bimodal solution for this asteroid. Further observations are strongly encouraged to nail down the actual period.

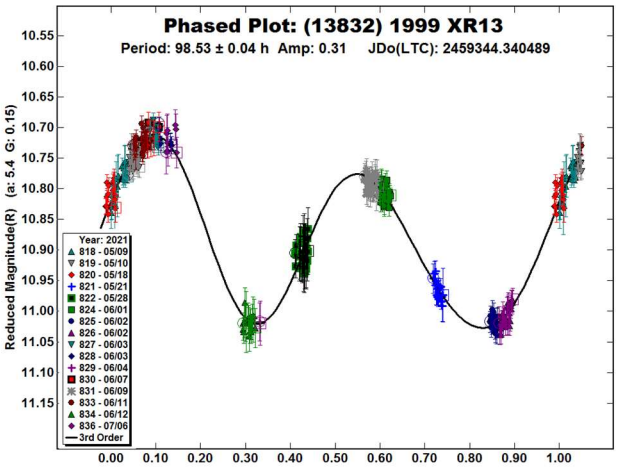

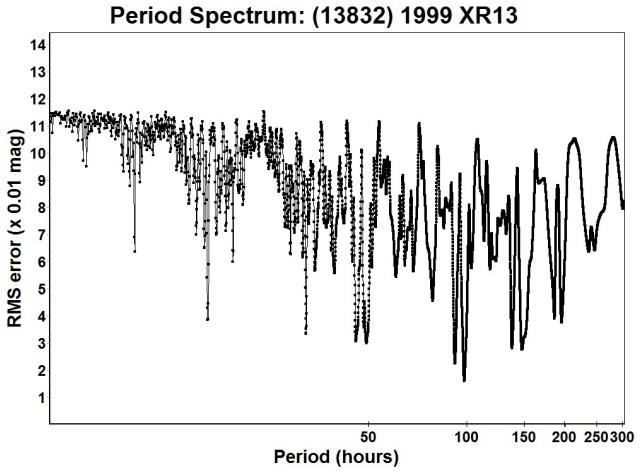

References

DSFTA (2021). Dipartimento di Scienze Fisiche, della Terra e dell'Ambiente – Astronomical Observatory. *https://www.dsfta.unisi.it/en/research/labs/astronomical-observatory*

Harris, A.W.; Young, J.W.; Scaltriti, F.; Zappala, V. (1984). "Lightcurves and phase relations of the asteroids 82 Alkmene and 444 Gyptis." *Icarus* **57**, 251-258.

JPL (2021). Small-Body Database Browser. *http://ssd.jpl.nasa.gov/sbdb.cgi#top*

Masiero, J.R.; Grav, T.; Mainzer, A.K.; Nugent, C.R.; Bauer, J.M.; Stevenson, R.; Sonnett, S. (2014). "Main-belt Asteroids with WISE/NEOWISE: Near-infrared Albedos." *Astrophys. J.* **791**, 121.

Warner, B.D.; Harris, A.W.; Pravec, P. (2009). "The Asteroid Lightcurve Database." *Icarus* **202**, 134-146. Updated 2020 Oct. *http://www.minorplanet.info/lightcurvedatabase.html*

Warner, B.D. (2018). MPO Software, MPO Canopus v10.7.7.0. Bdw Publishing. *http://minorplanetobserver.com*

Number	Name	2021/mm/dd	Phase	L_{PAB}	B_{PAB}	Period(h)	P.E.	Amp	A.E.	Grp
13832	1999 XR13	05/09-07/06	*5.4,15.4	239	8	98.53	0.04	0.31	0.03	MB-O

Table I. Observing circumstances and results. The phase angle is given for the first and last date. If preceded by an asterisk, the phase angle reached an extrema during the period. L_{PAB} and B_{PAB} are the approximate phase angle bisector longitude/latitude at mid-date range (see Harris et al., 1984). Grp is the asteroid family/group (Warner et al., 2009).

LIGHTCURVES, SIDEREAL ROTATION PERIOD, SPIN POLE, AND CONVEX MODEL SHAPE OF KORONIS FAMILY MEMBER (1443) RUPPINA

Stephen M. Slivan
Massachusetts Institute of Technology,
Dept. of Earth, Atmospheric, and Planetary Sciences
77 Mass. Ave. Rm. 54-410, Cambridge, MA 02139
slivan@mit.edu

(Received: 2021 June 16, Revised: 2021 July 28)

Rotation lightcurves of Koronis asteroid family member (1443) Ruppina were observed during its consecutive apparitions in 2015, 2016, and 2017-18, the latter yielding an improved synodic rotation period of 5.8796 ± 0.0002 h. In combination with the previously published lightcurves recorded in 2007 and 2014 the resulting data set is confirmed to be sufficient to unambiguously determine the sidereal rotation period, and the corresponding results for spin vector and convex model shape are presented.

Koronis family member (1443) Ruppina was observed during three apparitions between 2015 and 2018 as part of an ongoing program to study rotation properties of the family's brighter objects (Slivan et al., 2008). Lightcurve observations of Ruppina have been previously reported by Neugent and Slivan (2008), Arredondo et al. (2014), Stephens (2018), and Stephens and Warner (2020); the corresponding four independent determinations of the synodic rotation period all agree. The latter paper also presents an analysis for sidereal period and spin vector whose outcome is discussed at length by Slivan (2021; this issue).

The program of observations reported here was designed specifically to build a lightcurve data set that would be demonstrably sufficient for sidereal period and spin vector analyses, in part by improving the determination of the synodic rotation period (Slivan, 2012) and by assembling a suitable progression of epoch intervals (Slivan, 2013). The lightcurves from the two apparitions that had been published prior to the observations reported here served as a starting place, establishing an epoch interval of length five apparitions apart.

The observations were made during Ruppina's three consecutive apparitions in 2015, 2016, and 2017-18, using a series of CCD cameras at the Cassegrain focus of the the 0.61m Sawyer telescope at the Whitin Observatory in Wellesley, MA. Nightly observing information is summarized in Table I, and details about the instruments used are given in Table II. Image integrations were 240 s using an *R* filter. The observing strategy used to calibrate the lightcurves to standard magnitudes is described by Slivan et al. (2008), as are the procedures used for image processing and measurement. The resulting lightcurves were reduced for light-time and to unit distances.

2015 apparition: (Fig. 1, top panel) This viewing aspect had not yet been observed. Lightcurves were observed on two nights which together cover about 2/3 of the rotation phase, sufficient to record an amplitude, and also to measure an epoch interval of one apparition with respect to the lightcurves from 2014.

2016 apparition: (Fig. 1, center panel) This viewing aspect at an ecliptic longitude about 100° different from that in 2015 had not yet been observed. A lightcurve was observed on a single night covering just over 1/2 of the rotation phase, sufficient to record an amplitude, and also to measure an epoch interval of two apparitions with respect to 2014.

2017–18 apparition: (Fig. 1, bottom panel) At this viewing aspect near the reflex of that in 2015, lightcurves observed on six nights recorded complete coverage in rotation phase, and define an epoch interval of three apparitions with respect to 2014. The data span a 113-night interval in order to maximize the precision of the derived synodic rotation period. The improved period of 5.8796 ± 0.0002 h is consistent with the previously published periods and has been used to fold all of the lightcurves presented in Fig. 1.

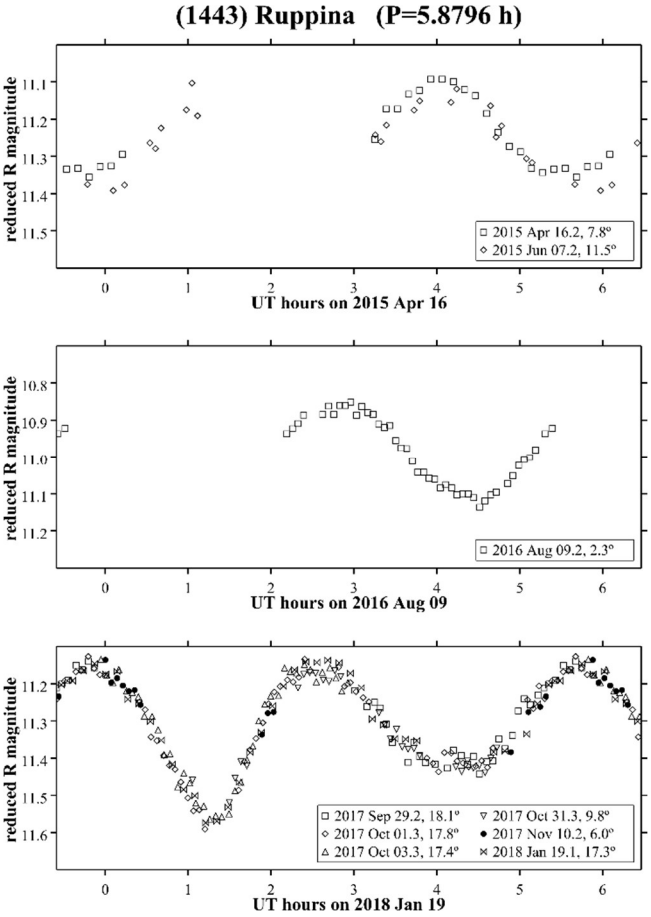

Figure 1. Folded composite lightcurves of (1443) Ruppina showing one rotation period plus the earliest and latest 10% repeated. (Top panel) 2015 apparition; both nights are calibrated to *R* magnitudes and reduced for changing solar phase angle using the MPC adopted value of G = 0.15 for the slope parameter. (Center panel) 2016 apparition. (Bottom panel) 2017–18 apparition; the nights of uncalibrated relative photometry have been shifted in brightness for best fit to the Jan 19 calibrated *R* lightcurve.

Applying the "sieve algorithm" of Slivan (2013) to the epochs measured from these lightcurves, in combination with epochs from the lightcurves recorded in 2007 and 2014 (Neugent and Slivan, 2008; Arredondo et al., 2014), confirms that these five apparitions (Table III) are sufficient to unambiguously count rotations over the entire data set—there is only one possible solution for the sidereal rotation period (Fig. 2) which indicates that the data are suitable to credibly attempt analysis for the spin pole.

Sidereal Photometric Astrometry (SPA) (Slivan, 2014; Drummond et al., 1988) locates a single merged pole region surrounding the north ecliptic pole (Fig. 3, left panel) with a corresponding sidereal period of 5.87941 h. Having thus determined that the rotation is prograde, convex inversion (CI) (Kaasalainen et al., 2001) trial poles were then run for the north ecliptic hemisphere (Fig. 3, right panel). Even though this lightcurve data set from only five apparitions is sufficient to determine an unambiguous sidereal period and prograde rotation, the trial pole fits from CI do not fully resolve the pole location, identifying instead two pairs of symmetric possible pole regions. Agreement with the SPA pole region distinguishes the correct solution regions as the pair closest to the north ecliptic pole. A summary of the analysis results is presented in Table V, and graphs of the P_1 solution model lightcurve fits to the entire data set used are presented in Fig. 4. As is discussed in a companion paper (Slivan, 2021; this issue) the pole results reported here differ markedly from those of Stephens and Warner (2020). Finally, a rendering of the P_1 CI model shape is shown in Fig. 5, mindful that any model shape based on a limited lightcurve data set such as that used here is necessarily very coarse.

UT date	Inst. ID	Observer(s)
2015 Apr 16	Ap8p	Slivan
2015 Jun 07	Ap8p	Slivan, Kurzner
2016 Aug 09	Ap8p	Slivan
2017 Sep 29	SBIG	Miller, Gordon, Sheraden Cox
2017 Oct 01	SBIG	Slivan, Shi
2017 Oct 03	SBIG	Sheraden Cox, Gordon
2017 Oct 31	SBIG	Gordon, Zdanky, Sheraden Cox
2017 Nov 10	SBIG	Sheraden Cox
2018 Jan 19	FLI	Slivan

Table I: Nightly observing information. Columns are: UT date, instrument ID (see Table II), and observers.

Inst. ID	CCD camera	FOV (′)	Bin	Scale (″/pix)
Ap8p	Apogee AP8p	19×19	2×2	1.2
SBIG	SBIG STL-1001	16×16	1×1	0.9
FLI	FLI-PL23042	20×20	2×2	1.2

Table II: Cameras used. Columns are: instrument ID, CCD camera, detector field of view, image binning used, and binned image scale.

Years observed	Number of apparitions	λPAB observed (°)
2007–2018	5	62, 69, 147, 226, 322

Table III: Summary of lightcurve data set used for the period, pole, and shape analyses. Columns are: years spanned by the lightcurves, the number of different apparitions observed, and a list of the ecliptic longitudes of the phase angle bisector near the mid-date of the observations from each apparition.

Epoch pair index	Interval (d)	Interval (app.)	Epochs source apparitions
0	415.9	1	2016, 2017-18
1	417.0	1	2014, 2015
2	481.1	1	2015, 2016
3	897.0	2	2015, 2017-18
4	898.1	2	2014, 2016
5	1314.0	3	2014, 2017-18
6	2300.0	5	2007, 2014
7	2717.0	6	2007, 2015
8	3198.1	7	2007, 2016
9	3614.0	8	2007, 2017-18

Table IV: Time intervals between lightcurve epochs used to identify the ranges of possible sidereal periods. Columns are: the epoch pair index label used in Fig. 2, the interval length rounded to 0.1 d, the corresponding integer count of elapsed apparitions, and identification of the apparitions from which the defining epochs were measured.

		λ(°)	β(°)	ε(°)
sidereal period:	5.8794084 ± 0.0000014 h			
spin poles and obliquities:	P1	160 ± 3	+79 ± 5	11
	P2	358 ± 3	+79 ± 5	11
model axial ratios:	a/b ~ 1.2; b/c undetermined			

Table V: Summary of period, pole, and model shape results. The error for the sidereal period was calculated for the CI pole location using SPA, and the errors for the pole coordinates are given in degrees of arc and were estimated based on the chi-square distribution of the CI fits to trial poles. The spin obliquities ε are the angles between the orbit pole and the spin poles. The *a*/*b* axial ratio is a necessarily coarse estimate, and *b*/*c* cannot credibly be determined for this object whose viewing aspects are always close to equatorial.

Acknowledgments

I thank the service observers Leafia Sheraden Cox, Naomi Gordon, Cassie Miller, Chloe Shi, and Karisa Zdanky, all from the Corps of Loyal Observers, Wellesley Division (CLOWD) who were supported in part by grants from the Massachusetts Space Grant Consortium. I also thank Max Kurzner, who was supported as a Keck Northeast Astronomy Consortium summer student by National Science Foundation Grant No. AST-1005024.

Number	Name	yyyy mm/dd	Phase	L_{PAB}	B_{PAB}	Period(h)	P.E.	Amp	A.E.
1443	Ruppina	2015 04/16-06/07	*7.8,11.5	226	+2			0.25	0.02
1443	Ruppina	2016 08/09	2.3	322	+1			0.26	0.02
1443	Ruppina	2017 09/29-2018 01/19	*18.1,17.3	62	-2	5.8796	0.0002	0.43	0.03

Table V. Observing circumstances and results. Solar phase angle is given for the first and last dates; an asterisk indicates that the phase angle reached a minimum within that interval. L_{PAB} and B_{PAB} are the phase angle bisector longitude and latitude at mid-date range.

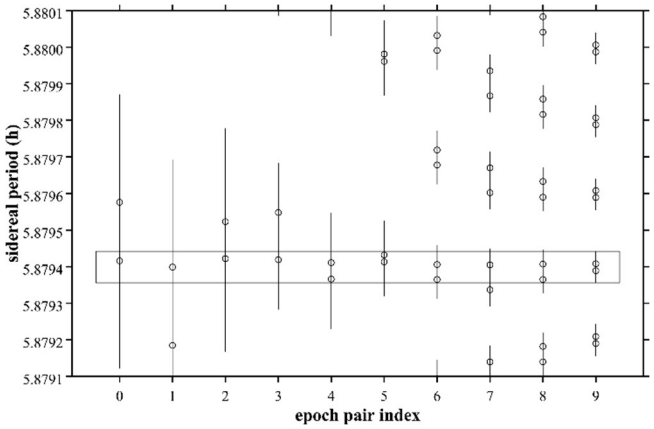

Figure 2: Confirmation of unambiguous sidereal rotation counting of (1443) Ruppina, based on epochs measured from the lightcurves from the five observed apparitions, 2007 through 2017–18. The synodic constraint is the improved period 5.8796, adopting 2.5σ = 0.0005 h, and the epoch measurement adopted errors are 15 min which is 1.5× the maximum observed asymmetry of the timing of the extrema in the composite lightcurves. Each horizontal coordinate index corresponds to the time interval between a pair of epochs as detailed in Table IV, ordered with longer intervals to the right. Open circles and vertical bars represent sidereal periods and period ranges, respectively, calculated from every possible number of rotations that could elapse during the interval. The thin horizontal rectangle identifies the single range of periods, 5.879356 to 5.879442 h, that is allowed by all ten time intervals.

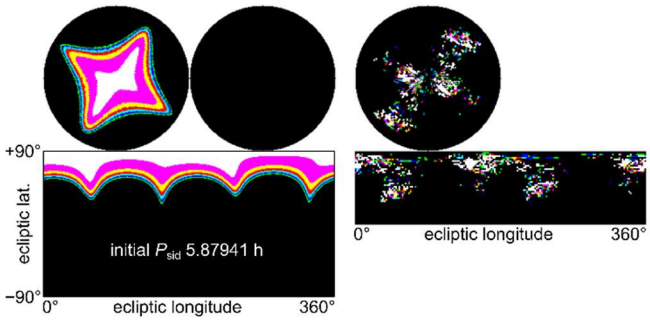

Figure 3: Contour graphs of the "goodness of fit" of trial poles for (1443) Ruppina. (Left panel) From SPA analysis of epochs measured from the lightcurves from the five apparitions observed from 2007 to 2017-18. Trial pole resolution is 1° and best-fit regions are colored white. In the lower half of the graph the celestial sphere is projected on a rectangular grid of ecliptic longitude and latitude. The same data in a polar format undistorted near the ecliptic poles appear in the upper half of the graph, where north- and south-hemisphere views are plotted separately. For Ruppina a single merged prograde pole region is found surrounding the north ecliptic pole. (Right panel) Similar to the left panel, but from CI analysis, for only the north ecliptic hemisphere, with a trial pole resolution of 2°, and using for clarity a color map which highlights only the regions of best fit. Two pairs of symmetric possible pole regions are found; the adopted pair is closest to the ecliptic pole as distinguished by using the SPA graph at left.

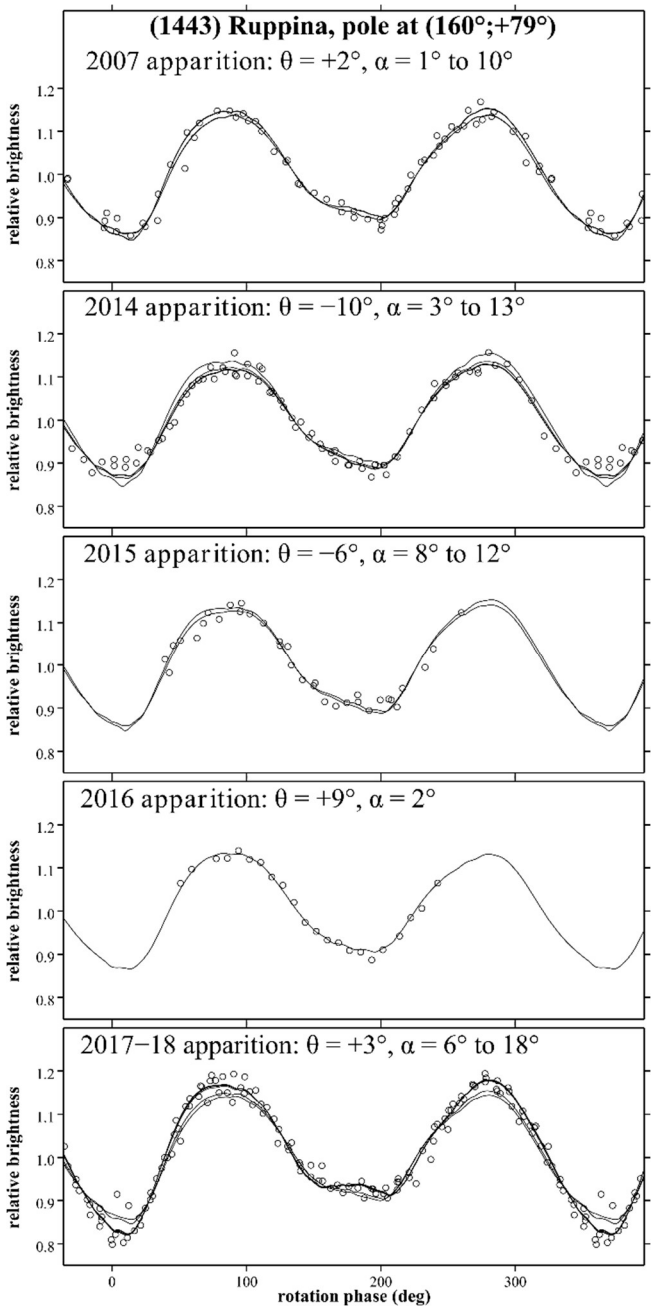

Figure 4: Lightcurve fits for (1443) Ruppina with pole P_1, plotted at identical vertical scales as brightness vs. sidereal rotation phase, with open circles for observed brightnesses and solid curves for the model. Changes in the lightcurve shape during the course of the observations appear as non-overlapping model curves. θ is the sub-PAB latitude and α is the included range of solar phase angles.

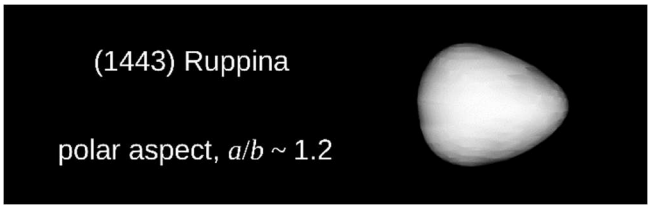

Figure 5: P_1 model rendering of (1443) Ruppina, fully illuminated using an artificial scattering law to better visualize the shape. In absence of information in the lightcurves to scale the model along the polar axis, only the pole-on view shown is constrained.

References

Arredondo, A.; Hartt, A.; Yazdi, S.K. (2014). "Rotation Periods and *R* Magnitudes of Three Koronis Family Members." *Minor Planet Bull.* **41**, 252-254.

Drummond, J.D.; Weidenschilling, S.J.; Chapman, C.R.; Davis, D.R. (1988). "Photometric geodesy of main-belt asteroids. II. Analysis of lightcurves for poles, periods, and shapes." *Icarus* **76**, 19-77.

Kaasalainen, M.; Torppa, J.; Muinonen, K. (2001). "Optimization methods for asteroid lightcurve inversion. II. The complete inverse problem." *Icarus* **153**, 37-51.

Neugent, K.F.; Slivan, S.M. (2008). "Rotation Periods and *H* Magnitudes of Two Koronis Family Members." *Minor Planet Bull.* **35**, 116-118.

Slivan, S.M.; Binzel, R.P.; Boroumand, S.C.; Pan, M.W.; Simpson, C.M.; Tanabe, J.T.; Villastrigo, R.M.; Yen, L.L.; Ditteon, R.P.; Pray, D.P.; Stephens, R.D. (2008). "Rotation Rates in the Koronis Family, Complete to $H \approx 11.2$." *Icarus* **195**, 226-276.

Slivan, S.M. (2012). "Epoch Data in Sidereal Period Determination. I. Initial Constraint from Closest Epochs." *Minor Planet Bull.* **39**, 204-206.

Slivan, S.M. (2013). "Epoch Data in Sidereal Period Determination. II. Combining Epochs from Different Apparitions." *Minor Planet Bull.* **40**, 45-48.

Slivan, S.M. (2014). "Sidereal Photometric Astrometry as Efficient Initial Search for Spin Vector." *Minor Planet Bull.* **41**, 282-284.

Slivan, S.M. (2021). "Caveat Emptor: Spurious Spin Vectors from Incorrect Sidereal Periods." *Minor Planet Bull.* **48**, 403-405.

Stephens, R.D. (2018). "Asteroids Observed from CS3: 2017 July-September." *Minor Planet Bull.* **45**, 50–54.

Stephens, R.D.; Warner, B.D. (2020). "Main-Belt Asteroids Observed from CS3: 2020 April to June." *Minor Planet Bull.* **47**, 275–284.

LIGHTCURVE ANALYSIS OF HILDA ASTEROIDS AT THE CENTER FOR SOLAR SYSTEM STUDIES: 2021 FEBRUARY-MARCH

Brian D. Warner
Center for Solar System Studies / MoreData!
446 Sycamore Ave.
Eaton, CO 80615 USA
brian@MinorPlanetObserver.com

Robert D. Stephens
Center for Solar System Studies / MoreData!
Rancho Cucamonga, CA

Daniel R. Coley
Center for Solar System Studies
Corona, CA

(Received: 2021 July 15)

New CCD photometric observations of the Hilda member 1038 Tuckia were made at the Center for Solar System Studies in 2021 February and March. Analysis of the resulting data indicate that the asteroid may be in non-principal axis rotation (NPAR), i.e., tumbling.

CCD photometric the Hilda asteroid 1038 Tuckia were made at the Center for Solar System Studies (CS3) as part of an ongoing study of this family/group that is located between the outer main-belt and Jupiter Trojans in a 3:2 orbital resonance with Jupiter. The goal is to determine the spin rate statistics of the Hildas and to find pole and shape models when possible. We also look to examine the degree of influence that the YORP (Yarkovsky–O'Keefe–Radzievskii–Paddack) effect (Rubincam, 2000) has on distant objects and to compare the spin rate distribution against the Jupiter Trojans, which can provide evidence that the Hildas are more "comet-like" than main-belt asteroids.

Telescopes	Cameras
0.30-m *f*/6.3 Schmidt-Cass	FLI Microline 1001E
0.35-m *f*/9.1 Schmidt-Cass	FLI Proline 1001E
0.35-m *f*/11 Schmidt-Cass	SBIG STL-1001E
0.40-m f/10 Schmidt-Cass	
0.50-m *f*/8.1 Ritchey-Chrétien	

Table I. List of available telescopes and CCD cameras at CS3. The exact combination for each telescope/camera pair can vary due to maintenance or specific needs.

Table I lists the telescopes and CCD cameras that are combined to make observations. Up to nine telescopes are commonly used for observations. All the cameras use CCD chips from the KAF blue-enhanced family and so have essentially the same response. The pixel scales ranged from 1.24-1.60 arcsec/pixel. All lightcurve observations were unfiltered since a clear filter can result in a 0.1-0.3 magnitude loss. The exposures varied depending on the asteroid's brightness.

To reduce the number of times and amounts of adjusting nightly zero points, we use the ATLAS catalog r´ (SR) magnitudes (Tonry et al., 2018). Those adjustments are usually ≤ ±0.03 mag. The rare greater corrections may have been related in part to using unfiltered observations, poor centroiding of the reference stars, and not correcting for second-order extinction. Another cause may be selecting what appears to be a single star but is actually an unresolved pair.

Number	Name	20yy/mm/dd	Phase	L_{PAB}	B_{PAB}	Period(h)	P.E.	Amp	A.E.
1038	Tuckia	21/03/18-04/04	5.7,8.7	154	10	T68.98	0.06	0.59	0.04
						44.42	0.03	0.29	0.04
1038	Tuckia	19/01/26-02/17	19.5,16.7	194	-11	T177.5	0.3	0.21	0.02
						9.55	0.01	0.07	0.01

Table II. Observing circumstances. T The dominant period of a tumbling asteroid. The phase angle (α) is given at the start and end of each date range. L_{PAB} and B_{PAB} are the average phase angle bisector longitude and latitude (see Harris *et al*., 1984).

The Y-axis values are ATLAS SR "sky" (catalog) magnitudes. The two values in the parentheses are the phase angle (a) and the value of *G* used to normalize the data to the comparison stars used in the earliest session. This, in effect, made all the observations seem to be made at a single fixed date/time and phase angle, leaving any variations due only to the asteroid's rotation and/or albedo changes. The X-axis shows rotational phase from –0.05 to 1.05. If the plot includes the amplitude, e.g., "Amp: 0.65", this is the amplitude of the Fourier model curve and *not necessarily the adopted amplitude for the lightcurve*.

1038 Tuckia. Dahlgren et al. (1998) reported a single-period result of 23.2 h, close to being Earth-day commensurate. Observations we made in 2019 (Warner and Stephens, 2019) led to a period of 18.020 h and amplitude of 0.21 mag.

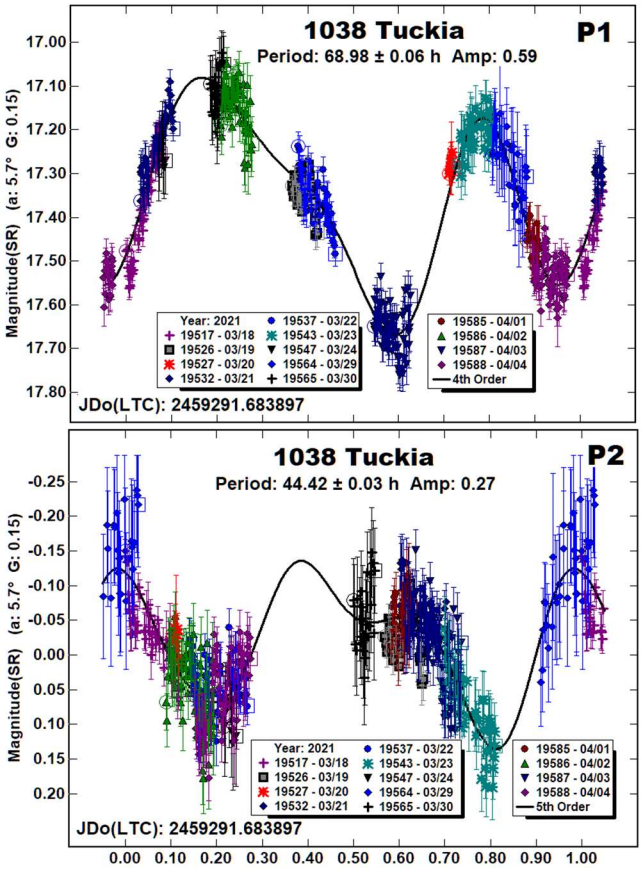

The 2021 data from March to April led to the conclusion that the asteroid is tumbling (Pravec et al., 2005; 2014). The two periods are best guesses since *MPO Canopus* cannot fully analyze tumbling asteroids.

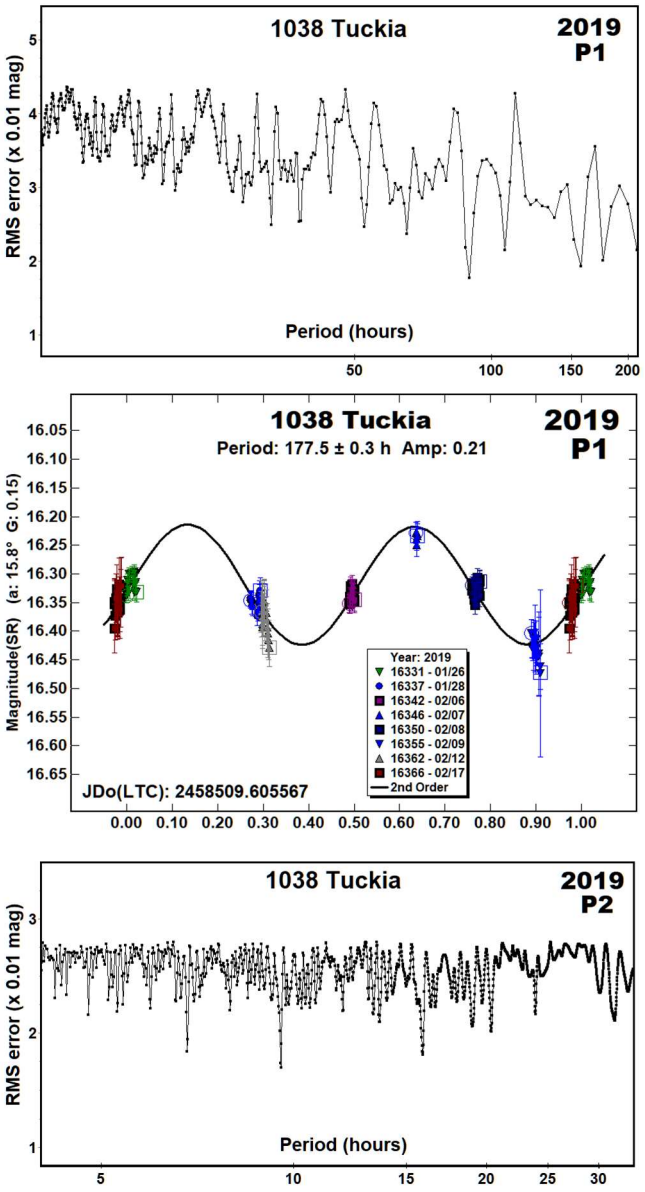

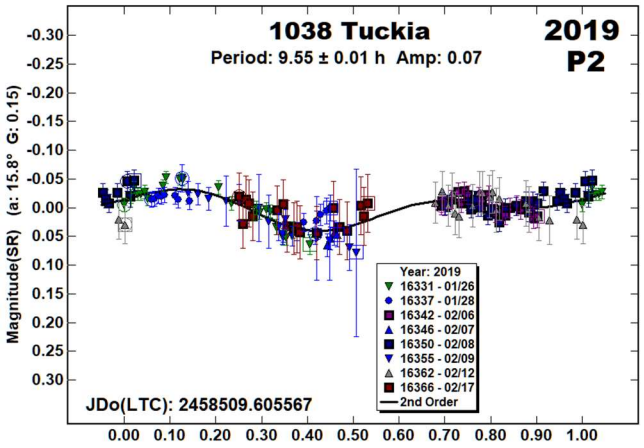

These results prompted a return to the 2019 data, which used V magnitudes derived from Sloan SG and SR magnitudes. The values for the comps were reset to use SR magnitudes from the ATLAS catalog (Tonry et al., 2018) and reset the nightly zero points to 0. As a result, none of the individual sessions needed more than 0.01 mag adjustment to the zero point.

The number of data in 2019 was about 25% of that in 2021, so getting similar results was very unlikely, especially since the Fourier analysis was limited to only second order. Forcing the 2019 data to the most recent results gave unconvincing fits. Instead, we found a dominant period of P_1 = 177.5 h and a second period P_2 = 9.55 h.

The 177-hour period could be the result of a fit by exclusion and so a solution between 40-50 h, still bimodal, might also be possible. When liming the search to that range, the fits of the slopes of the data to the Fourier curve on individual nights were considerably worse, even if taking tumbling into account.

Acknowledgements

Funding for observations at CS3 and work on the asteroid lightcurve database (Warner et al., 2009) and ALCDEF database (*alcdef.org*) were supported in part by NASA grant 80NSSC18K0851. This work includes data from the Asteroid Terrestrial-impact Last Alert System (ATLAS) project. ATLAS is primarily funded to search for near earth asteroids through NASA grants NN12AR55G, 80NSSC18K0284, and 80NSSC18K1575; byproducts of the NEO search include images and catalogs from the survey area. The ATLAS science products have been made possible through the contributions of the University of Hawaii Institute for Astronomy, the Queen's University Belfast, the Space Telescope Science Institute, and the South African Astronomical Observatory. The authors gratefully acknowledge Shoemaker NEO Grants from the Planetary Society (2007, 2013). These were used to purchase some of the telescopes and CCD cameras used in this research.

References

Dahlgren, M.; Lahulla, J.F.; Lagerkvist, C.-I.; Lagerros, J.; Mottola, S.; Erikson, A.; Gonano-Beurer, M.; Di Martino, M. (1998). "A Study of Hilda Asteroids. V. Lightcurves of 47 Hilda Asteroids." *Icarus* **133**, 247-285.

Harris, A.W.; Young, J.W.; Scaltriti, F.; Zappala, V. (1984). "Lightcurves and phase relations of the asteroids 82 Alkmene and 444 Gyptis." *Icarus* **57**, 251-258.

Pravec, P.; Harris, A.W.; Scheirich, P.; Kušnirák, P.; Šarounová, L.; Hergenrother, C.W.; Mottola, S.; Hicks, M.D.; Masi, G.; Krugly, Yu.N.; Shevchenko, V.G.; Nolan, M.C.; Howell, E.S.; Kaasalainen, M.; Galád, A.; Brown, P.; Degraff, D.R.; Lambert, J.V.; Cooney, W.R.; Foglia, S. (2005). "Tumbling asteroids." *Icarus* **173**, 108-131.

Pravec, P.; Scheirich, P.; Durech, J.; Pollock, J.; Kusnirak, P.; Hornoch, K.; Galad, A.; Vokrouhlicky, D.; Harris, A.W.; Jehin, E.; Manfroid, J.; Opitom, C.; Gillon, M.; Colas, F.; Oey, J.; Vrastil, J.; Reichart, D.; Ivarsen, K.; Haislip, J.; LaCluyze, A. (2014). "The tumbling state of (99942) Apophis." *Icarus* **233**, 48-60.

Rubincam, D.P. (2000). "Relative Spin-up and Spin-down of Small Asteroids." *Icarus* **148**, 2-11.

Tonry, J.L.; Denneau, L.; Flewelling, H.; Heinze, A.N.; Onken, C.A.; Smartt, S.J.; Stalder, B.; Weiland, H.J.; Wolf, C. (2018). "The ATLAS All-Sky Stellar Reference Catalog." *Astrophys. J.* **867**, A105.

Warner, B.D.; Harris, A.W.; Pravec, P. (2009). "The Asteroid Lightcurve Database." *Icarus* **202**, 134-146. Updated 2021 June. *http://www.minorplanet.info/lightcurvedatabase.html*

Warner, B.D.; Stephens, R.D. (2019). "Lightcurve Analysis of Hilda Asteroids at the Center for Solar System Studies: 2019 January-March." *Minor Planet Bull*. **46**, 294-297.

NEAR-EARTH ASTEROID LIGHTCURVE ANALYSIS AT THE CENTER FOR SOLAR SYSTEM STUDIES: 2021 MARCH - APRIL

Brian D. Warner
Center for Solar System Studies / MoreData!
446 Sycamore Ave.
Eaton, CO 80615 USA
brian@MinorPlanetObserver.com

Robert D. Stephens
Center for Solar System Studies / MoreData!
Rancho Cucamonga, CA

Daniel R. Coley
Center for Solar System Studies
Corona, CA

(Received: 2021 July 12)

Lightcurves of four near-Earth asteroids (NEAs) obtained at the Center for Solar System Studies (CS3) from 2021 March through April were analyzed for rotation period, peak-to-peak amplitude, and signs of satellites or tumbling.

CCD photometric observations of four near-Earth asteroids (NEAs) were made at the Center for Solar System Studies (CS3) from 2021 March through April. Table I lists the telescopes and CCD cameras that were combined to make observations.

Up to nine telescopes can be used for the campaign, although seven is more common. All the cameras use CCD chips from the KAF blue-enhanced family and so have essentially the same response. The pixel scales ranged from 1.24-1.60 arcsec/pixel.

Telescopes	Cameras
0.30-m *f*/6.3 Schmidt-Cass	FLI Microline 1001E
0.35-m *f*/9.1 Schmidt-Cass	FLI Proline 1001E
0.40-m *f*/10 Schmidt-Cass	SBIG STL-1001E
0.40-m *f*/10 Schmidt-Cass	
0.50-m *f*/8.1 Ritchey-Chrétien	

Table I. List of available telescopes and CCD cameras at CS3. The exact combination for each telescope/camera pair can vary due to maintenance or specific needs.

All lightcurve observations were unfiltered since a clear filter can cause a 0.1-0.3 mag loss. The exposure duration varied depending on the asteroid's brightness and sky motion. Guiding on a field star sometimes resulted in a trailed image for the asteroid.

Measurements were made using *MPO Canopus*. The Comp Star Selector utility in *MPO Canopus* found up to five comparison stars of near solar-color for differential photometry. To reduce the number of times and amounts of adjusting nightly zero points, we use the ATLAS catalog r´ (SR) magnitudes (Tonry et al., 2018). Those adjustments are usually $|\Delta| \leq 0.03$ mag. The larger corrections, which are rare, may have been related in part to using unfiltered observations, poor centroiding of the reference stars, and not correcting for second-order extinction. Another cause may be selecting what appears to be a single star but is actually an unresolved pair.

The Y-axis values are ATLAS SR "sky" (catalog) magnitudes. The two values in the parentheses are the phase angle (a) and the value of *G* used to normalize the data to the comparison stars used in the earliest session. This, in effect, had all the observations made at a single fixed date/time and phase angle, leaving any variations due only to the asteroid's rotation and/or albedo changes. The X-axis shows rotational phase from –0.05 to 1.05. If the plot includes the amplitude, e.g., "Amp: 0.65", this is the amplitude of the Fourier model curve and *not necessarily the adopted amplitude for the lightcurve*.

"LCDB" refers to Warner et al. (2009) from here on.

(5189) 1990 UQ. Warner (2018b) found a period of 6.676 h based on observations in 2017 November. We (Warner and Stephens, 2019) found a similar period of 6.640 h using data from 2019. Díaz-Vachier and Cotto-Figueroa (2020) reported a period of 6.653 h using data obtained in 2017. Oey (2020) followed the asteroid from 2017 September 25 to October 1. Due to a changing viewing aspect, he reported amplitudes range from 0.62–0.92 mag. At the time, he also suspected that the asteroid might be binary.

We observed the asteroid again in 2021 and derived a period of 6.654 h. Behrend (2021web) reported a period 6.644 h and Pravec et al. (2021web), observing six weeks earlier found 6.6570 h. An increasing synodic period as the asteroid approaches opposition usually indicates that the asteroid has retrograde rotation (a negative ecliptic latitude). This was supported by our shape model that found a pole of (λ, β, P) = (317, –79, 6.657399 h). The full results of that analysis are presented in a figure at the end of this paper.

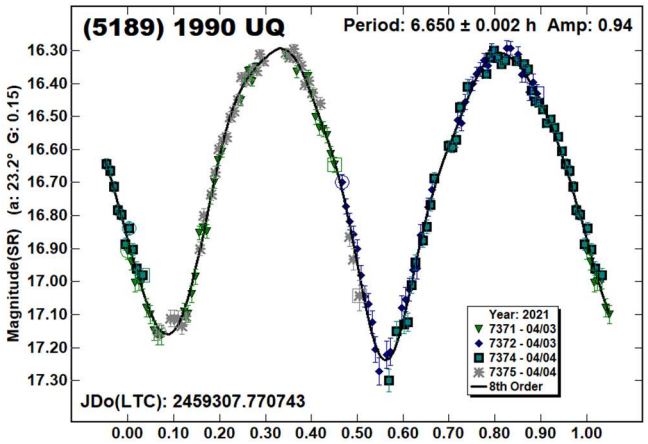

12923 Zephyr. The only previously reported period is from Pravec et al. (1999web) who found 3.891 h. Our observations in early 2021 April led to *P* = 3.893 h, which agrees with Pravec et al.

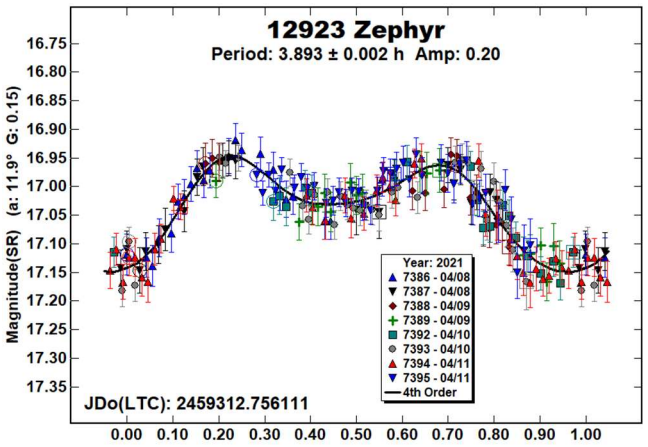

(142464) 2002 TC9. Warner (2018a) found a period of 2.320 h for this 890-m NEA (Mainzer et al., 2019). The solution was not fully secure (U = 2+). Our observations in 2021 led to, we believe, a secure period of 5.131 h. The bimodal lightcurve at 5.131 h with an amplitude of 0.21 mag is too asymmetrical, as shown in the split-halves plot, to adopt a shorter, monomodal solution (see Harris et al., 2014).

With this in mind, we re-examined the data from 2017 after resetting the comparison star magnitudes to those from the ATLAS catalog (Tonry et al, 2018). We tried fitting the data near the original period but the fit was unsatisfactory. We eventually found P = 5.134 h, which is not double the shorter period but close to a 9:4 ratio, suggesting that rotational aliasing and/or overzealous zero-point adjustments led to the shorter period.

(271480) 2004 FX31. Mainzer et al. (2019) used WISE data to find a diameter of 709 m using H = 17.5, which led to an albedo of 0.352. This is on the high end of the range for S-complex asteroids (Warner et al., 2009). Unfortunately, the LCDB has no entries for taxonomic class other than the assumed type S for near-Earth asteroids.

It seems likely that this is a tumbler (in non-principal axis rotation; see Pravec et al., 2005; 2014). *MPO Canopus* cannot fully analyze this type of object. Even so, we were able to extract a dominant period of 77.1 h. Subtracting that found secondary period of 44.9 h. Given the software deficiencies, low SNR, and observations being from a single longitude, these periods should not be taken at face value but may serve future observations. The next apparition is 2023 September when 2004 FX31 will reach V ~ 15.5 at –8° declination.

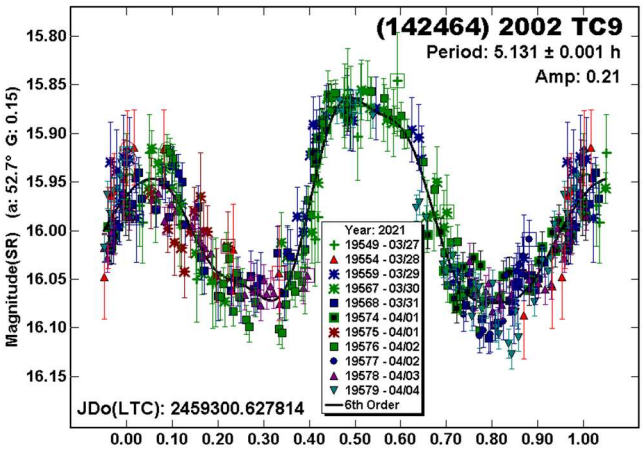

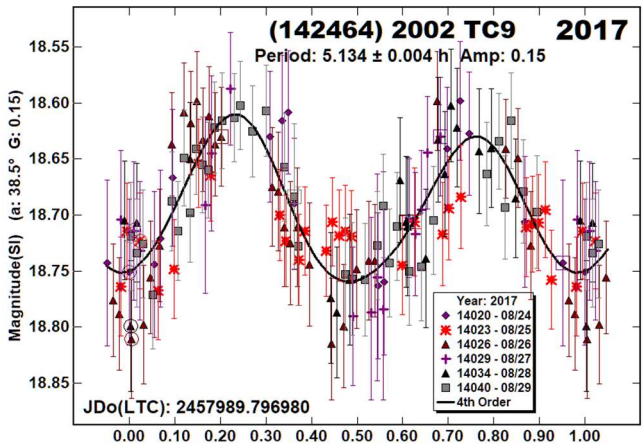

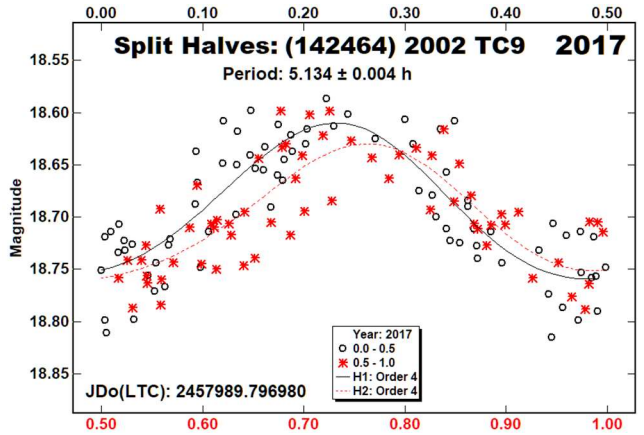

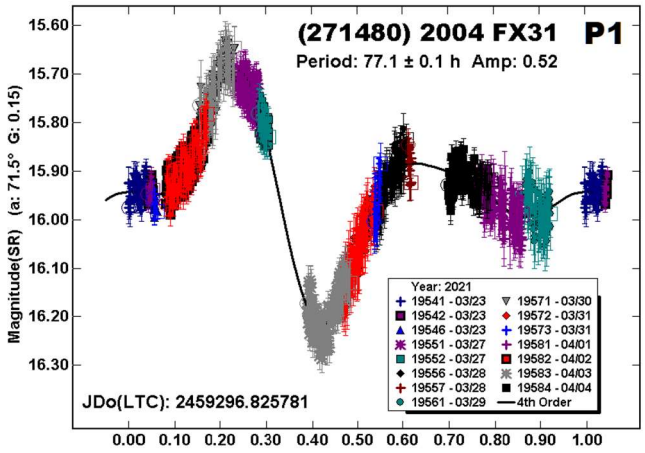

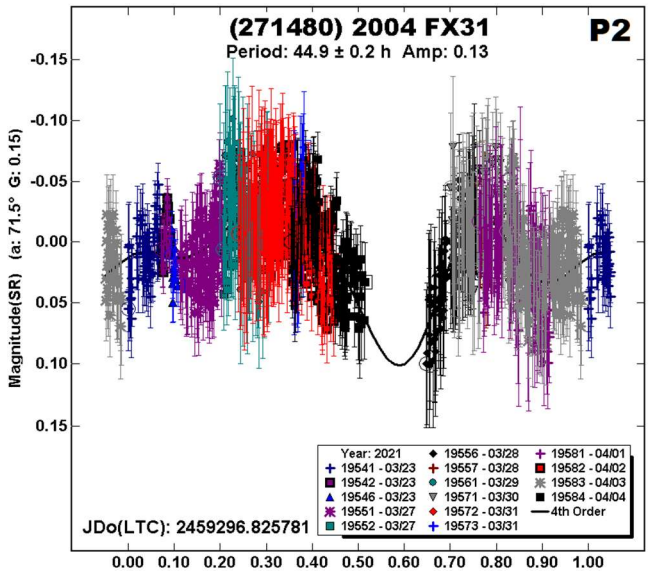

Number	Name	2021 mm/dd	Phase	L_{PAB}	B_{PAB}	Period(h)	P.E.	Amp	A.E.
5189	1990 UQ	04/03-04/07	23.2,22.9	210	9	6.654	0.002	0.91	0.02
12923	Zephyr	04/08-04/10	11.9,10.8	213	5	3.893	0.002	0.20	0.02
142464	2002 TC9	03/27-04/04	*52.8,57.3	155	-9	5.131	0.001	0.21	0.02
271480	2004 FX31	03/24-04/04	69.5,54.4	199	39	T77.1	0.1	0.52	0.04
						44.9	0.2	0.13	0.04

Table II. Observing circumstances and analysis results. TTumbling asteroid. The phase angle (α) is given at the start and end of each date range. If there is an asterisk before the first phase value, the phase angle reached a maximum or minimum during the period. L_{PAB} and B_{PAB} are, respectively the average phase angle bisector longitude and latitude (see Harris et al.,1984).

Number	Name	λ	β	Period	P.E.	a/b ratio	a/c ratio
5189	1990 UQ	317	-79	6.657399	0.000002	1.7	2.4

Table III. The pole solution for (5189) 1990 UQ. The pole coordinates are J2000.0 ecliptic. The a/b and a/c ratios are based on c = 1.0 in a triaxial ellipsoid.

Acknowledgements

Funding for observations at CS3 and work on the asteroid lightcurve database (Warner et al., 2009) and ALCDEF database (*alcdef.org*) were supported in part by NASA grant 80NSSC18K0851. The authors gratefully acknowledge Shoemaker NEO Grants from the Planetary Society (2007, 2013). These were used to purchase some of the telescopes and CCD cameras used in this research. This work includes data from the Asteroid Terrestrial-impact Last Alert System (ATLAS) project. ATLAS is primarily funded to search for near earth asteroids through NASA grants NN12AR55G, 80NSSC18K0284, and 80NSSC18K1575; byproducts of the NEO search include images and catalogs from the survey area. The ATLAS science products have been made possible through the contributions of the University of Hawaii Institute for Astronomy, the Queen's University Belfast, the Space Telescope Science Institute, and the South African Astronomical Observatory.

References

References from web sites should be considered transitory, unless from an agency with a long lifetime expectancy. Sites run by private individuals, even if on an institutional web site, do not necessarily fall into this category.

Behrend, R. (2021web) Observatoire de Geneve web site. *http://obswww.unige.ch/~behrend/page_cou.html*

Díaz-Vachier, I.; Cotto-Figueroa, D. (2020). "The Rotation Rates of Three Near-Earth Asteroids and a Mars-Crossing Asteroid." *Minor Planet Bull*. **47**, 149-150.

Harris, A.W.; Young, J.W.; Scaltriti, F.; Zappala, V. (1984). "Lightcurves and phase relations of the asteroids 82 Alkmene and 444 Gyptis." *Icarus* **57**, 251-258.

Harris, A.W.; Pravec, P.; Galad, A.; Skiff, B.A.; Warner, B.D.; Vilagi, J.; Gajdos, S.; Carbognani, A.; Hornoch, K.; Kusnirak, P.; Cooney, W.R.; Gross, J.; Terrell, D.; Higgins, D.; Bowell, E.; Koehn, B.W. (2014). "On the maximum amplitude of harmonics on an asteroid lightcurve." *Icarus* **235**, 55-59.

Mainzer, A.; Bauer, J.; Cutri, R.; Grav, T.; Kramer, E.; Masiero, J.; Sonnett, S.; Wright, E., Eds. (2019). "NEOWISE Diameters and Albedos V2.0." NASA Planetary Data System. urn:nasa:pds:neowise_diameters_albedos::2.0. *https://doi.org/10.26033/18S3-2Z54*

Oey, J. (2020). "Lightcurve Analysis of Near-Earth Asteroids in 2017 from BMO and JBL." *Minor Planet Bull*. **47**, 136-140.

Pravec, P.; Wolf, M.; Sarounova, L. (1999web; 2021web). *http://www.asu.cas.cz/~ppravec/neo.htm*

Pravec, P.; Harris, A.W.; Scheirich, P.; Kušnirák, P.; Šarounová, L.; Hergenrother, C.W.; Mottola, S.; Hicks, M.D.; Masi, G.; Krugly, Yu.N.; Shevchenko, V.G.; Nolan, M.C.; Howell, E.S.; Kaasalainen, M.; Galád, A.; Brown, P.; Degraff, D.R.; Lambert, J.V.; Cooney, W.R.; Foglia, S. (2005). "Tumbling asteroids." *Icarus* **173**, 108-131.

Pravec, P.; Scheirich, P.; Durech, J.; Pollock, J.; Kusnirak, P.; Hornoch, K.; Galad, A.; Vokrouhlicky, D.; Harris, A.W.; Jehin, E.; Manfroid, J.; Opitom, C.; Gillon, M.; Colas, F.; Oey, J.; Vrastil, J.; Reichart, D.; Ivarsen, K.; Haislip, J.; LaCluyze, A. (2014). "The tumbling state of (99942) Apophis." *Icarus* **233**, 48-60.

Tonry, J.L.; Denneau, L.; Flewelling, H.; Heinze, A.N.; Onken, C.A.; Smartt, S.J.; Stalder, B.; Weiland, H.J.; Wolf, C. (2018). "The ATLAS All-Sky Stellar Reference Catalog." *Ap. J.* **867**, A105.

Warner, B.D.; Harris, A.W.; Pravec, P. (2009). "The Asteroid Lightcurve Database." *Icarus* **202**, 134-146. Updated 2021 June. *http://www.minorplanet.info/lightcurvedatabase.html*

Warner, B.D. (2018a). "Near-Earth Asteroid Lightcurve Analysis at CS3-Palmer Divide Station: 2017 July Through October." *Minor Planet Bull*. **45**, 19-34.

Warner, B.D. (2018b). "Near-Earth Asteroid Lightcurve Analysis at CS3-Palmer Divide Station: 2017 October - December." *Minor Planet Bull*. **45**, 138-147.

Warner, B.D.; Stephens, R.D. (2019). "Near-Earth Asteroid Lightcurve Analysis at the Center for Solar System Studies: 2019 January - April." *Minor Planet Bull*. **46**, 304-314.

SPIN/SHAPE MODEL FOR (5189) 1990 UQ

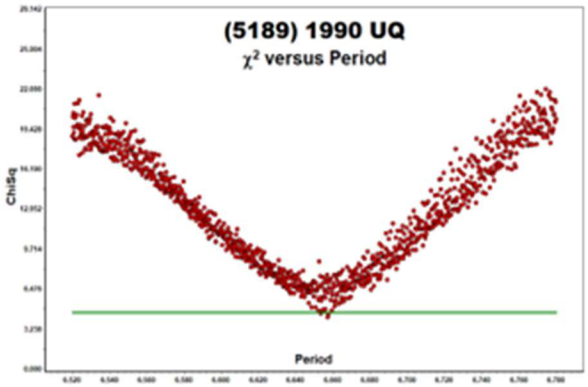

Figure 1. The initial period search results.

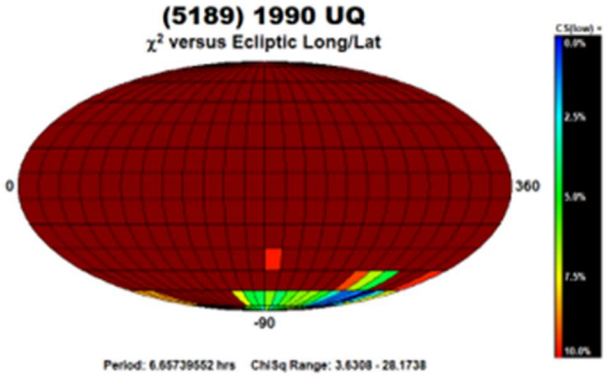

Figure 2. The pole search found one probable solution.

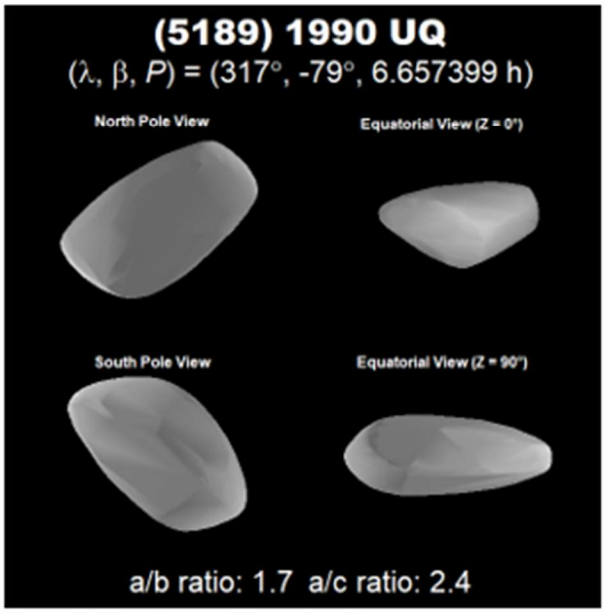

Figure 3. The shape of the asteroid.

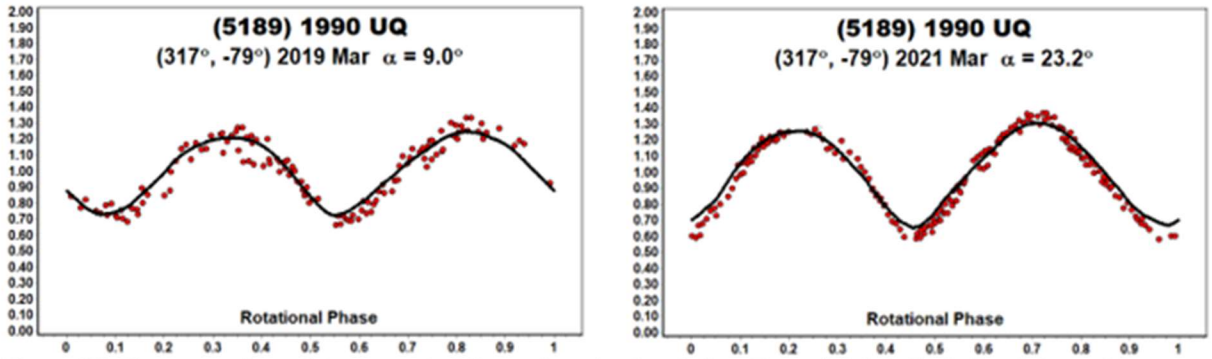

Figure 4/5. The comparison plots are against the preferred pole solution. The red dots indicate the data used for modeling while the black line is the smoothed lightcurve for generated by the shape at the time of the observations. The match is very close on both occasions, which gives confidence in the shape/spin axis model.

LIGHTCURVE ANALYSIS FOR SIX NEAR-EARTH ASTEROIDS

Peter Birtwhistle
Great Shefford Observatory
Phlox Cottage, Wantage Road
Great Shefford, Berkshire, RG17 7DA
United Kingdom
peter@birtwhistle.org.uk

(Received: 2021 July 9)

Lightcurves and amplitudes for six near-Earth asteroids observed from Great Shefford Observatory during close approaches in 2015 and 2021 are reported: 2015 HO116, 2021 GG11, 2021 HC3, 2021 JR3, 2021 JB6 and 2021 KN2. All are fast or superfast rotators and two appear to show signs of tumbling.

Photometric observations of near-Earth asteroids during close approaches to Earth in April 2015 and January - March 2021 were made at Great Shefford Observatory using a 0.40-m Schmidt-Cassegrain and Apogee Alta U47+ CCD camera. All observations were made unfiltered and with the telescope operating with a focal reducer at f/6. The 1Kx1K, 13-micron CCD was binned 2×2 resulting in an image scale of 2.16 arc seconds/pixel. All the images were calibrated with dark and flat frames and *Astrometrica* (Raab, 2018) was used to measure photometry using APASS Johnson V band data from the UCAC4 catalogue. *MPO Canopus* (Warner, 2021), incorporating the Fourier algorithm developed by Harris (Harris et al., 1989) was used for lightcurve analysis.

Unless otherwise noted, no previously reported results for any of the objects have been found in the LCDB (Warner et al., 2009), from searches via the Astrophysics Data System (ADS, 2021) or from wider searches.

2015 HO116. This Apollo object was discovered by the Catalina Sky Survey on 2015 Apr 25 (Nishiyama et al., 2015) two days before approaching Earth to within 1.7 Lunar Distances (LD). It was observed over a six-hour span starting on 2015 Apr 26.86 UTC as it brightened from 16th to 15th magnitude and the apparent speed against the sky increased from 150 to 275 arcsec/min. Exposures were limited to 1 and 2 seconds to keep trailing of the target well within the measurement annulus of *Astrometrica*. A total of 1404 images were taken, with the telescope being repositioned 45 times during the six hours. As no short-term magnitude variation was detected, but large variations were obvious over a period of tens of minutes, the *Astrometrica* Track and Stack function was used to combine on average groups of 15 individual exposures into a stacked image for photometry measurement, to increase the signal to noise ratio. The raw plot shows three deep minima with an apparent variation of shorter period and lower amplitude. To aid the analysis, the measurements were imported into separate sessions within *Canopus* by their placement within the raw curve rather than the more usual means of grouping measurements made from the same field of view into one session. The period spectrum shows a dominant solution at 1.455 h but phased solutions at that period (and at 2.91 h) fail to represent simple principal axis rotation well, the three deep minima are modelled well, but not the apparent minimum seen in the first set of measures, or the smaller ~0.6 mag amplitude variations away from the deep minima. Attempting to solve for a second period using the *Canopus* Dual-Period Search function was also unsuccessful. It is concluded that 2015 HO116 is tumbling, but neither period is resolved unambiguously and so it is expected to be rated as PAR = -1 (Non-Principal Axis rotation possible, but not conclusively) on the scale of Pravec et al. (2005).

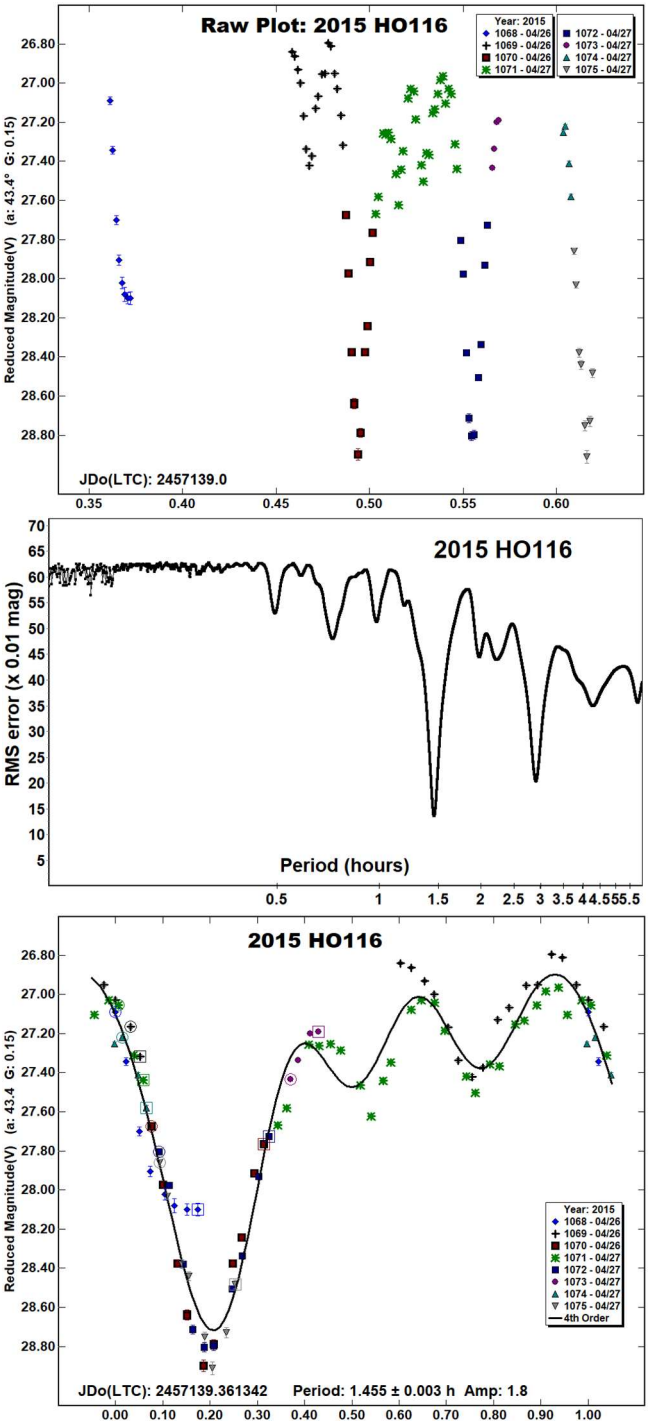

A lightcurve for 2015 HO116 has also been reported by Vaduvescu et al. (2018web), where a single clear maximum and apparent minimum were recorded during a short (probably < 1 h and possibly ~20 min) observing run starting at 2015 Apr 26.93 UTC (JD 2457139.43), i.e., completely within the six-hour span reported here, but probably entirely in the gap between *Canopus* sessions 1068 and 1069 (see the Raw plot). They report a 0.64 mag amplitude and a 0.45 ± 0.04 h monomodal or 0.90 ± 0.04 h bimodal period, flagged as tentative and to be regarded with caution, probably corresponding to quality code U ~ 1. The form of their lightcurve appears to have similar amplitude and periodicity to the short period variation seen in *Canopus* sessions 1069 and 1071 of the raw plot and as such appears consistent with the result presented here.

2021 GG11. The SBDB (JPL, 2021) lists this Apollo with H = 23.1, equating to a diameter of ~71 m assuming an albedo of 0.20. It was discovered from the Mt. Lemmon station of the Catalina Sky Survey (CSS) on 2021 Apr 15, with pre-discovery positions reported from the Mt. Bigelow CSS station 2 days before (Kowalski et al., 2021) and it made an approach to within 5 LD of Earth on 2021 Apr 27. Its ephemeris magnitude was expected to peak at +17.7 between Apr 25 and 26, but it would be moving at twice the speed on the latter date, favouring photometric observation on the earlier night. This was obtained over a period of 3.3 hours starting at 2021 Apr 24.96 UTC when 2021 GG11 was moving at 30 arcsec/min, at a distance of just under 9 LD. The telescope was repositioned 8 times, exposure length for the first 4 sessions limited to 6 s but this was increased to 13 s for the last 4 as large magnitude variations were obvious over a period of 1-2 minutes, indicating that no significant lightcurve smoothing would result with the longer exposure (Pravec et al., 2000). A period spectrum shows potential solutions in the range of 1 - 8 minutes, with an asymmetric bimodal lightcurve of period 2.6 minutes giving the best fit. 2021 GG11 completed 74 rotations during the period of observation.

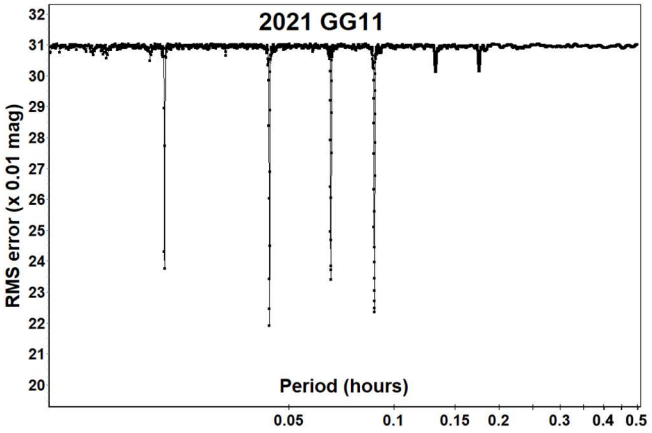

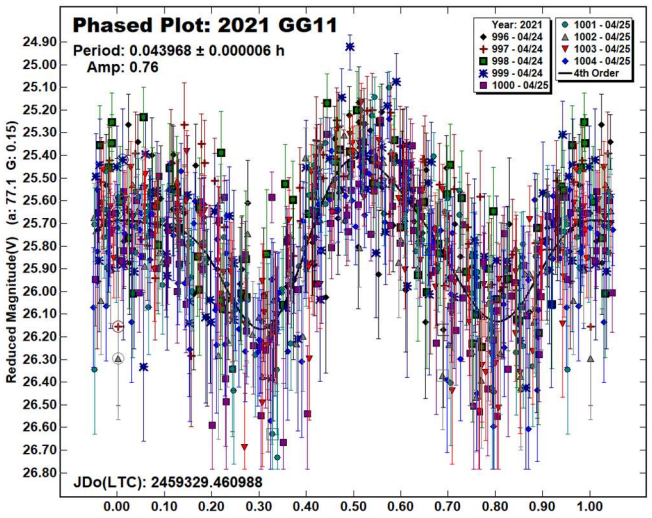

2021 HC3. This is the largest of the objects being reported, with the SBDB giving a value of H = 21.59 and with an assumed albedo of 0.20 suggesting a diameter of ~143 m. It was discovered by the ATLAS 0.5-m reflector on Haleakala (Pruyne et al., 2021) on 2021 Apr 30 and approached Earth to 19 LD on 2021 May 4. Photometry was obtained over a 2.6 h period on the night of closest approach and again, obvious magnitude variations within 1 minute were seen during image collection. Sky motion was 44 arcsec / min and exposures were limited to 9 s to reduce image trailing. Reduction in *Canopus* reveals a 1 mag amplitude bimodal lightcurve of period 2.3 minutes, indicating that 67 full revolutions occurred during the period of observation. The Frequency/Period vs. Diameter diagram, based on LCDB data (Warner et al., 2009) shows 2021 HC3 as a relatively large superfast rotator, which must have non-zero tensile strength, being well beyond the 2.2 h spin barrier and with H < 22 is positioned at the start of the range of small asteroids (0.15 km < D < 10 km) where superfast rotators become much less common.

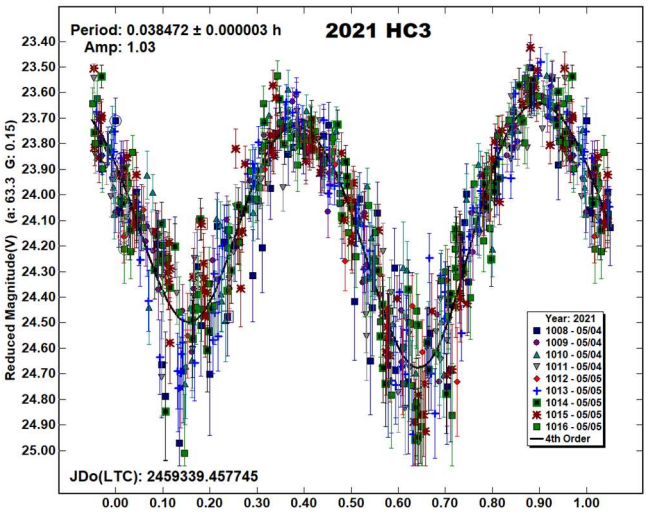

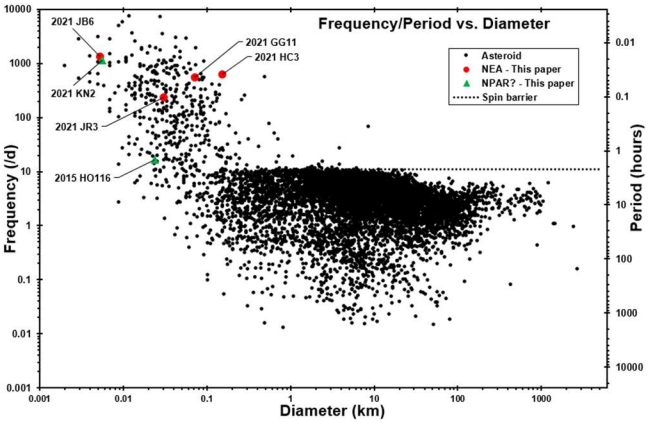

2021 JR3. This Apollo was discovered at 17th mag from the Piszkéstető Mountain Station of the Konkoly Observatory in Hungary on 2021 May 9.9 UTC, with 21st mag pre-discovery positions from May 1st reported from Mt. Lemmon (Pettarin et al., 2021). It passed the Earth at 2 LD on 2021 May 12.08 UT and was best placed for photometry from Great Shefford on the night of May 10 when it was 16th mag, 5 LD away and moving at 45-50 arcsec / min. It was observed for 1 h 16 m, allowing 411 exposures of 8 - 9 s duration to be obtained. Analysis in *Canopus* revealed a bimodal lightcurve with a rotation period of 6.2 min, indicating 12 revolutions had been observed. It is listed with H = 24.95 (JPL, 2021), implying a diameter of ~31 m.

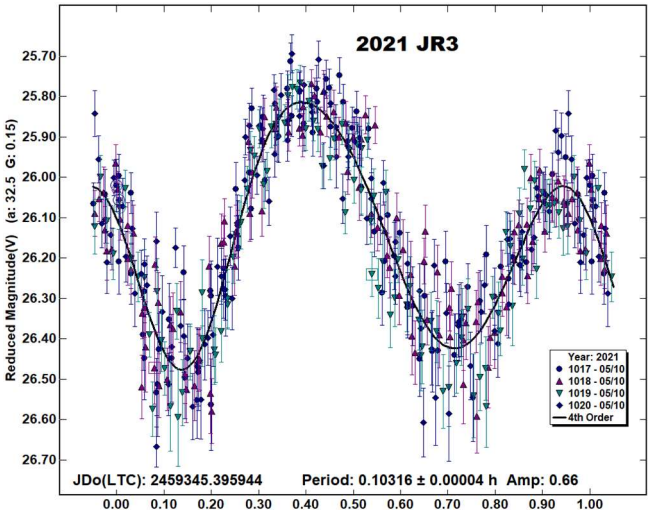

2021 JB6. A very small Apollo with an estimated diameter of ~5 m was discovered as a mag +22 object by the Pan-STARRS 1 team on 2021 May 8.3 UTC, 5.6 days before it made a very close pass to Earth at 0.27 LD (Beniyama et al., 2021a). It was only bright enough for photometry on the night of closest approach and was observed for 66 minutes starting at 2021 May 13.890 UTC. It was well placed, at an altitude of +73°, decreasing to +61°, but at a distance of 0.29 LD, decreasing to 0.26 LD (topocentric) it was moving very fast, speed increasing from 918 to 1086 arcsec/min during the period of observation and the telescope needed to be repositioned 24 times due to the fast motion. Exposures were reduced from 1 s down to 0.6 s to ensure trailing of the target was kept within the measurement annulus in *Astrometrica* and so even though 2021 JB6 was 16th mag, due to the short exposures the measurements are rather noisy. A period search in *Canopus* only found short period solutions, the four strongest shown in the period spectrum being monomodal at 0.009 h, increasing to quadrimodal at 0.037 h. The quadrimodal solution is marginally the strongest, but with the large amount of noise present, the bimodal solution at 0.018 h is preferred. 2021 JB6 completed 60 revolutions during the period of observation.

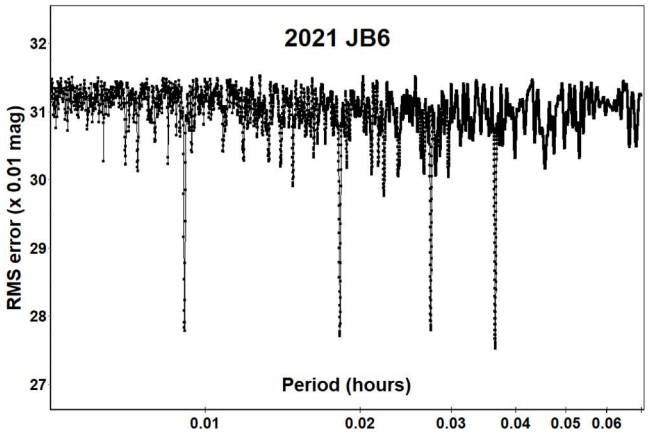

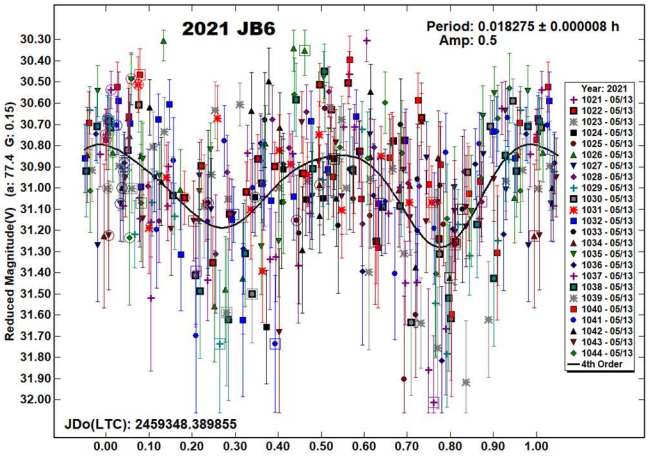

2021 KN2. Another very small Apollo, listed with H = 28.6 in the SBDB (JPL, 2021), equating to a likely size of ~6 m, assuming an albedo of 0.2. it was discovered with the 1.05-m Schmidt at the Tokyo-Kiso observatory on 2021 May 30.55 UTC (Beniyama et al., 2021b) when already just 1.2 LD from Earth and 13 hours later it passed Earth at 0.38 LD. Pre-discovery positions extending the observed arc by 3 hours were reported by the ATLAS team.

1457 images suitable for photometric measurement were obtained over a 2.73 h period starting 2021 May 30.91 UTC. With the speed increasing from 415 to 755 arcsec/min the telescope had to be repositioned 61 times and exposures were reduced from 1.4 to 0.6 s to keep trailing of the target within the measurement annulus in *Astrometrica*. As with 2021 JB6, the very short exposures used have resulted in measurements with relatively low S/Nr.

An initial reduction of the lightcurve in *Canopus*, assuming principal axis rotation (diagram labelled PAR assumed), indicated a period of 0.02101 h, but with even more scatter in the solution than would have been expected from the amount of noise in the measurements:

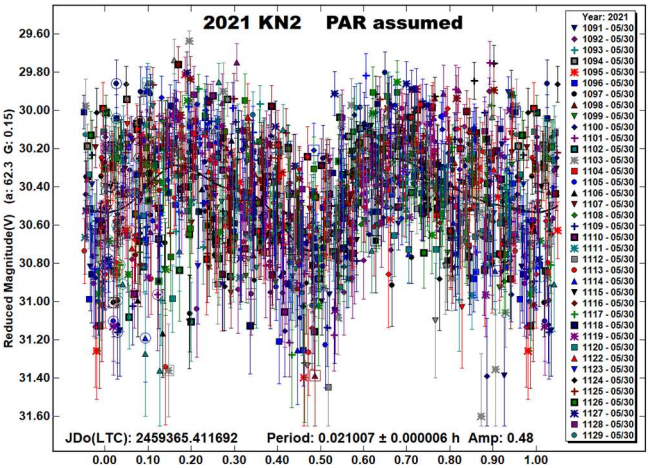

An examination of the period spectrum showed 15 minima in the range 0.006 - 0.0525 h (22.5 - 189 s) and the *Canopus* Dual-Period search function, seeded with 0.02101 h as the main period, resulted in two bimodal periods being resolved, P1 = 0.021007 h and P2 = 0.017825 h (diagrams labelled P1 and P2). Multiples of the values of P1/2 and P2/2 can be identified as the strongest 10 of the 15 minima, these indicated by arrows labelled P1 and P2 in the linearly scaled Period Spectrum diagram:

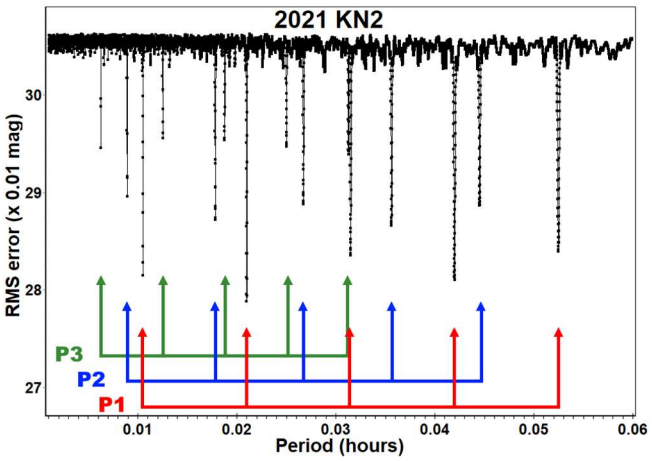

The remaining 5 minima were equally spaced, and apparently multiples of 0.006 h, so another Dual-Period search was done, starting with the P1 value and forcing *Canopus* to resolve a period near .012 h (the likely bimodal value amongst the unidentified 5 minima). The resulting lightcurve labelled P3 has a period of 0.012516 h. The three derived periods, their formal errors and amplitudes are:

P1 = 0.021007 ± 0.000002 h, amplitude = 0.50
P2 = 0.017825 ± 0.000002 h, amplitude = 0.38
P3 = 0.012516 ± 0.000002 h, amplitude = 0.27

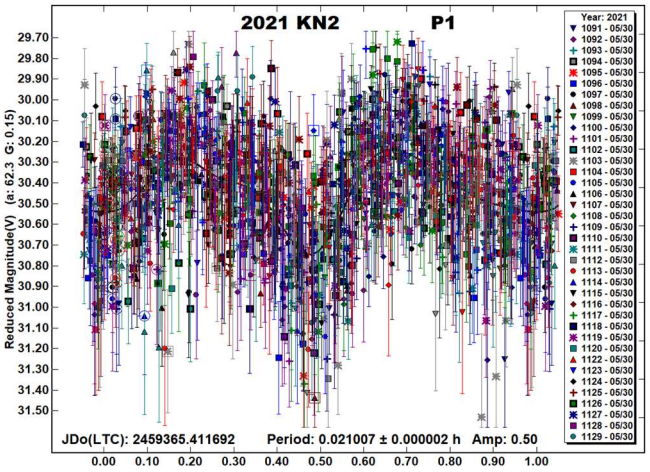

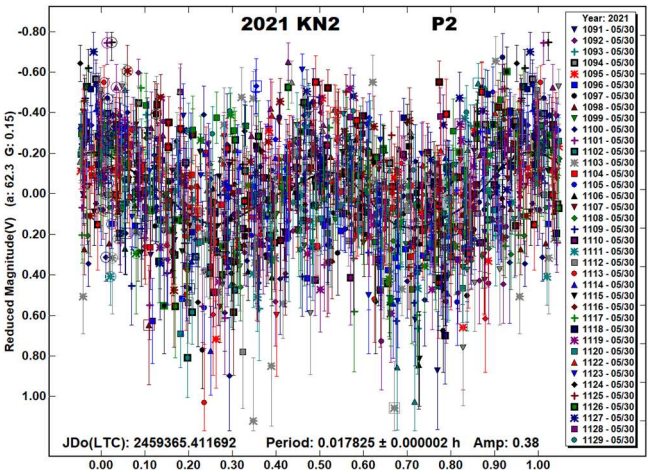

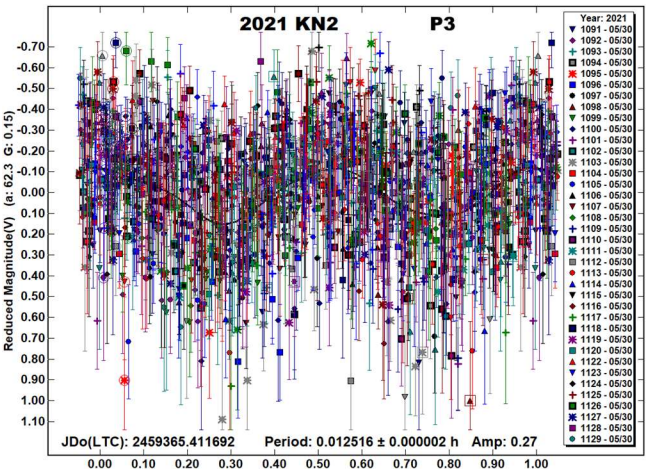

A Dual-Period solution using P1 and P2 gives the best fit to the data points but solutions for P1/P3 and also P2/P3 have similar fits, with the P2/P3 solution producing the largest RMS residuals, but these being only 8% larger than the P1/P2 result.

2021 KN2 is definitely tumbling and the three frequencies, 1/P1, 1/P2 and 1/P3 are linearly related, one of them is a linear combination of the other two, e.g.:

$$1/P1 = 2/P3 - 2/P2$$

and in rotations:

$$28\ P1 = 33\ P2 = 47\ P3$$

but without more data it is not clear which two of the periods are real periods of the tumbler and which one is only their linear combination. It is therefore expected this may be rated as PAR = -2 tending to -3. (Petr Pravec, personal communication). The slowest rotation period, of 75.6 s (P1) implies at least 129 rotations were completed during the 2.73 h of observation.

Number	Name	Integration times	Max intg./ Period	Min a/b	Points	Fields
	2015 HO116	134$^{\Sigma}$	0.026	2.1	91	45
	2021 GG11	13	0.082	1.2	530	5
	2021 HC3	8.8,8.9	0.064	1.4	681	9
	2021 JR3	8.1-8.7	0.023	1.4	411	4
	2021 JB6	0.6-1.0	0.015	1.1	346	24
	2021 KN2	0.6-1.4	0.031	1.2	1457	61

Table I. Ancillary information, listing the integration times used (seconds), the fraction of the period represented by the longest integration time (Pravec et al., 2000), the calculated minimum elongation of the asteroid (Kwiatkowski et al., 2010), the number of data points used in the analysis and the number of times the telescope was repositioned to different fields. Note: Σ = Longest elapsed integration time for stacked images (start of first to end of last exposure used).

Acknowledgements

The author would like to thank Petr Pravec for his continued support and help on the analysis of tumbling asteroids. The author also gratefully acknowledges a Gene Shoemaker NEO Grant from the Planetary Society (2005) and a Ridley Grant from the British Astronomical Association (2005), both of which facilitated upgrades to observatory equipment used in this study.

Number	Name	yyyy mm/ dd	Phase	L_{PAB}	B_{PAB}	Period(h)	P.E.	Amp	A.E	PAR	H
	2015 HO116	2015 04/26-04/27	22.1,43.5	218	17	1.455	0.003	1.8	0.2	-1	25.5
	2021 GG11	2021 04/24-04/25	77.1,78.8	196	36	0.043968	0.000006	0.8	0.3		23.13
	2021 HC3	2021 05/04-05/05	63.3,65.0	217	34	0.038472	0.000003	1.0	0.2		21.59
	2021 JR3	2021 05/10-05/10	32.4,33.7	214	4	0.10316	0.00004	0.7	0.1		24.95
	2021 JB6	2021 05/13-05/13	79.5,95.1	219	42	0.018275	0.000008	0.5	0.3		28.78
	2021 KN2	2021 05/30-05/31	60.2,86.1	232	32	0.021007	0.000002	0.5	0.3	-2/-3	28.63
						0.017825	0.000002	0.4	0.3		
						0.012516	0.000002	0.3	0.3		

Table II. Observing circumstances and results. Where more than one line is given, these include periods determined for NPA rotation. The phase angle is given for the first and last date. If preceded by an asterisk, the phase angle reached an extrema during the period. LPAB and BPAB are the approximate phase angle bisector longitude/latitude at mid-date range (see Harris et al., 1984). PAR is the expected Principal Axis Rotation quality detection code (Pravec et al., 2005) and H is the absolute magnitude at 1 au from Sun and Earth taken from the Small-Body Database Browser (JPL, 2021).

References

ADS (2021). Astrophysics Data System. *https://ui.adsabs.harvard.edu/*

Beniyama, J.; Ikari, Y.; Bulger, J.; Lowe, T.; Schultz, A.; Willman, M.; Chambers, K.; Chastel, S.; de Boer, T.; Denneau, L.; Fairlamb, J.; Flewelling, H.; Huber, M.; Lin, C.-C.; Magnier, E. and 8 colleagues (2021a). "2021 JB6" MPEC 2021-J203. *https://minorplanetcenter.net/mpec/K21/K21JK3.html*

Beniyama, J.; Sako, S.; Pettarin, E.; Ikari, Y.; Emmerich, M.; Melchert, S.; Felber, T.; Losse, F.; Briggs, D.; Birtwhistle, P.; Korlevic, K.; Arena, C.; Elenin, L.; Denneau, L.; Tonry, J. and 7 colleagues (2021b). "2021 KN2" MPEC 2021-K100. *https://minorplanetcenter.net/mpec/K21/K21KA0.html*

Harris, A.W.; Young, J.W.; Scaltriti, F.; Zappala, V. (1984). "Lightcurves and phase relations of the asteroids 82 Alkmene and 444 Gyptis." *Icarus* **57**, 251-258.

Harris, A.W.; Young, J.W.; Bowell, E.; Martin, L.J.; Millis, R.L.; Poutanen, M.; Scaltriti, F.; Zappala, V.; Schober, H.J.; Debehogne, H.; Zeigler, K. (1989). "Photoelectric Observations of Asteroids 3, 24, 60, 261, and 863." *Icarus* **77**, 171-186.

JPL (2021). Small-Body Database Browser. *https://ssd.jpl.nasa.gov/sbdb.cgi*

Kowalski, R.A.; Gray, B.; Rankin, D.; Shelly, F.C.; Christensen, E.J.; Farneth, G.A.; Fuls, D.C.; Gibbs, A.R.; Grauer, A.D.; Groeller, H.; Larson, S.M.; Leonard, G.J.; Pruyne, T.A.; Seaman, R.L.; Wierzchos, K.W. and 2 colleagues (2021) "2021 GG11" MPEC 2021-G223. *https://minorplanetcenter.net/mpec/K21/K21GM3.html*

Kwiatkowski, T.; Buckley, D.A.H.; O'Donoghue, D.; Crause, L.; Crawford, S.; Hashimoto, Y.; Kniazev, A.; Loaring, N.; Romero Colmenero, E.; Sefako, R.; Still, M.; Vaisanen, P. (2010). "Photometric survey of the very small near-Earth asteroids with the SALT telescope - I. Lightcurves and periods for 14 objects.", *Astronomy & Astrophysics* **509**, A94.

Nishiyama, K.; Urakawa, S.; Okumura, S.; Fuls, D.C.; Christensen, E.J.; Gibbs, A.R.; Grauer, A.D.; Hill, R.E.; Johnson, J.A.; Kowalski, R.A.; Larson, S.M.; Matheny, R.G.; Shelly, F.C.; Ikari, Y. (2015). "2015 HO116" MPEC 2015-H122. *https://minorplanetcenter.net/mpec/K15/K15HC2.html*

Pettarin, E.; Rankin, D.; Gray, B.; Shelly, F.C.; Holmes, R.; Linder, T.; Horn, L.; Leonard, G.J.; Christensen, E.J.; Farneth, G.A.; Fuls, D.C.; Gibbs, A.R.; Grauer, A.D.; Groeller, H.; Kowalski, R.A. and 13 colleagues (2021). "2021 JR3" MPEC 2021-J144. *https://minorplanetcenter.net/mpec/K21/K21JE4.html*

Pravec, P.; Hergenrother, C.; Whiteley, R.; Sarounova, L.; Kusnirak, P.; Wolf, M. (2000). "Fast Rotating Asteroids 1999 TY2, 1999 SF10, and 1998 WB2." *Icarus* **147**, 477-486.

Pravec, P.; Harris, A.W.; Scheirich, P.; Kušnirák, P.; Šarounová, L.; Hergenrother, C.W.; Mottola, S.; Hicks, M.D.; Masi, G.; Krugly, Yu.N.; Shevchenko, V.G.; Nolan, M.C.; Howell, E.S.; Kaasalainen, M.; Galád, A.; Brown, P.; DeGraff, D.R.; Lambert, J.V.; Cooney Jr., W.R.; Foglia, S. (2005). "Tumbling Asteroids." *Icarus* **173**, 108-131.

Pruyne, T.A.; Christensen, E.J.; Farneth, G.A.; Fuls, D.C.; Gibbs, A.R.; Grauer, A.D.; Groeller, H.; Kowalski, R.A.; Larson, S.M.; Leonard, G.J.; Rankin, D.; Seaman, R.L.; Shelly, F.C.; Wierzchos, K.W.; Dupouy, P. and 25 colleagues (2021). "2021 HC3" MPEC 2021-J16. *https://minorplanetcenter.net/mpec/K21/K21J16.html*

Raab, H. (2018). Astrometrica software, version 4.12.0.448. *http://www.astrometrica.at/*

Vaduvescu, O.; Cornea, R.; Aznar Macias, A.; Sonka, A.; Predatu, M.; Serra-Ricart, M. (2018web). "The EURONEAR Lightcurve Survey of Near-Earth Asteroids - Teide Observatory, Tenerife, 2015." Astronomy scientific papers by Ovidiu Vaduvescu web site. *http://www.ovidiuv.ca/papers/Vaduvescu_Paper113.pdf*

Warner, B.D.; Harris, A.W.; Pravec, P. (2009). "The Asteroid Lightcurve Database." *Icarus* **202**, 134-146. Updated 2021 June. *https://minplanobs.org/mpinfo/php/lcdb.php*

Warner, B.D. (2021). MPO Software Canopus, version 10.8.4.2. Bdw Publishing. Colorado Springs, CO.

ULTRA-FAST ROTATORS: RESULTS AND RECOMMENDATIONS FOR OBSERVING STRATEGIES

Peter Birtwhistle
Great Shefford Observatory
Phlox Cottage, Wantage Road
Great Shefford, Berkshire, RG17 7DA
United Kingdom
peter@birtwhistle.org.uk

(Received: 2021 July 9, Revised: 2021 August 23)

Lightcurves and amplitudes for two ultra-fast rotating near-Earth asteroids with rotation periods < 20 s observed from Great Shefford Observatory during close approaches in April 2021 are reported: 2021 GQ10 and 2021 HN. The interpretation of lightcurves where exposure length is likely to be a sizable fraction of the rotation period is discussed. Observing strategy recommendations are made to optimize exposure length in near-real time, maximizing the chance of detecting ultra-fast rotation in small objects.

Photometric observations of near-Earth asteroids during close approaches to Earth during April 2021 were made at Great Shefford Observatory using a 0.40-m Schmidt-Cassegrain and Apogee Alta U47+ CCD camera. All observations were made unfiltered and with the telescope operating with a focal reducer at f/6. The 1K×1K, 13-micron CCD was binned 2×2 resulting in an image scale of 2.16 arc seconds/pixel. All the images were calibrated with dark and flat frames and *Astrometrica* (Raab, 2018) was used to measure photometry using APASS Johnson V band data from the UCAC4 catalogue. *MPO Canopus* (Warner, 2021), incorporating the Fourier algorithm developed by Harris (Harris et al., 1989) was used for lightcurve analysis.

No previous results for 2021 GQ10 or 2021 HN are contained in the LCDB (Warner et al., 2009) and no previously reported results have been found in searches of the Astrophysics Data System (ADS, 2021) or from wider searches.

Number	Name	Integration times	Max intg./ Period	Min a/b	Points	Fields
	2021 GQ10	4.6-6.3	0.326	1.03	1384	14
	2021 HN	2.7-3.7	0.236	1.3	1062	13

Table I. Ancillary information, listing the integration times used (seconds), the fraction of the period represented by the longest integration time (Pravec et al., 2000), the calculated minimum elongation of the asteroid (Kwiatkowski et al., 2010), the number of data points used in the analysis and the number of times the telescope was repositioned to different fields.

2021 GQ10. Discovered on 2021 Apr 14 with the 1.05-m Schmidt at the Tokyo-Kiso station, 9 hours after a very close approach to within 0.5 Lunar distances (LD) of Earth (Melnikov et al., 2021). It was observed from Great Shefford for a continuous period of 3.5 h starting at 2021 Apr 14.95 UTC, sky motion was high but decelerating, from 83 to 59 arcsec/min by the end. Due to the apparent speed, the telescope was repositioned 14 times and for each new field, the exposure length was adjusted if necessary to ensure the object trailed 3 pixels, for consistency when measuring in Astrometrica. This resulted in exposures being increased from an initial 4.6 s to 6.3 s at the end. The average gap between consecutive images was 1.7 s. Analysis of the 1384 measurable images initially indicated little or no periodic variation over a range of 0.01 – 6 h. A raw plot has indications of small variations between individual Canopus sessions but attempting a solution results in an unsatisfactory period (3.7 h), similar to the span of observations and an amplitude smaller than the underlying noise in the measurements. However, checking for very short periods revealed a set of solutions with P < 75 s. As discussed in Birtwhistle (2021b), RMS minima at very small P are very narrow and need investigating with the step size in Canopus set to the highest resolution to determine the best fit. The period spectrum here has a linear x-axis and shows 6 RMS minima between 10 and 77 s, with a monomodal solution at 0.0027 h, bimodal solution at 0.0054 h and quadrimodal at 0.011 h. When investigated individually the bimodal and quadrimodal minima have the strongest signals and match each other to 0.00001 magnitudes. Examining the quadrimodal solution with the Canopus Split Halves function shows the two halves matching to within 0.02 magnitudes and with the overall RMS fit of the solution being 0.07 the two halves are essentially the same and the bimodal solution is taken in preference here.

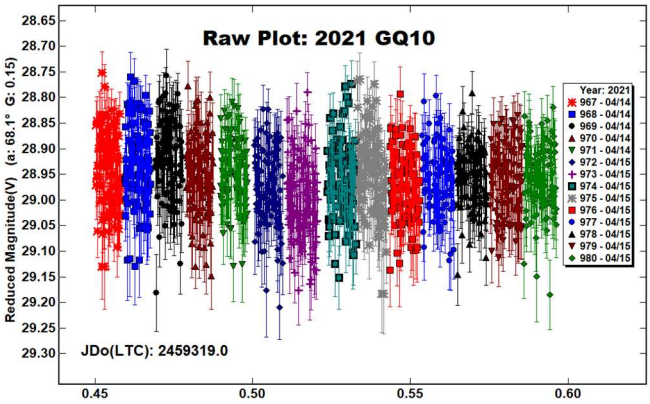

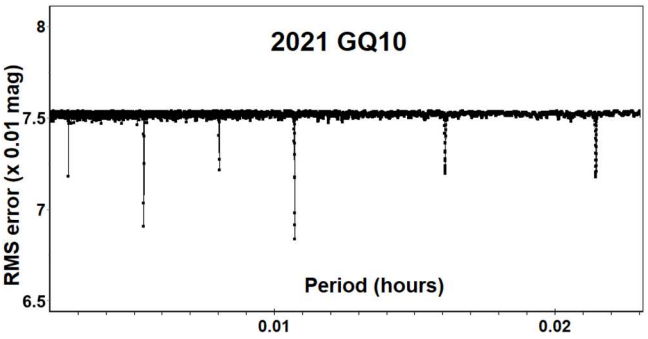

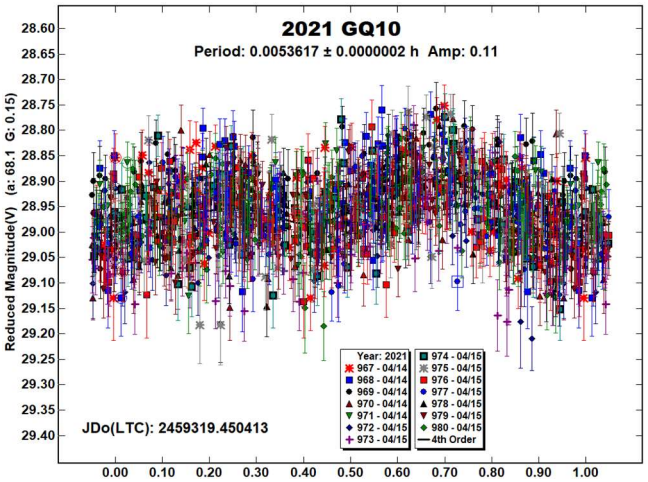

Number	Name	yyyy mm/ dd	Phase	L_{PAB}	B_{PAB}	Period(h)	P.E.	Amp	A.E	H
	2021 GQ10	2021 04/14-04/15	69.5,70.7	213	34	0.0053617	0.0000002	0.11	0.05	26.7
	2021 HN	2021 04/18-04/18	52.2,56.1	203	27	0.0043581	0.0000001	0.74	0.15	26.9

Table II. Observing circumstances and results. The phase angle is given for the first and last date. If preceded by an asterisk, the phase angle reached an extrema during the period. LPAB and BPAB are the approximate phase angle bisector longitude/latitude at mid-date range (see Harris et al., 1984). H is the absolute magnitude at 1 au from Sun and Earth taken from the Small-Body Database Browser (JPL, 2021).

It is possible that exposure length or exposure cadence can cause artificial periodic effects in a short period lightcurve, but due to the exposure length being changed throughout, these effects are likely to be minimised in this analysis. During the observing period, exposure length was increased by 37% and overall cadence (exposure length + gap between consecutive exposures) changed by 21%, with the largest number of exposures using the same settings being 15% of the total. The lightcurve is noisy, with a small amplitude of 0.11 and an ultra-fast rotation period of 19.3 s. This is discussed later due to the likelihood of significant lightcurve smoothing being present. During the 3.5 h of observation the 19.3 s period indicates that 2021 GQ10 completed 657 revolutions. The estimated diameter is ~14 m based on the value of H = 26.65 (JPL, 2021) assuming the NEO default albedo value of 0.20 (Warner et al., 2009).

2021 HN. JPL lists this Apollo with H = 26.9 (JPL, 2021), suggesting an approximate diameter of 12 m. It was discovered at the Mt. Lemmon station of the Catalina Sky Survey 2 days before passing Earth at 0.66 LD (Bacci et al., 2021) and followed from 2021 Apr 18.89 UTC for 109 min during the last part of its approach, at a range of 1.6 LD. Its sky motion increased from 107 to 147 arcsec/min during that period. As with 2021 GC10, exposures were automatically adjusted to keep the trailing of the object 3 pixels long, decreasing from 3.7 to 2.7 s during the period of observation. The telescope was repositioned 13 times and exposure lengths were changed 11 times, in 0.1 s decrements. The average gap between images was again 1.7 s. During image capture large variations in magnitude were obvious between consecutive exposures, with the object being visible in all images, though faint at some minima. A period search revealed 6 potential solutions, all at values of P < 63 s. Similar to 2021 GQ10, in this linear scaled Period Spectrum, the monomodal solution is on the left at 0.0022 h, with bimodal at 0.0044 h and the apparently strongest signal from the quadrimodal solution at 0.008 h. However, investigating each minima individually with the highest resolution, smallest step size in Canopus shows the bimodal solution actually gives the best fit.

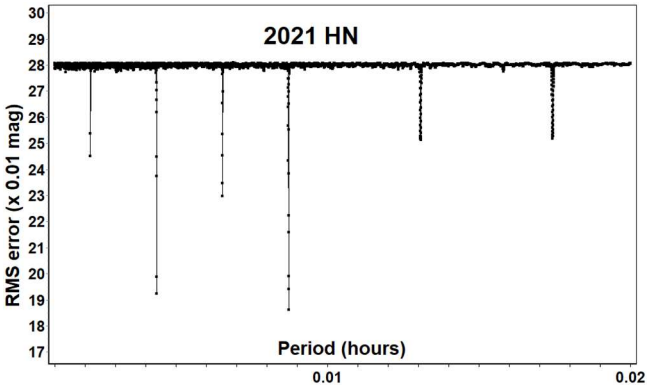

2021 HN has an ultra-fast rotation period of 15.7 s with amplitude of 0.74 and completed 417 rotations while under observation.

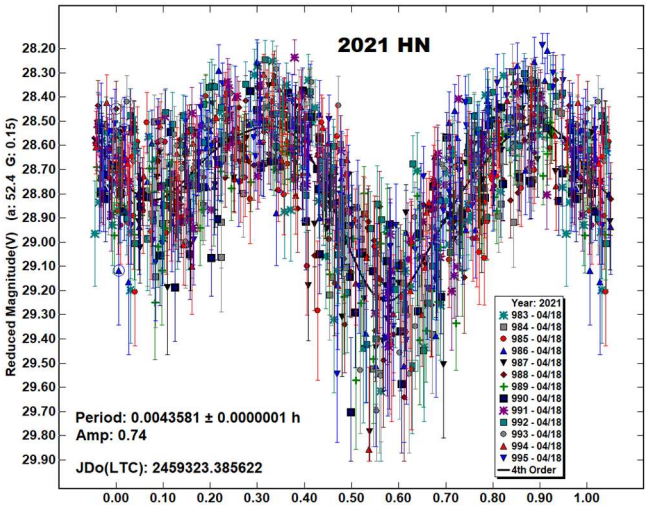

Interpreting lightcurves of ultra-fast rotators.

The optimum exposure time Δt required to detect the second (and normally strongest) harmonic in a lightcurve of period P is developed in Pravec et al. (2000), examining the trade-off between a longer exposure giving better signal to noise ratio but also causing increasing smoothing of the lightcurve as Δt approaches or exceeds 0.5 P. The optimum integration time for a detection of the second harmonic is determined there to be 0.185 P. Further, the apparent lightcurve, observed with exposure length Δt is shown to not have the same shape as the real lightcurve, instead, its Fourier coefficients are the Fourier coefficients of the true lightcurve multiplied by factors:

$$f_n = \frac{P}{\pi n \Delta t} \sin\left(\frac{\pi n \Delta t}{P}\right) \quad \text{for n = 1 to m} \qquad (1)$$

where m is the highest significant order in the Fourier series.

It can be seen that when fn = 0 then the contribution of the nth harmonic to the overall lightcurve will be zero, i.e., that harmonic is completely smoothed out. This occurs when $n\Delta t/P$ is integer, therefore in the intuitively obvious case where Δt = P all harmonics are smoothed out and the lightcurve becomes a straight line. The second harmonic is smoothed out when Δt = P / 2, the third when Δt = P / 3 and 2 P / 3 and so on. Depending on the (unknown) amplitude of the individual harmonics in the real lightcurve, the observed lightcurve can radically change shape with an unfortunate choice of Δt. To examine this further, Eq. 1 is used to plot values of fn for the first 5 harmonics, for Δt / P in the range of 0 to 2:

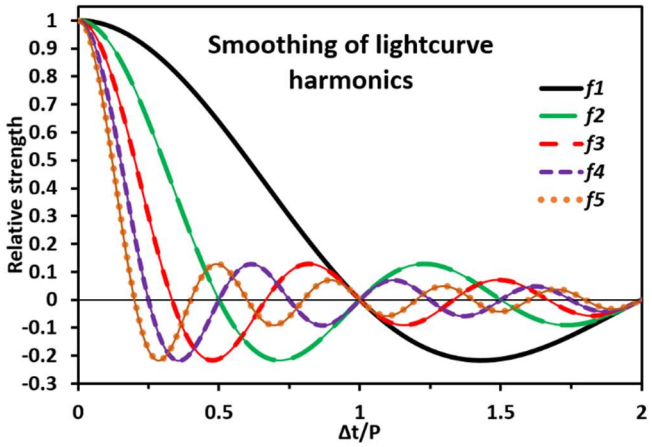

As $\Delta t \rightarrow 0$, all the factors, $fn \rightarrow 1$, the result being an observed lightcurve with no smoothing, matching the real lightcurve of the object, but of course at Δt = 0, no signal would be recorded. As Δt increases, each factor in turn reduces to 0 when $n\Delta t/P$ is integer and soon afterwards reaches a small negative extreme, before oscillating between positive and negative peaks of decreasing amplitude. In most lightcurves, where the second harmonic is the strongest, selecting exposure time Δt = 0.5 P will completely remove the contribution of the 2nd (and also the 4th) harmonic. Doing so will also cause the amplitude due to the 1st harmonic to reduce to 0.64 of its real value and likewise, the 3rd and 5th harmonics reduce to -0.21 and 0.13 of their real values respectively. At any value of non-integer Δt / P, the individual harmonics will be unequally affected. Depending on the values of the real Fourier coefficients and of Δt, these changing strengths of individual harmonics can result in the observed lightcurve having drastically reduced amplitude, reversal of phase and apparent corruption of shape, for instance, a real bimodal lightcurve may appear monomodal, trimodal or with a higher order shape. The observed lightcurve of any object with a strong 2nd harmonic in its real lightcurve, if observed with a value of Δt approaching or exceeding 0.5 P is likely to be so severely distorted as to make interpretation of the real curve difficult or impossible.

To assess the effect of smoothing on real lightcurves, a set of bimodal lightcurves previously reported (Birtwhistle, 2018, 2021a, 2021c) and listed in Table III were selected to represent a range of harmonic strengths. In all cases, during data collection, Δt ≤ 0.10 P and therefore smoothing effects can be expected to be minimal in the dominant lower order harmonics (at Δt = 0.10, $f1$ = 0.98, $f2$ = 0.94) and so are referred to here as their "real" lightcurves.

Number	Name	Δt/P Obs	P(s)	Ampl.	H	Ref.
	2012 XE54	0.039	101.8	0.29	25.4	2018
	2018 CB	0.003	326.6	0.24	25.9	2021a
	2018 GE3	0.004	1113	0.92	23.8	2021a
	2020 KK7	0.082	46.4	1.44	26.2	2021a
	2021 FH	0.101	64.5	0.21	26.7	2021c

Table III. NEOs used in lightcurve modelling, listing the fraction of the period represented by the longest integration time (Pravec et al., 2000), rotation period in seconds, amplitude in magnitudes, the absolute magnitude at 1 au from Sun and Earth taken from the Small-Body Database Browser (JPL, 2021) and the (Birtwhistle) reference to the original lightcurve.

Two figures are given for each object, labelled "Δt ≤ 0.5 P" and "Δt > 0.5 P", both include a solid line representing the real lightcurve. Broken lines are given in the first figure for the calculated smoothing effects of Δt = 0.2, 0.25, 0.333 and 0.5 P, i.e., matching the 5th, 4th, 3rd and 2nd harmonics respectively and the second figure for the effects of Δt = 0.6, 0.667, 0.75 and 0.8 P matching the 5th, 3rd, 4thand 5th harmonics respectively. Inset into each plot is a small figure showing the relative strengths of harmonics 1 to 5 in the real lightcurve.

For all objects, the first figure shows that the real curves are only recognisable for Δt ≤ 0.333 P. With increasing Δt the amplitude decreases and in addition, small, higher order detail is smoothed out occasionally (e.g., 2021 FH between 0.75 < P < 1). Again, for all objects, at Δt = 0.5 P, where the amplitudes due to the 2nd and 4th harmonics are reduced to zero, significant distortion occurs and the strongest remaining harmonics dominate the lightcurve. In most cases this is the 1st harmonic and result in apparent monomodal lightcurves but occasionally the 3rd harmonic is strong enough to cause visible effects. The diagrams are summarised below:

2nd harmonic dominant, 1st harmonic weak. (2020 KK7). A shallow monomodal lightcurve results after removal of the dominant 2nd (and the weaker 4th) harmonic contribution at Δt = 0.5 P.

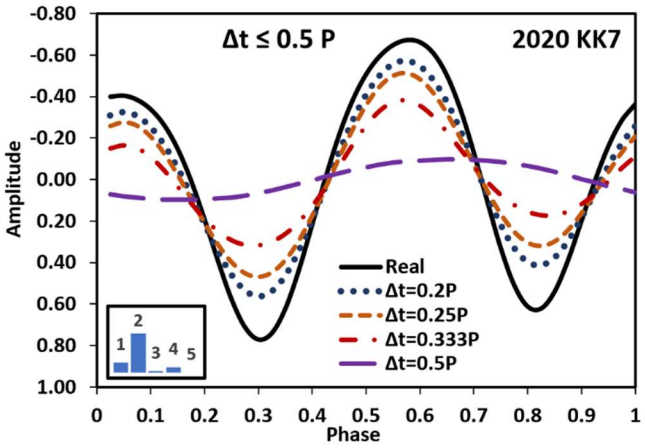

Values of Δt > 0.5 P all show low amplitude bimodal variation but with the opposite phase to the real curve:

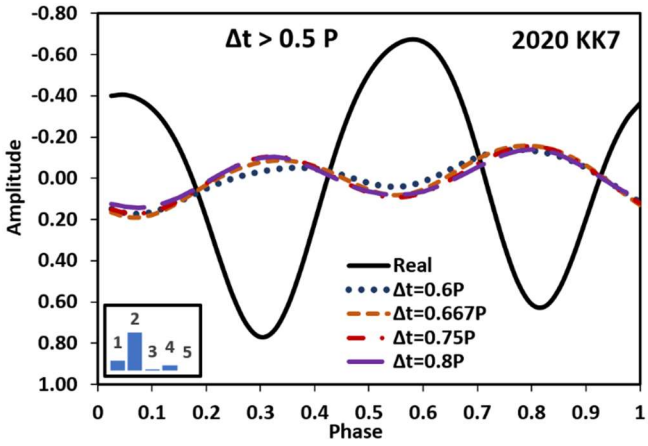

2nd harmonic dominant, 1st harmonic weak, 3rd harmonic rivals 1st. (2018 GE3). At Δt = 0.5 P, again, a very shallow lightcurve and with the 1st and 3rd harmonics being of almost equal strengths, this shows up as slight irregularities in the otherwise monomodal curve.

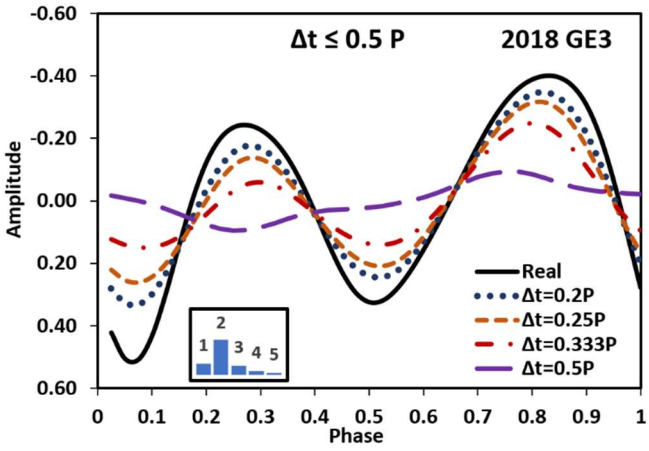

Again, for values of Δt > 0.5 P, all show low amplitude bimodal variation with the opposite phase to the real curve:

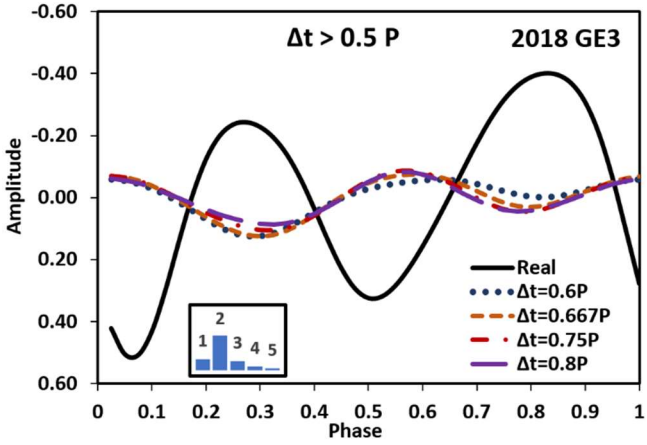

2nd harmonic dominant, 3rd harmonic weak but stronger than 1st. (2021 FH). The 3rd harmonic is revealed as a very low amplitude trimodal lightcurve at Δt = 0.5 P.

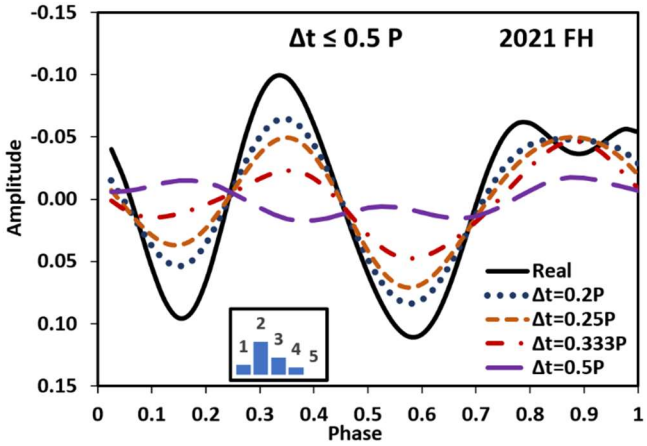

All the curves of Δt > 0.5 P are similar, bimodal, with very low amplitudes and again, with the opposite phase to the real lightcurve:

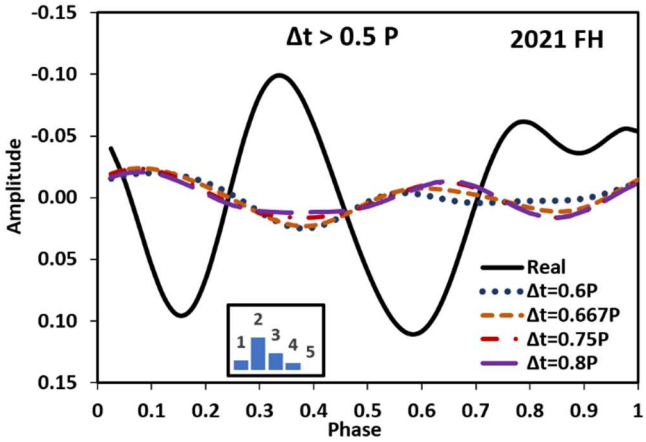

2nd harmonic dominant, 1st harmonic strong. (2012 XE54). A relatively strong 1st harmonic produces a well-defined, and regular monomodal curve at Δt = 0.5 P and with moderate amplitude compared to the real lightcurve:

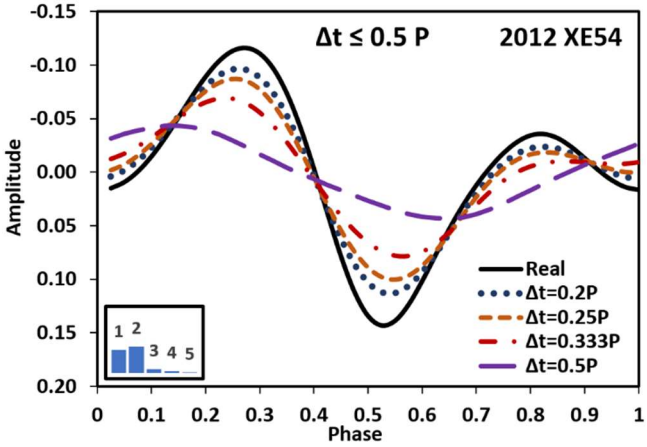

For values of Δt > 0.5 P, the low amplitude bimodal curves bear little resemblance to the real curve, but again have the opposite phase:

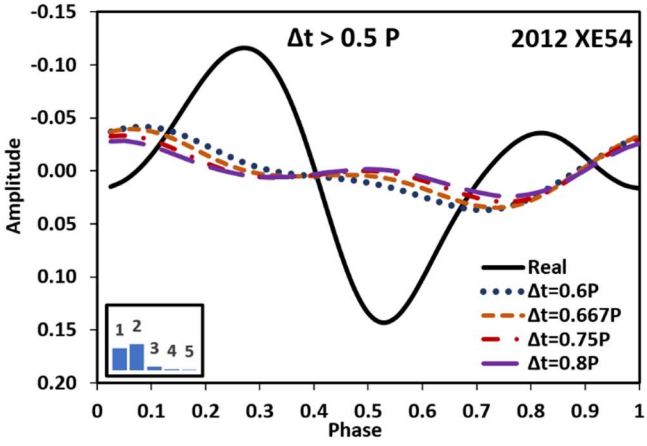

1st harmonic dominant, 2nd harmonic strong. (2018 CB). In this uncommon situation, the result of the 2nd harmonic being suppressed when Δt = 0.5 P leaves the dominant 1st harmonic to produce a relatively strong monomodal curve, with the amplitude being ~0.5 of the real amplitude. The curve at Δt = 0.333 P is smoothed enough to also be interpreted as monomodal:

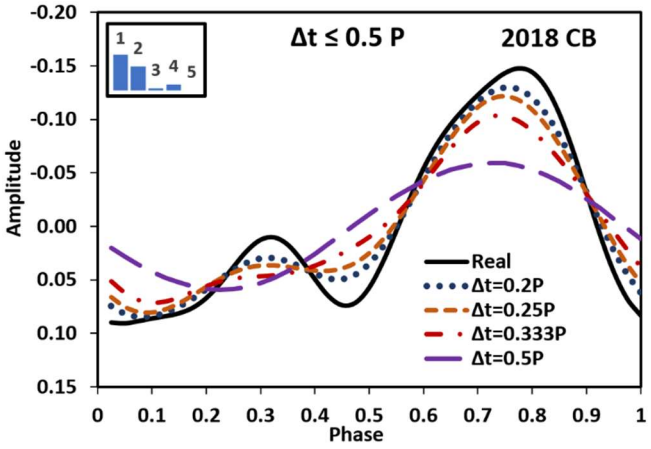

For all values of Δt > 0.5 P, all curves appear monomodal with still moderate but successively decreasing amplitudes:

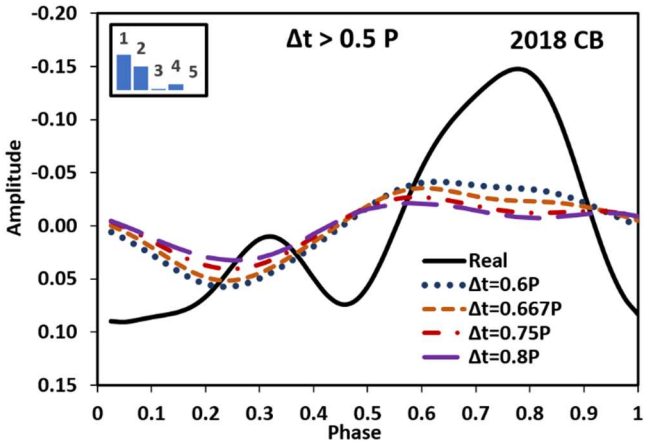

Of course, when imaging a minor planet with unknown period, the observer is initially not able to make the choice of Δt = 0.185 P, however for all but the fastest rotators, exposures will probably be shorter than this optimum level and smoothing will not be an issue. By chance, 2021 HN was observed with exposure lengths spanning the optimal value for recording the 2nd harmonic, with Δt spanning 0.172 - 0.236 P but still, this range will have reduced the strength of the 2nd harmonic by up to 1/3 and significantly distorted the values of the potentially weaker 3rd, 4th and 5th harmonics, see Table IV.

Δt / P	*f*1	*f*2	*f*3	*f*4	*f*5	Relates to
0.172	0.95	0.82	0.62	0.38	0.16	2021 HN
0.236	0.91	0.67	0.36	0.06	-0.14	2021 HN
0.238	0.91	0.67	0.35	0.05	-0.15	2021 GQ10
0.326	0.83	0.43	0.02	-0.20	-0.18	2021 GQ10

Table IV. Factors from Eq. 1 reducing the real amplitude of harmonics 1 - 5 for the exposure lengths used for 2021 GQ10 and 2021 HN.

However, the exposure lengths for 2021 GQ10, with Δt ranging between 0.238 and 0.326 P, will have had a more dramatic consequence, effectively suppressing most and negating some of the amplitude due to the 3rd, 4th and 5th harmonics and reducing the 2nd harmonic to 0.43 of its real value, significantly more than the reduction to the 1st harmonic, to 0.83 of its real value.

If a factor *f*n is close to unity and therefore the contribution from the related harmonic only moderately affected by smoothing, to get a first order approximation of the real lightcurve, the factor can be used to remove its effect from the Fourier coefficients obtained from the observed lightcurve. But as the factor approaches 0 at Δt = *P* / *n* and beyond, the contribution of that harmonic to the real lightcurve cannot be reconstructed safely, lack of precision in the observed Fourier coefficients being compounded by numerically small values of *f*n with a dependency on $f n^{-1}$. With the assumption that the contribution from the 3rd and higher harmonics in the real lightcurves of 2021 GQ10 and 2021 HN are relatively minor, only the 1st and 2nd harmonics from the observed lightcurves have been adjusted by $f n^{-1}$ to reconstruct a first order estimate of what the "real" lightcurves may have been. Figures labelled "Est. lightcurve before smoothing" include a solid line for the lightcurve as derived from observations and broken curves estimating the real lightcurve for the range of Δt used in the observations of that object. As with the other figures, the inset plots of relative harmonic strengths are for the observed lightcurves.

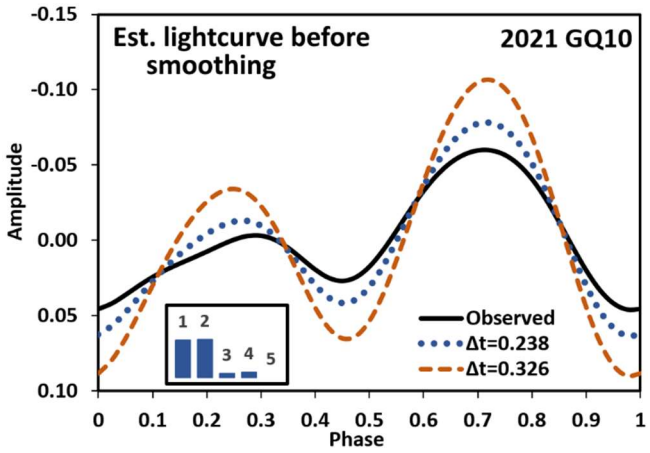

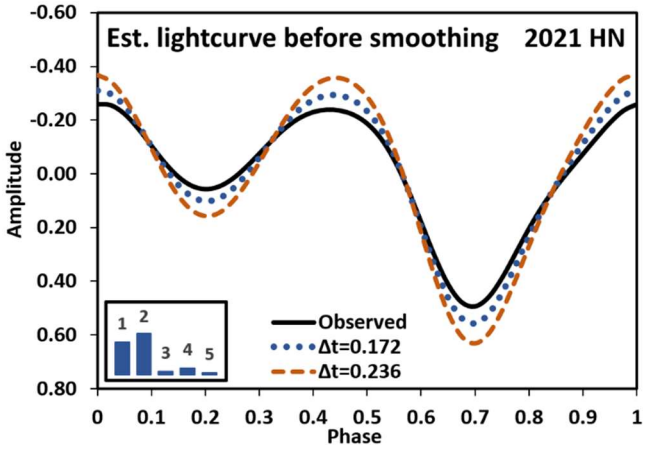

These estimates imply the amplitude for 2021 GQ10 may have ranged between 0.14 and 0.20 in the absence of lightcurve smoothing, rather than the observed 0.11 amplitude. Similarly, for 2021 HN the real amplitude is estimated to be between 0.87 and 1.00, compared to the observed amplitude of 0.74. For both objects, the range of amplitudes due to changing exposure lengths will have contributed to the amount of scatter in the phased lightcurve plots.

The observed lightcurve shape and period determined for 2021 HN is expected to be close to reality, the large observed amplitude and the dominance of the 2nd harmonic both imply only moderate smoothing, as would also be expected from the values of Δt utilised. However, the same is not true for 2021 GQ10, where the observed amplitude is small and the 1st and 2nd harmonics are of approximately equal strength. It is of course possible for the object to be relatively spherical and for it to have been presenting an approximately pole-on aspect to produce the observed lightcurve.

But can the question be answered whether smoothing has modified the real lightcurve to the point where the period and shape are being misinterpreted? Firstly, it is noted that in the set of real lightcurves presented earlier, even in the range $0.5 \leq \Delta t < P$, with significant smoothing and drastically reduced amplitudes, they still reveal periodicity related to the strongest remaining harmonics, so in practice, a real bimodal lightcurve could be interpreted as having a period 2, 1, 2/3 or 1/2 of the real period, assuming the effects of harmonics higher than the 4th will be insignificant. The observed bimodal lightcurve for 2021 GQ10 is distinctly asymmetric, most clearly seen in the "Est. lightcurve before smoothing" figure, suggesting that monomodal and trimodal solutions are unlikely. The period spectrum also indicates a bimodal or quadrimodal solution is preferred. If quadrimodal, then the period would be 38.6 s and the largest Δt / P value of 6.3 / 38.6 = 0.163 would imply there would not be enough lightcurve smoothing in the principal harmonics to radically change the overall lightcurve shape (where $f1 = 0.96$, $f2 = 0.84$, $f3 = 0.66$, $f4 = 0.45$). However, in forcing the observed data points to a quadrimodal solution, the values of $f2$ and $f4$ applied to the amplitude of the 2nd and 4th harmonics imply that the 4th harmonic in the real lightcurve would have to be an implausible 1.9 times larger than the 2nd harmonic. The figure labelled "Quadrimodal assumed" shows this solution, together with dashed lines for the estimated lightcurves before smoothing and as with the other figures, the inset plot of relative harmonic strengths is for the observed lightcurve.

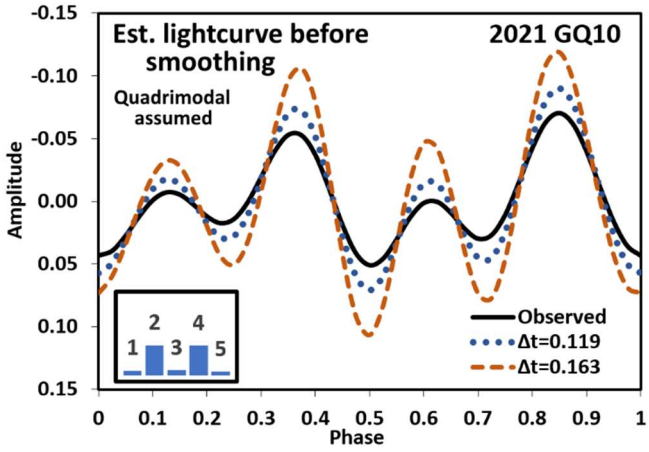

With other interpretations improbable, it is concluded that most likely, 2021 GQ10 does have an ultra-fast rotation period of 19.3 s and a bimodal lightcurve of observed amplitude 0.11 that, if observed with shorter exposure times would have been ~ 0.2 magnitudes.

Conclusions and Recommendations.

Both 2021 GQ10 and 2021 HN are very small objects of estimated diameter < 15 m and were making very close approaches to Earth, causing them to be bright enough (16th magnitude) to record with short exposures and also moving fast enough that exposures had to be kept short to stop the objects trailing excessively. This combination was conducive to revealing their very short periods. However, in different circumstances, for slower moving small objects (say H > ~ 24, where rotation period could be expected to be anywhere from a few hours to sub-minute) and where longer exposures *could* be used, a visual check of the images in near real-time to look for variation is worthwhile.

- If regular variation is apparent, then making an estimate of the period, to allow for an initial determination of 0.185 P will allow exposure length to be optimised accordingly if needed.
- If there is no obvious variation up to some tens of minutes it may be worth sacrificing some S/Nr and shortening exposures to a few seconds to see whether any very short-term magnitude variation can be detected, before reverting to longer exposures if nothing is apparent.
- If significant amplitude variations are seen between consecutive exposures, it is unlikely the true period will be obvious during data collection, especially if exposure cadence is a significant fraction, or longer than the true period. Therefore, acquiring several sets of images with differing but short exposure lengths may allow the true period to be resolved more clearly in later analysis than keeping to a single exposure length for the entire duration of observation.

Acknowledgements

The author is very grateful for the help and encouragement given by Petr Pravec during the drafting of this paper. The author also gratefully acknowledges a Gene Shoemaker NEO Grant from the Planetary Society (2005) and a Ridley Grant from the British Astronomical Association (2005), both of which facilitated upgrades to observatory equipment used in this study.

References

ADS (2021). Astrophysics Data System *https://ui.adsabs.harvard.edu/*

Bacci, P.; Maestripieri, M.; Tesi, L.; Fagioli, G.; Foglia, S.; Galli, G.; Bressi, T.H.; Pettarin, E.; Choi, P.; Saini, N.; Zhai, C.; Trahan, R.; Shao, M.; Groeller, H.; Christensen, E.J. and 20 colleagues (2021). "2021 HN." MPEC 2021-H51. *https://minorplanetcenter.net/mpec/K21/K21H51.html*

Birtwhistle, P. (2018). "Lightcurve Analysis for Two Near-Earth Asteroids Eclipsed by the Earth's Shadow." *Minor Planet Bull.* **45**, 215-219.

Birtwhistle, P. (2021a). "Lightcurve Analysis for Four Near-Earth Asteroids." *Minor Planet Bull.* **48**, 26-29.

Birtwhistle, P. (2021b). "Lightcurve Analysis for Ten Near-Earth Asteroids." *Minor Planet Bull.* **48**, 180-186.

Birtwhistle, P. (2021c). "Lightcurve Analysis for Nine Near-Earth Asteroids." *Minor Planet Bull.* **48**, 286-293.

Harris, A.W.; Young, J.W.; Scaltriti, F.; Zappala, V. (1984). "Lightcurves and phase relations of the asteroids 82 Alkmene and 444 Gyptis." *Icarus* **57**, 251-258.

Harris, A.W.; Young, J.W.; Bowell, E.; Martin, L.J.; Millis, R.L.; Poutanen, M.; Scaltriti, F.; Zappala, V.; Schober, H.J.; Debehogne, H.; Zeigler, K. (1989). "Photoelectric Observations of Asteroids 3, 24, 60, 261, and 863." *Icarus* **77**, 171-186.

JPL (2021). Small-Body Database Browser. *https://ssd.jpl.nasa.gov/sbdb.cgi*

Kwiatkowski, T.; Buckley, D.A.H.; O'Donoghue, D.; Crause, L.; Crawford, S.; Hashimoto, Y.; Kniazev, A.; Loaring, N.; Romero Colmenero, E.; Sefako, R.; Still, M.; Vaisanen, P. (2010). "Photometric survey of the very small near-Earth asteroids with the SALT telescope - I. Lightcurves and periods for 14 objects." *Astronomy & Astrophysics* **509**, A94.

Melnikov, S.; Hoegner, C.; Laux, U.; Ludwig, F.; Stecklum, B.; Beniyama, J.; Dupouy, P.; Holmes, R.; Foglia, S.; Buzzi, L.; Linder, T.; Losse, F.; Birtwhistle, P.; Gerhard, C.; Korlevic, K. and 6 colleagues (2021). "2021 GQ10." MPEC 2021-G218. *https://minorplanetcenter.net/mpec/K21/K21GL8.html*

Pravec, P.; Hergenrother, C.; Whiteley, R.; Sarounova, L.; Kusnirak, P.; Wolf, M. (2000). "Fast Rotating Asteroids 1999 TY2, 1999 SF10, and 1998 WB2." *Icarus* **147**, 477-486.

Raab, H. (2018). Astrometrica software, version 4.12.0.448. *http://www.astrometrica.at/*

Warner, B.D.; Harris, A.W.; Pravec, P. (2009). "The Asteroid Lightcurve Database." *Icarus* **202**, 134-146. Updated 2021 June. *https://minplanobs.org/mpinfo/php/lcdb.php*

Warner, B.D. (2021). MPO Software, Canopus version 10.8.4.2. Bdw Publishing, Colorado Springs, CO.

SERENDIPITOUS ASTEROIDS

Iga Mieczkowska
Astronomical Observatory Institute, Faculty of Physics,
A. Mickiewicz University, Słoneczna 36, 60-286
Poznań, POLAND
igamie@st.amu.edu.pl

Anna Marciniak, Roman Hirsch, Krzysztof Kamiński,
Monika K. Kamińska, Magdalena Polińska,
Dagmara Oszkiewicz, Krzysztof Sobkowiak,
Radosław Wróblewski, Kamil Żukowski
Astronomical Observatory Institute, Faculty of Physics,
A. Mickiewicz University, Słoneczna 36, 60-286
Poznań, POLAND

Erika Pakštienė
Institute of Theoretical Physics and Astronomy, Vilnius University, Saulėtekio al. 3, 10257 Vilnius, LITHUANIA

Waldemar Ogłoza, Marek Dróżdż
Mt. Suhora Observatory, Pedagogical University, Podchorążych 2, 30-084, Cracow, POLAND

(Received: 2021 July 3)

We present here a byproduct of a large photometric survey of slow rotators led since the year 2013. The observations within the campaign sometimes serendipitously registered additional asteroids moving in the same field with the main target. Here we gather all 24 such asteroids, which had strong enough S/N, and also presented any traceable brightness variations, and we estimate their rotation periods and amplitudes. For best covered lightcurves we also present their plots. For ten asteroids there were apparently no previous period determinations. All the lightcurve data for these serendipitous asteroids are now uploaded to ALCDEF for the use in future spin/shape studies.

Since the year 2013 a worldwide photometric campaign of slowly rotating asteroids has been conducted at AOI AMU, led by coauthor A. Marciniak. The campaign is aimed at reducing the selection effects against slow rotators and low amplitude targets, to complement the set of asteroid spin and shape models for more realistic picture of the main-belt asteroids, and also for determinations of their sizes and thermal properties (see Marciniak et al. 2015 for the campaign description, and, e.g., Marciniak et al. 2019 for the results).

As a byproduct, sometimes additional asteroids are unexpectedly captured in the same field of view with the main target. When their signal-to-noise ratio is high enough for photometry of acceptable quality we measure them as well in an additional circular aperture. Moreover, there are cases when the on-sky movement of the main target is similar to that of the additional asteroid. Then the other can also be captured in more than one night, enabling to complement its lightcurve and to determine rotation period with greater precision.

Such serendipitous asteroids with strong enough signal were not found often in our programme, due to small fields of view and small sizes of most of the telescopes used. Still, over the years we gathered a substantial collection containing 24 targets, that is summarised in Table 1.

The main instrument used in our campaign is a 40-cm Newtonian with SBIG ST7 CCD camera located in the Borowiec station near Poznań, Poland. For most of the observations a clear (C) filter was used.

Another instrument is a 70-cm Dall-Kirkham telescope located in Winer Observatory near Sonoita, Arizona, and remotely operated from AOI UAM institute in Poland. In is equipped with Andor iXon CCD with a broad "Luminance" (L) filter, and a set of Johnson's filters, from which R filter was used for brighter targets, otherwise we observed in aforementioned L filter.

An additional telescope that was extensively used in the campaign is a robotic 80-cm TJO telescope at Montsec Observatory (OAdM), Catalonia. Specific, semi-sparse observing cadence was used there, registering one frame per 0.5 hour. MEIA and MEIA-2 CCD cameras were used there for observations in R filter.

Thanks to collaboration with Pedagogical University in Cracow, Poland, we also obtained data from 60-cm Cassegrain telescope at Suhora Observatory. The camera used there is Apogee Aspen-47m, and observations were done in R filter.

We also used the IAC80 telescope located in Observatorio del Teide on Tenerife. This is an 80-cm instrument with CAMELOT CCD camera. Our observations there were done with Johnson's R filter.

Within our campaign we were also granted a 5-nights run at 120-cm Mercator telescope based on Observatorio Roque de los Muchachos, on La Palma. The MAIA camera (Raskin et al., 2013) splits the light into three passbands: R, G, and B, where R band gave the best S/N, thus it was used here.

Data came also from 76 cm telescope at South African Astronomical Observatory equipped with 0.76M WRT1 CCD and R filter.

Lastly, thanks to a new collaboration with Vilnius University our targets have also been observed at Moletai Observatory, Lithuania, at 35/51-cm Maksutov telescope with Apogee Alta U47-BB camera. Unfiltered or R filter exposures were acquired there.

All the raw data, after standard bias, dark and flatfield corrections were applied, were semi-automatically processed using aperture photometry procedures of the *CLR Starlink* package. Three comparison stars were used, where the relative magnitudes were usually obtained by comparison with the brightest from the comparison stars, provided its brightness was stable. Before that step, additional asteroids were searched for via blink-comparison procedure, and identified using *XEphem* software (*https://github.com/XEphem/XEphem*) with an up-to-date asteroid orbit database from Minor Planet Center (*https://www.minorplanetcenter.net/iau/mpc.html*). All the frames were checked for star passages and removed in such an instance.

Below we describe targets with best covered lightcurves in more detail. For other targets, where only a fragment of a lightcurve was captured, we could only estimate a lower limit for its period and the amplitude (see Table 1).

34 Circe. This large, middle main-belt asteroid, was previously observed for lightcurve by Magnusson and Lagerkvist (1991), and Pilcher (2008). It displayed a 12.15 - 12.17-hour period and 0.17 - 0.25 mag amplitudes. We serendipitously captured it on three nights in 2020 September during an observing run at 35-cm telescope at Moletai Observatory, Lithuania. In spite of its long period, which is commensurate with an Earth day, we managed to capture both peaks of its lightcurve. Our result (P =12.15 h and A = 0.22mag) is in line with previous determinations.

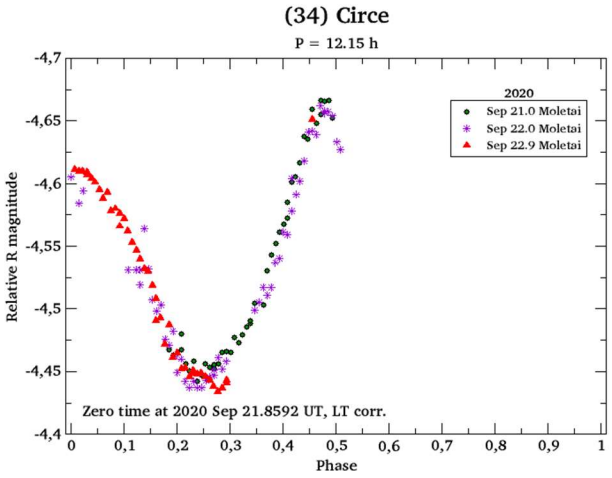

3478 Fanale. This asteroid belonging to Flora family was captured one time in 2015 July at 60-cm telescope at Mt. Suhora, Poland. We obtained a double-peaked lightcurve that clearly covered full rotation. Fanale was previously observed by Stephens (2013) and Owings (2013). It then displayed a 3.245-hour period and 0.47-0.60 mag amplitude. Our result for the period (P = 3.25 h) is consistent with those determinations, and various amplitudes registered (here A = 0.38 mag) are indicative of variable viewing aspects of the spin axis.

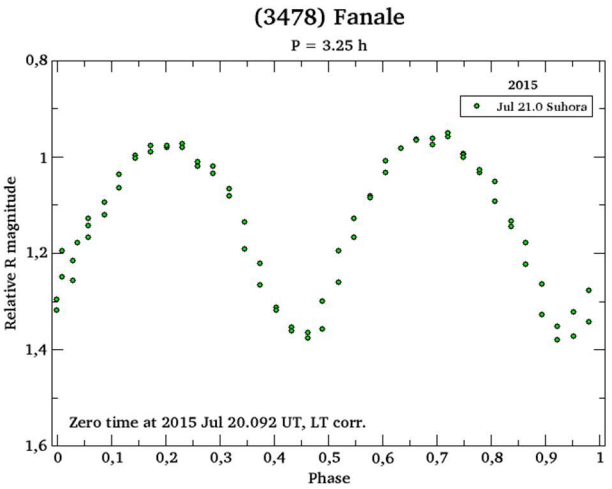

Number	Name	yyyy mm/dd	Phase	L_{PAB}	B_{PAB}	Period(h)	P.E.	Amp	A.E.	Grp
34	Circe	2020 09/20-09/22	13.3-13.9	33	-3	12.15	0.02	0.22	0.02	MB-M
535	Montague	2015 05/15	13.8	204	7	>10.2		>0.12		MB-I
2549	Baker	2015 07/20	5.2	310	0	>5.3		>0.36		THM
2875	Lagerkvist	2008 06/12	15.7	307	-7	>5.		>0.6		MB-O
3478	Fanale	2015 07/20	7.4	309	0	3.25	0.02	0.38	0.01	FLOR
3955	Bruckner	2016 06/01	19.4	150	7	>7.6		>0.4		EOS
4004	List'ev	2018 03/27-03/28	3.9-4.0	199	1	>8.6		>0.25		MB-O
5245	Maslyakov	2019 12/31	7.8	113	-3	10.2	0.1	0.62	0.03	FLOR
6353	Semper	2020 08/22	3.1	337	-3	>6.		>0.3		THM
6520	Sugawa	2013 08/07	6.7	320	7	>5.		>0.18		FLOR
6600	Qwerty	2015 07/20	7.6	309	0	>11.		>0.6		MB-I
7052	Octaviabutler	2020 01/07	27.4	21	-7	6.1	0.2	0.68	0.02	MB-O
7327	Crawford	2016 10/04	23.0	56	2	2.7	0.2	0.26	0.03	MB-I
8361	1990 JN1	2020 09/27	16.4	49	0	>3.		>0.8		EUN
13374	1998 VT10	2017 08/27-08/31	12.4-14.2	316	-6	3.235	0.002	0.43	0.04	FLOR
14381	1990 CE	2021 03/04	12.3	143	-1	5.7	0.2	0.8	0.2	BAP
14411	Clerambault	2019 12/31	8.7	112	-3	3.07	0.05	0.4	0.1	BAP
15375	Laetitiafoglia	2021 03/03	6.7	151	1	3.9	0.2	0.7	0.2	FLOR
17431	Sainte-Colombe	2018 09/20	17.6	30	8	>5.		>1.1		MB-I
31146	1997 UV3	2020 09/27	24.0	46	0	>9.		>0.4		NYS
33785	1999 RD192	2015 05/06	13.6	198	6	7.13	0.08	0.33	0.02	MB-M
37870	1998 FJ23	2020 02/17	16.4	32	3	4.23	0.08	0.9	0.2	MB-I
69695	1998 HL36	2019 02/11-02/15	10.1-11.7	153	13	4.78	0.07	0.13	0.02	MB-I
163799	2003 QR69	2019 07/26	17.4	301	-6	>2.5		>0.6		MC

Table I. Observing circumstances and results. The phase angle is given for the first and last date. L_{PAB} and B_{PAB} are the approximate phase angle bisector longitude/latitude at mid-date range (see Harris et al., 1984). Grp is the asteroid family/group (Warner et al., 2009).

3955 Bruckner. This minor body belonging to the Eos family was previously observed by Behrend et al. (2021web) and displayed a 7.5513-hour period with 0.36 mag amplitude. Also observed by Polakis (2021), it displayed a 7.566-hour period and 0.25 mag amplitude. We captured it once in 2017 May using the 70-cm telescope at Winer Observatory. Due to covering only a short segment of the complete lightcurve, we can only estimate the period as being around 7.6 hours and amplitude of at least 0.4 magnitudes.

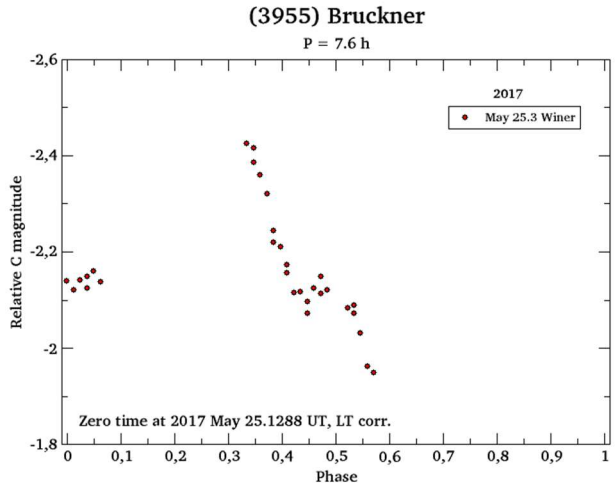

5245 Maslyakov. This Flora family asteroid was serendipitously captured on one night in 2019 December during an observing run at the robotic 80-cm telescope in Montec Observatory. Previously observed by Behrend et al. (2021web), Maslyakov displayed a 10.2-hour period and 0.63-mag amplitude. Our result (P = 10.2 h and A = 0.62 mag) is very close to earlier work.

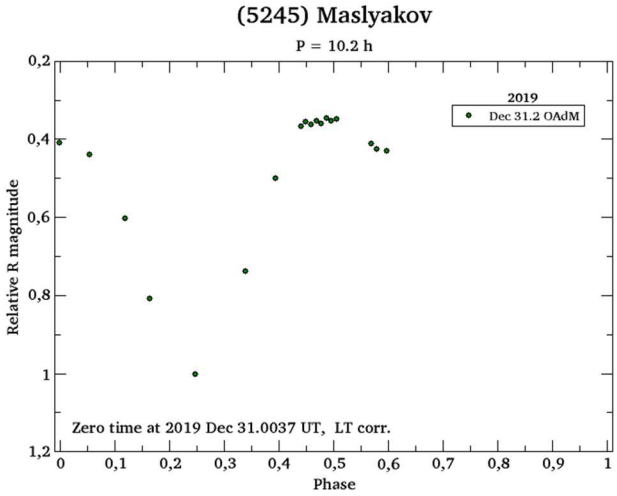

7052 Octaviabutler. This outer main-belt asteroid and has no previous period determination that could be found in literature. It was captured once during 3-hours observations with the 70-cm telescope in Winer Observatory. The resulting one-peaked lightcurve of 0.68 mag amplitude seems to cover half of full rotation. From this, we determined a 6.1-hour period.

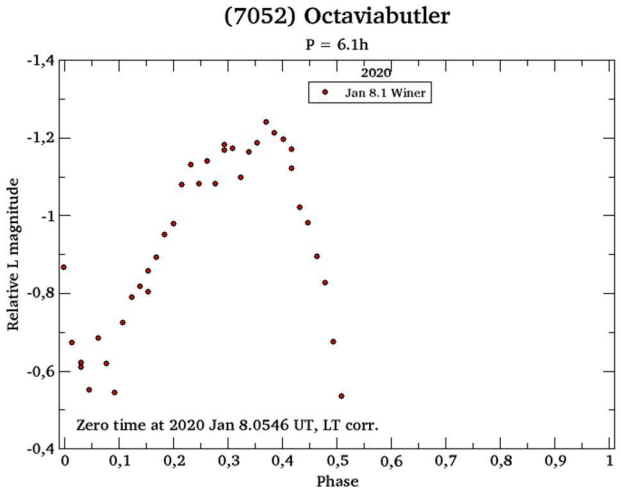

7327 Crawford. This is an inner main-belt asteroid with apparently no previous rotation period determination. On one night, during the observing run at 120-cm Mercator telescope at La Palma in 2016 October, we registered it displaying a double-peaked, asymmetric lightcurve that seems to cover full rotation. We estimate the period at 2.7 hours and the amplitude at 0.26 magnitudes.

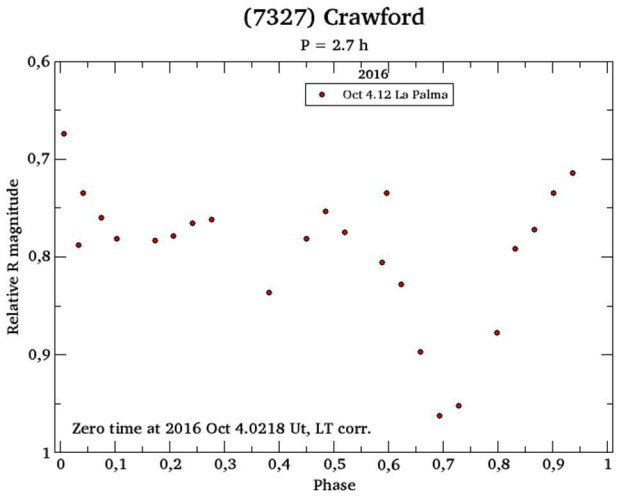

(13374) 1998 VT10. This asteroid belonging to Flora family was serendipitously captured during two nights in 2017 August during our observing run at 80-cm IAC telescope at Teide Observatory. Previously observed by Behrend et al. (2021web), it displayed a 3.23-hour period and 0.41 mag amplitude. We managed to obtain a lightcurve clearly covering full rotation with many overlapping segments from two nights. Our result for the period (P = 3.236 h) is consistent with previously published results.

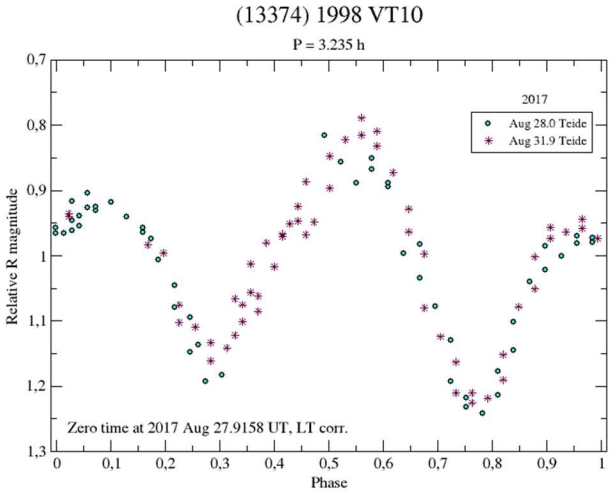

(14381) 1990 CE. This Baptistina family asteroid has no previous rotation period determination that could be found in literature. It was captured during one night in 2021 March during our observing run at 35-cm telescope at Moletai Observatory. The rather noisy lightcurve points to a 5.7-hour rotation period and a large, 0.8 mag amplitude.

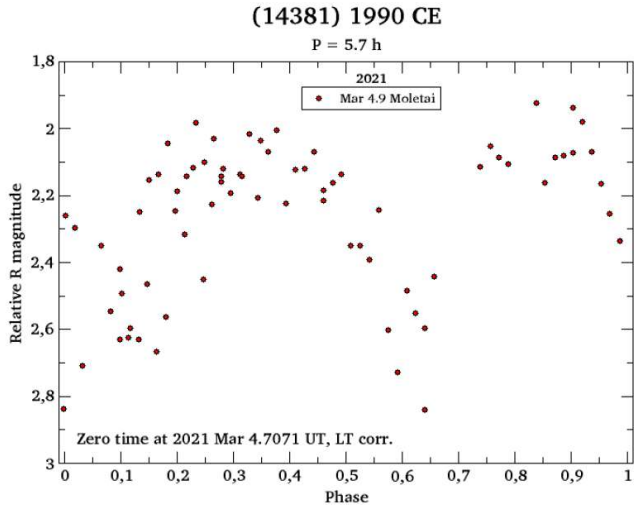

14411 Clerambault. This Baptistina asteroid was serendipitous captured once, together with 5245 Maslyakov, in 2019 December 2019 during an observing run with the 80-cm telescope at Montec Observatory. Previously it displayed 3.053 to 3.07-hour period and a 0.41 to 0.44-mag amplitude (Behrend et al., 2021web; Waszczak et al., 2015). Our result (P =3.07 h, A = 0.4 mag) is consistent with earlier works.

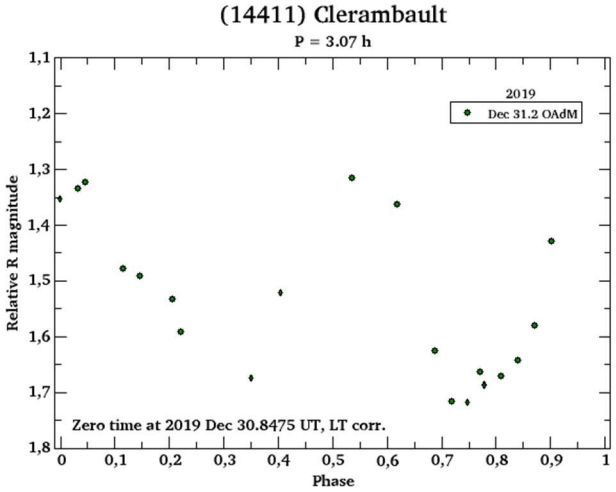

15375 Laetitiafoglia. This target is a Flora family asteroid with apparently no previous rotation period determination. It was captured once in March 2021 at 35-cm telescope at Moletai observatory. We estimate its period at 3.9 hours, and amplitude at 0.7 mag.

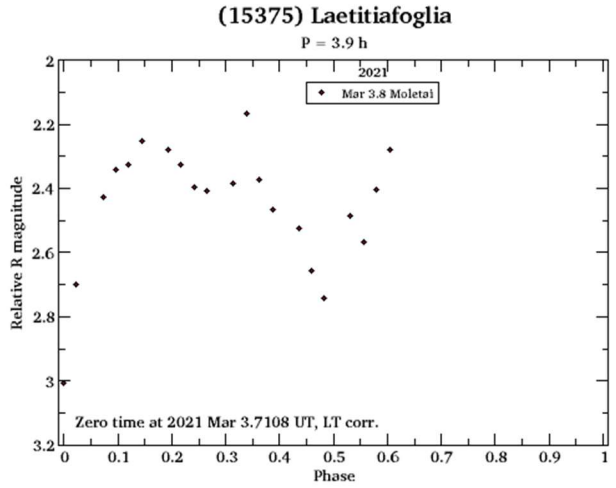

(33785) 1999 RD192. The lightcurve of this middle-main belt asteroid was previously published by Waszczak et al. (2015). It then displayed a 7.126-hour period and a 0.29-mag amplitude. We captured it with a single night of observations in 2015 May using the 70-cm telescope in Winer Observatory. The double-peaked lightcurve covers exactly one full rotation. Our result (P = 7.13 h; A = 0.33 mag) is in line with previously published values.

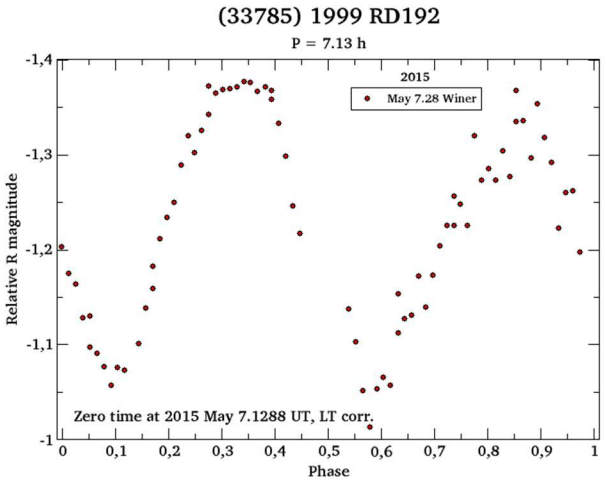

(37870) 1998 FJ23. This in an inner main-belt asteroid with apparently no previous rotation period determination. It was captured during one night of observations in 2020 February 2020 with the 35-cm telescope at Moletai Observatory. We obtained a double-peaked lightcurve that seems to cover full rotation, and determined a 4.23-hour period with a large 0.90-mag amplitude.

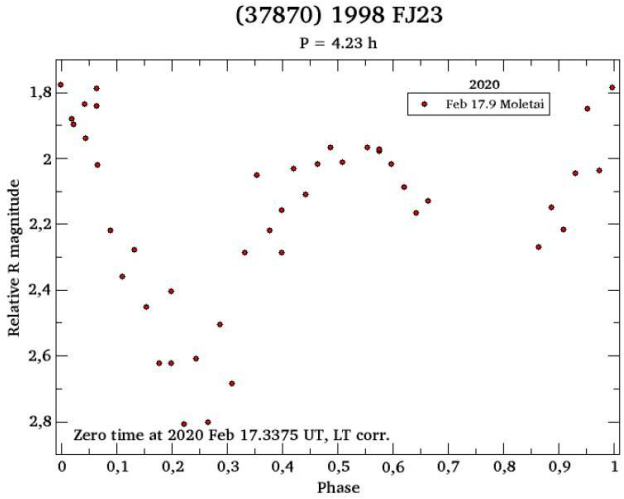

(69695) 1998 HL36. This target is an inner main-belt asteroid with no previous rotation period determination that could be found in literature. It was captured during as many as four nights in 2019 February in the data from the 80-cm telescope in Montsec Observatory. We determined a 4.78-h period and a 0.13- mag amplitude.

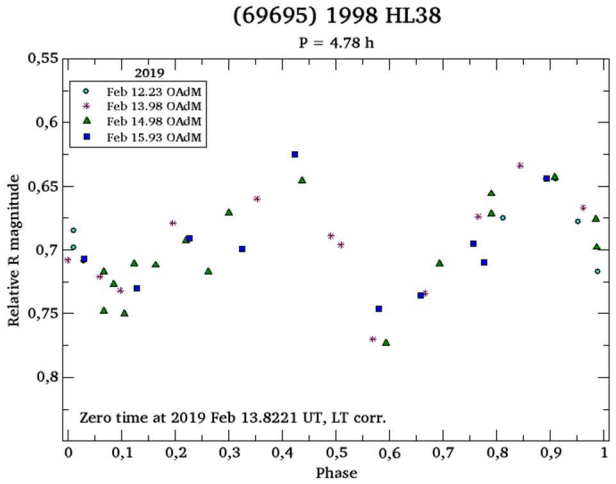

Acknowledgements

The Joan Oró Telescope (TJO) of the Montsec Astronomical Observatory (OAdM) is owned by the Catalan Government and operated by the Institute for Space Studies of Catalonia (IEEC).

This article is based on observations made in the Observatorios de Canarias del IAC with the 0.82-m IAC80 telescope operated on the island of Tenerife by the Instituto de Astrofísica de Canarias (IAC) in the Observatorio del Teide.

Based on observations made with the Mercator Telescope, operated on the island of La Palma by the Flemmish Community, at the Spanish Observatorio del Roque de los Muchachos of the Instituto de Astrofísica de Canarias. Based on observations obtained with the MAIA camera, which was built by the Institute of Astronomy of KU Leuven, Belgium, thanks to funding from the European Research Council under the European Community's Seventh Framework Programme (FP7/2007-2013)/ERC grant agreement no 227224 (PROSPERITY, PI: Conny Aerts) and from the Research Foundation - Flanders (FWO) grant agreement G.0410.09. The CCDs of MAIA were developed by e2v in the framework of the ESA Eddington space mission project; they were offered by ESA on permanent loan to KU Leuven.

Erika Pakštienė acknowledges the Europlanet 2024 RI project funded by the European Union's Horizon 2020 Research and Innovation Programme (Grant agreement No. 871149).

References

Behrend, R. (2021web) Observatoire de Geneve web site. *http://obswww.unige.ch/~behrend/page_cou.html*

Harris, A.W.; Young, J.W.; Scaltriti, F.; Zappala, V. (1984). "Lightcurves and phase relations of the asteroids 82 Alkmene and 444 Gyptis." *Icarus* **57**, 251-258.

Magnusson, P.; Lagerkvist, C.-I. (1991). "Physical studies of asteroids. XXII - Photometric photometry of the asteroids 34, 98, 115, 174, 270, 389, 419 and 804." *Astronomy Astrophys.* **87**, 269-275.

Marciniak, A.; Pilcher, F.; Oszkiewicz D.; and 21 colleagues (2015). "Against the Biases in Spins and Shapes of Asteroids." *Planet. Space Sci.* **118**, 256-266.

Marciniak, A.; Alí-Lagoa, V.; Müller, T.G.; and 54 colleagues (2019). "Thermal Properties of Slowly Rotating Asteroids: Results from a Targeted Survey." *Astronomy Astrophys.* **625** A139.

Owings, L. (2013). "Lightcurves for 1560 Strattonia, 1928 Summa, 2763 Jeans, 3478 Fanale, 3948 Bohr, 5275 Zdislava, and 5369 Virgiugum." *The Minor Planet Bulletin* **40**, 104-106.

Pilcher, F. (2008). "Period Determinations for 26 Proserpina, 34 Circe 74 Galatea, 143 Adria, 272 Antonia, 419 Aurelia, and 557 Violetta." *The Minor Planet Bulletin* **35**, 135-138.

Polakis, T. (2021). "Period Determinations for Twenty Asteroids." *The Minor Planet Bulletin* **48**, 239-245.

Raskin, G.; Bloemen, S.; Morren, J.; and 12 colleagues (2013). "MAIA, a three-channel imager for asteroseismology: Instrument design." *Astronomy Astrophys.* **559**, A26.

Stephens, R.D. (2013). "Asteroids Observed from Santana and CS3 Observatories: 2012 October - December." *The Minor Planet Bulletin* **40**, A92.

Warner, B.D.; Harris, A.W.; Pravec, P. (2009). "The Asteroid Lightcurve Database." *Icarus* **202**, 134-146. Updated 2020 Oct. *http://www.minorplanet.info/lightcurvedatabase.html*

Waszczak, A.; Chang, Ch.; Ofek, E.; and 10 colleagues (2015). "Asteroid Light Curves from the Palomar Transient Factory Survey: Rotation Periods and Phase Functions from Sparse Photometry." *The Astronomical Journal* **150**, A75.

ON CONFIRMED AND SUSPECTED BINARY ASTEROIDS OBSERVED AT THE CENTER FOR SOLAR SYSTEM STUDIES

Brian D. Warner
Center for Solar System Studies / MoreData!
446 Sycamore Ave.
Eaton, CO 80615 USA
brian@MinorPlanetObserver.com

Robert D. Stephens
Center for Solar System Studies / MoreData!
Rancho Cucamonga, CA 91730

Daniel R. Coley
Center for Solar System Studies
Corona, CA

(Received: 2021 July 15)

Using data from observations made at the Center for Solar System Studies from 2021 May to July, we report that minor planets 6009 Yuzuruyoshii and (18503) 1996 PY4 are very likely binary systems. The lightcurves for (18503) changed significantly over the range of observations, including the near disappearance of mutual events by the end of the observing sessions.

Data from CCD photometric observations made at the Center for Solar System Studies in 2021 May to July were used to look for indications of an asteroid being binary. Confirmed binaries are those that show mutual events (occultations/eclipses) while suspected binaries include those with two periods, no obvious mutual events, and periods consistent with binary asteroids.

Table I lists the telescopes and CCD cameras that were combined to make the observations. The cameras use CCD chips from the KAF blue-enhanced family and so have essentially the same response. The pixel scales were 1.24 arcsec/pixel.

Telescopes	Cameras
0.40-m *f*/10 Schmidt-Cass	FLI Proline 1001E
0.40-m *f*/10 Schmidt-Cass	FLI Proline 1001E

Table I. List of available telescopes and CCD cameras at CS3. The exact combination for each telescope/camera pair can vary due to maintenance or specific needs.

All lightcurve observations were unfiltered since a clear filter can cause a 0.1-0.3 mag loss. The exposure duration varied depending on the asteroid's brightness and sky motion.

Measurements were made using *MPO Canopus*. The Comp Star Selector utility in *MPO Canopus* found up to five comparison stars of near solar-color for differential photometry. To reduce the number of adjusted nightly zero points and their amounts, the analysis of the 2021 data used the ATLAS catalog r´ (SR) magnitudes (Tonry et al., 2018). The rare zero-point adjustments ≥ ±0.03 mag may be related in part to using unfiltered observations, poor centroiding of the reference stars, not correcting for second-order extinction, or selecting a star that is an unresolved pair.

The Y-axis shows the catalog ("sky") magnitudes for the "primary" period (P_1) while the "secondary" (P_2) plots give the differential from the average magnitude in the P_1 plot. "SR" indicates that the ATLAS catalog was used.

The two values in the parentheses are the phase angle (a) and the value of *G* used to normalize the data to the comparison stars used in the earliest session as well as the mid-date/time of that session. Ideally, this leaves any variations due only to the asteroid's rotation and/or albedo changes. The X-axis shows rotational phase from –0.05 to 1.05. If the plot includes the amplitude, e.g., "Amp: 0.65", this is the amplitude of the Fourier model curve and *not necessarily the adopted amplitude for the lightcurve*.

From here on, "LCDB" refers to the asteroid lightcurve database (Warner et al., 2009).

6009 Yuzuruyoshii. Three previous works found similar periods for the now presumed primary: Behrend (2006web, 3.03038 h) and Pravec et al. (2006web, 3.0302 h; 2017web, 3.0306 h). Pál et al. (2020), however, reported a period of 14.6585 h. Our results support the previous works giving a period near 3.03 h.

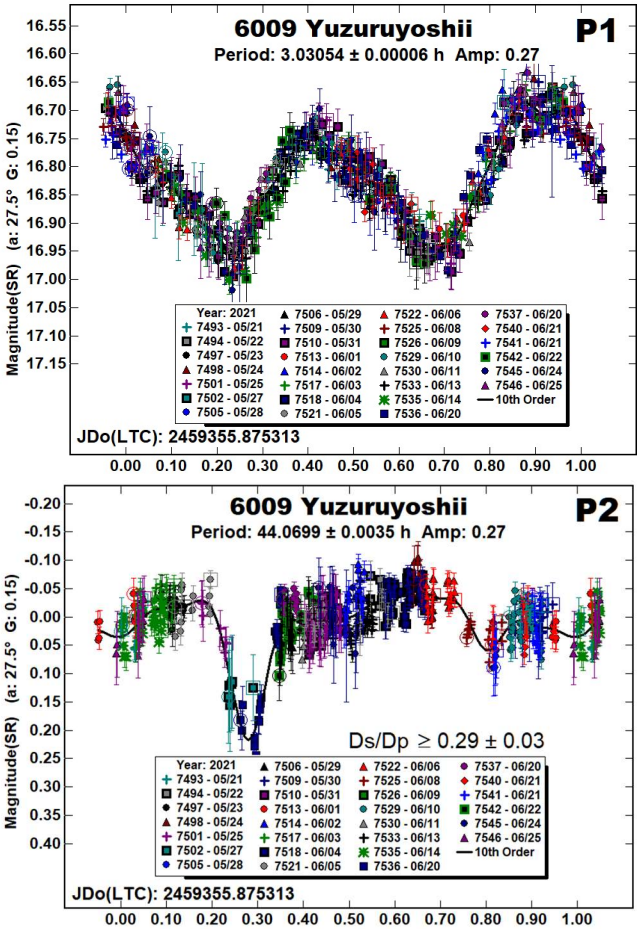

None of those previous works indicated the likelihood of a satellite, let alone confirm that one existed. However, our observations revealed the mutual events (occultation/eclipse), ranging from 0.09 to 0.20 mag, that give evidence to the presence of a satellite. The coverage of the events, in particular the secondary one, is less than ideal, making future observations required to improve the putative orbital period.

Even when taking phase angle into account, the amplitude of the primary lightcurve in 2021 was the deepest reported to-date. This implies a more equatorial view and so possibly why mutual events were reported for the 2021 apparition and not at those previous.

Number	Name	20yy mm/dd	Phase	L_{PAB}	B_{PAB}	Period(h)	P.E.	Amp	A.E.	Grp/Dr
6009	Yuzuruyoshii	05/21-07/06	27.5,21.0	298	29	3.03067	3.0E-5	0.27	0.01	9104
						44.0699	0.0035	0.27	0.03	≥0.29
18503	1996 PY4	05/31-06/28	25.2,22.2	265	33	3.43912	0.00003	0.36	0.02	701
						19.914	0.003	0.09	0.01	≥0.24
18503	1996 PY4	06/28-07/06	22.2,22.4	268	31	3.4391	0.0001	0.37	0.02	701
						19.904	0.001	0.05	0.02	?

Table II. Observing circumstances. The first line for each object gives the primary period for the system and the second line gives the orbital/secondary period. The two solutions for (18503) are based on different date ranges. The phase angle (α) is given at the start and end of each date range. L_{PAB} and B_{PAB} are, respectively the average phase angle bisector longitude and latitude (see Harris et al.,1984). For the Grp/Dr column, the first line gives the group/family based on the families list from the LCDB: 9104: inner main-belt; 701: Phocaea. See the LCDB documentation (*https://minplanobs.org/MPInfo/docs/lcdb_readme.pdf)* for a full list. The Dr column on the second line indicates a confirmed binary and is the estimated diameter ratio of the secondary to primary (Ds/Dp).

(18503) 1996 PY4. The only previously reported rotation period in the LCDB is from Pravec et al. (2010web), who found a period of 3.4390 h but did not report signs of a satellite. Mainzer et al. (2019) used WISE data to find an effective diameter for the system of 3.53 ± 0.05 km and, when using H = 13.8, an albedo of p_V = 0.429 ± 0.033. This seems inordinately high for the Phocaea family, which has an average value nearer p_V = 0.24.

Applying the correction from Harris and Harris (1997) and the current value from the MPCORB file (H = 14.51), the albedo becomes p_V = 0.24 ± 0.02, the average value for the Phocaea family, and a revised diameter D = 3.38 km. This demonstrates the strong dependency of albedos on H and so the need to confirm or improve H values whenever possible.

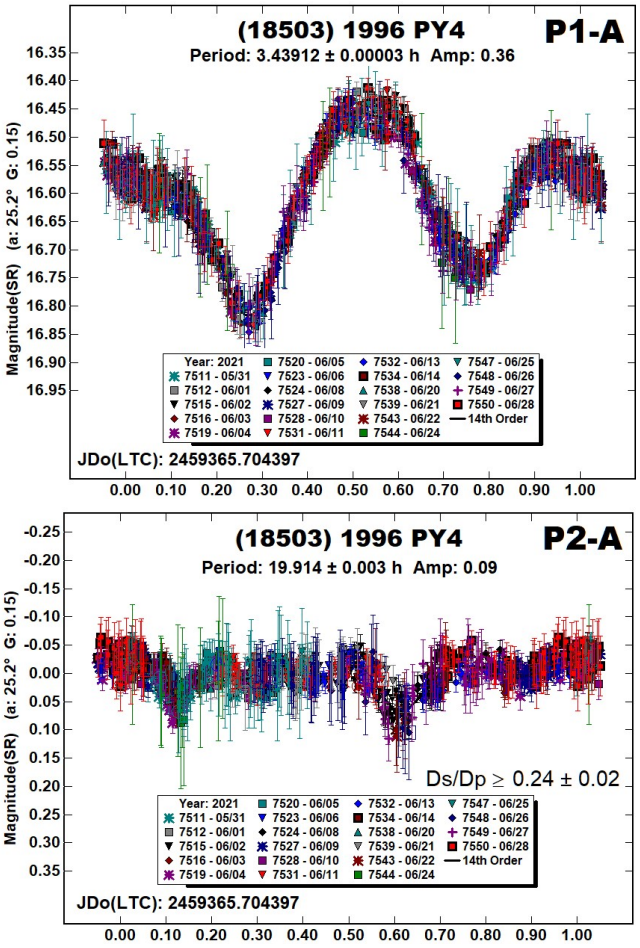

During the overall span of our observations, 2021 May 31 to July 6, the primary lightcurve shape and, to a lesser degree the amplitude, changed. Also changing, more dramatically, were the mutual events seen at the start of observations versus the end. This would seem to indicate that the viewing geometry of the system was leaving the "eclipse season" when mutual events can be observed. This information can be useful for finding a solution for the poles of the primary's spin axis and the satellite's orbit.

We've isolated two sets of data, the first ("A") covering most of 2021 June and the second ("B") the end of June into early July. In the first set, the mutual events are well-defined despite their amplitudes versus the error bars of the data. The shallower event, but only so by about 0.01 mag, gives an effective primary-to-secondary diameter ratio of Ds/Dp ≥ 0.24 ± 0.02.

The second data set, shows scant trace of the mutual events with the P_2 solution having been forced to a value near the one found with the first data set. In addition, the difference between the two maximums in the primary lightcurve increased from 0.10 mag in the first set to 0.15 mag in the second while the difference in the minimums remained about the same. These are both important data for future modeling.

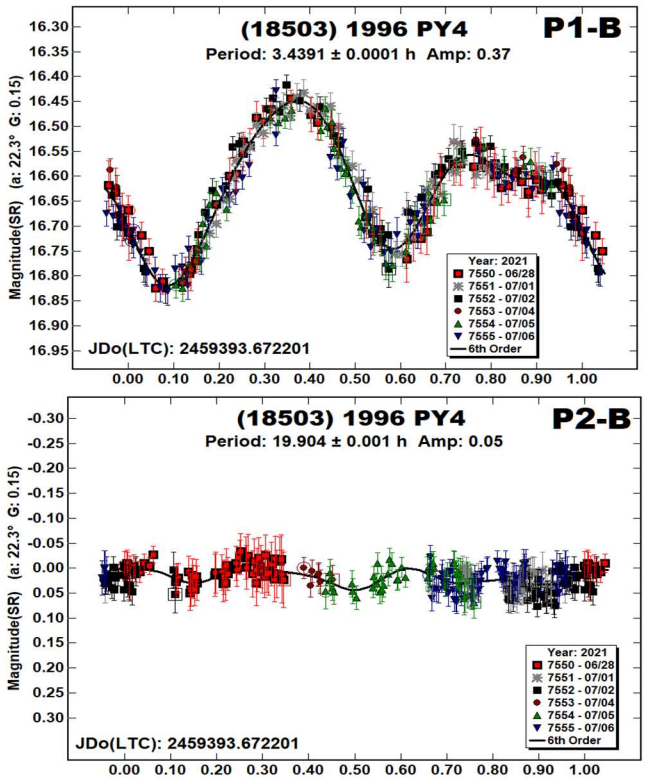

Acknowledgements

Funding for observations at CS3 and work on the asteroid lightcurve database (Warner et al., 2009) and ALCDEF database (*alcdef.org*) were supported by NASA grant 80NSSC18K0851. The authors gratefully acknowledge Shoemaker NEO Grants from the Planetary Society (2007, 2013). These were used to purchase some of the telescopes and CCD cameras used in this research. This work includes data from the Asteroid Terrestrial-impact Last Alert System (ATLAS) project. ATLAS is primarily funded to search for near earth asteroids through NASA grants NN12AR55G, 80NSSC18K0284, and 80NSSC18K1575; byproducts of the NEO search include images and catalogs from the survey area. The ATLAS science products have been made possible through the contributions of the University of Hawaii Institute for Astronomy, the Queen's University Belfast, the Space Telescope Science Institute, and the South African Astronomical Observatory.

References

References from web sites should be considered transitory, unless from an agency with a long lifetime expectancy. Sites run by private individuals, even if on an institutional web site, do not necessarily fall into this category.

Behrend, R. (2006web) Observatoire de Geneve web site. *http://obswww.unige.ch/~behrend/page_cou.html*

Harris, A.W.; Young, J.W.; Scaltriti, F.; Zappala, V. (1984). "Lightcurves and phase relations of the asteroids 82 Alkmene and 444 Gyptis." *Icarus* **57**, 251-258.

Harris, A.W., Harris, A.W. (1997). "On the Revision of Radiometric Albedos and Diameters of Asteroids." *Icarus* **126**, 450-454.

Mainzer, A.; Bauer, J.; Cutri, R.; Grav, T.; Kramer, E.; Masiero, J.; Sonnett, S.; Wright, E; Eds. (2019). "NEOWISE Diameters and Albedos V2.0." NASA Planetary Data System. urn:nasa:pds:neowise_diameters_albedos::2.0. *https://doi.org/10.26033/18S3-2Z54*

Pál, A.; Szakáts, R.; Kiss, C.; Bódi, A.; Bognár, Z.; Kalup, C.; Kiss, L.L.; Marton, G.; Molnár, L.; Plachy, E.; Sárneczky, K.; Szabó, G.M.; Szabó, R. (2020). "Solar System Objects Observed with TESS – First Data Release: Bright Main-belt and Trojan Asteroids from the Souther Survey." *Ap. J. Suppl Ser*. **247**, id. 26.

Pravec, P.; Wolf, M.; Sarounova, L. (2006web, 2010web. 2017web). *http://www.asu.cas.cz/~ppravec/neo.htm*

Tonry, J.L.; Denneau, L.; Flewelling, H.; Heinze, A.N.; Onken, C.A.; Smartt, S.J.; Stalder, B.; Weiland, H.J.; Wolf, C. (2018). "The ATLAS All-Sky Stellar Reference Catalog." *Ap. J.* **867**, A105.

Warner, B.D., Harris, A.W., Pravec, P. (2009). "The Asteroid Lightcurve Database." *Icarus* **202**, 134-146. Updated 2020 Aug. *http://www.minorplanet.info/lightcurvedatabase.html*

LIGHTCURVES AND ROTATION PERIODS OF 420 BERTHOLDA, 664 JUDITH, AND 2779 MARY

Frederick Pilcher
Organ Mesa Observatory (G50)
4438 Organ Mesa Loop
Las Cruces, NM 88011 USA
fpilcher35@gmail.com

(Received: 2021 June 19)

Synodic rotation periods and amplitudes are found for 420 Bertholda 10.987 ± 0.001 h, 0.32 ± 0.02 magnitudes; 664 Judith 19.305 ± 0.001 h, 0.32 ± 0.02 magnitudes; 2779 Mary 3.583 ± 0.001h, 0.11 ± 0.02 magnitudes.

Observations to produce the results reported in this paper were made at the Organ Mesa Observatory with a Meade 35-cm LX200 GPS Schmidt-Cassegrain, SBIG STL-1001E CCD, unguided. Exposure times were 60 seconds for 420 Bertholda and 664 Judith, 120 seconds for 2779 Mary, with a clear filter. Image photometric measurement and lightcurve construction were done by *MPO Canopus* software. To reduce the number of data points on the lightcurves and make them easier to read, data points have been binned in sets of 3 with maximum time difference 5 minutes.

420 Bertholda. The Lightcurve Data Base (Warner et al., 2009) states a rotation period of 11.04 hours based on four independent determinations all between 10.97 hours and 11.04 hours. New observations on 9 nights 2021 May 9 at phase angle 9.3º to June 10 at phase angle 0.9º can be fit to a phased lightcurve with period 10.987 ± 0.001 hours, maximum amplitude 0.32 ± 0.02 magnitudes. The shape and amplitude of the lightcurve changed considerably as the phase angle decreased, but the period as shown by the timings of maxima and minima remained stable and may be considered secure. This new value of the rotation period is consistent with all previously published values.

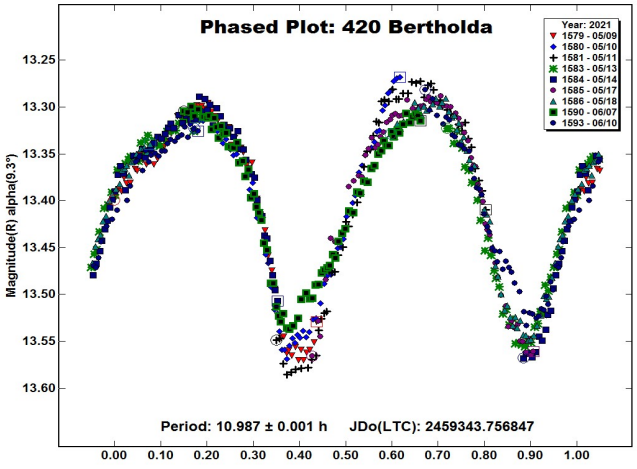

Number	Name	yyyy/mm/dd	Phase		LPAB	BPAB	Period(h)	P.E	Amp	A.E.
420	Bertholda	2021/05/09-2021/06/10	9.3	0.9	256	2	10.987	0.001	0.32	0.02
664	Judith	2021/03/27-2021/05/12	*14.1,	6.1	222	8	19.305	0.001	0.32	0.02
2779	Mary	2021/05/20-2021/06/11	* 5.6,	7.1	248	1	3.583	0.001	0.11	0.02

Table I. Observing circumstances and results. Pts is the number of data points. The phase angle is given for the first and last date, unless a minimum (second value) was reached. LPAB and BPAB are the approximate phase angle bisector longitude and latitude at mid-date range (see Harris *et al.*, 1984).

664 Judith. Almost all previously published rotation periods are different: Degraff et al. (1998), 10.76 h; Behrend (2009), >12. h; Garceran et al. (2015), 18.51 h; Hosek at al. (2011), 10.6829 h; Melton et al. (2012), 19.35 h; Pal et al. (2020), 19.3709 h. New observations on 7 nights 2021 Mar. 27 - May 12 provide a good fit to a bimodal lightcurve with period 19.305 ± 0.001 hours, amplitude 0.32 ± 0.02 magnitudes. This value is fairly close to Melton et al. (2012) and to Pal et al. (2020) and completely incompatible with all other previously published period determinations.

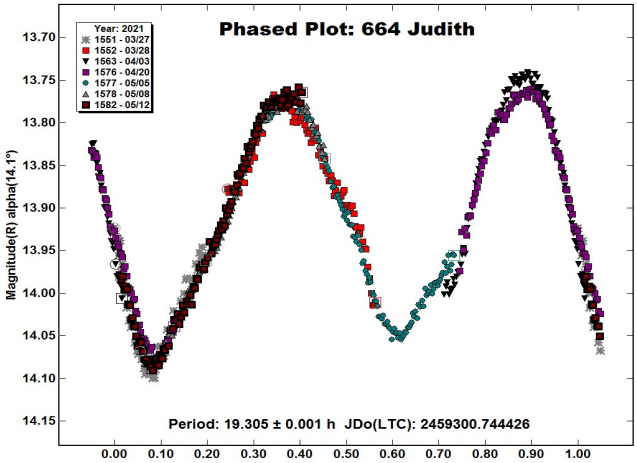

2779 Mary. The only previously published rotation period is 3.36 hours (Behrend, 2006) based on a one-night noisy lightcurve. New observations on 6 nights 2021 May 20 - June 11 can be fit to a lightcurve with period 3.583 ± 0.001 hours, amplitude 0.11 ± 0.02 magnitudes. At 15.5 magnitude, the scatter in the data points is large, but the lightcurve amplitude is larger. A period spectrum shows a narrow minimum at 3.583 hours much deeper than any other minimum between 3.2 hours and 4.2 hours. Despite the large scatter in the data points, all other periods within this range are ruled out and a 3.583-hour period should be considered secure. This value is compatible with the 3.36-hour period found by Behrend (2006).

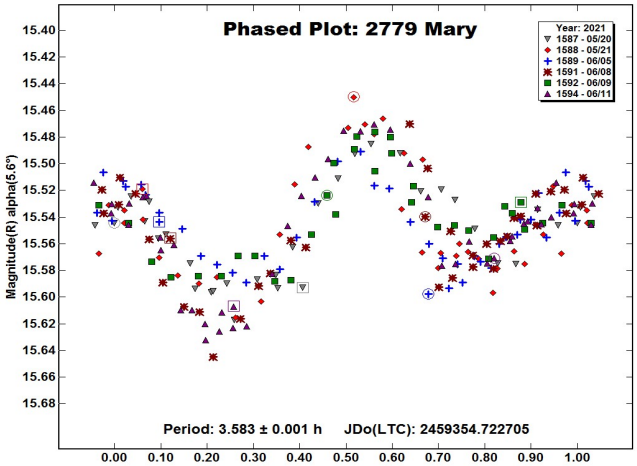

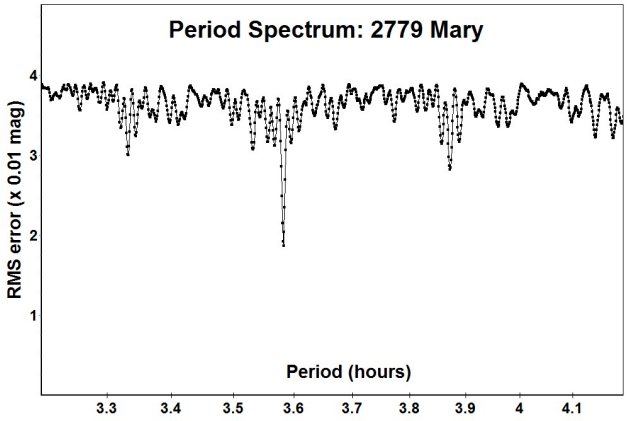

References

Behrend, R. (2006, 2009). Observatoire de Geneve web site. *http://*obswww.unige.ch/*~behrend/page_cou.html*.

Degraff, D.R.; Robbins, A.M.; Gutermuth, R.A. (1998). "Rotation curves for 13 asteroids." *Bull. Amer. Astron. Soc.* **30**, 1390.

Garceran, A.C.; Aznar Macias, A.; Mansego, E.A.; Rodriguez, P.B.; Lozano de Haro, J. (2015). "Lightcurve analysis of six asteroids." *Minor Planet Bull.* **42**, 235-237.

Harris, A.W., Young, J.W., Scaltriti, F., Zappala, V. (1984). "Lightcurves and phase relations of the asteroids 82 Alkmene and 444 Gyptis." *Icarus* **57**, 251-258.

Hosek, M.; Cooke, W.J.; Suggs, R.M. (2011). "Lightcurve analysis of asteroids 664 Judith and (20453) 1999 KL6." *Minor Planet Bull.* **38**, 11-12.

Melton, E.; Carver, S.; Harris, A.; Karnemaat, R.; Klaase, M.; Ditteon, R. (2012). "Asteroid analysis at the Oakley Southern Sky Observatory: 2011 November - December." *Minor Planet Bull.* **39**, 131-133.

Pal, A.; Szakáts, R.; Kiss, C.; Bódi, A.; Bognár, Z.; Kalup, C.; Kiss, L.L.; Marton, G.; Molnár, L.; Plachy, E.; Sárneczky, K.; Szabó, G.M.; Szabó, R. (2020). "Solar System Objects Observed with TESS – First Data Release: Bright Main-belt and Trojan Asteroids from the Southern Survey." *Ap. J. Supl. Ser.* **247**, 26-34.

Warner, B.D., Harris, A.W., Pravec, P. (2009). "The Asteroid Lightcurve Database." *Icarus* **202**, 134-146. Updated 2021 June. *https://minplanobs.org/mpinfo/php/lcdb.php*

PHOTOMETRIC OBSERVATIONS OF 755 QUINTILLA AND 1132 HOLLANDIA

Michael Fauerbach
Florida Gulf Coast University
and SARA Observatories
10501 FGCU Blvd.
Ft. Myers, FL 33965-6565
mfauerba@fgcu.edu

Matthew Fauerbach
NYU
Tandon School of Engineering
6 MetroTech Center
Brooklyn, NY 11201

(Received: 2021 July 13)

Photometric observations of 755 Quintilla and 1132 Hollandia were obtained on four nights 2021 May 15 to 2021 June 21. The following rotational periods were determined: 755 Quintilla: 4.552 ± 0.001 h; 1132 Hollandia: 5.322 ± 0.001 h.

Photometric observations obtained with the 0.6m telescope of the Southeastern Association for Research in Astronomy (SARA) consortium at Cerro Tololo Inter-American Observatory are reported. The telescope is coupled with an Andor iKon-L series CCD. A detailed description of the instrumentation and setup can be found in the paper by Keel et al. (2017). The data were calibrated using *MaximDL* and photometric analysis was performed using *MPO Canopus* (Warner, 2017). Both asteroids were observed by FGCU's Asteroid Research Group previously and are shape modelling targets of our group.

755 Quintilla. A preliminary shape model was published by Franco et al. (2020b). Large uncertainties in the pole position made the need for additional data obvious. Since the apparition of 2021 was a favorable one, it was decided to focus our spring 2021 observation campaign on 755 Quintilla. Results from our observations before opposition are reported in an accompanying paper (Fauerbach, 2021).

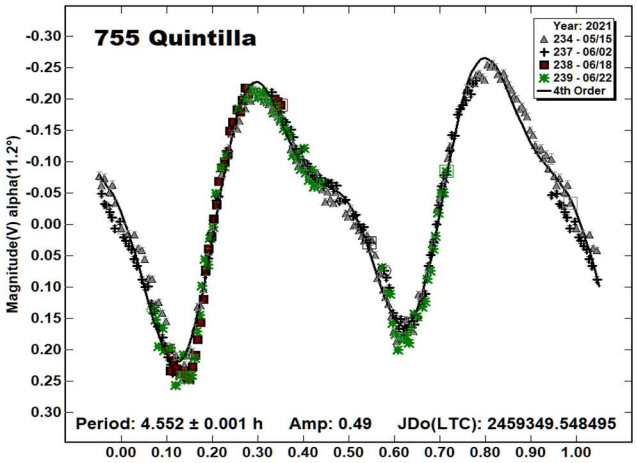

Opposition for 755 Quintilla was on 2021 April 18. We were able to observe the asteroid at large phase angles on each of our four nights allocated during the 2021 May-June timeframe. Our analysis yields a rotational period of 4.552 ± 0.001 h with an amplitude of 0.49 mag. This is in excellent agreement with previous publications by Behrend (2004web; 2005web), Buchheim and Prey (2005), Ďurech et al. (2020), Franco et al. (2020a), as well as our previous result (Fauerbach and Fauerbach, 2019). It should be pointed out that the amplitude reported here is larger than that in the accompanying paper. It appears that the minima of the lightcurve are significantly deeper at the larger phase angles.

1132 Hollandia. This main-belt asteroid was observed by our group during two previous oppositions and is one of our shape modelling targets. Our analysis yields a rotational period of 5.322 ± 0.001 h with an amplitude of 0.27 mag. This is not in agreement with Behrend (2003web; 5.586 h), but is in excellent agreement with previous publications by Sauppe et al. (2007; 5.326 h) and Clark (2015; 5.360 h), as well as our previous results (Fauerbach and Brown, 2018; 5.312 h) and Fauerbach (2020; 5.322 h).

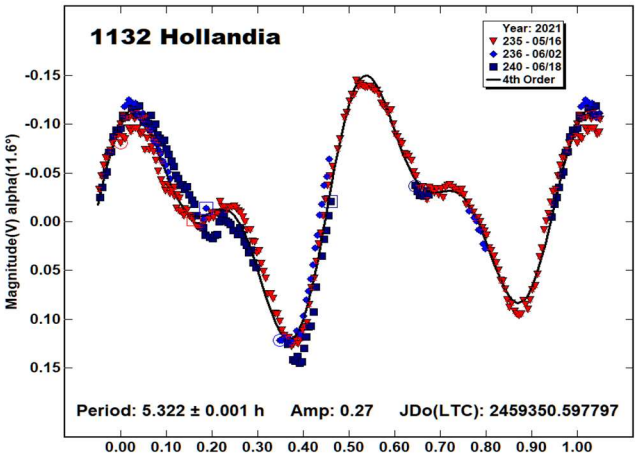

References

Behrend, R. (2003web, 2004web, 2005web). Observatoire de Geneve web site. *http://obswww.unige.ch/~behrend/page_cou.html*

Buchheim, R.K.; Pray, D. (2005). "Lightcurve of 755 Quintilla." *Minor Planet Bulletin* **32**, 1.

Clark, M. (2015). "Asteroid Photometry from the Preston Gott Observatory." *Minor Planet Bulletin* **42**, 15-20.

Ďurech, J.; Tonry, J.; Erasmus, N.; Denneau, L.; Heinze, A.N.; Flewelling, H.; Vančo, R. (2020). "Asteroid models reconstructed from ATLAS photometry." *Astronomy & Astrophysics*, **643**, A59.

Fauerbach, M. (2020). "Measured Lightcurves and Rotational Periods of 1132 Hollandia and 1184 Gaea." *Minor Planet Bulletin* **47**, 343-344.

Number	Name	yyyy mm/dd	Phase	L_{PAB}	B_{PAB}	Period(h)	P.E.	Amp	A.E.
755	Quintilla	2021 05/15,06/21	11.1,19.9	210	3	4.552	0.001	0.49	0.03
1132	Hollandia	2021 05/16,06/18	3.2,16.1	239	-6	5.322	0.001	0.27	0.02

Table I. Observing circumstances and results. The phase angle is given for the first and last date. If preceded by an asterisk, the phase angle reached an extremum during the period. L_{PAB} and B_{PAB} are the approximate phase angle bisector longitude/latitude at mid-date range (see Harris et al., 1984).

Fauerbach, M. (2021). "Rotational Period and Lightcurve Determination of 755 Quintilla, 2699 Kalinin, 3523 Arina, 5182 Bray, 5401 Minamioda, 5405 Neverland, (7288) 1991 FE1, and 18418 Ujibe." *Minor Planet Bulletin* **48**, 388-391.

Fauerbach, M.; Brown, A. (2018). "Lightcurve Analysis of Minor Planets 1132 Hollandia, 1184 Gaea 1322 Coppernicius, 1551 Argelander, and 3230 Vampilov." *Minor Planet Bulletin* **45**, 240-241.

Fauerbach, M.; Fauerbach, M. (2019). "Rotational Period Determination for Asteroids 755 Quintilla, 1830 Pogson, 5076 Lebedev-Kumach, and (29153) 1998 SY2." *Minor Planet Bulletin* **46**, 138-139.

Franco, L.; Marchini, A.; Saya, L.-F.; Galli, G.; Baj, G.; Ruocco, N.; Tinelli, L.; Scarfi, G.; Aceti, P.; Banfi, M.; Bacci, P.; Maestripieri, M.; Papini, R.; Salvaggio, F.; Mortari, F.; Bachini, M.; Casalnuovo, G.B.; Chinaglia, B. (2020a). "Collaborative Asteroid Photometry from UAI: 2020 January - March." *Minor Planet Bulletin* **47**, 242-246.

Franco, L.; Buchheim, R.K.; Pray, D.; Fauerbach, M.; Mortari, F.; Casalnuovo, G.B.; Chinaglia, B.; Scarfi, G.; Papini, R.; Salvaggio, F. (2020b). "Preliminary Spin-Shape Model for 755 Quintilla." *Minor Planet Bulletin* **47**, 267-269.

Harris, A.W.; Young, J.W.; Scaltriti, F.; Zappala, V. (1984). "Lightcurves and phase relations of the asteroids 82 Alkmene and 444 Gyptis." *Icarus* **57**, 251-258.

Keel, W.C.; Oswalt, T.; Mack, P.; Henson, G.; Hillwig, T.; Batcheldor, D.; Berrington, R.; De Pree, C.; Hartmann, D.; Leake, M.; Licandro, J.; Murphy, B.; Webb, J.; Wood, M.A. (2017). "The Remote Observatories of the Southeastern Association for Research in Astronomy (SARA)." *Publications of the Astronomical Society of the Pacific* **129**:015002 (12pp). *http://iopscience.iop.org/article/10.1088/1538-3873/129/971/015002/pdf*

Sauppe, J.; Torno, S., Lemke-Oliver, R., Ditteon, R. (2007). "Asteroid Lightcurve Analysis at the Oakley Observatory - March/April 2007." *Minor Planet Bulletin* **34**, 119-122.

Warner, B.D. (2017). *MPO Canopus* software version 10.7.10.0. *http://www.bdwpublishing.com*

ASTEROID PHOTOMETRY AND LIGHTCURVE ANALYSIS AT GORA'S OBSERVATORIES, PART V.

Milagros Colazo
Instituto de Astronomía Teórica y Experimental
(IATE-CONICET), ARGENTINA
Facultad de Matemática, Astronomía y Física,
Universidad Nacional de Córdoba, ARGENTINA
Grupo de Observadores de Rotaciones de Asteroides (GORA),
ARGENTINA
milirita.colazovinovo@gmail.com

César Fornari, Aldo Wilberger, Mario Morales,
Ezequiel Bellocchio, Eduardo Pulver, Damián Scotta,
Néstor Suárez, Raúl Melia, Francisco Santos, Aldo Mottino,
Ariel Stechina, Alberto García, Andrés Chapman, Carlos Colazo

Grupo de Observadores de Rotaciones de Asteroides (GORA),
ARGENTINA

Observatorio Cruz del Sur (MPC I39) -
San Justo (Buenos Aires-Argentina)

Observatorio de Sencelles (MPC K14) -
Sencelles (Mallorca-Islas Baleares-España)

Observatorio Los Cabezones (MPC X12) -
Santa Rosa (La Pampa-Argentina)

Observatorio Galileo Galilei (MPC X31) -
Oro Verde (Entre Ríos-Argentina)

Observatorio Antares (MPC X39) -
Pilar (Buenos Aires-Argentina)

Observatorio AstroPilar (GORA APB) -
Pilar (Buenos Aires-Argentina)

Observatorio de Aldo Mottino (GORA OAM) -
Rosario (Santa Fe-Argentina)

Observatorio Astro Pulver (GORA OAP) -
Rosario (Santa Fe-Argentina)

Observatorio de Ariel Stechina 1 (GORA OAS) -
Reconquista (Santa Fe-Argentina)

Observatorio de Damián Scotta 1 (GORA ODS) -
San Carlos Centro (Santa Fe-Argentina)

Observatorio de Damián Scotta 2 (GORA OD2) -
San Carlos Centro (Santa Fe-Argentina)

Observatorio Astronómico Giordano Bruno (GORA OGB) -
Piconcillo (Córdoba-España)

Observatorio Río Cofio (GORA ORC) -
Robledo de Chavela (Madrid-España)

Observatorio de Raúl Melia (GORA RMG) -
Gálvez (Santa Fe-Argentina)

(Received: 2021 May 3)

Synodic rotation periods and amplitudes are reported for 153 Hilda, 357 Ninina, 366 Vincentina, 709 Fringilla, and 739 Mandeville.

Observatory	Telescope	Camera
I39 Obs.Astr.Cruz del Sur	Telesc. Newtoniano (D=200mm; f=4.0)	CMOS QHY174
K14 Obs.Astr.de Sencelles	Telesc. Newtoniano (D=250mm; f=4.0)	CCD SBIG ST-7XME
X12 Obs.Astr.Los Cabezones	Telesc. Newtoniano (D=200mm; f=5.0)	CMOS QHY174MGPS
X31 Obs.Astr.Galileo Galilei	Telesc. RCT ap (D=405mm; f=8.0)	CCD SBIG STF8300M
X39 Obs.Astr.Antares	Telesc. Newtoniano (D=250mm; f=4.7)	CCD QHY9 Mono
APB Obs.Astr.AstroPilar	Telesc. Refractor (D=150mm; F=7.0)	CCD ZWO-ASI183OAM
Obs.Astr.de Aldo Mottino	Telesc. Newtoniano (D=250mm; f=4.7)	CCD SBIG STF8300M
OAP Obs.Astr.Astro Pulver	Telesc. SCT (D=203mm; f=7.0)	CMOS QHY5 LII M
OAS Obs.Astr.de Ariel Stechina 1	Telesc. Newtoniano (D=254mm; f=4.7)	CCD SBIG STF402
ODS Obs.Astr.de Damián Scotta 1	Telesc. Newtoniano (D=300mm; f=4.0)	CCD SBIG St-402 XME
OD2 Obs.Astr.de Damián Scotta 2	Telesc. Newtoniano (D=250mm; f=4.0)	CCD Atik 314L+
OGB Obs.Astr.Giordano Bruno	Telesc. SCT (D=203mm; f=6.0)	CCD Atik 420 m
ORC Obs.Astr.Río Cofio	Telesc. SCT (D=254mm; f=6.3)	CCD SBIG ST8-XME
RMG Obs.Astr.de Raúl Melia	Telesc. SCT (D=200mm; f=10.0)	CCD Meade DSI Pro II

Table I. List of observatories and equipment.

Number	Name	20yy/ mm/dd- 20yy/ mm/dd	Phase	L_{PAB}	B_{PAB}	Period(h)	P.E.	Amp	A.E.	Grp
153	Hilda	21/02/19-21/04/02	2.4,10.4	150	-8	5.962	0.005	0.040	0.007	HIL
357	Ninina	21/01/10-21/03/03	3.3,15.5	112	-7	35.982	0.010	0.17	0.01	MB-O
366	Vincentina	21/03/21-21/04/17	1.5,10.2	177	-3	17.338	0.010	0.09	0.01	MB-O
709	Fringilla	21/03/06-21/04/06	*3.3,10.0	169	-9	52.172	0.011	0.23	0.02	MB-O
739	Mandeville	20/11/07-21/01/25	*12.9,18.9	69	-23	35.842	0.008	0.09	0.01	MB-O

Table II. Observing circumstances and results. The phase angle is given for the first and last date. If preceded by an asterisk, the phase angle reached an extremum during the period. L_{PAB} and B_{PAB} are the approximate phase angle bisector longitude/latitude at mid-date range (see Harris et al., 1984). Grp is the asteroid family/group (Warner et al., 2009). MB-O: main-belt outer.

The periods and amplitudes of asteroid lightcurves presented here are the product of a collaborative work by GORA (Grupo de Observadores de Rotaciones de Asteroides). In all the studies we have applied relative photometry assigning V magnitudes to the calibration stars.

The image acquisition was performed without filters and with exposure times of a few minutes. All images used were corrected using dark frames and in some cases bias and flat-field were also used. Photometry measurements were performed using *FotoDif* software and for the analysis we employed *Periodos* software (Mazzone, 2012).

Below, we present the results for each asteroid under study. The lightcurve figures contain the following information: the estimated period and period error and the estimated amplitude and amplitude error. In the reference boxes the columns represent, respectively, the marker, observatory MPC code or, failing that, the GORA internal code, session date, session off-set, and number of data points.

Targets were selected based on the following criteria: 1) those asteroids with magnitudes accessible to the equipment of all participants, 2) those with favorable observation conditions from Argentina, i.e., with negative declinations, and 3) objects with few periods reported in the literature and/or with Lightcurve Database (LCDB) (Warner et al., 2009) quality codes (U) of less than 3.

153 Hilda is a dark P-type asteroid. It was discovered in 1875 by Johann Palisa. Our analysis yields a period of $P = 5.962 \pm 0.005$ h with $\Delta m = 0.040 \pm 0.007$ mag. This period is in agreement with the one measured by Shevchenko et al. (2009), who obtained $P = 5.9587 \pm 0.0005$ h with $\Delta m = 0.20 \pm 0.02$ mag. The difference in Δm is likely due to a change in the aspect angle.

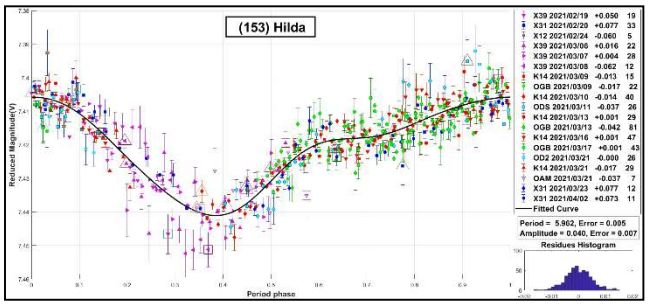

357 Ninina is a main-belt asteroid. It was discovered in 1893 by Auguste Charlois. The latest periods reported in the literature are $P = 35.98 \pm 0.07$ h with $\Delta m = 0.12 \pm 0.01$ mag (Behrend, 2005web) and $P = 35.9 \pm 0.1$ h with $\Delta m = 0.12 \pm 0.01$ mag (Oey, 2014). The results we obtained, $P = 35.982 \pm 0.010$ h with $\Delta m = 0.17 \pm 0.01$ mag, are consistent with those presented by the authors mentioned above.

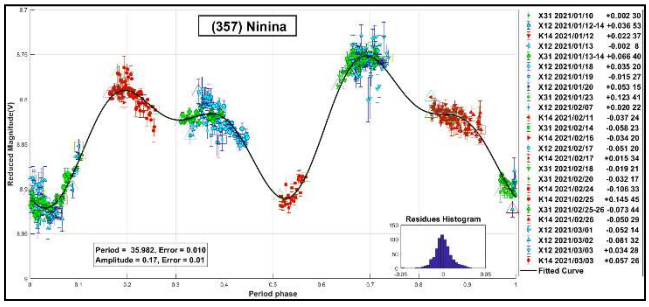

366 Vincentina was discovered in 1893 by Auguste Charlois. The periods published for this asteroid are P = 15.5 ± 0.1 h with Δm = 0.08 ± 0.03 mag (Robinson, 2002) and P = 12.7365 ± 0.0005 h with Δm = 0.05 ± 0.01 mag (Benishek, 2013). Our results show a period longer than those previously reported. Our data give P = 17.338 ± 0.010 h and Δm = 0.09 ± 0.01 mag.

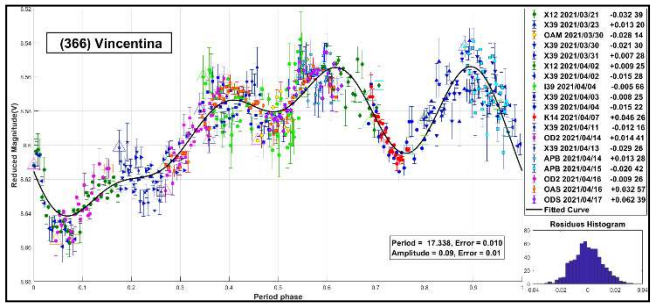

709 Fringilla is a X-type asteroid. It was discovered in 1911 by Joseph Helffrich. We found in the literature two different periods calculated for this object: P = 52.4 ± 0.2 h with Δm = 0.18 ± 0.02 mag (Harris & Young, 1980) and P = 20 h with Δm = 0.05 mag (Behrend, 2008web). The results we obtained are P = 52.172 ± 0.011 h and Δm = 0.23 ± 0.02. Our period well agrees with the one measured by Harris & Young (1980), which is also the one exhibiting the highest U quality code.

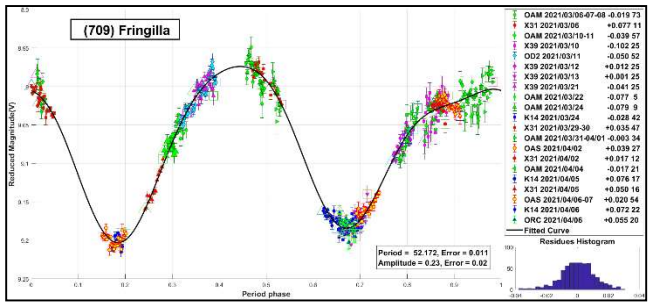

739 Mandeville is classified as type X in the Tholen taxonomy. It was discovered by Joel Hastings Metcalf. This was a very difficult case to solve since we had to deal with candidate periods that were integer multiple or divisors of 12 h. Harris & Young (1989) reported a period of 11.931 ± 0.010 h. Our own previous estimation (Colazo et al., 2020) was 23.92 ± 0.02 h, twice the period proposed by Harris & Young. We are currently proposing a new period, different from all those reported previously. We have determined a period of 35.842 ± 0.008 h (~1.5 times our last published period). Our new contribution is based on several observations including five performed linking two or three consecutive nights. The same equipment, identical configurations and calibration stars were used in these particular observations. Further coordinated observations from different longitudes would help confirm our latest result.

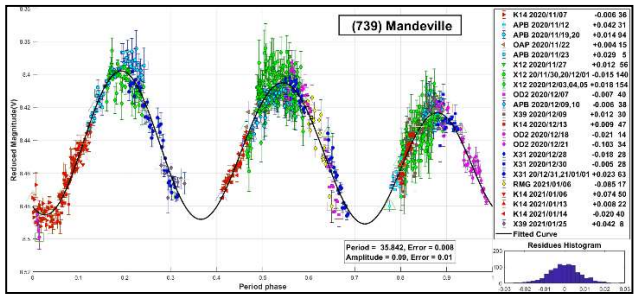

Acknowledgements

We want to thank Julio Castellano as we use his *FotoDif* program for preliminary analyses, Fernando Mazzone for his *Periods* program, used in final analyses and Matías Martini for his *CalculadorMDE_v0.2* used for generate ephemerides used in the planning stage of the observations. This research has made use of the Small Bodies Data Ferret (*http://sbn.psi.edu/ferret/*), supported by the NASA Planetary System and made use of data and/or services provided by the International Astronomical Union's Minor Planet Center.

References

Behrend, R. (2005web, 2008web). Observatoire de Geneve web site. *http://obswww.unige.ch/~behrend/page_cou.html*

Benishek, V. (2013). "Lightcurves for 366 Vincentina, 592 Bathseba, and 1554 Yugoslavia from Belgrade Astronomical Observatory." *Minor Planet Bulletin* **40**, 100-101.

Colazo, M.; Fornari, C.; Santucho, M.; Mottino, A.; Colazo, C.; and 16 colleagues (2020). "Asteroid Photometry and Lightcurve Analysis at Gora's Observatories." *Minor Planet Bulletin* **47**, 188-191.

Harris, A.W.; Young, J.W. (1980). "Asteroid rotation: III. 1978 Observations." *Icarus* **43**, 20-32.

Harris, A.W.; Young, J.W.; Scaltriti, F.; Zappala, V. (1984). "Lightcurves and phase relations of the asteroids 82 Alkmene and 444 Gyptis." *Icarus* **57**, 251-258.

Harris, A.W.; Young, J.W. (1989). "Asteroid lightcurve observations from 1979-1981." *Icarus* **81**, 314-364.

Mazzone, F.; Colazo, C.; Mina, F.; Melia, R.; Spagnotto, J.; Bernal, A. (2014). "Collaborative asteroid photometry and lightcurve analysis at observatories OAEGG, OAC, EABA, AND OAS." *Minor Planet Bull.* **41**, 17-18

Oey, J. (2014). "Lightcurve Analysis of Asteroids from Blue Mountains Observatory in 2013." *Minor Planet Bulletin* **41**, 276-281.

Robinson, L.E. (2002). "Photometry of Five Difficult Asteroids: 309 Fraternitas, 366 Vincentina, 421 Zahringia, 578 Happelia, 959 Anne." *Minor Planet Bulletin* **29**, 30-31.

Shevchenko, V.G.; Tungalag, N.; Chiorny, V.G.; Gaftonyuk, N.M.; Krugly, Yu.N.; Harris, A.W. (2009). "CCD-photometry and pole coordinates for eight asteroids." *Planetary and Space Science* **57**, 1514-1520.

Warner, B.D.; Harris, A.W.; Pravec, P. (2009) "The asteroid lightcurve database." *Icarus* **202**, 134-146. Updated 2021 April 1. *http://www.minorplanet.info/lightcurvedatabase.html*

DETERMINING LIGHTCURVES AND ROTATIONAL PERIODS OF FOUR MAIN BELT ASTERIODS

Allan Teer
Kent Montgomery
Texas A&M University–Commerce
P.O. Box 3011
Commerce, TX 75429-3011
Kent.Montgomery@tamuc.edu

(Received: 2021 May 14, Revised: 2021 August 2)

Lightcurves and rotational periods were determined for the following four asteroids: 2394 Nadeev: 6.539 ± 0.001 h; 3717 Thorenia: 4.365 ± 0.001 h; 4700 Carusi: 10.798 ± 0.002 h; and (29032) 2059 T-1: 5.238 ± 0.001 h.

Introduction

This research was performed to determine the rotational period of four main belt asteroids: 2394 Nadeev, 3717 Thorenia, 4700 Carusi, and (29032) 2059 T-1. Data was taken over several nights of observations to produce photometric lightcurves that were then analyzed to determine rotational periods. For an optimal signal to noise ratio, these asteroids needed to have a brightness of 16 mag or less. The telescope used, residing in the northern hemisphere, dictated that these asteroids have a positive declination.

Asteroid 2394 Nadeev was discovered in 1973 by N. Chernykh at Nauchnyj. This asteroid has an orbital eccentricity of 0.214 and a semi-major axis of 3.175 AU (JPL). Asteroid 3717 Thorenia was discovered in 1964 by the Indiana Asteroid Program at the Goeth Link Observatory in Brooklyn, Indiana. It has an orbital eccentricity of 0.171 and a semi-major axis of 3.159 AU (JPL). Asteroid 4700 Carusi was discovered in 1986 by E. Bowell at Flagstaff. It has an orbital eccentricity of 0.201 and a semi-major axis of 2.563 AU (JPL). Asteroid (29032) 2059 T-1 was discovered in 1971 by C.J. Houten, I. van Houten-Groeneveld, and T. Gehrels at Palomar. It has an orbital eccentricity of 0.206 and a semi-major axis of 2.347 AU (JPL).

Method

The telescope used is a 0.7-m CDK 700 Planewave corrected Dall-Kirkham design telescope with an Andor Technologies CCD camera at Texas A&M University-Commerce Observatory (TAMUC) in Commerce, Texas. The camera was thermoelectrically cooled to between -60ºC and -100ºC to reduce background noise in the images.

In order to reduce the images, flats, bias, and dark calibration images were taken each night. The flat field images were taken against the twilight sky. The darks were exposed for the same time as the respective light images, three minutes. A Luminance filter that allowed the visible portion of the spectrum to be recorded while blocking the infrared was used in front of the CCD camera.

The software *MaxImDL* was used to calibrate and align the asteroid images. Afterward, the program *MPO Canopus* v10.4.0.8 (Warner, 2011) was used to perform differential photometry on the reduced data. For each data set, five stars within an image were used for brightness comparison to the asteroid. Aperture photometry was used to determine the brightness of these comparison stars and the asteroid. The average of the difference in mag. between the stars and the asteroid was found for each image and then plotted in a phased plot, mag. versus time, to create a lightcurve. A Fourier transform was then applied to the lightcurve to determine the rotational period and error in the period.

Results

2394 Nadeev was imaged on 2019 December 4, 124 times and on 2019 December 18, 110 times. A rotation period of 6.539 ± 0.001 h with an amplitude variance of 0.05 mag was found. Behrend (2019) found a similar rotation period of 6.54 hours.

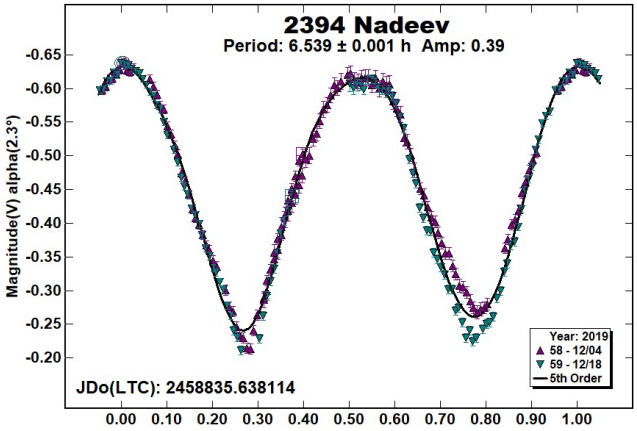

3717 Thorenia was imaged on 2020 February 9, 138 times and on 2020 March 25, 65 times. A rotation period of 4.365 ± 0.001 h with an amplitude variance of 0.02 mag was found. No previous studies regarding the rotation period were found in either the JPL Small-Body Database or the Minor Planet Light Curve Database (MPC).

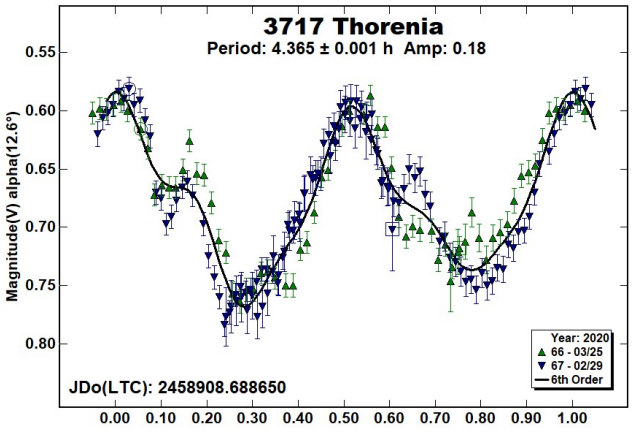

4700 Carusi was imaged 2019 December 19, 150 times and on 2019 December 31, 139 times. A rotation period of 10.798 ± 0.002 h with an amplitude variance of 0.47 mag was found. Odden et al. (2020) found a period of 11.656 ± 0.001 h with an amplitude of 0.49 ± 0.05 mag. The discrepancy in the two rotation periods is interesting since both studies had well sampled lightcurves.

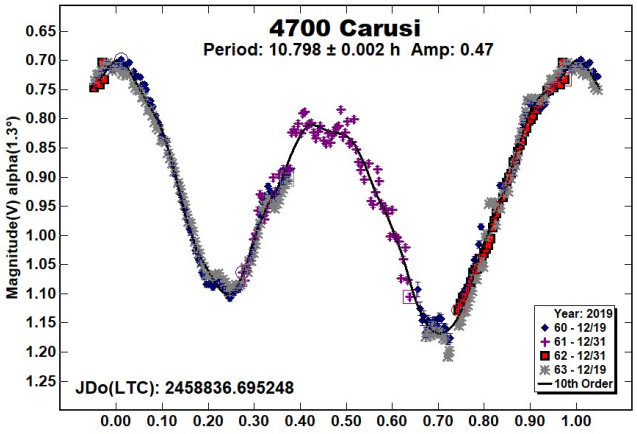

29032 (2059 T-1) The asteroid 29032 (2059 T-1) was imaged on 2019 October 5, 43 times, 2019 October 6, 110 times, and on 2019 October 19, 90 times. A rotation period of 5.238 ± 0.001 h with an amplitude variance of 0.05 mag was found. Benishek (2020) found a similar rotation period of 5.2393 ± 0.0006 h and an amplitude of 0.41 mag.

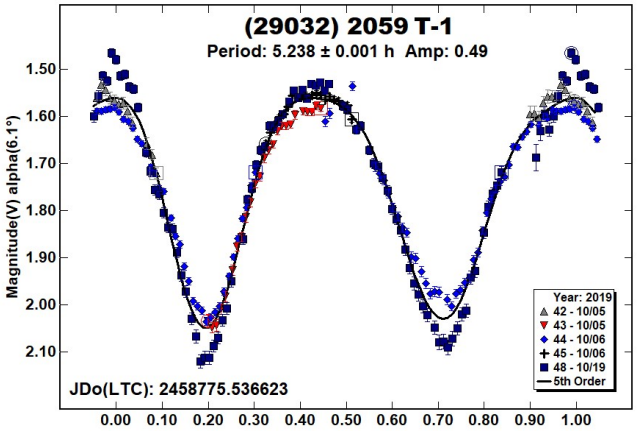

Acknowledgments

This work is supported in part by the Physics and Astronomy Scholarship for Success (PASS) project at Texas A&M University-Commerce funded by the NSF under grant No. 1643567.

References

Behrend, R. (2019) Observatoire de Geneve, *http://obswww.unige.ch/~behrend/page_cou.html*

Benishek, V. (2020), "Photometry of 39 Asteroids at Sopot Astronomical Observatory: 2019 September - 2020 March," *Minor Planet Bulletin* **47-3**, 231-240.

Harris, A.W.; Young, J.W.; Scaltriti, F.; Zappala, V. (1984). "Lightcurves and phase relations of the asteroids 82 Alkmene and 444 Gyptis." *Icarus* **57**, 251-258.

JPL Small-Body Database Browser. *http://ssd.jpl.nasa.gov/sbdb.cgi#top*

MaxIm DL by Diffraction Limited. *http://diffractionlimited.com/product/maxim-dl/*

MPC Database Search. *https://minorplanetcenter.net/db_search/*

Odden, C.E.; Zhu, J.; Barakaiev, I.; Bilokur, M.; Colleye, Z.A.; de Saint-Exupery, M.P.; Lee, Y.; Mundra, I.R.; Nazzaro, H.A.; Nyiha, I.R.; Pedroza, A.; Prabhakar, P.S.; Taylor, A.C.; Xie, Y.; Yoon, C.S.; Yusuf, S.M.; Zhu, E.C.; Zhu, S.; Kemp, J.; Sliski, A. (2020), "Lightcurve Analysis of Asteroid 4700 Carusi," *Minor Planet Bulletin* **47-3,** 252-253.

Warner, B.D. (2011) *MPO Canopus* Software. Version 10.2.1.0 Bdw Publishing. *http://www.minorplanetobserver.com/*

Number	Name	yyyy mm/dd	Phase	L_{PAR}	B_{PAR}	Period(h)	P.E.	Amp	A.E.
2394	Nadeev	2019/12/04-2019/12/18	2.1, 8.4	67.6	-1.8	6.539	0.001	0.39	0.05
3717	Thorenia	2020/02/09-2020/03/25	6.9, 12.6	154.8	+2.7	4.365	0.001	0.18	0.02
4700	Carusi	2019/12/19-2019/12/31	1.5, 6.2	88.6	+1.8	10.798	0.002	0.47	0.02
29032	2059 T-1	2019/10/05-2019/10/19	5.9, 14.7	4.0	+4.8	5.238	0.001	0.49	0.05

Table I. Observing circumstances and results. The phase angle is given for the first and last date. If preceded by an asterisk, the phase angle reached an extrema during the period. L PAB and B PAB are the approximate phase angle bisector longitude/latitude at mid-date range (see Harris et al., 1984).

CCD PHOTOMETRIC OBSERVATIONS OF ASTEROIDS 2984 CHAUCER, (26206) 1997 PJ4, (87035) 2000 KE2, AND 2015 NU13

Kenneth Zeigler
Star Z Research Ranch
PO Box 1464, George West, Texas 78022 USA
Dylan_lucard@yahoo.com

(Received: 2021 June 11, Revised: 2021 August 2)

CCD photometric observations of asteroids 2984 Chaucer, (26206) 1997 PJ4, (87035) 2000 KE2, and 2015 NU13 were conducted from the Star Z Research Ranch in South Texas. The rotational period of asteroid 2984 Chaucer is 9.016 ± 0.010 h, with an amplitude of 0.98 mag. The rotational period of asteroid (26206) 1997 PJ4 is 3.293 ± 0.010 h with an amplitude of 0.13 mag. The rotational period of asteroid (87035) 2000 KE2 is 6.14 ± 0.01 h with an amplitude of 0.13 mag. The rotational period of asteroid 2015 NU13 is 2.4 ± 0.1 h, with an amplitude of 0.26 mag.

The photometric observations described in this paper were conducted from the Star Z Research Ranch, which is located at a dark sky site, 19 kilometers south of the Town of George West, Texas.

Throughout this research program, a Meade 0.35-meter LX600 Schmidt Cassegrain telescope was used. The telescope is housed within a converted eight by sixteen-foot Wells Cargo trailer with a hinged roof, which in turn sets upon four steel jacks resting on a concrete slab. The telescope pier itself rests upon a heavy steel tripod, independent of the trailer, to minimize vibrations. An SBIG STXL 6303 camera thermoelectrically cooled to -35°C was used to make the photometric observations. The photometric exposures were all 120 seconds in length and were dark subtracted and flat fielded. To preserve the maximum light intensity of the objects observed, no filters were placed in the optical path during the observations.

The brightness of the asteroid was compared to that of three comparison stars in the same CCD frame. The average instrumental magnitude of the three stars was determined and this average was subtracted from the instrumental magnitude of the asteroid. A constant was then added to approximate the visual magnitude. The instrumental magnitude of the three comparison stars with respect to one another was continuously monitored in the event that one of them was determined to be a short period variable star. The target brightness was determined by measuring a 121 pixels (11 pixel by 11 pixel) sample surrounding the asteroid or star in question. This corresponds to a 7.15 by 7.15 arcsec box. When possible, the same comparison stars were used during consecutive nights of observation. The coordinates of the asteroid and its approximate visual magnitude on any specific night were obtained from the online Lowell Minor Planet Services. This information was also used to compensate for the effect of the asteroid's changing distance from the sun and earth on its visual magnitude when vertically aligning the photometric data points from different nights in the construction of a composite lightcurve.

2984 Chaucer was discovered by Edward Bowell at Lowell's Anderson Mesa Station in Flagstaff, Arizona, on 30 December 1981. It is named after Geoffrey Chaucer (1343–1400), the medieval English poet. The orbit of the asteroid has a semi-major axis of 2.500 a.u., eccentricity of 0.136, and an orbital period of 3.88 years. This places it within the inner region of the main belt. This asteroid was observed from the Star Z Research Ranch on three separate nights between January 16 and 18, 2021. The asteroid's lightcurve is characterized by two broad and nearly identical maxima, and two narrow minima per rotational cycle. A composite lightcurve with a period of 9.016 ± 0.01 h best fit the available data. The lightcurve has an amplitude of 0.98 mag, as shown in the figure.

A search of the literature revealed no previously published rotational period for 2984 Chaucer.

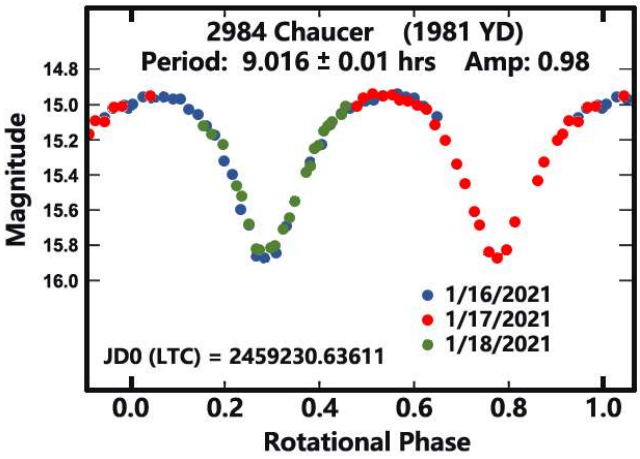

(26206) 1997 PJ4 was discovered on 1997 Aug 11 by P. Antonini, at the Bedoin Observatory in Southern France. With a semi-major axis of 2.867 a.u., eccentricity of 0.138, and orbital period of 4.36 years it is located in the middle of the main belt. According to the Lightcurve Data Base, as of October 2020, a rotational period for this asteroid has not yet as been determined. This asteroid was observed from the Star Z Research Ranch on the nights of January 13, 14, and 15, 2021. The asteroid was determined to have a rotational period of 3.293 ± 0.010 h, with a lightcurve amplitude of 0.13 mag. The lightcurve is very asymmetrical, characterized by three separate maxima and minima per rotational cycle. The three minima are of approximately the same magnitude; however, the three maxima are not. Two are broad while the third is far narrower, lasting only a matter of minutes. This peculiar lightcurve feature was observed on all three nights of observation.

Number	Name	yyyy mm/dd	Phase	L_{PAB}	B_{PAB}	Period(h)	P.E.	Amp	A.E.	Grp
2984	Chaucer	2021 1/16-1/18	1.5,2.2	116	3	9.016	0.010	0.98	0.02	
26206	1997 PJ4	2021 1/13-1/15	-2.5,2.2	116	-5	3.293	0.010	0.13	0.02	
87035	2000 KE2	2021 2/2 -2/7	-3.8,3.5	143	5	6.14	0.010	0.13	0.02	Amor
	2015 NU13	2021 1/23	-9.4,-9.3	123	-10	2.4	0.100	0.26	0.02	Apollo

Table I. Observing circumstances and results. The phase angle is given for the first and last date. If preceded by an asterisk, the phase angle reached an extrema during the period. L_{PAB} and B_{PAB} are the approximate phase angle bisector longitude/latitude at mid-date range (see Harris et al., 1984). Grp is the asteroid family/group (Warner et al., 2009).

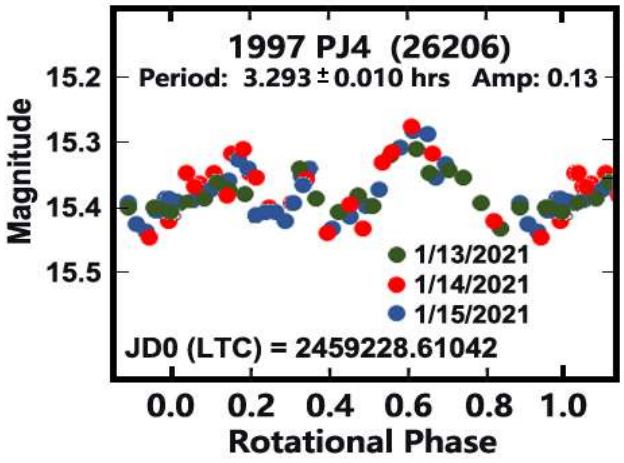

(87035) 2000 KE2 was discovered on 26-May-2000 by the LINEAR Survey at Socorro, New Mexico. Its orbit has a semi-major axis of 2.352 a.u., eccentricity of 0.343, and an orbital period of 3.61 years. Its high eccentricity makes it a Mars crossing asteroid. This asteroid was observed from the Star Z Research Ranch on the nights of February 2 and 7, 2021. At the time of observation, it was just beyond the orbit of Mars. It should be noted that the reported rotational period of this asteroid has some uncertainty associated with it. The composite lightcurve presented here is the most likely one, however there are other possibilities. The composite lightcurve is very asymmetrical displaying three minima and three maxima per rotational cycle. A rotational period of 6.14 ± 0.01 h, with a lightcurve amplitude of 0.13 mag best fits the observations, as shown in the figure.

According to the October 2020 update of the LCDB, Asteroid 87035, has, as yet, no published rotational period.

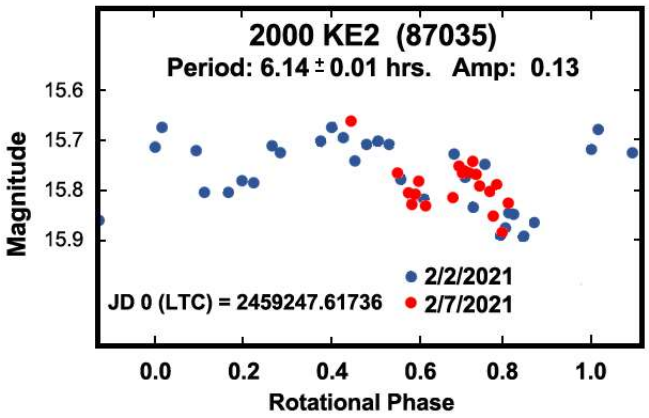

2015 NU13 is classified as an Apollo asteroid and also a potentially hazardous asteroid. Its orbit has a semi-major axis of 1.830 a.u., an eccentricity of 0.590, and an orbital period of 2.48 years. At perihelion it is just beyond the orbit of Venus. It has been estimated to be about half a kilometer in diameter. On 9-January-2021 it passed within 0.038 a.u. of Earth. However, at the time it had a far southern declination and was moving very rapidly across the sky. On the night of the observations, it was 0.126 a.u. from Earth and much further north. Its angular speed had slowed sufficiently to conduct CCD photometry. It was only observed during a single night, the other nights around this date being cloudy. Its lightcurve displays two maxima and two minima per rotational cycle. The maxima are of nearly identical brightness; however, one minimum is a full 0.1 mag fainter than the other. The asteroid was observed for a bit over one rotation before clouds moved in. An examination of the October 2020 update of the Asteroid Lightcurve Database reveals that this asteroid currently has no published lightcurve.

The single night lightcurve for this asteroid is shown in the figure.

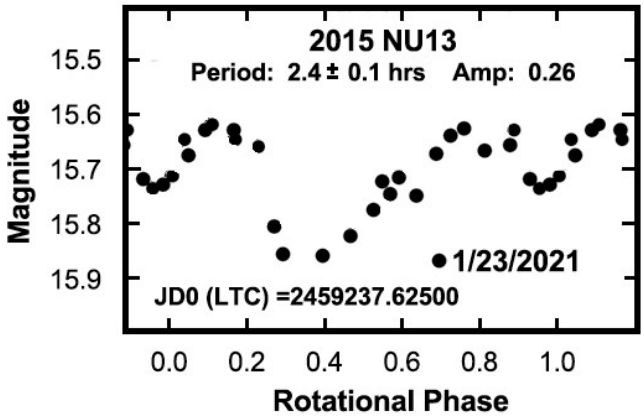

References

Harris, A.W.; Young, J.W.; Scaltriti, F.; Zappala, V. (1984). "Lightcurves and phase relations of the asteroids 82 Alkmene and 444 Gyptis." *Icarus* **57**, 251-258.

JPL (2018). Small Body Database Browser. *http://ssd.jpl.nasa.gov/sbdb.cgi*

Lowell Minor Planet Services. *https://asteroid.lowell.edu/gui/*

Warner, B.D.; Harris, A.W.; Pravec, P. (2009). "The Asteroid Lightcurve Database." *Icarus* **202**, 134-146. Updated 2020 Oct. *http://www.minorplanet.info/lightcurvedatabase.html*

LIGHTCURVE ANALYSIS OF ASTEROIDS 1228 SCABIOSA AND 12016 GREEN

Caroline Odden, Lola Bingham, Sofia Cordover, Victoria Darling, Amanda DiNatale, George Hsieh, Reimi Kusaka, Jeremy Lin, Troy Mao, Katherine Marquis, Paulkichna Merove, Tanush Mittal, Olha Yarynich
Phillips Academy Observatory (MPC I12)
180 Main Street
Andover, MA 01810 USA
ceodden@andover.edu

(Received: 2021 July 15)

Photometric observations of asteroids 1228 Scabiosa and 12016 Green were made from the Phillips Academy Observatory (PAO) from 2021 March 14 to May 16. The rotational periods and amplitudes were determined to be: 1228 Scabiosa, P = 22.769 ± 0.001 h, A = 0.75 ± 0.02 mag; 12016 Green, P = 4.911 ± 0.001 h, A = 0.52 ± 0.05 mag.

CCD photometric observations of asteroids 1228 Scabiosa and 12016 Green were made from the Phillips Academy Observatory. The asteroids were chosen from the CALL website. All observations were made with a 0.50-m *f*/6.8 Ritchey-Chrétien (RC) Astrograph telescope manufactured by PlaneWave Instruments and Andor Tech iKon DW436 CCD camera with a 2048×2048 array of 13.5-micron pixels. The resulting image scale was 0.81 arcseconds per pixel. All images were corrected using dark frames, flat-fields, and bias frames using *AstroImageJ* Software v. 3.2.21 (Collins et. al., 2018). All exposures were taken through a luminance filter at -50°C and were unbinned. Exposures were 300 s in length and unguided.

MPO Canopus (Warner, 2018) was used to make photometric measurements of the images using differential photometry as well as to generate the final lightcurves. Comparison stars were chosen to have near solar-color, a B-V value close to 0.8, and a V-R value close to 0.45 (Warner, 2012). In addition, brighter comparison stars were favored. Data merging and period analysis were done with *MPO Canopus* using the Fourier Analysis for Lightcurves (FALC) algorithm developed by Alan Harris (Harris et al., 1989) and modified by Petr Pravec (Warner, 2012). The research was conducted for the Astronomy Research course at Phillips Academy, a high school in Andover, Massachusetts.

1228 Scabiosa was discovered on 5 October 1931 by K. Reinmuth (JPL, 2021). This object did not have any previous rotational period results in the Asteroid Lightcurve Database (LCDB; Warner et al., 2009). Images were taken over fifteen nights from 2021 March 14 to May 25. Analysis of 500 data points indicated a rotational period of 22.769 ± 0.001 h with amplitude 0.75 ± 0.03 mag. The composite lightcurve is well covered, and a bimodal solution is expected given the amplitude (Harris et. al, 2014). Because this is a slow rotator with a period close to Earth's rotation period, many sessions and a little bit of luck were required to achieve full coverage of the lightcurve. The group was unable to obtain full coverage due to a combination of poor weather and moon placement. Nevertheless, four consecutive nights of imaging in March helped to constrain the period, and the period spectrum strongly favors the reported period.

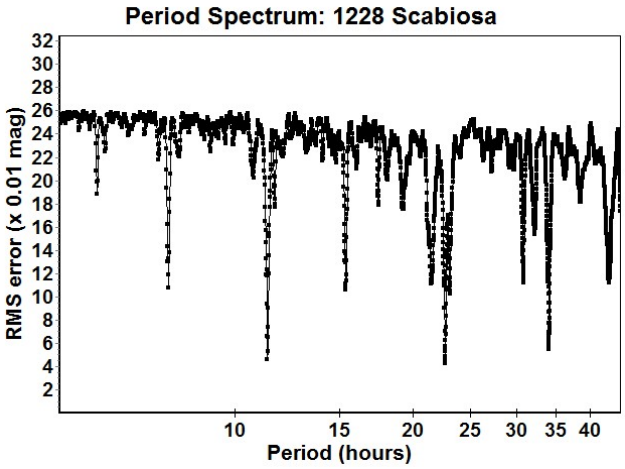

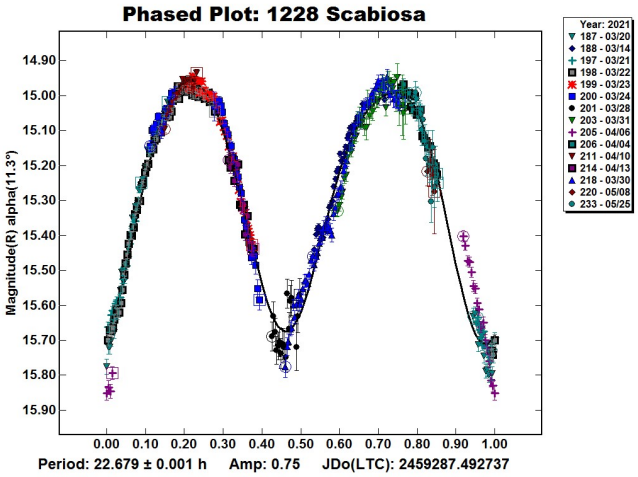

12016 Green was discovered on 1 December 1996 by P. G. Comba and was named after George Green (JPL, 2021), the self-taught physicist who is associated with "Green's Function." This object has a previously reported period of 5.055 h (Behrend, 2006web) with a quality rating of 2 (LCDB; Warner et al., 2009).

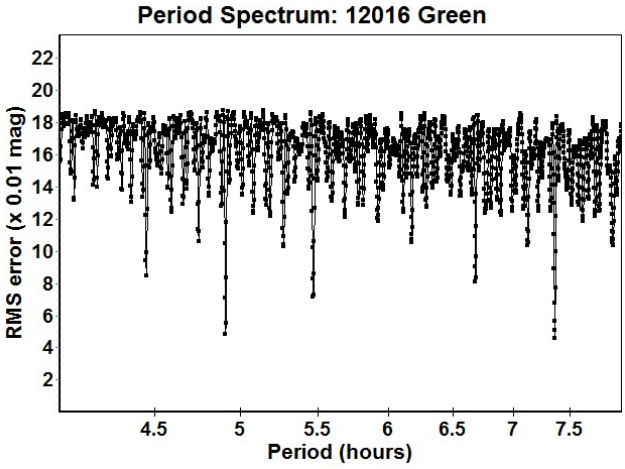

Number	Name	yyyy mm/dd	Phase	L_{PAB}	B_{PAB}	Period(h)	P.E.	Amp	A.E.	Grp
1228	Scabiosa	2021 03/14-05/21	8.9,22.3	156	-2	22.679	0.001	0.75	0.02	MB-M
12016	Green	2021 04/21-05/16	10.1,20.6	197	9	4.911	0.001	0.52	0.05	MB-M

Table I. Observing circumstances and results. The phase angle is given for the first and last date. If preceded by an asterisk, the phase angle reached an extremum during the period. L_{PAB} and B_{PAB} are the approximate phase angle bisector longitude/latitude at mid-date range (see Harris et al., 1984). Grp is the asteroid family/group (Warner et al., 2009).

Images were taken over six nights from 2021 April 21 to May 16. Analysis of 193 data points indicated a period of 4.911 ± 0.001 h with amplitude 0.52 ± 0.03 mag. The period spectrum also includes relative minima at 4.455 h and 5.470 h, but when the data are phased to these periods, the fit is noticeably worse. The data do not phase at all well to the previously reported period of 5.055 hrs.

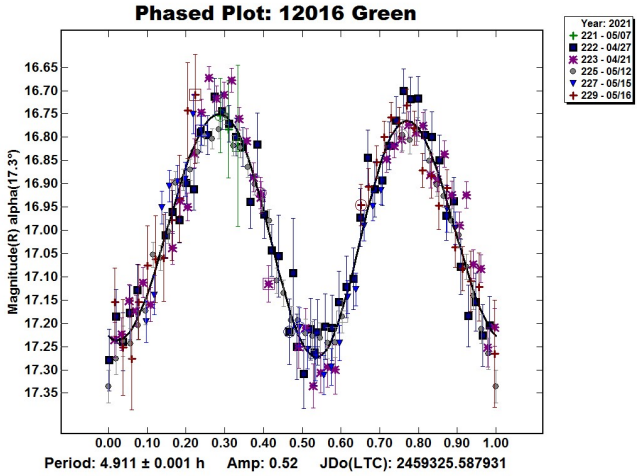

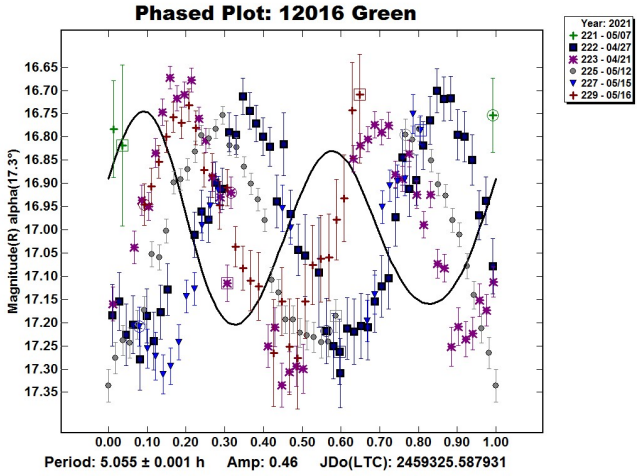

Acknowledgements

Research at the Phillips Academy Observatory is supported by the Israel Family Foundation. Funding for the Andor Tech camera and PlaneWave telescope at Phillips Academy was provided by the Abbot Academy Association, the Donald T. Ganem Fund, and the Taylor Family.

References

Behrend, R. (2006web) Observatoire de Geneve web site. *http://obswww.unige.ch/~behrend/page_cou.html*

CALL: Potential Lightcurve Targets (with LCDB data) Query. *http://www.minorplanet.info/PHP/call_OppLCDBQuery.php*

Collins, K.A.; Kielkopf, J.F.; Stassun, K.G.; Hessman, F.V. (2018). "AstroImageJ: Image processing and photometric extraction for ultra-precise astronomical light curves." *Astronomical Journal* **153-2**, 77. *http://www.astro.louisville.edu/software/astroimagej/*

Harris, A.W.; Young, J.W.; Scaltriti, F.; Zappala, V. (1984). "Lightcurves and phase relations of the asteroids 82 Alkmene and 444 Gyptis." *Icarus* **57**, 251-258.

Harris, A.W.; Young, J.W.; Bowell, E.; Martin, L.J.; Millis, R.L.; Poutanen, M.; Scaltriti, F.; Zappala, V.; Schober, H.J.; Debehogne, H.; Zeigler, K. (1989). "Photoelectric Observations of Asteroids 3, 24, 60, 261, and 863." *Icarus* **77**, 171-186.

Harris, A.W.; Pravec, P.; Galad, A.; Skiff, B.A.; Warner, B.D.; Vilagi, J.; Gajdos, S.; Carbognani, A.; Hornoch, K.; Kusnirak, P.; Cooney, W.R.; Gross, J.; Terrell, D.; Higgins, D.; Bowell, E.; Koehn, B.W. (2014). "On the maximum amplitude of harmonics on an asteroid lightcurve." *Icarus* **235**, 55-59.

JPL (2021). Small Body Database Browser. *http://ssd.jpl.nasa.gov/sbdb.cgi*

Warner, B.D. (2012). *The MPO Users Guide: A Companion Guide to the MPO Canopus/PhotoRed Reference Manuals*. BDW Publishing, Colorado Springs, CO.

Warner, B.D. (2018). MPO Software, *MPO Canopus* v10.7.12.2. Bdw Publishing. *http://bdwpublishing.com*

Warner, B.; Harris, A.W.; Pravec, P. Eds., Asteroid Lightcurve Data Base (LCDB) V3.0 urn:nasa:pds:ast-lightcurve-database::3.0. NASA Planetary Data System, 2019; doi: 10.26033/7h40-8s80.

COLLABORATIVE ASTEROID PHOTOMETRY FROM UAI: 2021 APRIL-JUNE

Lorenzo Franco
Balzaretto Observatory (A81), Rome, ITALY
lor_franco@libero.it

Alessandro Marchini
Astronomical Observatory, DSFTA - University of Siena (K54)
Via Roma 56, 53100 - Siena, ITALY

Marco Iozzi
HOB Astronomical Observatory (L63), Capraia Fiorentina, ITALY

Giulio Scarfi
Iota Scorpii Observatory (K78), La Spezia, ITALY

Nico Montigiani, Massimiliano Mannucci
Osservatorio Astronomico Margherita Hack (A57)
Florence, ITALY

Pietro Aceti, Massimo Banfi
Seveso Observatory (C24), Seveso, ITALY

Fabio Mortari
Hypatia Observatory (L62), Rimini, ITALY

Gianni Galli
GiaGa Observatory (203), Pogliano Milanese, ITALY

Paolo Bacci, Martina Maestripieri
GAMP - San Marcello Pistoiese (104), Pistoia, ITALY

Adriano Valvasori, Ernesto Guido
ALMO Observatory (G18), Padulle (BO), ITALY

(Received: 2021 July 12)

Photometric observations of eight asteroids were made in order to acquire lightcurves for shape/spin axis modeling. The synodic period and lightcurve amplitude were found for 81 Terpsichore, 363 Padua, 563 Suleika, 909 Ulla, 929 Algunde, 1048 Feodosia, 3385 Bronnina, 3760 Poutanen.

Collaborative asteroid photometry was done inside the Italian Amateur Astronomers Union (UAI; 2021) group. The targets were selected mainly in order to acquire lightcurves for shape/spin axis modeling. Table I shows the observing circumstances and results.

CCD observations of eight asteroids were made in 2021 April-June using the instrumentation described in the Table II. Lightcurve analysis was performed at the Balzaretto Observatory with *MPO Canopus* (Warner, 2021). All the images were calibrated with dark and flat frames and converted to R magnitudes using solar colored field stars from CMC15 catalogue, distributed with *MPO Canopus*. For brevity, the following citations to the asteroid lightcurve database (LCDB; Warner et al., 2009) will be summarized only as "LCDB."

81 Terpsichore is a Cb-type (Bus & Binzel, 2002) outer main-belt asteroid discovered on 1864 September 30 by E.W. Tempel at Marseille. Collaborative observations were made over seven nights. The analysis shows a synodic period of P = 10.950 ± 0.003 h with an amplitude A = 0.02 ± 0.01 mag. The period is close to the previously published results in the LCDB.

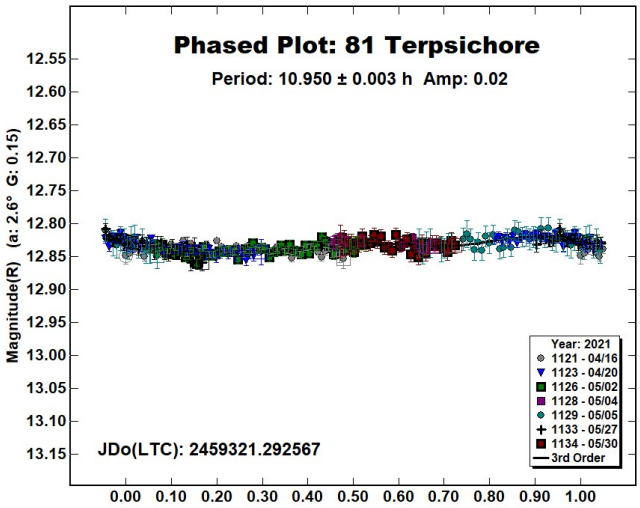

363 Padua is an X-type (Bus & Binzel, 2002) outer main-belt asteroid discovered on 1893 March 17 by A. Charlois at Nice. Collaborative observations were made over six nights. The analysis shows a synodic period of P = 8.400 ± 0.001 h with an amplitude A = 0.08 ± 0.02 mag. The period is close to the previously published results in the LCDB.

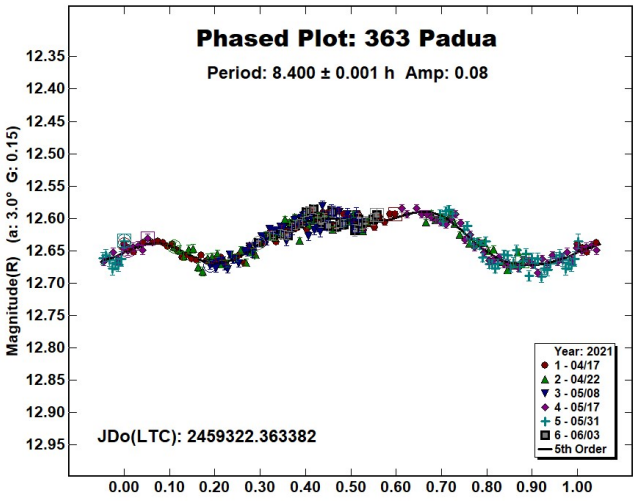

563 Suleika is an Sl-type (Bus & Binzel, 2002) outer main-belt asteroid discovered on 1905 April 6 by P. Gotz at Heidelberg. Collaborative observations were made over six nights. We found a synodic period of P = 5.630 ± 0.001 h with an amplitude A = 0.18 ± 0.03 mag. The period is close to the previously published results in the LCDB.

Number	Name	2021 mm/dd	Phase	L_{PAB}	B_{PAB}	Period(h)	P.E.	Amp	A.E.	Grp
81	Terpsichore	04/16-05/30	2.6,14.4	200	-4	10.950	0.003	0.02	0.01	MB-O
363	Padua	04/17-06/03	3.0,17.1	202	4	8.400	0.001	0.08	0.02	MB-O
563	Suleika	04/20-05/27	4.5,13.8	205	10	5.630	0.001	0.18	0.03	MB-O
909	Ulla	05/17-06/02	*7.0,6.8	245	22	8.714	0.002	0.21	0.03	MB-O
929	Algunde	06/13-06/15	7.9,9.0	251	2	3.302	0.002	0.13	0.02	MB-I
1048	Feodosia	03/24-05/02	9.0,19.8	180	15	10.417	0.001	0.09	0.05	MB-O
3385	Bronnina	04/23-05/08	*2.3,7.3	216	3	2.959	0.001	0.22	0.03	FLOR
3760	Poutanen	04/23-05/08	11.4,8.7	226	14	2.9560	0.0002	0.18	0.05	MB-I

Table I. Observing circumstances and results. The first line gives the results for the primary of a binary system. The second line gives the orbital period of the satellite and the maximum attenuation. The phase angle is given for the first and last date. If preceded by an asterisk, the phase angle reached an extremum during the period. L_{PAB} and B_{PAB} are the approximate phase angle bisector longitude/latitude at mid-date range (see Harris et al., 1984). Grp is the asteroid family/group (Warner et al., 2009).

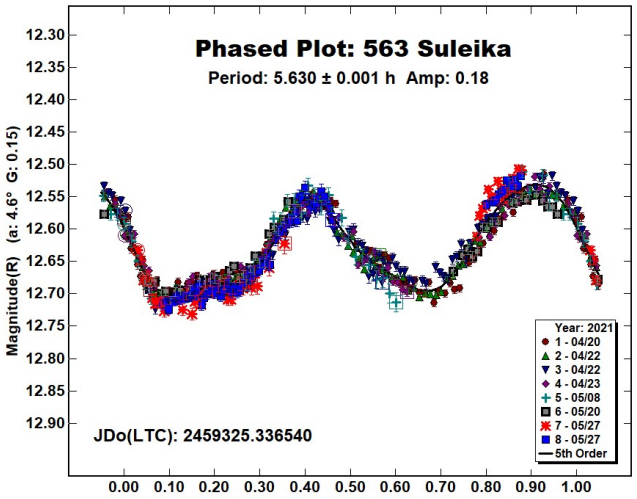

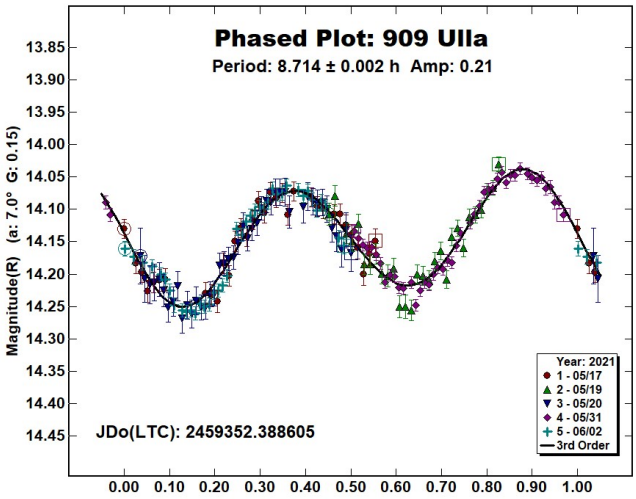

909 Ulla is an X-type (Tholen, 1984) outer main-belt asteroid member of the Cybele group that was discovered on 1919 February 7 by K. Reinmuth at Heidelberg. Collaborative observations were made over five nights. We found a synodic period of $P = 8.714 \pm 0.002$ h with an amplitude $A = 0.21 \pm 0.03$ mag. The period is close to the previously published results in the LCDB.

929 Algunde is an S-type (Bus & Binzel, 2002) inner main-belt asteroid discovered on 1920 March 10 by K. Reinmuth at Heidelberg. Collaborative observations were made over three nights. We found a synodic period of $P = 3.302 \pm 0.002$ h with an amplitude $A = 0.13 \pm 0.02$ mag. The period is close to the previously published results in the LCDB.

Observatory (MPC code)	Telescope	CCD	Filter	Observed Asteroids (#Sessions)
Astronomical Obs. of the University of Siena(K54)	0.30-m MCT f/5.6	SBIG STL-6303e (2x2)	C,Rc	81(7), 363(3), 909(1), 929(2), 3385(1), 3760(2)
HOB Astronomical Observatory (L63)	0.20-m SCT f/6.8	CMOS ASI 294 (2x2)	C	363(3), 1048(8)
Iota Scorpii(K78)	0.40-m RCT f/8.0	SBIG STXL-6303e (2x2)	Rc	563(1), 909(2), 3760(1)
Osservatorio Astronomico Margherita Hack (A57)	0.35-m SCT f/8.3	SBIG ST10XME (2x2)	Rc	563(1), 3760(2)
Seveso Observatory (C24)	0.30-m SCT f/6.3	SBIG ST9	Rc	563(1), 909(2)
Hypatia Observatory (L62)	0.25-m RCT f/5.4	SBIG ST8-XE	Rc	563(3)
GiaGa Observatory (203)	0.36-m SCT f/5.8	Moravian G2-3200	Rc	563(1), 929(1)
GAMP (104)	0.60-m NRT f/4.0	Apogee Alta	C	3385(2)
ALMO Observatory (G18)	0.24-m SCT f/5.1	Atik 4000	Rc	563(1)

Table II. Observing Instrumentations. MCT: Maksutov-Cassegrain, NRT: Newtonian Reflector, RCT: Ritchey-Chretien, SCT: Schmidt-Cassegrain.

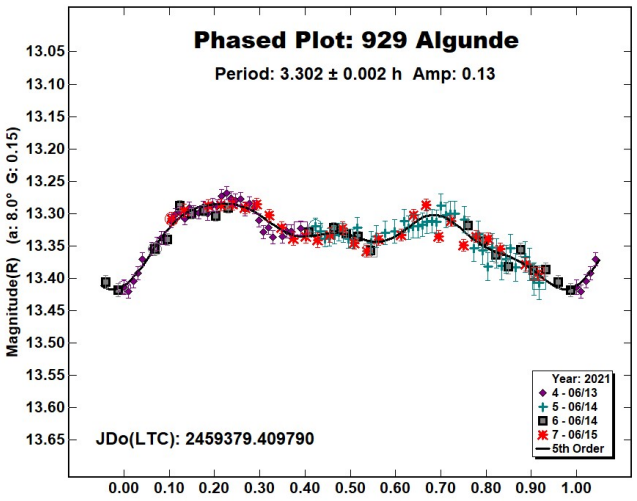

1048 Feodosia is a Ch-type (Bus & Binzel, 2002) outer main-belt asteroid discovered on 1924 November 29 by K. Reinmuth at Heidelberg. Collaborative observations were made over eight nights. We found a synodic period of $P = 10.417 \pm 0.001$ h with an amplitude $A = 0.09 \pm 0.05$ mag. The period is close to the previously published results in the LCDB.

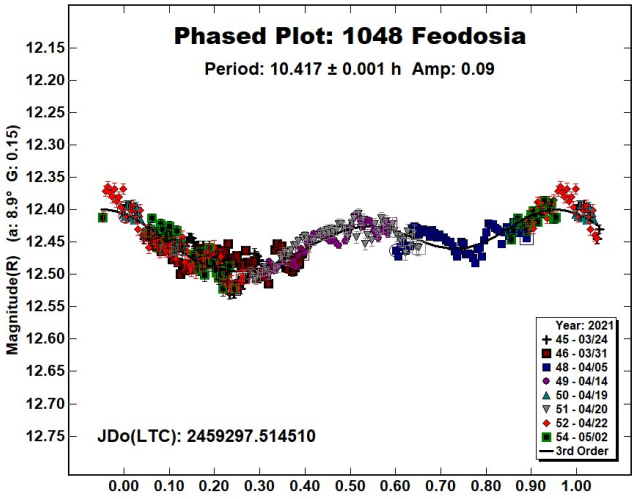

3385 Bronnina is an S-type (Bus & Binzel, 2002) inner main-belt asteroid member of the Flora family; it was discovered on 1979 September 24 by N. Chernykh at Nauchnyj. Collaborative observations were made over two nights. We found a synodic period of $P = 2.959 \pm 0.001$ h with an amplitude $A = 0.22 \pm 0.03$ mag. The period is close to the previously published results in the LCDB.

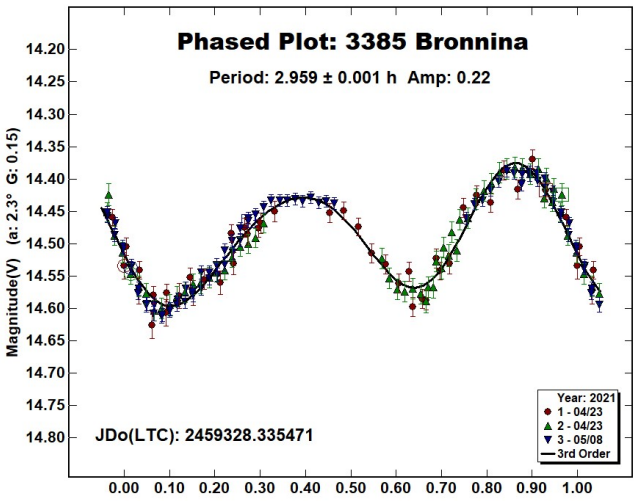

3760 Poutanen is a medium-albedo inner main-belt asteroid discovered on 1984 January 8 by E. Bowell at Flagstaff. Collaborative observations were made over four nights. We found a synodic period of $P = 2.9560 \pm 0.0002$ h with an amplitude $A = 0.18 \pm 0.05$ mag. The period is close to the previously published results in the LCDB.

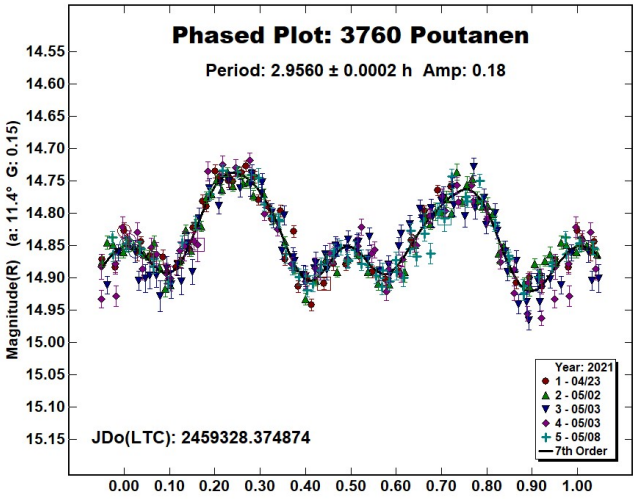

References

Bus, S.J.; Binzel, R.P. (2002). "Phase II of the Small Main-Belt Asteroid Spectroscopic Survey - A Feature-Based Taxonomy." *Icarus* **158**, 146-177.

Harris, A.W.; Young, J.W.; Scaltriti, F.; Zappala, V. (1984). "Lightcurves and phase relations of the asteroids 82 Alkmene and 444 Gyptis." *Icarus* **57**, 251-258.

Tholen, D.J. (1984). "Asteroid taxonomy from cluster analysis of Photometry." Doctoral Thesis. University Arizona, Tucson.

UAI (2021), "Unione Astrofili Italiani" web site. *https://www.uai.it*

Warner, B.D.; Harris, A.W.; Pravec, P. (2009) "The asteroid lightcurve database." *Icarus* **202**, 134-146. Updated 2021 July 6. *http://www.minorplanet.info/lightcurvedatabase.html*

Warner, B.D. (2021). MPO Software, *MPO Canopus* v10.8.4.2. Bdw Publishing. *http://minorplanetobserver.com*

LIGHTCURVES OF TWELVE ASTEROIDS

Eric V. Dose
3167 San Mateo Blvd NE #329
Albuquerque, NM 87110
mp@ericdose.com

(Received: 2021 July 13, Revised: 2021 August 16)

We present lightcurves, synodic rotation periods, and G value (H-G) estimates for twelve asteroids, obtained by applying dozens of comparison stars from the ATLAS refcat2 catalog to each working image.

We present asteroid lightcurve photometry results obtained by following the workflow process described by Dose (2020a), with later improvements (Dose, 2020b). This workflow applies to each image an ensemble of typically 20-60 nearby ATLAS refcat2 catalog (Tonry et al., 2018) comparison ("comp") stars as a basis for asteroid photometry. Diagnostic plots and numerous comp stars allow for effective identification and removal of outlier, variable, and poorly measured comp stars.

The custom workflow produces a time series of asteroid magnitude estimates on Sloan r' (SR) catalog basis, unreduced and without H-G adjustment. These magnitudes are imported directly into *MPO Canopus* software (Warner, 2018) where they are adjusted for distances and phase-angle dependence, fit by Fourier analysis including identifying and ruling out of aliases, and plotted. Phase-angle dependence is corrected with a H-G model, using $G = 0.15$ for each asteroid unless otherwise specified.

No nightly zero-point adjustments (DeltaComps in *MPO Canopus* terminology) were made to any session herein, other than by adjusting the G value (H-G phase model). All lightcurve data herein have been submitted to ALCDEF.

Lightcurve Results

Twelve asteroids were observed from Deep Sky West observatory (IAU V28) at 2210 meters elevation in northern New Mexico. Images were acquired with a 0.35-meter SCT reduced to f/7.7; a SBIG STXL-6303E camera cooled to -35 C and fitted with a Clear filter (Astrodon); and a PlaneWave L-500 mount. The equipment was operated remotely via ACP software version 8.3 (DC-3 Dreams), running plan files generated for each night by the author's python scripts (Dose, 2020a). Observations often cycled between 2-4 asteroids. Exposure times targeted 5-8 millimagnitudes uncertainty in asteroid instrumental magnitude, subject to a minimum of 120 seconds to ensure suitable comp-star photometry, and to a maximum of 900 seconds. All exposures were autoguided.

FITS images were plate-solved by *PinPoint* (DC-3 Dreams) or *TheSkyX* (Software Bisque) and were calibrated using temperature-matched, median-averaged dark images and recent flat images of a flux-adjustable flat panel. Every photometric image was visually inspected; all images with poor tracking, obvious interference by cloud or moon, or having stars or other light sources within 10 arcseconds of the target asteroid were excluded. Photometry-ready images that pass these screens were submitted to the workflow, which applies separately measured second-order transforms from Clear filter to deliver asteroid magnitudes in Sloan r' passband.

In this work, "period" refers to an asteroid's synodic rotation period, and "SR" denotes the Sloan r' passband.

329 Svea. This bright inner main-belt asteroid was found to have a period of 22.777 ± 0.005 hours, in agreement with several previous reports (22.770 h, Behrend, 2006web; 22.6 h, Menke et al., 2008; 22.778 h, Marciniak et al., 2015; and 22.777 h, Marciniak et al. 2018) and consistent with another (>12 h, Behrend, 2017web), but differing from two reports (15 h, Weidenschilling et al., 1990; 15.201 h, Pray, 2006). Fourier fit to the present data has RMS error of 7 millimagnitudes and indicates a G value (H-G phase model) close to 0.20.

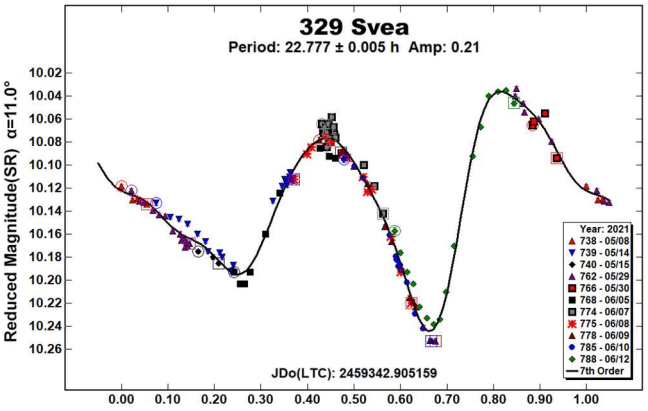

486 Cremona. This inner main-belt asteroid was found to have a period of 65.203 ± 0.027 h, in general agreement with most previous reports (65.90 h, Warner, 2006; 65.15 h, Cooney Jr. et al., 2007; 65.151 h, Hanuš et al., 2011; 65.178 h, McNeill et al., 2019; 65.0918 h, Pál et al., 2020), but differing from one early report (77.5 h, Behrend, 2006web). Fourier fit to the present data has RMS error of 7 millimagnitudes and indicates a G value close to 0.18.

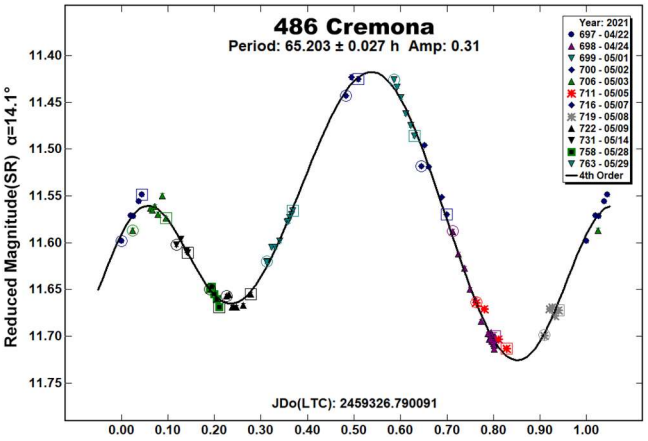

527 Euryanthe. This asteroid of unknown family was found to have a period 42.854 ± 0.008 h, agreeing at least generally with several recent reports (42.986 h, Polakis and Skiff, 2019; 42.9 h, Behrend, 2020web; 42.93 h, Pilcher, 2020; 43.40 h, Polakis, 2020; 42.3819 h, Pál et al., 2020; 42.75 h, Pilcher, 2021), but differing from one earlier report (26.06 h, Brinsfield, 2010). Our Fourier fit has RMS error of 9 millimagnitudes and indicates a G value close to 0.09.

When adjusted for differing starting phases, the present lightcurve closely resembles the more complete lightcurve of (Pilcher, 2021), taken near the same date. They match especially in that the two minima appear to differ in shape; both lightcurves support a bimodal interpretation.

Number	Name	yyyy mm/dd	Phase	L_{PAB}	B_{PAB}	Period(h)	P.E.	Amp	A.E.	Grp
329	Svea	2021 05/09-06/12	*10.9,13.8	240	19	22.777	0.005	0.21	0.02	MB-I
486	Cremona	2021 04/22-05/29	*14.3,11.8	231	12	65.203	0.027	0.31	0.02	MB-I
527	Euryanthe	2021 03/27-05/27	*10.6,14.6	210	12	42.854	0.008	0.14	0.02	UNK
664	Judith	2021 03/28-04/24	13.9,5.4	221	8	19.306	0.002	0.32	0.02	UNK
1056	Azalea	2021 03/23-05/03	*5.8,15.9	191	7	15.032	0.002	0.53	0.04	FLOR
1118	Hanskya	2020-21 12/22-03/08	4.4,17.1	90	11	25.310	0.002	0.29	0.04	MB-O
1428	Mombasa	2021 05/05-06/10	*7.6,13.6	224	20	25.621	0.004	0.16	0.03	MB-O
1504	Lappeenranta	2021 04/11-05/30	*15.3,11.7	228	11	15.187	0.002	0.18	0.02	MB-I
1886	Lowell	2021 03/27-06/12	*13.9,19.7	215	14	157.872	0.074	0.72	0.10	EUN
2261	Keeler	2021 03/23-05/01	*23.4,25.7	195	34	22.813	0.004	0.10	0.02	PHO
4107	Rufino	2021 03/29-05/09	17.4,25.1	158	8	22.371	0.004	0.15	0.05	MB-I
5551	Glikson	2021 03/20-04/19	20.9,23.8	184	33	148.352	0.144	0.82	0.10	PHO

Table I. Observing circumstances and results. The phase angle is given for the first and last date. If preceded by an asterisk, the phase angle reached an extrema during the period. L_{PAB} and B_{PAB} are the approximate phase angle bisector longitude/latitude at mid-date range (see Harris et al., 1984). Grp is the asteroid family/group (Warner et al., 2009).

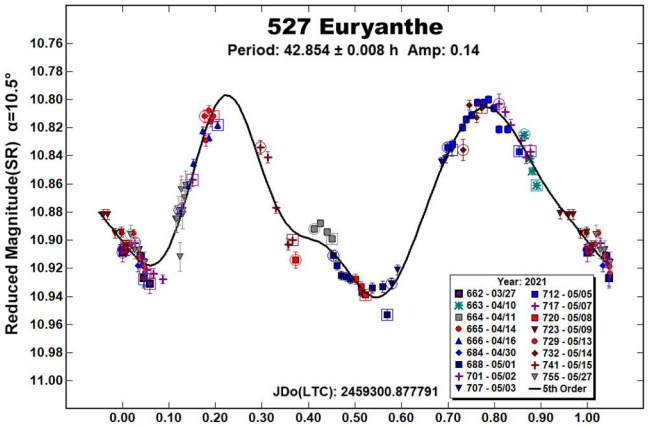

664 Judith. This asteroid of unknown family was found to have a period of 19.3065 ± 0.0025 h, in fair agreement with two previous reports (19.35 h, Melton et al., 2012; 19.3709 h, Pál et al., 2020) and consistent with another (>12 h, Behrend, 2009web), but differing from several others (10.76 h, Degraff et al., 1998; 13.764 h, Behrend, 2010web; 10.6829 h, Hosek et al., 2011; and 18.51 h, Garceràn et al., 2015).

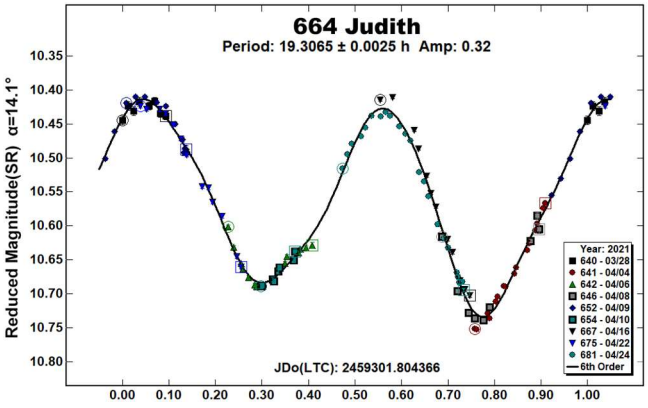

The previously reported period of 10.6829 h is an alias by exactly 1 period per 24 hours of our 19.3065 h; the previously reported 13.764 h is similarly an alias by exactly ½ period per 24 hours. Fourier fit to the present data has RMS error of 10 millimagnitudes and indicates a G value close to 0.07.

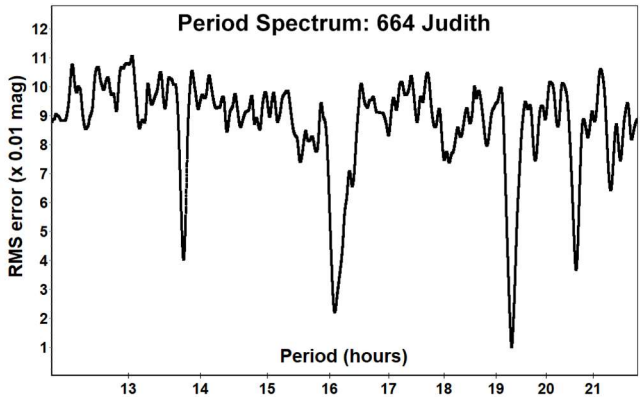

1056 Azalea. This Flora asteroid was found to have a period of 15.032 ± 0.002 h, agreeing with previous reports (15.15 h, Behrend, 2004web; 15.03 h, Kryszczyńska et al., 2012; 15.0276 h, Hanuš et al., 2013; 15.034 h, Erasmus et al., 2020). Fourier fit to the present data has RMS error of 18 millimagnitudes and indicates a G value close to 0.30.

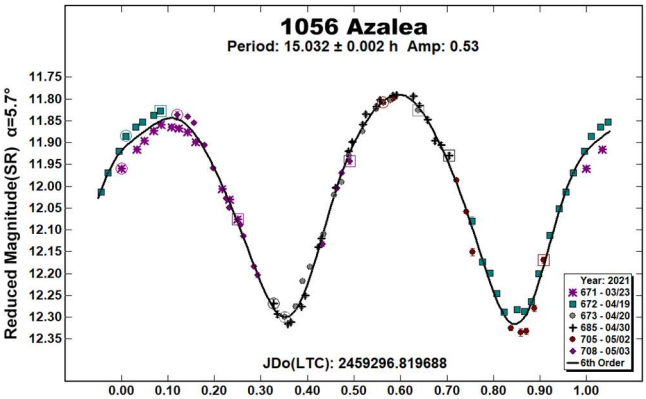

1118 Hanskya. This outer main-belt asteroid was found to have a period of 25.310 ± 0.002 h, differing from one early report (15.61 h, Robinson, 2002) but agreeing with all other period reports found (25.31 h, Behrend, 2007web; 25.348 h, Waszczak et al., 2015; 25.38 h, Ditteon and Young, 2018; 25.305 h, Ďurech and Hanuš, 2018). Fourier fit to the present data has RMS error of 15 millimagnitudes and indicates a G value close to 0.12.

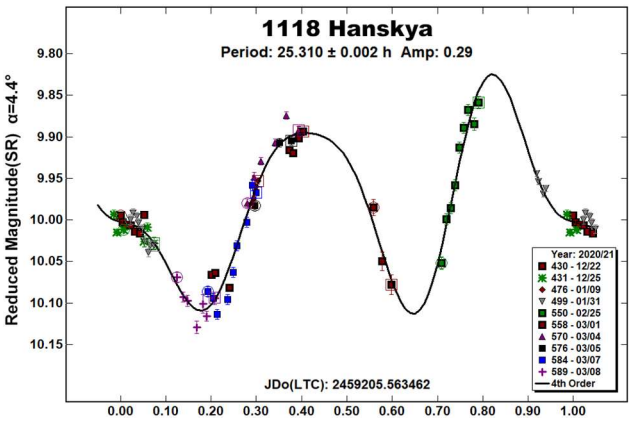

Despite sparser than ideal phase coverage within the current lightcurve, the 11 weeks' observing span and the resulting period spectrum strongly support the proposed period.

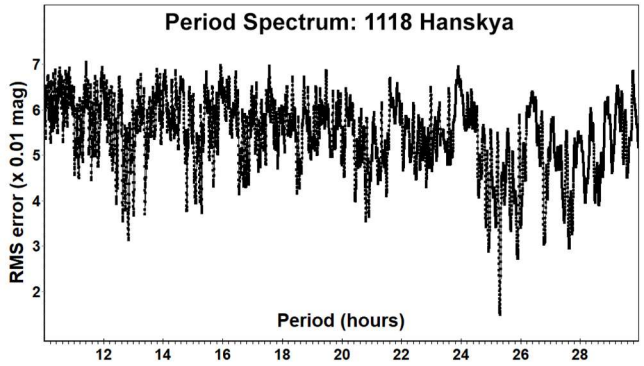

1428 Mombasa. This outer main-belt asteroid was found to have a period of 25.621 ± 0.004 h, agreeing only with one recent survey estimate (25.646 h, Pál et al., 2020), and differing from all three other reports known (17.6 h, Behrend, 2006web; 17.12 h, Hawkins and Ditteon, 2008; and 16.67 h, Stephens, 2012web). Fourier fit to the present data has RMS error of 12 millimagnitudes and indicates a G value close to 0.10.

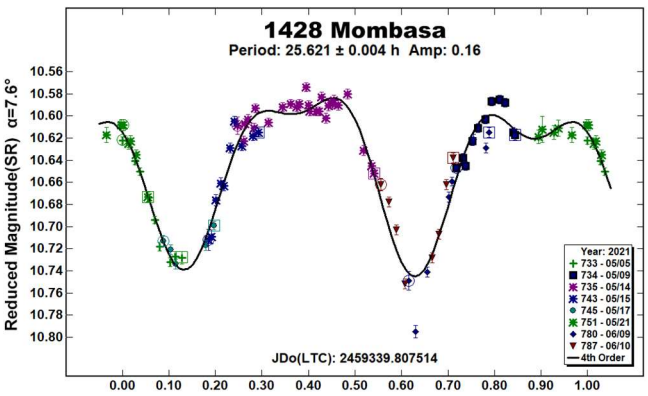

We note that a period estimate of 16.67 h is almost exactly an alias, by ½ period per 24 hours, of our proposed period. Period candidates in the 16-18 h range are essentially absent from our period spectrum.

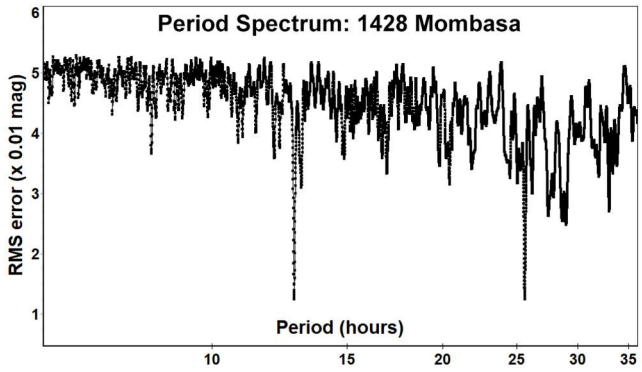

1504 Lappeenranta. This inner main-belt asteroid was found to have a period of 15.187 ± 0.002 h, agreeing with four recent reports (15.190 h, Garlitz, 2013web; 15.16 h, Polakis and Skiff, 2017; 15.18 h, Ditteon et al., 2019; 15.2385 h, Pál et al., 2020), but differing from three earlier reports (10.44 h, Binzel, 1987; 8 h, Behrend, 2002web; 8 h Behrend, 2006web). We find no evidence favoring a bimodal lightcurve shape (period ca. 30.4 h) over the proposed monomodal lightcurve shape, which is dominated by the sharp brightening from phase 0.9 to 0.15 (see phase plot). Fourier fit to the present data has RMS error of 10 millimagnitudes and yields G value close to 0.32.

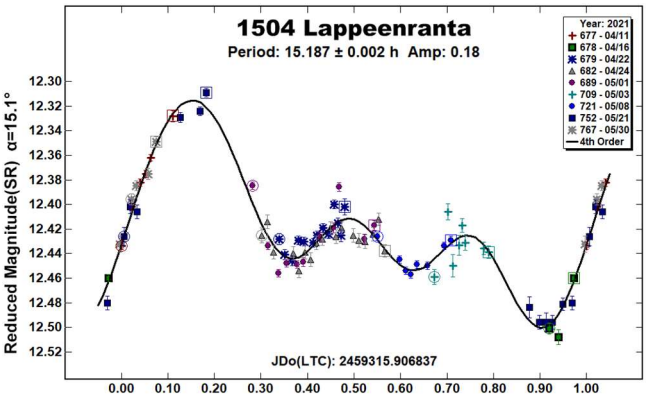

1886 Lowell. This Eunomia-family asteroid was found to have a period 157.872 ± 0.074 h. The lightcurve shape is bimodal, and is roughly twice the only known previous period report, a survey result (80.1898 h, Pál et al., 2020). The very high amplitude of the present lightcurve does not support a monomodal interpretation (Harris et al., 2014), and the two minima differ in shape, as well. Fourier fit to the present data has RMS error of 28 millimagnitudes and indicates a G value close to 0.45.

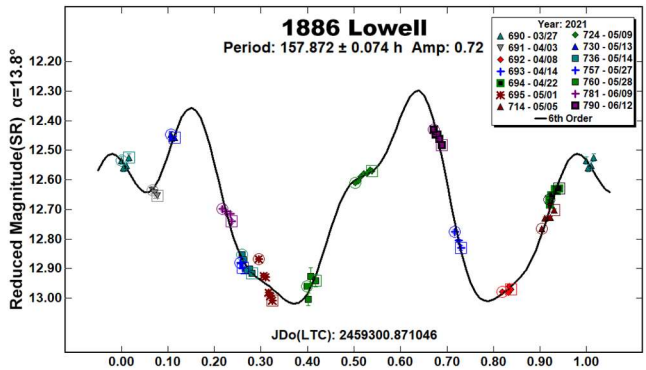

2261 Keeler. This Phocaea asteroid was found to have a period of 22.813 ± 0.004 h, agreeing approximately with both known previous reports (22.810 h, Warner et al., 2011; 22.7596 h, Pál et al., 2020). The lightcurve is clearly bimodal and appears to rule out the monomodal alternative interpretation mentioned by Warner et al (2011). Fourier fit to the present data has RMS error of 7 millimagnitudes, and though the observations' phase angle range is narrow, the best fits indicate a remarkable G value close to 1.05.

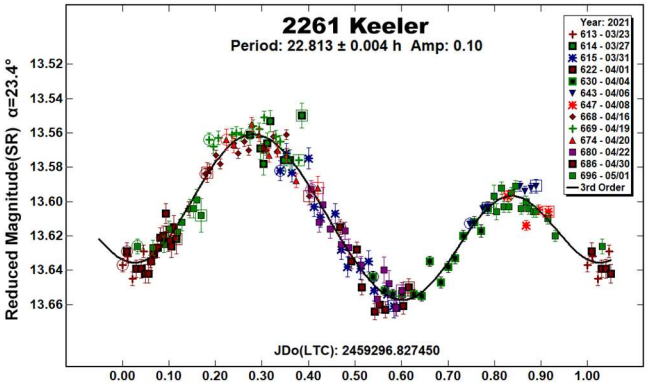

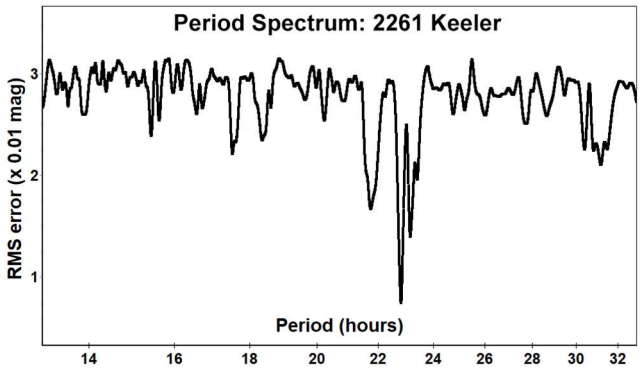

4107 Rufino. This inner main-belt asteroid was found to have a period of 22.371 ± 0.004 h, agreeing with one survey report of 22.352 h (Waszczak et al., 2015) but differing from a report of 15.31 h (Behrend, 2017 web) which appears to be an alias by ½ rotation per 24 hours from our result. Fourier fit to the present data has RMS error of 9 millimagnitudes and indicates a G value close to 0.20.

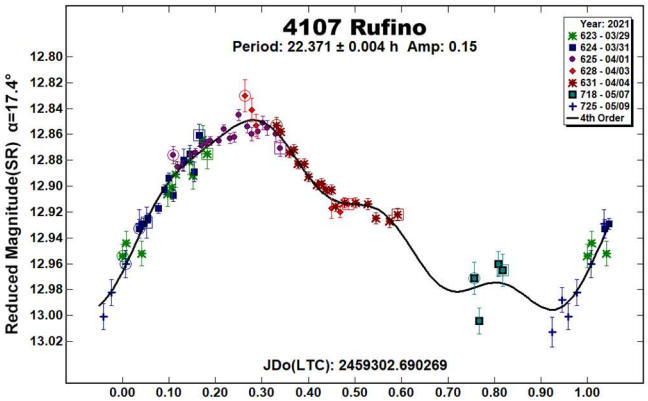

Our lightcurve suffers incomplete phase coverage, but with 7 nights' observations the period spectrum supports the proposed period, certainly in preference to candidate periods of 15-16 h.

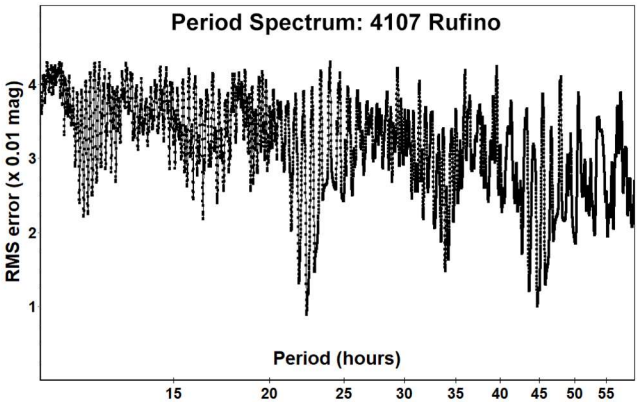

5551 Glikson. This Phocaea asteroid was found to have a period of 148.352 ± 0.144 h, differing from the sole known previous period report of 91.43 h (Pravec et al., 2014web). The lightcurve shape is trimodal and suggests some tumbling effect. Fourier fit to the present data has RMS error of 46 millimagnitudes and indicates a G value close to 0.60.

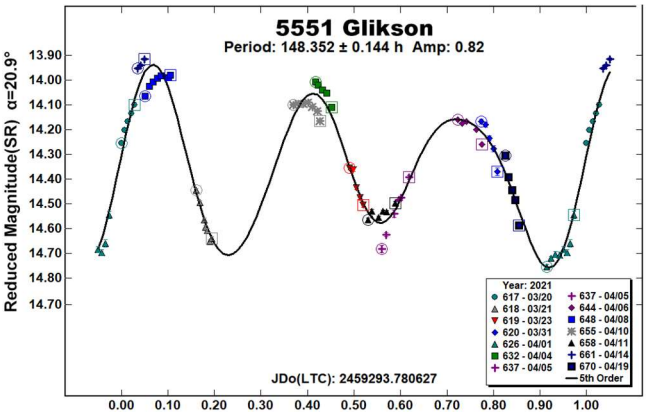

The previously reported period of 91.43 h and the 2/3 (bimodal) candidate period of ca. 99 h appear as minor signals in the period spectrum. But from our 14 nights' observations, the trimodal period proposed here emerges as a superior fit to the observations.

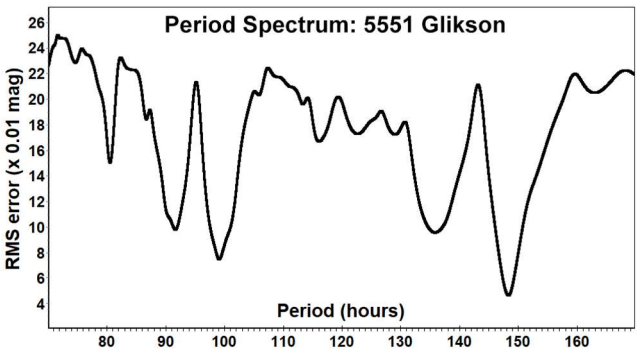

Acknowledgements

The author thanks all authors of the ATLAS paper (Tonry et al, 2018) and numerous contributors for providing without cost the ATLAS refcat2 release catalog and its technical descriptions. This project makes extensive use of the python language interpreter and of several supporting packages (notably: pandas, ephem, matplotlib, requests, astropy, and statsmodels), all provided without cost, and without which this work would have been infeasible.

References

Behrend, R. (2002web, 2004web, 2006web, 2007web, 2009web, 2010web, 2017web, 2020web). Observatoire de Genève web site. *http://obswww.unige.ch/~behrend/page_cou.html*

Binzel, R.P. (1987). "A photoelectric survey of 130 asteroids." *Icarus* **72**, 135-208.

Brinsfield, J.W. (2010). "Asteroid Lightcurve Analysis at the Via Capote Observatory: 4th Quarter 2009." *Minor Planet Bull.* **37**, 50-53.

Cooney Jr., W.R.; Gross, J.; Terrell, D.; Reddy, V.; Dyvig, R. (2007). "Lightcurve Results for 486 Cremona, 855 Newcombia, 942 Romilda, 3908 Nyx, 5139 Rumoi, 5653 Camarillo, (102866) 1999 WA5." *Minor Planet Bull.* **34**, 47-49.

Degraff, D.R.; Robbins, A.M.; Gutermuth, R.A. (1998). "Rotation Curves for 13 Asteroids." *Bull. Amer. Astron. Soc.* **30**, 1390.

Ditteon, R.; Young, J. (2018). "Lightcurve Analysis of Minor Planets Observed at the Oakley Southern Sky Observatory: 2017 March - May." *Minor Planet Bull.* **45**, 117-119.

Ditteon, R.; Johnson, D.; Weichang, L.; Zibo, W.; Zhao, B. (2019). "Lightcurve Analysis of Minor Planets Observed at the Oakley Southern Sky Observatory: 2018 August-September." *Minor Planet Bull.* **46**, 280-282.

Dose, E. (2020a). "A New Photometric Workflow and Lightcurves of Fifteen Asteroids." *Minor Planet Bull.* **47**, 324-330.

Dose, E. (2020b). "Lightcurves of Nineteen Asteroids." *Minor Planet Bull.* **48**, 69-76.

Ďurech, J.; Hanuš, J. (2018). "Reconstruction of asteroid spin states from Gaia DR2 photometry." *Astron. Astrophys.* **620**, A91.

Erasmus, N.; Navarro-Meza, S.; McNeill, A.; Trilling, D.E.; Sickafoose, A.A.; Denneau, L.; Flewelling, H.; Heinze, A.; Tonry, J.L. (2020). "Investigating Taxonomic Diversity within Asteroid Families through ATLAS Dual-band Photometry." *Astrophys. J. Suppl. Series* **247**, 13.

Garceràn, A.C.; Macias, A.A.; Mansego, E.A.; Rodriguez, P.B.; de Haro, J.L. (2015). "Lightcurve Analysis of Six Asteroids." *Minor Planet Bull.* **42**, 235-237.

Garlitz, J. (2013web). Posting on the CALL website. *http://www.minorplanet.info/call.html*

Hanuš, J. and 14 colleagues (2011). "A study of asteroid pole-latitude distribution based on an extended set of shape models derived by the lightcurve inversion method." *Astron. Astrophys.* **530**, A134.

Hanuš, J. and 119 colleagues (2013). "Asteroids' physical models from combined dense and sparse photometry and scaling of the YORP effect by the observed obliquity distribution." *Astron. Astrophys.* **551**, A67.

Harris, A.W.; Young, J.W.; Scaltriti, F.; Zappalà, V. (1984). "Lightcurves and phase relations of the asteroids 82 Alkmene and 444 Gyptis." *Icarus* **57**, 251-258.

Harris, A.W.; Pravec, P.; Galád, A.; Skiff, B.A.; Warner, B.D.; Világi, J.; Gajdoš, Š.; Carbognani, A.; Hornoch, K.; Kušnirák, P.; Cooney, W.R.; Gross, J.; Terrell, D.; Higgins, D.; Bowell, E.; Koehn, B.W. (2014). "On the maximum amplitude of harmonics on an asteroid lightcurve." *Icarus* **235**, 55-59.

Hawkins, S.; Ditteon, R. (2008). "Asteroid Lightcurve Analysis at the Oakley Observatory - May 2007." *Minor Planet Bull.* **35**, 1-4.

Hosek, M.; Cooke, W.J.; Suggs, R.M. (2011). "Lightcurve Analysis of Asteroids 664 Judith and (20453) 1999 KL6." *Minor Planet Bull.* **38**, 11-12.

Kryszczyńska, A. and 29 colleagues (2012). "Do Slivan states exist in the Flora family? I. Photometric survey of the Flora region." *Astron. Astrophys.* **546**, A72.

Marciniak, A. and 23 colleagues (2015). "Against the biases in spins and shapes of asteroids." *Planetary Space Sci.*, **118**, 256-266.

Marciniak, A. and 42 colleagues (2018). "Photometric survey, modelling, and scaling of long-period and low-amplitude asteroids." *Astron. Astrophys.*, **610**, A7.

McNeill, A.; Mommert, M.; Trilling, D.E.; Llama, J; Skiff, B. (2019). "Asteroid Photometry from the Transiting Exoplanet Survey Satellite: A Pilot Study." *Astrophys. J. Suppl. Series.* **245**, 29.

Melton, E.; Carver, S.; Harris, A.; Karnemaat, R.; Klaasse, M.; Ditteon, R. (2012). "Asteroid Lightcurve Analysis at the Oakley Southern Sky Observatory: 2011 November-December." *Minor Planet Bull.* **39**, 131-133.

Menke, J.; Cooney, W.; Gross, J.; Terrell, D.; Higgins, D. (2008). "Asteroid Lightcurve Analysis at Menke Observatory." *Minor Planet Bull.* **35**, 155-160.

Pál, A.; Szakáts, R.; Kiss, C.; Bódi, A.; Bognár, Z.; Kalup, C.; Kiss, L.L.; Marton, G.; Molnár, L.; Plachy, E.; Sárneczky, K.; Szabó, G.M.; Szabó, R. (2020). "Solar System Objects Observed with TESS-First Data Release: Bright Main-belt and Trojan Asteroids from the Southern Survey." *Astrophys. J. Suppl. Series* **247**, 26.

Pilcher, F. (2020). "Lightcurves and Rotation Periods of 83 Beatrix, 86 Semele, 118 Peitho, 153 Hilda, 527 Euryanthe, and 549 Jessonda." *Minor Planet Bull.* **47**, 192-195.

Pilcher, F. (2021). "Lightcurves and Rotation Periods of 47 Aglaja, 504 Cora, 527 Euryanthe, 593 Titania, and 594 Mireille." *Minor Planet Bull.* **48**, 217-218.

Polakis, T.; Skiff, B. (2017). "Lightcurve Analysis for 341 California, 594 Mireille, 1115 Sabauda, 1504 Lappeenranta, and 1926 Demiddelaer." *Minor Planet Bull.* **44**, 299-302.

Polakis, T.; Skiff, B. (2019). "Lightcurves of Eleven Main-belt Minor Planets." *Minor Planet Bull.* **46**, 132-137.

Polakis, T. (2020). "Photometric Observations of Thirty Minor Planets." *Minor Planet Bull.* **47**, 177-186.

Pravec, P.; Wolf, M.; Saruonova, L. (2014web). Entry on the Ondrejov Asteroid Photometry Project web page (as cited on LCDB web site). *http://www.asu.cas.cz/~ppravec/neo.htm*

Pray, D.P. (2006). "Lightcurve analysis of asteroids 326, 329, 426, 619, 1829, 1967, 2453, 10518 and 42267." *Minor Planet Bull.* **33**, 4-5.

Robinson, L.E. (2002). "Lightcurve Photometry of 551 Ortrud, 1118 Hanskya, and 1916 Boreas from Sunflower Observatory." *Minor Planet Bull.* **29**, 37-38.

Stephens, R.D. (2012web). Posting on the CALL web site, *http://www.minorplanet.info/call.html*

Tonry, J.L.; Denneau, L.; Flewelling, H.; Heinze, A.N.; Onken, C.A.; Smartt, S.J.; Stalder, B.; Weiland, H.J.; Wolf, C. (2018). "The ATLAS All-Sky Stellar Reference Catalog." *Astrophys. J.* **867**, A105, 1-16.

Warner, B.D. (2006). "Asteroid Lightcurve Analysis at the Palmer Divide Observatory - February-March 2006." *Minor Planet Bull.* **33**, 82-84.

Warner, B.D.; Harris, A.W.; Pravec, P. (2009). "The asteroid lightcurve database." *Icarus* **202**, 134-146. Updated 2020 August. *http://www.minorplanet.info/lightcurvedatabase.html*

Warner, B.D.; Pravec, P.; Kušnirák, P.; Pray, D.P.; Durkee, R.; Galád, A. (2011). "Lightcurve Analysis of 2261 Keeler." *Minor Planet Bull.* **38**, 3.

Warner, B.D. (2018). *MPO Canopus* Software, version 10.7.12.9, BDW Publishing. *http://www.bdwpublishing.com*

Waszczak, A.; Chang, C.-K.; Ofek, E.O.; Laher, R.; Masci, F.; Levitan, D.; Surace, J.; Cheng, Y.-C.; Ip, W.-H.; Kinoshita, D.; Helou, G.; Prince, T.A.; Kulkarni, S. (2015). "Asteroid Light Curves from the Palomar Transient Factory Survey: Rotation Periods and Phase Functions from Sparse Photometry." *Astron. J.* **150**, 75.

Weidenschilling, S.J.; Chapman, C.R.; Davis, D.R.; Greenberg, R.; Levy, D.H.; Binzel, R.P.; Vail, S.M.; Magee, M.; Spaute, D. (1990). "Photometric Geodesy of main-belt asteroids: III. Additional Lightcurves." *Icarus* **86**, 402-447.

MAIN-BELT ASTEROIDS OBSERVED FROM CS3: 2021 APRIL-MAY

Robert D. Stephens
Center for Solar System Studies (CS3) / MoreData!
11355 Mount Johnson Ct., Rancho Cucamonga, CA 91737 USA
rstephens@foxandstephens.com

Daniel R. Coley
Center for Solar System Studies (CS3)
Corona, CA

Brian D. Warner
Center for Solar System Studies (CS3) / MoreData!
Eaton, CO

(Received: 2021 July 12)

CCD photometric observations of 11 main-belt asteroids were obtained at the Center for Solar System Studies (CS3) from 2021 April-May. In addition, recovered data from 2019 allowed finding lightcurve parameters for 1413 Roucarie. New pole/shape modeling results are presented for 323 Brucia and 1106 Cydonia. The recovered data for 1413 Roucarie did not have an effect on a previously published shape model.

The Center for Solar System Studies (CS3) has nine telescopes which are normally used in program asteroid family studies. The focus is on near-Earth asteroids, but when suitable targets are not available, Jovian Trojans and Hildas are observed. When a nearly full moon is too close to the family targets being studied, targets of opportunity amongst the main-belt families were selected.

Table I lists the telescopes and CCD cameras that were used to make the observations. Images were unbinned with no filter and had master flats and darks applied. The exposures depended upon various factors including magnitude of the target, sky motion, and Moon illumination.

Telescope	Camera
0.30-m f/6.3 Schmidt-Cass	SBIG 1001E
0.35-m f/9.1 Schmidt-Cass	FLI Microline 1001E
0.35-m f/9.1 Schmidt-Cass	FLI Microline 1001E
0.35-m f/9.1 Schmidt-Cass	FLI Microline 1001E
0.35-m f/10 Schmidt-Cass	SBIG 1001E
0.35-m f/10 Schmidt-Cass	FLI Proline 1001E
0.40-m f/10 Schmidt-Cass	FLI Proline 1001E
0.40-m f/10 Schmidt-Cass	FLI Proline 1001E
0.50-m F8.1 R-C	FLI Proline 1001E

Table I: List of CS3 telescope/CCD camera combinations.

Image processing, measurement, and period analysis were done using *MPO Canopus* (Bdw Publishing), which incorporates the Fourier analysis algorithm (FALC) developed by Harris (Harris et al., 1989). For the images reduced in 2021, the Comp Star Selector feature in *MPO Canopus* was used to limit the comparison stars to near solar color. Night-to-night calibration was done using field stars from the ATLAS catalog (Tonry et al., 2018), which has Sloan *griz* magnitudes that were derived from the GAIA and Pan-STARR catalogs and are "native" magnitudes of the catalog. Those adjustments are usually $\leq \pm 0.03$ mag. The rare greater corrections may have been related in part to using unfiltered observations, poor centroiding of the reference stars, and not correcting for second-order extinction.

The Y-axis values are ATLAS SR "sky" magnitudes. The two values in the parentheses are the phase angle (a) and the value of *G* used to normalize the data to the comparison stars used in the earliest session. This, in effect, made all the observations seem to be made at a single fixed date/time and phase angle, leaving any variations due only to the asteroid's rotation and/or albedo changes. The X-axis shows rotational phase from –0.05 to 1.05. If the plot includes the amplitude, e.g., "Amp: 0.65", this is the amplitude of the Fourier model curve and *not necessarily the adopted amplitude for the lightcurve*.

For brevity, only some of the previously reported rotational periods may be referenced. A complete list is available at the asteroid lightcurve database (LCDB; Warner et al., 2009).

323 Brucia. This member of the Phocaea dynamical family has been observed several times in the past. Schober et al. (1993) and Behrend (2006web) who both reported periods near 9.46 h. We observed it twice (Warner 2014; 2018) also finding a period near 9.46 h. Our results this year is in good agreement with those prior results.

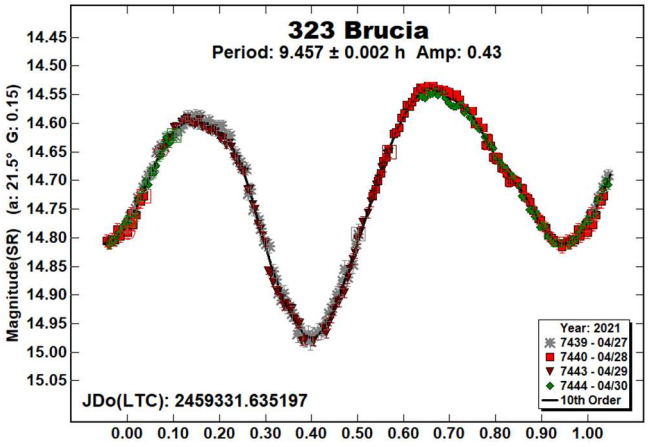

In addition to our dense data from the two apparitions, we used sparse data from the AstDyS-2 site to solve for the sidereal period and pole position and to create a shape model using *MPO LCInvert* (Bdw Publishing).

The model showed two possible solutions 180° apart; (λ, β, *P*) = (237°, 16°, 9.459492 h) and (λ, β, *P*) = (57°, -19°, 9.459500 h). Our preferred solution is (237°, 16°). Assuming c = 1.0 for a triaxial ellipsoid, a/b = 1.2 and a/c ratio 1.6.

1106 Cydonia. This member of the Eunomia dynamical family has been observed three times in the past. Klinglesmith et al. (2016) and Aznar (2017) each found a period near 2.67 h. We observed it (Stephens and Warner 2020) finding a period of 2.678 h. Our result this year is in good agreement with these prior periods.

Using the Klinglesmith et al. data found on the ALCDEF website, our dense data from the two apparitions, and sparse data from the AstDyS-2 site to solve for the sidereal period and pole position and create a shape model, using *MPO LCInvert* (Bdw Publishing).

Our pole model showed two possible solutions about 180° apart: (λ, β, *P*) = (336°, -25°, 2.679720 h) and (λ, β, *P*) = (145°, -22°, 2.679720 h). Our preferred solution is (336°, -25°). Assuming c = 1.0 for a triaxial ellipsoid, a/b = 1.2 and a/c = 1.5.

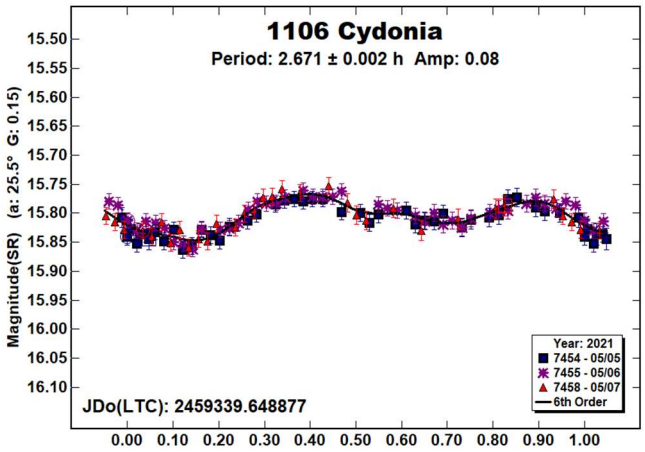

1257 Mora. This inner main-belt asteroid was originally observed by Binzel (1987). Periods were later reported twice by Behrend (2009web; 2011web). All of the prior periods were near 5.3 h. Our results this year is in good agreement with those prior results.

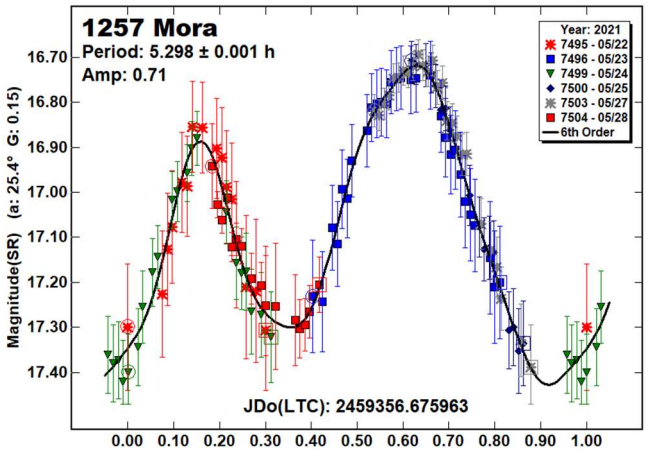

1413 Roucarie. We observed this member of the EOS dynamical family in 2011, 2013 and 2021 finding periods near 6.53 h (Stephens et al., 2021; and references therein). Subsequent to that report, we recovered more data from 2019 which are consistent with the prior results.

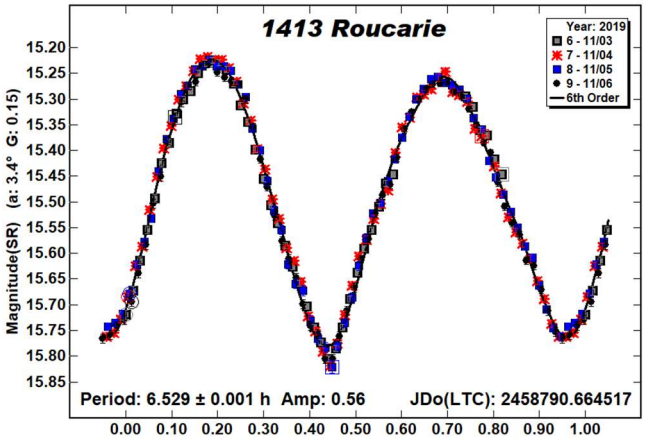

Using sparse data from the Lowell Photometric Database and WISE data, Ďurech et al. (2018) reported a spin axis model with (λ, β) = (124°, 5°) or (310°, 5°) and a sidereal period of 6.53058 h. Without including our new data from 2019, we previously found two possible pole solutions that are about 180° apart: (λ, β, *P*) = (122°, 10°, 6.530557 h) and (311°, 37°, 6.530558 h). Our preferred solution is (122°, 10°).

(7792) 1995 WZ3. This inner main-belt asteroid was observed by the Photometric Survey for Asynchronous Binary Asteroids (Pravec et al., 2007web) who found a period of 3.16001 h. Our results this year is in good agreement with that prior result.

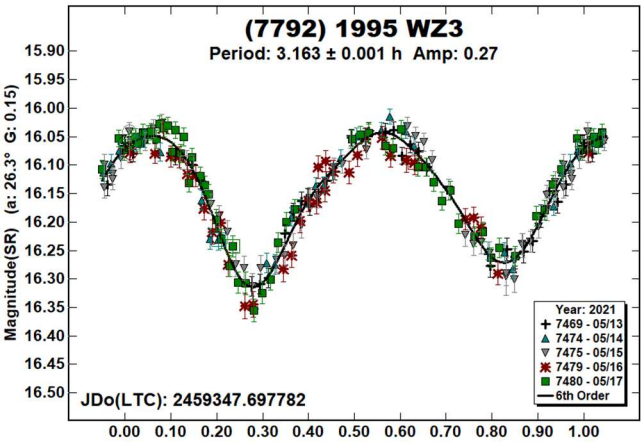

10177 Ellison. This member of the Vesta dynamical family has been observed only once in the past. Erasmus et al. (2020) using data from the ATLAS survey found a period of 7.271 h. Our result this year is in good agreement with that prior result. With an amplitude of only 0.10 mag., there is no assurance of a bimodal lightcurve (Harris et al., 2014). The period spectrum shows possible solutions near 3.5 h, 10.8 h, and 14.4 h. However, those solutions are single modal, trimodal, and quadrimodal lightcurves, and are not more likely than our bimodal solution.

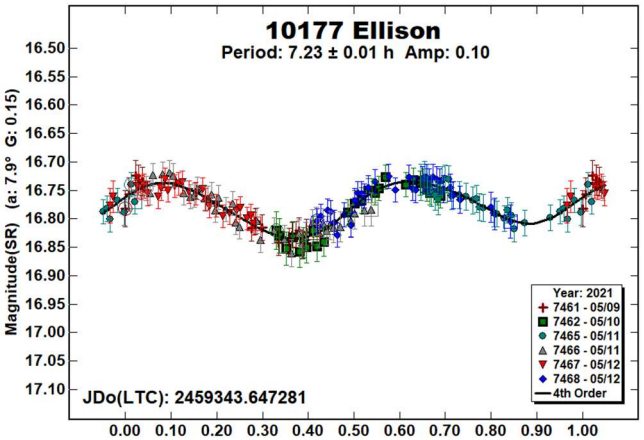

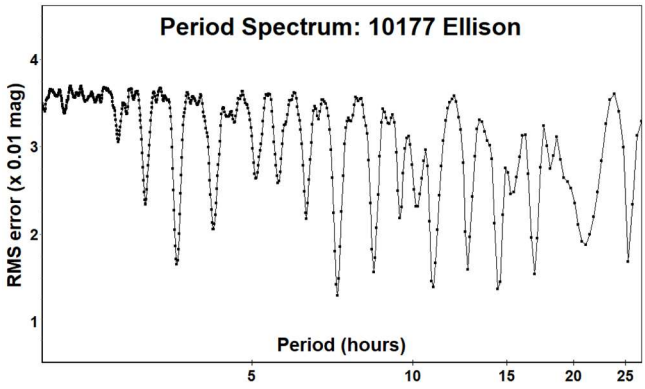

(14653) 1998 YV11. This Mars-crosser was observed by Higgins (2005) finding a period of 11.389 h. Using TESS survey data, Pál et al. (2020) found a period of 11.391 h. Our results this year is in good agreement with those prior results.

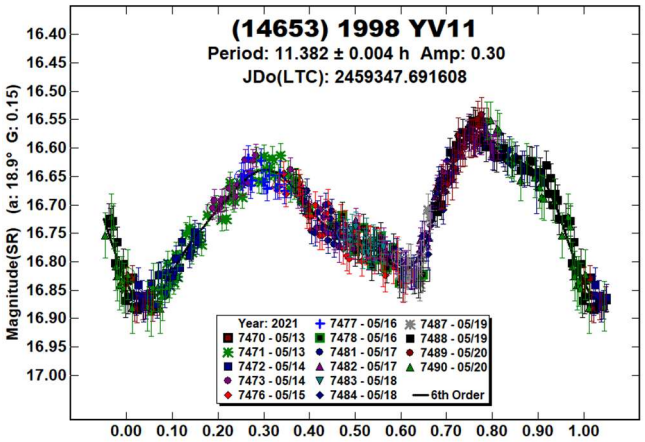

18434 Mikesandras. Carbo et al. (2009) found a period of 3.137 h for this 5.3 km member of the Phocaea dynamical family (LCDB: 701). On the other hand, Pál et al. (2020) used data from the TESS mission to find a period of 42.8675 h. This raised the possibility that they had found a long-period component and overlooked the shorter period found by Carbo et al. (2009).

However, after importing their data into *MPO Canopus*, a period search from 2-100 hours found what was an essentially flat line for the period spectrum and a plot to their period showed only the slightest trace of a period within a significant amount of noise.

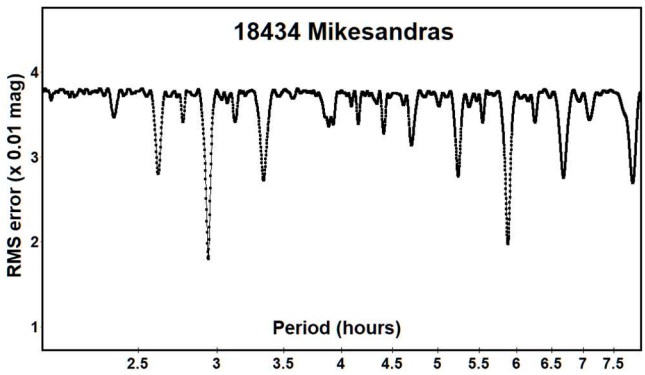

Our period spectrum showed two distinct possibilities, a monomodal solution at 2.940 h and a bimodal solution at 5.870 h. As noted by Harris et al. (2014), given the low amplitude and relatively small phase angle, either solution was plausible and so we used a split-halves plot to see which period to favor. That showed highly-symmetrical halves for the 5.879 h period, too symmetrical for out liking, and so we adopted a period of 2.940 h for this paper despite the somewhat unusual lightcurve shape.

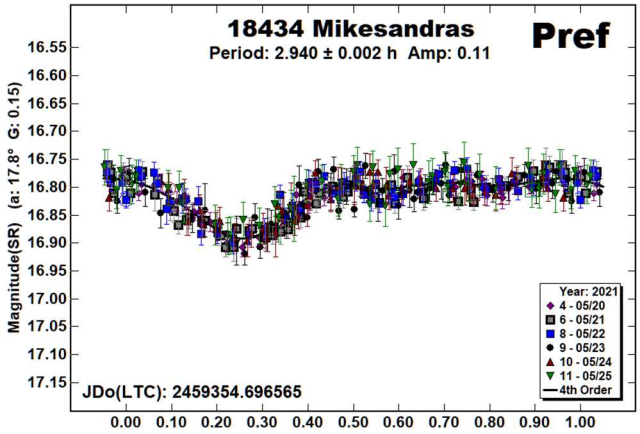

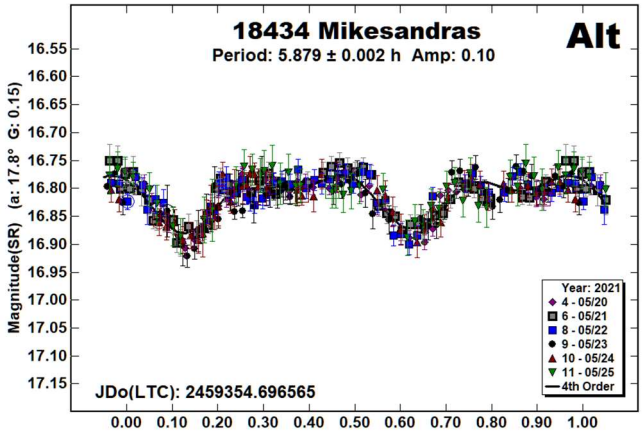

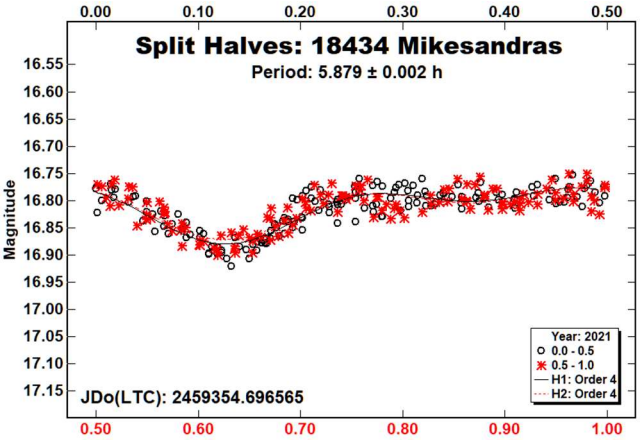

(30958) 1994 TV3. We observed this member of the Hungaria dynamical family twice in the past (Warner, 2014; Stephens, 2017) finding periods near 5.8 h. Our results this year is in good agreement with those prior results.

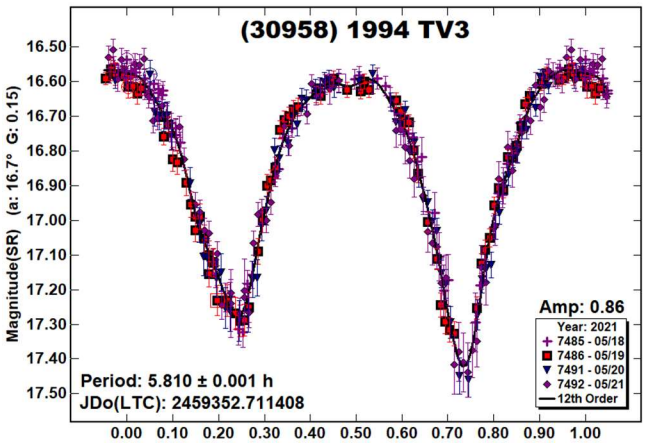

(53134) 1999 BG1. The estimated diameter is 7.7 km for this middle main-belt asteroid. Based on observations made about two weeks before ours, Behrend (2021web) found a period of 2.6109 h and lightcurve amplitude of 0.11 mag. At that time, the phase angle was 17.1°. During our observations, the phase angle averaged about 21.0°, and so the slightly larger amplitude would be expected (Zappala et al., 1990).

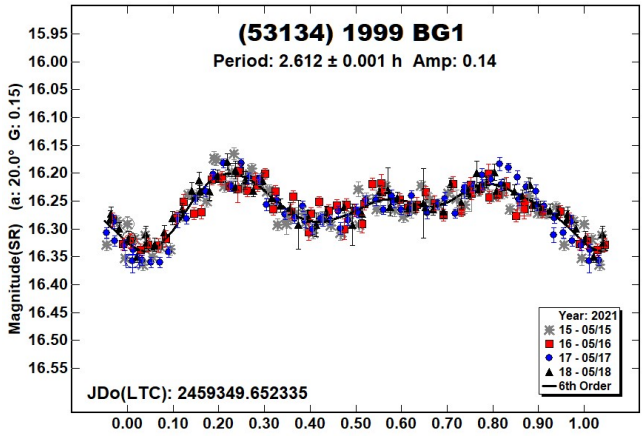

66846 Frankllederer. There were no previous lightcurve entries in the LCDB for this 5-km asteroid, which a member of the Pallas dynamical family. The phase angle and phase angle bisector were nearly the same over the 9-day span of observations and so the slight deviation between 0.0 and 0.2 rotation is somewhat unexpected. However, there were no signs of a second period when doing a dual-period search of *MPO Canopus*.

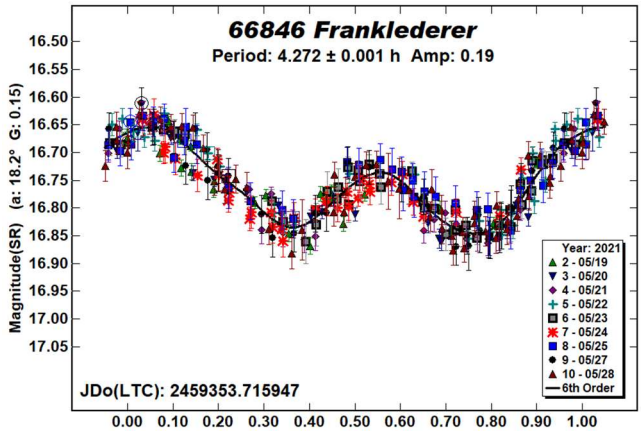

Number	Name	2021/mm/dd	Phase	L_{PAB}	B_{PAB}	Period(h)	P.E.	Amp	A.E.	Grp
323	Brucia	04/27-04/30	21.5,21.6	148	24	9.457	0.002	0.43	0.01	701
1106	Cydonia	05/05-05/07	25.5,25.7	159	-6	2.671	0.002	0.08	0.02	502
1257	Mora	05/22-05/28	25.4,25.6	169	-2	5.298	0.001	0.71	0.03	9104
1413	Roucarie	2019/11/03-11/06	3.4,3.9	38	-8	6.529	0.001	0.56	0.01	606
7792	1995 WZ3	05/13-05/17	26.4,27.3	187	6	3.163	0.001	0.27	0.02	9104
10177	Ellison	05/09-05/12	7.9,9.2	216	8	7.23	0.01	0.10	0.02	401
14653	1998 YV11	05/13-05/20	19.0,22.4	206	9	11.382	0.004	0.30	0.02	9103
18434	Mikesandras	05/20-05/25	17.8,17.4	244	32	[P]2.940	0.002	0.11	0.01	701
						5.879	0.002	0.11	0.01	
30958	1994 TV3	05/18-05/21	16.7,17.2	237	24	5.81	0.001	0.86	0.02	003
53134	1999 BG1	05/15-05/18	20.0,20.9	211	21	2.612	0.001	0.14	0.01	9105
66846	Frankle derer	05/19-05/28	*18.2,18.4	252	27	4.272	0.001	0.19	0.01	801
80366	1999 XA142	04/04-05/04	*20.5,22.7	194	24	580	20	0.6	0.3	701

Table II. Observing circumstances and results. [P]Preferred solution for an ambiguous result. The phase angle is given for the first and last date. If preceded by an asterisk, the phase angle reached an extremum during the period. L_{PAB} and B_{PAB} are the approximate phase angle bisector longitude/latitude at mid-date range (see Harris et al., 1984). Grp is the asteroid family/group (Warner et al., 2009; Warner and Harris, 2021). A number < 2000 indicates a dynamical family member as determined from Nesvorny (2015) and Nesvorny et al. (2015). Numbers in the range of 2000-3000 are additional families from the AstDys site (2021June). Numbers > 9000 are objects in an orbital space defined by osculating orbital elements. See the recent LCDB documentation or use *https://minplanobs.org/MPInfo/php/oneasteroidinfo.php* to look up an asteroid's family or group number.

Number	Name	λ	β	Period	λ	β	Period	a/b ratio	a/c ratio
323	Brucia	**237**	**16**	**9.459492**	57	-19	9.459500	1.2	1.6
1106	Cydonia	**336**	**-25**	**2.679720**	145	-22	2.679720	1.2	1.5

Table III. Results of Pole/Shape modeling. The preferred solution is listed first in bold text. For the ratios, c = 1.0.

(80366) 1999 XA142. There are no entries in the LCDB for this Mars-crosser estimated to be 3 km in size. That is not a surprise given its long period and that the asteroid is tumbling, which is likely given the period (Pravec et al., 2005; 2014). The tumbling frequencies cannot be confirmed from our data set alone.

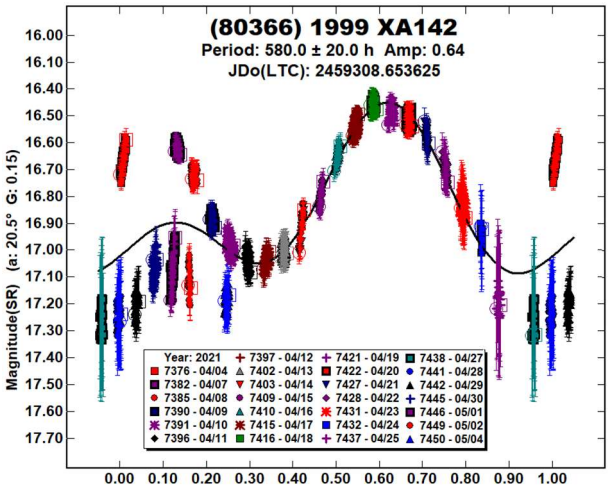

Acknowledgements

Observations at CS3 and continued support of the asteroid lightcurve database (LCDB; Warner et al., 2009) were supported in part by NASA grant 80NSSC18K0851.

This work includes data from the Asteroid Terrestrial-impact Last Alert System (ATLAS) project. ATLAS is primarily funded to search for near earth asteroids through NASA grants NN12AR55G, 80NSSC18K0284, and 80NSSC18K1575; byproducts of the NEO search include images and catalogs from the survey area. The ATLAS science products have been made possible through the contributions of the University of Hawaii Institute for Astronomy, the Queen's University Belfast, the Space Telescope Science Institute, and the South African Astronomical Observatory.

The authors gratefully acknowledge Shoemaker NEO Grants from the Planetary Society (2007, 2013). These were used to purchase some of the telescopes and CCD cameras used in this research.

References

ALCDEF (2021). Asteroid Lightcurve Data Exchange Format database. *https://www.minplanobs.org/alcdef*

AstDys-2 (2020). Asteroids - Dynamic site. *https://newton.spacedys.com/astdys/*

Aznar, M.A. (2017). "Density and Axis-size Relationship of Five Main-belt Asteroids: 2017 January - March." *Minor Planet Bull.* **44**, 276-279.

Behrend, R., (2006web; 2009web, 2011web, 2021web). Observatoire de Geneve web site. *http://obswww.unige.ch/~behrend/page_cou.html*

Binzel, R.P. (1987). "A photoelectric survey of 130 asteroids." *Icarus* **72**, 135-208.

Carbo, L.; Green, D.; Kragh, K.; Krotz, J.; Meiers, A.; Patino, B.; Pligge, Z.; Shaffer, N.; Getteon, R. (2009). "Asteroid Lightcurve Analysis at the Oakley Southern Sky Observatory: 2008 October thru 2009 March." *Minor Planet Bull.* **36**, 152-157.

Ďurech, J.; Hanuš, J.; Alí-Lagoa, V. (2018). "Asteroid models reconstructed from the Lowell Photometric Database and WISE data." *Astron. Astrophys*. **617**, A57.

Erasmus, N.; Navarro-Meza, S.; McNeill, A.; Trilling, D.E.; Sickafoose, A.A.; Denneau, L.; Flewelling, H.; Heinze, A.; Tonry, J.L. (2020). "Investigating Taxonomic Diversity within Asteroid Families through ATLAS Dual-band Photometry." *Ap. J. Suppl. Ser.* **247**, A13.

Harris, A.W.; Young, J.W.; Scaltriti, F.; Zappala, V. (1984). "Lightcurves and phase relations of the asteroids 82 Alkmene and 444 Gyptis." *Icarus* **57**, 251-258.

Harris, A.W.; Young, J.W.; Contreiras, L.; Dockweiler, T.; Belkora, L.; Salo, H.; Harris, W.D.; Bowell, E.; Poutanen, M.; Binzel, R.P.; Tholen, D.J.; Wang, S. (1989). "Phase relations of high albedo asteroids: The unusual opposition brightening of 44 Nysa and 64 Angelina." *Icarus* **81**, 365-374.

Harris, A.W.; Pravec, P.; Galad, A.; Skiff, B.A.; Warner, B.D.; Vilagi, J.; Gajdos, S.; Carbognani, A.; Hornoch, K.; Kusnirak, P.; Cooney, W.R.; Gross, J.; Terrell, D.; Higgins, D.; Bowell, E.; Koehn, B.W. (2014). "On the maximum amplitude of harmonics on an asteroid lightcurve." *Icarus* **235**, 55-59.

Higgins, D.J. (2005). "Lightcurve periods for 1701 Okavango, 689 Zita, 981 Martina and (14653) 1998 YV11." *Minor Planet Bull.* **32**, 13-14.

Klinglesmith, D.A. III; Hendrickx, S.; Madden, K.; Montgomery, S. (2016). "Asteroid Lightcurves from Estcorn Observatory." *Minor Planet Bull.* **43**, 234-239.

Nesvorny, D. (2015). "Nesvorny HCM Asteroids Families V3.0." NASA Planetary Data Systems, id. EAR-A-VARGBET-5-NESVORNYFAM-V3.0.

Nesvorny, D.; Broz, M.; Carruba, V. (2015). "Identification and Dynamical Properties of Asteroid Families." In *Asteroids IV* (P. Michel, F. DeMeo, W.F. Bottke, R. Binzel, Eds.). Univ. of Arizona Press, Tucson, also available on astro-ph.

Pál, A.; Szakáts, R.; Kiss, C.; Bódi, A.; Bognár, Z.; Kalup, C.; Kiss, L.L.; Marton, G.; Molnár, L.; Plachy, E.; Sárneczky, K.; Szabó, G.M.; Szabó, R. (2020). "Solar System Objects Observed with TESS-First Data Release: Bright Main-belt and Trojan Asteroids from the Southern Survey." *Ap. J.* **247**, A26.

Pravec, P.; Harris, A.W.; Scheirich, P.; Kušnirák, P.; Šarounová, L.; Hergenrother, C.W.; Mottola, S.; Hicks, M.D.; Masi, G.; Krugly, Yu.N.; Shevchenko, V.G.; Nolan, M.C.; Howell, E.S.; Kaasalainen, M.; Galád, A.; Brown, P.; Degraff, D.R.; Lambert, J. V.; Cooney, W.R.; Foglia, S. (2005). "Tumbling asteroids." *Icarus* **173**, 108-131.

Pravec, P.; Wolf, M.; Sarounova, L. (2007web). *http://www.asu.cas.cz/~ppravec/neo.htm*

Pravec, P.; Scheirich, P.; Durech, J.; Pollock, J.; Kusnirak, P.; Hornoch, K.; Galad, A.; Vokrouhlicky, D.; Harris, A.W.; Jehin, E.; Manfroid, J.; Opitom, C.; Gillon, M.; Colas, F.; Oey, J.; Vrastil, J.; Reichart, D.; Ivarsen, K.; Haislip, J.; LaCluyze, A. (2014). "The tumbling state of (99942) Apophis." *Icarus* **233**, 48-60.

Schober, H.J.; Erikson, A.; Hahn, G.; Lagerkvist, C.I.; Oja, T. (1993). "Physical Studies of Asteroids. Part XXVI. Rotation and Photoelectric Photometry of Asteroids 323, 350, 582, 1021 and 1866." *Astron. Astrophys*. *Supp*. **101**, 507.

Stephens, R.D. (2017). "Asteroids Observed from CS3: 2016 - September." *Minor Planet Bull.* **44**, 49-52.

Stephens, R.D.; Warner, B.D. (2020). "Main-belt Asteroids Observed from CS3: 2020 January to March." *Minor Planet Bull.* **47**, 224-230.

Stephens, R.D.; Coley, D.R.; Warner, B.D. (2021). "Main-belt Asteroids Observed from CS3: 2021 January to March." *Minor Planet Bull.* **48**, 246-267.

Tonry, J.L.; Denneau, L.; Flewelling, H.; Heinze, A.N.; Onken, C.A.; Smartt, S.J.; Stalder, B.; Weiland, H.J.; Wolf, C. (2018). "The ATLAS All-Sky Stellar Reference Catalog." *Astrophys. J.* **867**, A105.

Warner, B.D.; Harris, A.W.; Pravec, P. (2009). "The Asteroid Lightcurve Database." *Icarus* **202**, 134-146. Updated 2020 Oct. *http://www.minorplanet.info/lightcurvedatabase.html*

Warner, B.D. (2014). "Asteroid Lightcurve Analysis at CS3-Palmer Divide Station: 2013 June- September." *Minor Planet Bull.* **41**, 27-32.

Warner, B.D. (2018). "Asteroid Lightcurve Analysis at CS3-Palmer Divide Station: 2018 April-June." *Minor Planet Bull.* **45**, 380-386.

Warner, B.D.; Harris, A.W. (2021). "All in the Family: Upcoming Changes in the LCDB." *Minor Planet Bull.* **48**, 313-315.

Zappala, V.; Cellini, A.; Barucci, A.M.; Fulchignoni, M.; Lupishko, D.E. (1990). "An anlaysis of the amplitude-phase relationship among asteroids." *Astron. Astrophys*. **231**, 548-560.

SPIN/SHAPE MODEL FOR 323 Brucia

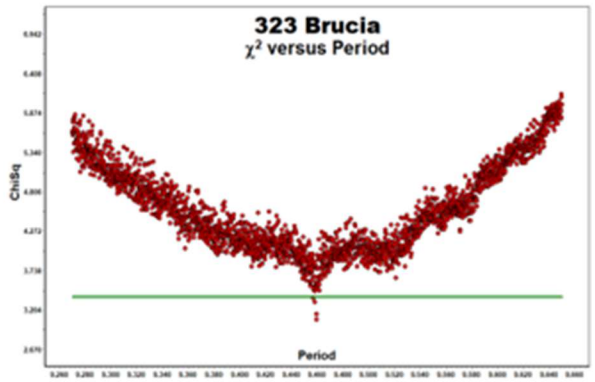

Figure 1. The initial period search results.

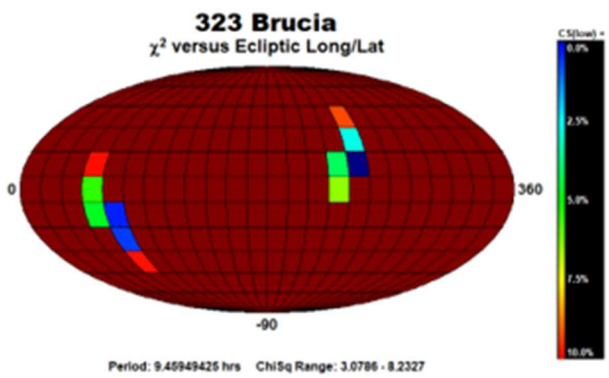

Figure 2. The pole search found two probable solutions.

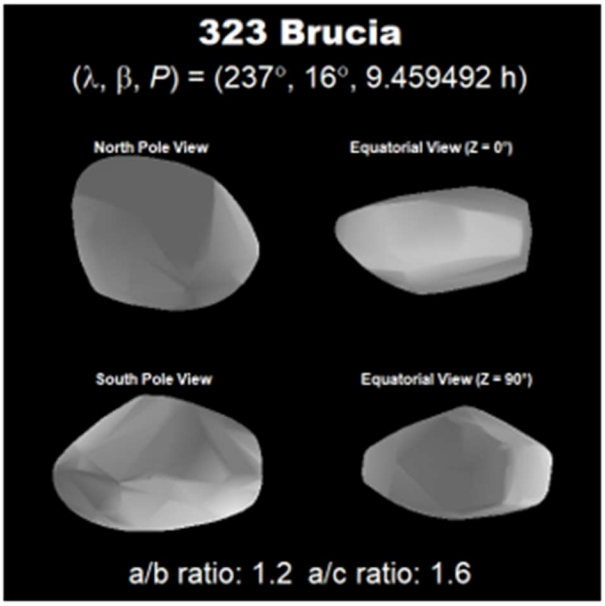

Figure 3. The shape of the asteroid based on the preferred solution.

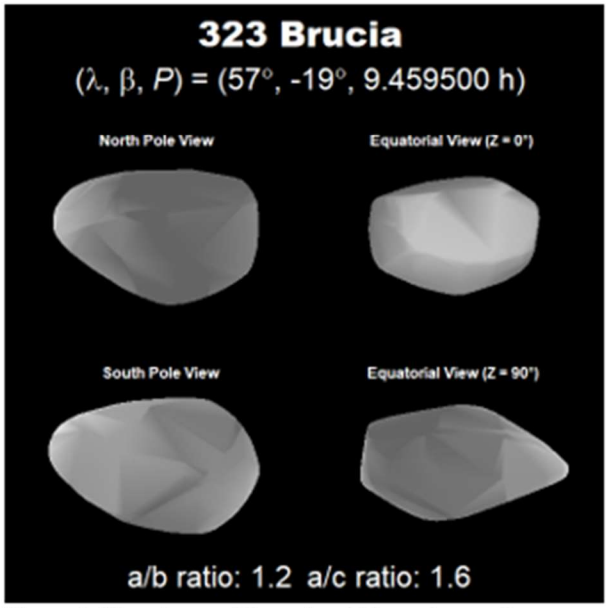

Figure 4. The shape of the asteroid based upon the secondary solution.

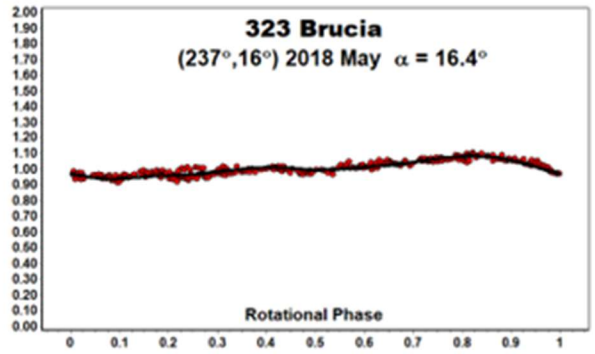

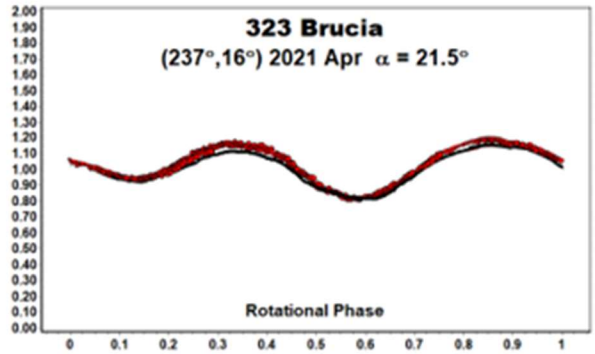

Figure 5/6. The comparison plots are against the preferred pole solution. The red dots indicate the data used for modeling while the black line is the smoothed lightcurve for generated by the shape at the time of the observations. The match is very close on both occasions, which gives confidence in the shape/spin axis model.

SPIN/SHAPE MODEL FOR 1106 Cydonia

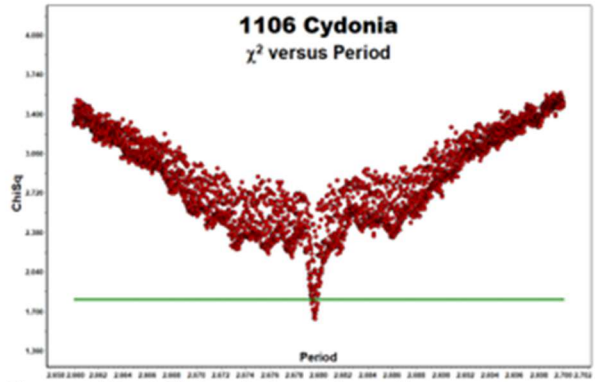

Figure 1. The initial period search results.

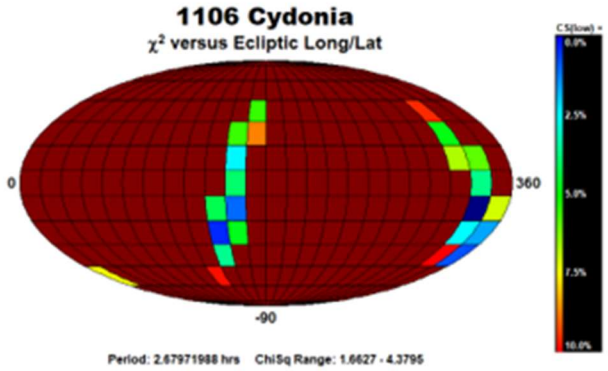

Figure 2. The pole search found two probable solutions.

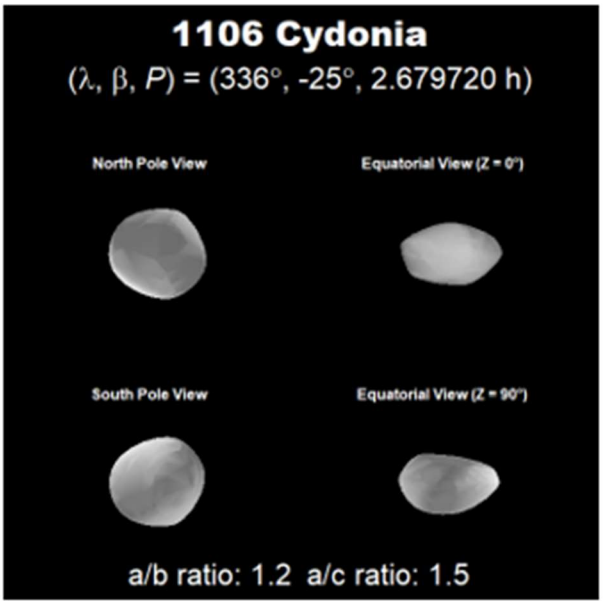

Figure 3. The shape of the asteroid based on the preferred solution.

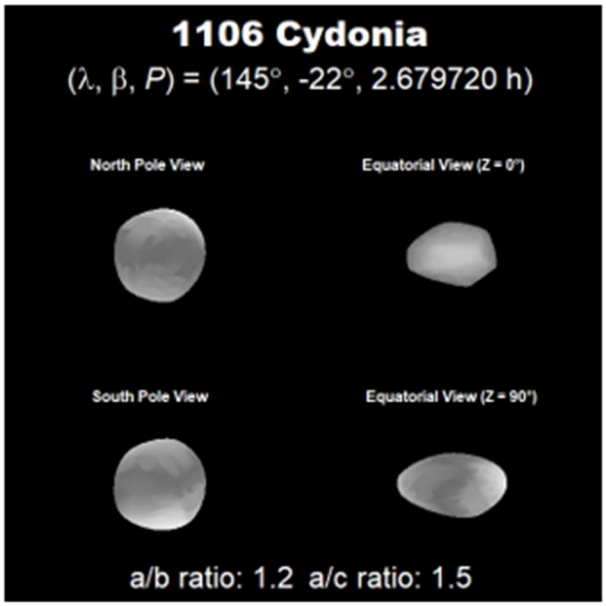

Figure 4. The shape of the asteroid based upon the secondary solution.

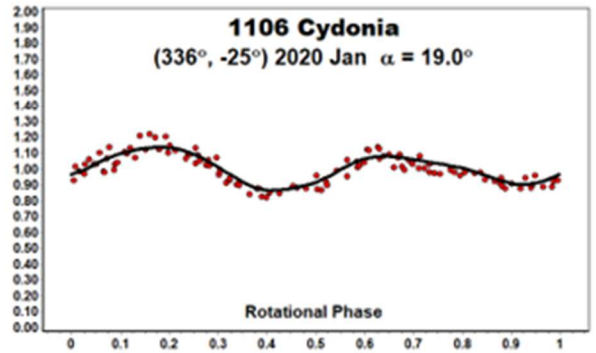

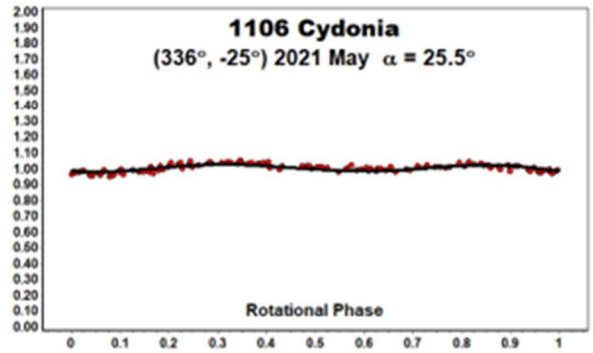

Figure 5/6. The comparison plots are against the preferred pole solution. The red dots indicate the data used for modeling while the black line is the smoothed lightcurve for generated by the shape at the time of the observations. The match is very close on both occasions, which gives confidence in the shape/spin axis model.

ROTATIONAL PERIOD AND LIGHTCURVE DETERMINATION OF 755 QUINTILLA, 2699 KALININ, 3523 ARINA, 5182 BRAY, 5401 MINAMIODA, 5405 NEVERLAND, (7288) 1991 FE1, AND 18418 UJIBE

Michael Fauerbach
Florida Gulf Coast University
and SARA Observatories
10501 FGCU Blvd.
Ft. Myers, FL 33965-6565
mfauerba@fgcu.edu

(Received: 2021 July 13)

Photometric observations of eight main-belt asteroids were obtained on eight nights between 2020 November 17 and 2021 April 11. The following rotational periods were determined: 755 Quintilla: 4.552 ± 0.001 h; 2699 Kalinin: 2.928 ± 0.001 h; 3523 Arina: 2.674 ± 0.001 h; 5182 Bray: 2.89 ± 0.04 h; 5401 Minamioda: 4.388 ± 0.001 h; 5405 Neverland: 3.181 ± 0.001 h; (7288) 1999 FE1: 4.889 ± 0.001 h; 18418 Ujibe: 3.470 ± 0.001 h.

Photometric observations obtained with the Southeastern Association for Research in Astronomy (SARA) consortium 1-m Jacobus Kapteyn Telescope at the Observatorio del Roque de los Muchachos on the Spanish island of La Palma are presented. The telescope is coupled with an Andor iKon-L series CCD. A detailed description of the instrumentation and setup can be found in Keel et al. (2017). The data were calibrated using *MaximDL* and photometric analysis was performed using *MPO Canopus* (Warner, 2017).

755 Quintilla. This main-belt asteroid is a shape model target. A preliminary shape model was published by Franco et al. (2020b). Large uncertainties in the pole position made the need for additional data obvious. Since the apparition of 2021 was a favorable one, it was decided to focus our spring 2021 observation campaign on 755 Quintilla. We were able to observe the asteroid on three of the four nights allocated during the 2021 March - April timeframe. Despite the apparition being favorable, it was a challenging target since the asteroid never reached an altitude of more than 52° at our observatory. This limited our nightly observations to about the same time as the rotational period.

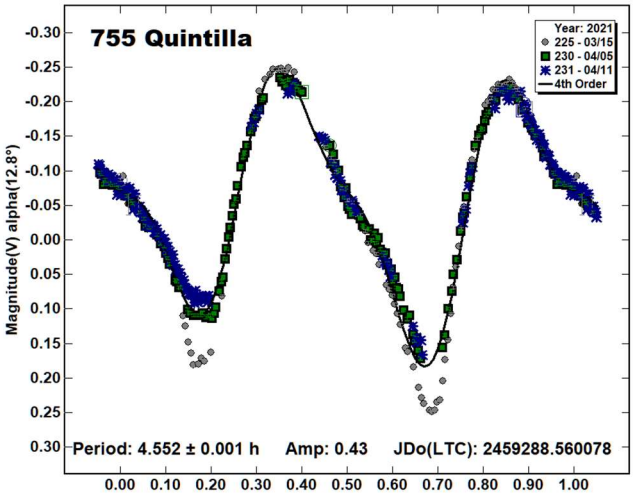

When looking at the data set, it is obvious that the data from the first night, with the largest phase angle, appear to show much deeper minima than the other two nights, which were closer to opposition. In an accompanying paper (Fauerbach and Fauerbach, 2021) we will report the results taken 1-2 months after opposition, again at large phase angles. That data also shows the deeper minima, thereby showing that the deep minima reported here are not an artifact of the data. Our analysis yields a rotational period of 4.552 ± 0.001 h with an amplitude of 0.43 mag. This is in excellent agreement with previous publications by Behrend (2004web, 2005web), Buchheim and Prey (2005), Ďurech et al. (2020), Franco et al. (2020a), as well as our previous result (Fauerbach and Fauerbach, 2019).

2699 Kalinin. This asteroid was observed by FGCU's Asteroid Research Group before and is a shape modelling target for our group. Ďurech et al. (2020) recently published a shape model for this asteroid and we intend to use our data to confirm and improve on this model. We observed 2699 Kalinin on two nights over a 12-day period. A rotational period of 2.928 ± 0.001 h with an amplitude of 0.23 mag was obtained. This is in excellent agreement with the result by Ambrosioni (2011; 2.9279 h) and by our group (Fauerbach and Zabala, 2019; 2.928 h) and Fauerbach (2021; 2.928 h).

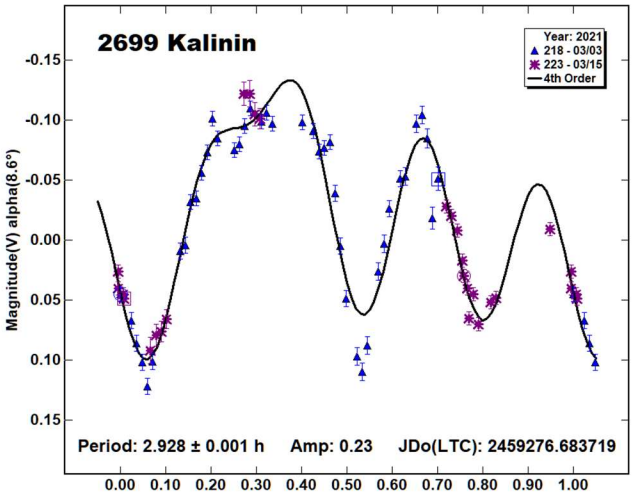

3523 Arina was observed on three nights over a three-week timespan. At the time of our observations, only one prior period determination was known (Schmidt, 2015; 2.67 h). The current data yield a period of 2.674 ± 0.001 h with an amplitude of 0.10 mag. This is in excellent agreement with the result from Schmidt (2015). Unbeknown to us Behrend (2021web; 2.672 h) and Benishek et al. (2021; 2.6742 h) also observed this asteroid. All four published periods are in excellent agreement with each other.

Both Behrend and Benishek et al. report this asteroid is binary. Behrend reports a period of the secondary of 5.344 ± 0.005 h, whereas Benishek reports an orbital period of 29.26 ± 0.02 hr. An attempt was made to derive the orbital period or the period of the secondary using *MPO Canopus*. The results are presented below, but due to the limited amount of data used to derive them, their validity should be questioned. The best fit for the period of the secondary yields 4.714 ± 0.001 h. This solution is not unique. Subtracting the data from the secondary lightcurve yields a much cleaner solution for the primary without changing the period, as shown below. An attempt was made to use the secondary period provided by Behrend, but it yielded a worse result than the uncorrected lightcurve.

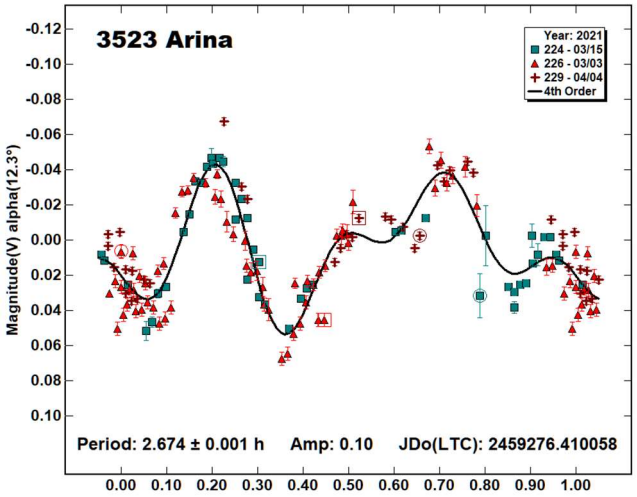

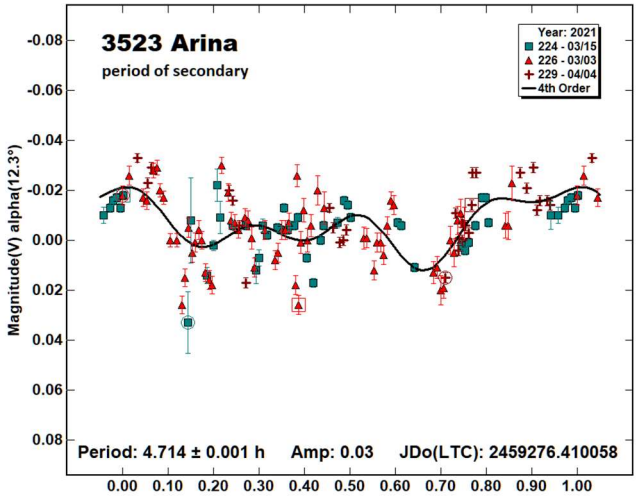

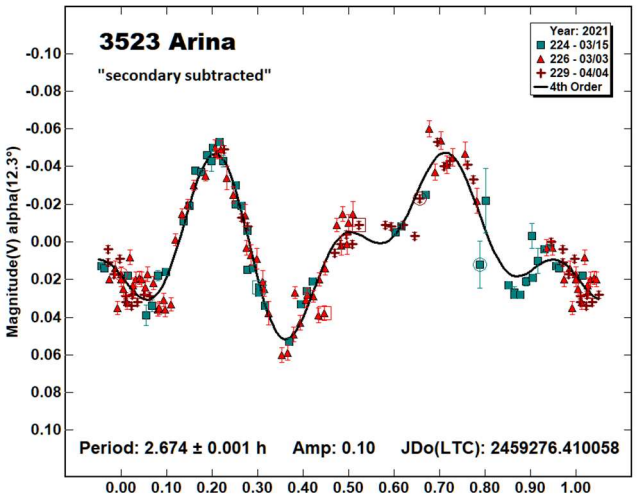

5182 Bray is another of our shape model targets. Unfortunately, due to poor weather, several scheduled nights were lost so the asteroid was observed only on a single night. The measured rotational period of 2.89 ± 0.04 h with an amplitude of 0.29 mag is in excellent agreement with previous publications by Klinglesmith III (2014; 2.883 h), Behrend (2018; 2.884 h), as well as our previous result (Fauerbach, 2019; 2.86 h) and (Fauerbach, 2021; 2.88 h).

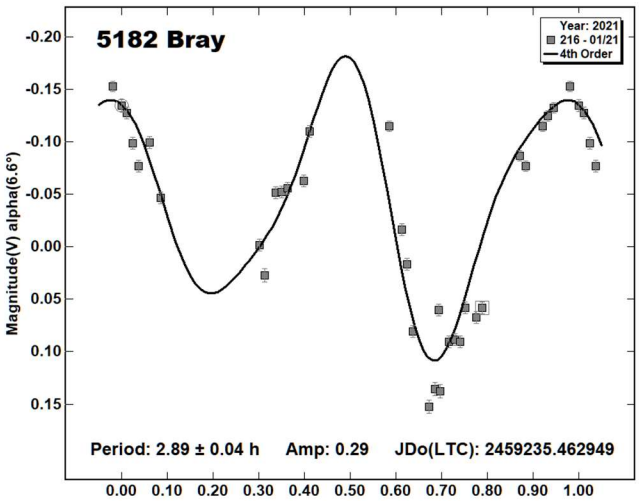

5401 Minamioda was observed on two nights over a period of approximately 4 h and 5 h respectively. The best fit to the data provides a period of 4.388 ± 0.001 h with an amplitude of 0.09 mag. The only prior period determination was by Marchini et al. (2016). They reported a period of either 3.949 ± 0.001 h or 7.897 ± 0.003 h, with the accepted value being 3.949 h. Unfortunately, the current result does not agree with either result and further study is necessary to determine the correct value.

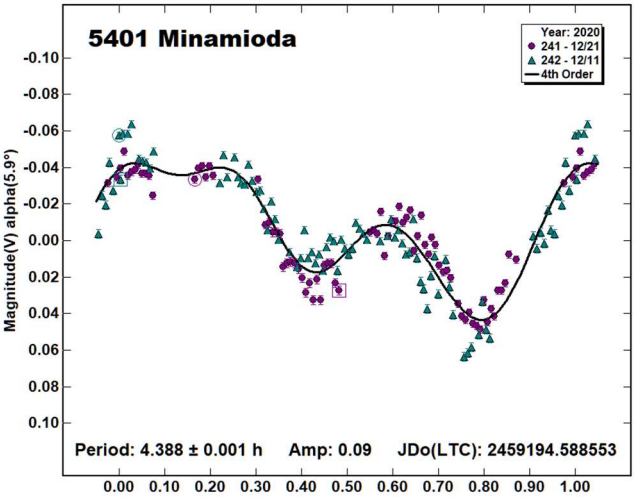

5405 Neverland. This main-belt asteroid was observed for two nights, separated by 6 weeks, for 3.5 h and 5.5 h respectively. The current data yields a period of 3.181 ± 0.001 h with an amplitude of 0.19 m. This is in excellent agreement with Waszczak et al. (2015; 3.181 ± 0.0012 h) and our previous result (Fauerbach, 2019; 3.181 ± 0.001 h). The results by Behrend (2017web; 7.1414 ± 0.0002 h) and Mas et al. (2018; 3.149 ± 0.025 h) cannot be reproduced with the current data set.

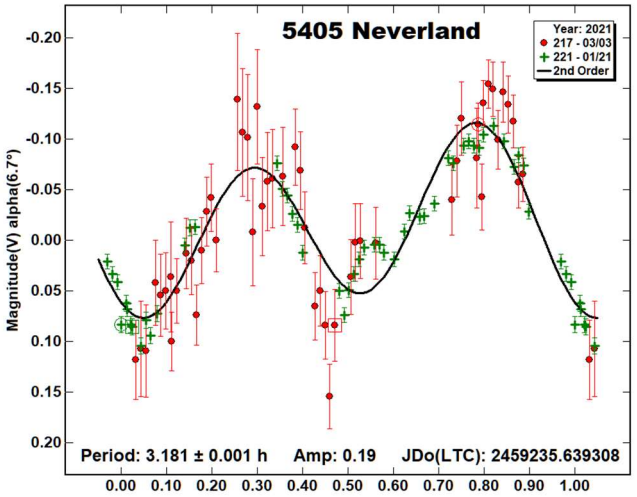

(7288) 1991 FE1. At the time of our observations there were two previous period determinations, both based on sparse data. Waszczak et al. (2015) reported a period of 4.890 ± 0.0022 h, whereas Erasmus et al. (2020) reported a period of 4.436 ± 0.002 h. We observed the asteroid on four nights over the period of a month. The current data provides a period of 4.889 ± 0.001 h with an amplitude of 0.48 mag. This is in excellent agreement with the result by Waszczak et al. and excludes the period determined by Erasmus et al. We learned that Pravec et al (2021web) also observed (7288) 1991 FE1. They derived a period of 4.8889 ± 0.0001 h, which is in agreement with our observations.

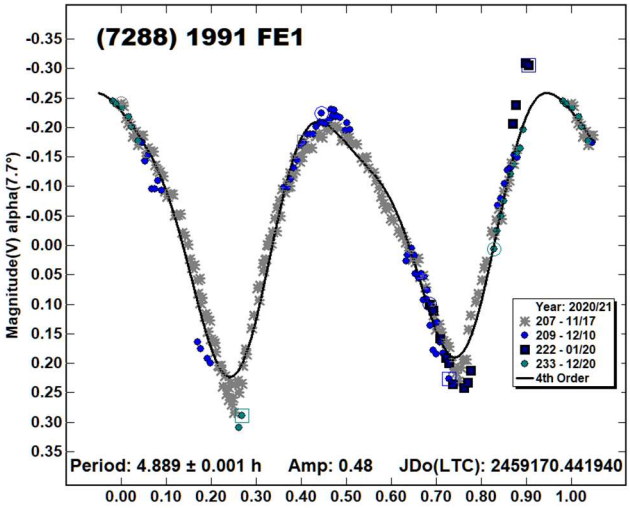

18418 Ujibe was observed over a period of twelve days on three nights. A period of 3.470 ± 0.001 h with an amplitude of 0.28 mag was derived. This is in excellent agreement with the result by Waszczak et al. (2015) of 3.470 ± 0.0005 h.

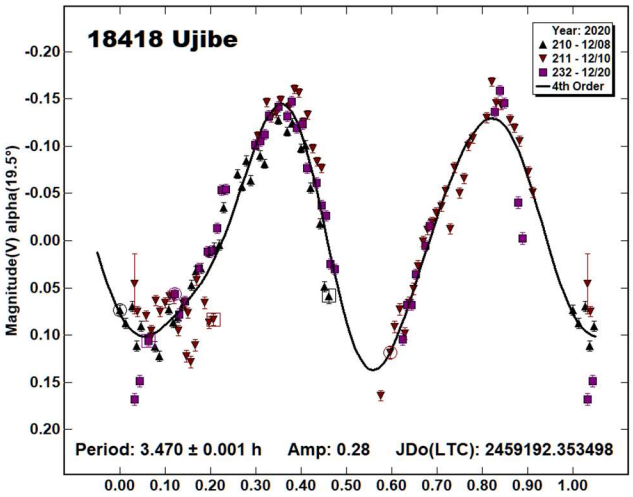

References

Ambrosioni, C., Colazo, C., Mazzone, F. (2011). "Period Determination for 1996 Adams and 2699 Kalinn by AOACM." *Minor Planet Bulletin* **38**, 102.

Behrend, R. (2004web, 2005web, 2017web, 2018web, 2021web). Observatoire de Geneve web site. *http://obswww.unige.ch/~behrend/page_cou.html*

Benishek, V.; Pravec, P.; Husarik, M.; Pikler, M.; Cervak, G.; Marchini, A.; Papini, R.; Salvaggio, F.; Cooney, W.; Aznar, A.; Santos-Sanz, P.; Sota, A.; Aceituno, F.J.; Durkee, R. *Central Bureau for Astronomical Telegrams* **4967**.

Buchheim, R.K.; Pray, D. (2005). "Lightcurve of 755 Quintilla," *Minor Planet Bulletin* **32**, 1.

Ďurech, J.; Tonry, J.; Erasmus, N.; Denneau, L.; Heinze, A.N.; Flewelling, H.; Vančo, R. (2020). "Asteroid models reconstructed from ATLAS photometry." *Astronomy & Astrophysics*, **643**, A59.

Erasmus, N.; Navarro-Meza, S.; McNeill, A.; Trilling, D.E.; Sickafoose, A.A.; Denneau, L.; Flewelling, H.; Heinze, A.; Tonry, J.L. (2020). "Investigating Taxonomic Diversity within Asteroid Families through ATLAS Dual-band Photometry." *The Astrophysical Journal Supplement Series,* **247:13**.

Fauerbach, M. (2019). "Photometric Observations for 8 Main-belt Asteroids: 2017 April - May." *Minor Planet Bulletin* **46**, 15-19.

Number	Name	yyyy mm/dd	Phase	L_{PAB}	B_{PAB}	Period(h)	P.E.	Amp	A.E.
755	Quintilla	2021 03/15,04/11	12.8,2.8	207	2	4.552	0.001	0.43	0.06
2699	Kalinin	2021 03/03,03/15	8.5,6.9	177	18	2.928	0.001	0.23	0.02
3523	Arina	2021 03/15,04/04	12.6,20.2	157	12	2.674	0.001	0.10	0.01
						4.714	0.001		
5182	Bray	2021 01/21	6.2	137	-2	2.89	0.04	0.29	0.03
5401	Minamioda	2020 12/11,12/21	9.2,5.8	95	10	4.388	0.001	0.09	0.01
5405	Neverland	2021 01/21,03/03	*11.8,7.0	149	10	3.181	0.001	0.19	0.02
7288	1991 FE1	2020/21 11/17,01/20	*7.1,25.4	67	4	4.889	0.001	0.48	0.04
18418	Ujibe	2020 12/08,12/20	19.4,23.5	46	3	3.470	0.001	0.28	0.02

Table I. Observing circumstances and results. The first line gives the results for the primary of a binary system. The second line gives the orbital period of the satellite The phase angle is given for the first and last date. If preceded by an asterisk, the phase angle reached an extremum during the period. L_{PAB} and B_{PAB} are the approximate phase angle bisector longitude/latitude at mid-date range (see Harris et al., 1984).

Fauerbach, M. (2021). "Lightcurve Analysis of Asteroids 1939 Loretta, 2099 Opik, 2699 Kalinin, 2779 Mary, 3108 Lyubov, 5182 Bray, and 9098 Toshihiko." *Minor Planet Bulletin* **48**, 225-227.

Fauerbach, M.; Fauerbach, M. (2019). "Rotational Period Determination for Asteroids 755 Quintilla, 1830 Pogson, 5076 Lebedev-Kumach, and (29153) 1998 SY2." *Minor Planet Bulletin* **46**, 138-139.

Fauerbach, M.; Fauerbach, M. (2021). "Photometric observations of 755 Quintilla and 1132 Hollandia." *Minor Planet Bulletin* **48**, 362-363.

Fauerbach, M., Zabala F. (2019). "Photometric Observations of Asteroids 570 Kythera, 1334 Lundmarka, 2699 Kalinin, and 5182 Bray." *Minor Planet Bulletin* **46**, 3-4.

Franco, L.; Marchini, A.; Saya, L.-F.; Galli, G.; Baj, G.; Ruocco, N.; Tinelli, L.; Scarfi, G.; Aceti, P.; Banfi, M.; Bacci, P.; Maestripieri, M.; Papini, R.; Salvaggio, F.; Mortari, F.; Bachini, M.; Casalnuovo, G.B.; Chinaglia, B. (2020a). "Collaborative Asteroid Photometry from UAI: 2020 January - March." *Minor Planet Bulletin* **47**, 242-246.

Franco, L.; Buchheim, R.K.; Pray, D.; Fauerbach, M.; Mortari, F.; Casalnuovo, G.B.; Chinaglia, B.; Scarfi, G.; Papini, R.; Salvaggio, F. (2020b). "Preliminary Spin-Shape Model for 755 Quintilla." *Minor Planet Bulletin* **47**, 267-269.

Harris, A.W.; Young, J.W.; Scaltriti, F.; Zappala, V. (1984). "Lightcurves and phase relations of the asteroids 82 Alkmene and 444 Gyptis." *Icarus* **57**, 251-258.

Keel, W.C.; Oswalt, T.; Mack, P.; Henson, G.; Hillwig, T.; Batcheldor, D.; Berrington, R.; De Pree, C.; Hartmann, D.; Leake, M.; Licandro, J.; Murphy, B.; Webb, J.; Wood, M.A. (2017). "The Remote Observatories of the Southeastern Association for Research in Astronomy (SARA)." *Publications of the Astronomical Society of the Pacific* **129**:015002 (12pp). *http://iopscience.iop.org/article/10.1088/1538-3873/129/971/015002/pdf*

Klinglesmith III, D.A. (2014). Posting on CALL web site. *http://www.MinorPlanet.info/call.html*

Marchini, A.; Franco, L.; Papini, R.; Salvaggio, F. (2016). "Rotation Period Determination for 5401 Minamioda." *Minor Planet Bulletin* **43***, 188-190.*

Mas, V.; Fornas, G.; Lozano, J.; Rodrigo, O.; Fornas, A.; Carreño, A.; Arce, E.; Brines, P.; Herrero, D. (2018). "Twenty-one Asteroid Lightcurves at Asteroids Observers (OBAS) - MPPD: Nov 2016 - May 2017." *Minor Planet Bulletin* **45**, 76-82.

Pravec, P.; Wolf, M.; Sarounova, L. (2021web) *http://www.asu.cas.cz/~ppravec/neo.htm*

Schmidt, R.E. (2015). "NIR Minor Planet Photometry from Burleith Observatory: 2014 February - June." *Minor Planet Bulletin* **42**, 1-3.

Warner, B.D. (2017). *MPO Canopus* software version 10.7.10.0. *http://www.bdwpublishing.com*

Waszczak, A.; Chang, C.-K.; Ofek, E.O.; Laher, R.; Masci, F.; Levitan, D.; Surace, J.; Cheng, Y.-C.; Ip, W.-H.; Kinoshita, D.; Helou, G.; Prince, T.A.; Kulkarni, S. (2015). "Asteroid Light Curves from the Palomar Transient Factory Survey: Rotation Periods and Phase Functions from Sparse Photometry," *The Astronomical Journal* **150**, article id. 75, 35 pp.

ROTATION PERIOD ANALYSIS FOR FIVE ASTEROIDS

Milagros Colazo
Instituto de Astronomía Teórica y Experimental
(IATE-CONICET), ARGENTINA
Facultad de Matemática, Astronomía y Física,
Universidad Nacional de Córdoba, ARGENTINA

Grupo de Observadores de Rotaciones de Asteroides (GORA), ARGENTINA
milirita.colazovinovo@gmail.com

Francisco Santos, César Fornari, Damián Scotta, Néstor Suárez, Alberto García, Mario Morales, Ariel Stechina, Matías Martini, Raúl Melia, Andrés Chapman, Ezequiel Bellocchio, Aldo Wilberger, Marcos Anzola, Aldo Mottino, Carlos Colazo.

Grupo de Observadores de Rotaciones de Asteroides (GORA), ARGENTINA

Grupo de Astrometría y Fotometría (GAF), ARGENTINA

Estación Astrofísica Bosque Alegre (MPC 821) -
Bosque Alegre (Córdoba- ARGENTINA)

Observatorio Astronómico Giordano Bruno (MPC G05) -
Piconcillo (Córdoba-ESPAÑA)

Observatorio Cruz del Sur (MPC I39) -
San Justo (Buenos Aires-ARGENTINA)

Observatorio de Sencelles (MPC K14) -
Sencelles (Mallorca-Islas Baleares- ESPAÑA)

Observatorio Los Cabezones (MPC X12) -
Santa Rosa (La Pampa-ARGENTINA)

Observatorio Galileo Galilei (MPC X31) -
Oro Verde (Entre Ríos- ARGENTINA)

Observatorio Antares (MPC X39) -
Pilar (Buenos Aires- ARGENTINA)

Observatorio AstroPilar (GORA APB) -
Pilar (Buenos Aires- ARGENTINA)

Observatorio Astronómico Aficionado Omega (GORA OAO) -
Córdoba (Córdoba- ARGENTINA)

Observatorio de Ariel Stechina 1 (GORA OAS) -
Reconquista (Santa Fe- ARGENTINA)

Observatorio de Ariel Stechina 2 (GORA OA2) -
Reconquista (Santa Fe- ARGENTINA)

Observatorio de Damián Scotta 1 (GORA ODS) -
San Carlos Centro (Santa Fe- ARGENTINA)

Observatorio de Damián Scotta 2 (GORA OD2) -
San Carlos Centro (Santa Fe- ARGENTINA)

Observatorio Astronómico Vuelta por el Universo (GORA OMA)
Córdoba (Córdoba- ARGENTINA)

Observatorio Río Cofio (GORA ORC) -
Robledo de Chavela (Madrid- ESPAÑA)

Observatorio de Raúl Melia (GORA RMG) -
Gálvez (Santa Fe- ARGENTINA)

(Received: 2021 June 29)

Synodic rotation periods and amplitudes are reported for 318 Magdalena, 455 Bruchsalia, 486 Cremona, 503 Evelyn, and 664 Judith.

The periods and amplitudes of asteroid lightcurves presented here are the product of collaborative work by GORA (Grupo de Observadores de Rotaciones de Asteroides) group. In all the studies we have applied relative photometry assigning V magnitudes to the calibration stars.

The image acquisition was performed without filters and with exposure times of a few minutes. All images used were corrected using dark frames and, in some cases, bias and flat-field were also used. Photometry measurements were performed using *FotoDif* software and for the analysis, we employed *Periodos* software (Mazzone, 2012).

Below, we present the results for each asteroid under study. The lightcurve figures contain the following information: the estimated period and period error and the estimated amplitude and amplitude error. In the reference boxes, the columns represent, respectively, the marker, observatory MPC code, or - failing that - the GORA internal code, session date, session offset, and several data points.

Targets were selected based on the following criteria: 1) those asteroids with magnitudes accessible to the equipment of all participants, 2) those with favorable observation conditions from Argentina or Spain, i.e., with negative or positive declinations, respectively, and 3) objects with few periods reported in the literature and/or with light curve Database (LCDB) (Warner et al., 2009) quality codes (U) of less than 3.

318 Magdalena was discovered in 1891 by Charlois, A. The two more recent periods published in the literature correspond to $P = 42.49 \pm 0.01$ h with $\Delta m = 0.06 \pm 0.01$ mag (Pilcher & Martinez, 2015) and $P = 42.65 \pm 0.01$ h with $\Delta m = 0.08 \pm 0.01$ mag (Pilcher, 2019). The results we obtained, $P = 45.251 \pm 0.012$ h with $\Delta m = 0.16 \pm 0.02$ mag, are consistent with those presented by Pilcher. Moreover, our analysis shows an asymmetric bimodal light curve, quite similar to the one presented by this same author.

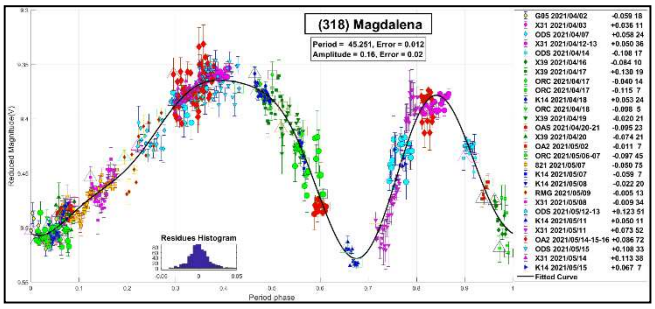

455 Bruchsalia was discovered in 1900 by M. Wolf and A. Schwassmann. Ferrero (2020) and Pilcher (2020) reported a period of 11.839 ± 0.001 h. Although they measured the same period, they reported different amplitudes, which were 0.42 mag (Ferrero, 2020) and 0.50 ± 0.03 mag (Pilcher, 2020). Our analysis yields a period of $P = 11.838 \pm 0.014$ h with $\Delta m = 0.13 \pm 0.02$ mag. The difference in amplitude with respect to previous observations likely reflects a significant change in the viewing aspect angle of the asteroid.

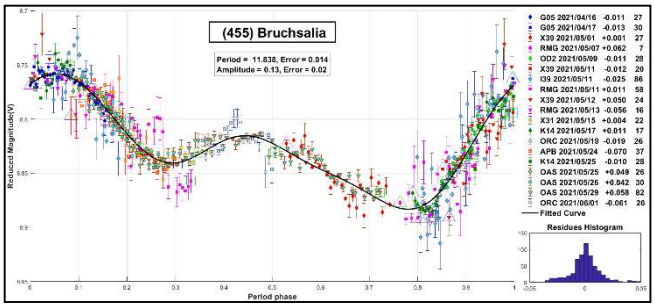

486 Cremona was discovered in 1902 by Carnera, L. The two more recent periods reported in literature are $P = 65.151 \pm 0.005$ h (Hanuš et al., 2011) and $P = 65.15 \pm 0.10$ h with $\Delta m = 0.80 \pm 0.05$ mag (Cooney et al., 2007). Our observations determined a period of $P = 64.941 \pm 0.010$ h with an amplitude of $\Delta m = 0.36 \pm 0.01$ mag. This result is in good agreement with those mentioned above. Also, we noted that our light curve is bimodal with little asymmetric peaks as also shown by Hanuš and Cooney.

Observatory	Telescope	Camera
821 Est.Astrof.Bosque Alegre	Telesc. Newtoniano (D=1540mm; f=4.9)	CCD APOGEE Alta U9
G05 Obs.Astr.Giordano Bruno	Telesc. SCT (D=203mm; f=6.0)	CCD Atik 420 m
I39 Obs.Astr.Cruz del Sur	Telesc. Newtoniano (D=254mm; f=4.7)	CMOS QHY174
K14 Obs.Astr.de Sencelles	Telesc. Newtoniano (D=250mm; f=4.0)	CCD SBIG ST-7XME
X12 Obs.Astr.Los Cabezones	Telesc. Newtoniano (D=200mm; f=5.0)	CMOS QHY174MGPS
X31 Obs.Astr.Galileo Galilei	Telesc. RCT ap (D=405mm; f=8.0)	CCD SBIG STF8300M
X39 Obs.Astr.Antares	Telesc. Newtoniano (D=250mm; f=4.7)	CCD QHY9 Mono
APB Obs.Astr.AstroPilar	Telesc. Refractor (D=150mm; f=7.0)	CCD ZWO-ASI183
OAO Obs.Astr.Aficionado Omega	Telesc. Newtoniano (D=150mm; f=5.0)	CMOS ZWO ASI178mm
OAS Obs.Astr.de Ariel Stechina 1	Telesc. Newtoniano (D=254mm; f=4.7)	CCD SBIG STF402
OA2 Obs.Astr.de Ariel Stechina 2	Telesc. Newtoniano (D=305mm; f=5.0)	CMOS QHY 174M
ODS Obs.Astr.de Damián Scotta 1	Telesc. Newtoniano (D=300mm; f=4.0)	CCD SBIG St-402 XME
OD2 Obs.Astr.de Damián Scotta 2	Telesc. Newtoniano (D=250mm; f=4.0)	CCD Atik 314L+
OMA Obs.Astr.Vuelta por el Universo	Telesc. Newtoniano (D=150mm; f=5.0)	CMOS Qhy5III 290
ORC Obs.Astr.RíoCofio	Telesc. SCT (D=254mm; f=6.3)	CCD SBIG ST8-XME
RMG Obs.Astr.de Raúl Melia	Telesc. SCT (D=200mm; f=10.0)	CCD Meade DSI Pro II

Table II. List of observatories and equipment.

Number	Name	yy/ mm/dd- yy/ mm/dd	Phase	L_{PAB}	B_{PAB}	Period(h)	P.E.	Amp	A.E.	Grp
318	Magdalena	21/04/02-21/05/16	*4.6,11.4	202	9	45.251	0.012	0.16	0.02	MB-O
455	Bruchsalia	21/04/16-21/06/01	*5.4,13.4	215	9	11.838	0.014	0.13	0.02	MB-M
486	Cremona	21/05/06-21/06/14	8.6,18.4	233	10	64.941	0.010	0.36	0.01	MB-I
503	Evelyn	21/05/12-21/06/11	*7.8,03.6	251	0	38.871	0.011	0.44	0.02	MB-O
664	Judith	21/04/03-21/06/05	*12.2,14.4	222	9	19.303	0.012	0.30	0.02	MB-O

Table I. Observing circumstances and results. The phase angle is given for the first and last date. If preceded by an asterisk, the phase angle reached an extremum during the period. L_{PAB} and B_{PAB} are the approximate phase angle bisector longitude/latitude at mid-date range (see Harris et al., 1984). Grp is the asteroid family/group (Warner et al., 2009). MB-O: main-belt outer.

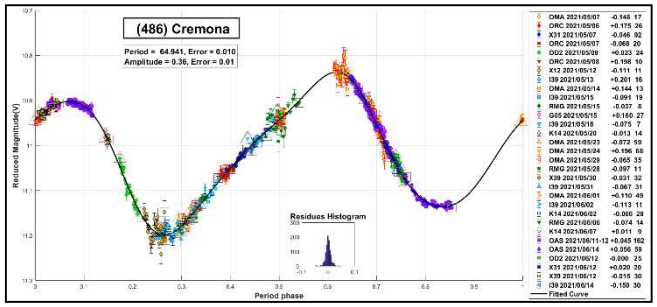

503 Evelyn was discovered in 1903 by R.S. Dugan. We measured a period of 38.871 ± 0.011 with Δm = 0.44 ± 0.02 mag. These results agree well with those reported by Fauerbach (2007): P = 38.70 ± 0.01 with Δm = 0.30 ± 0.03 mag. As a further contribution, our lightcurve provides more coverage on the rotational phase space.

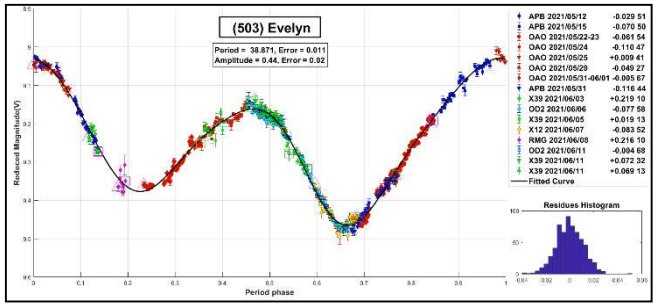

664 Judith was discovered in 1908 by A. Kopff. We found two different periods reported in the literature: P = 19.35 ± 0.06 h with Δm = 0.35 ± 0.02 mag (Melton et al., 2012) and P = 18.51 ± 0.01 h with Δm = 0.37 ± 0.03 mag (Garcerán, 2015). Our period agrees well with the one measured by Melton et al. (2012). The bimodal shape of the lightcurve is also in good agreement with that from Melton et al. (2012). As a further contribution, we provide almost full coverage of this lightcurve.

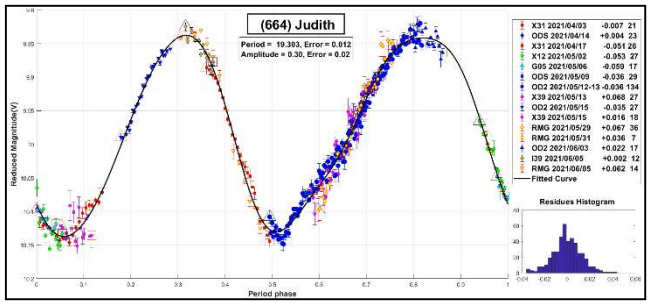

Acknowledgements

We want to thank Julio Castellano as we use his *FotoDif* program for preliminary analyses, Fernando Mazzone for his *Periods* program, used in final analyses, and Matías Martini for his *CalculadorMDE_v0.2* used for generating ephemerides used in the planning stage of the observations. This research has made use of the Small Bodies Data Ferret (*http://sbn.psi.edu/ferret/*), supported by the NASA Planetary System and made use of data and/or services provided by the International Astronomical Union's Minor Planet Center.

References

Cooney Jr, W.R.; Gross, J.; Terrell, D.; Reddy, V.; Dyvig, R. (2007). "Lightcurve Results for 486 Cremona, 855 Newcombia, 942 Romilda, 3908 Nyx, 5139 Rumoi, 5653 Camarillo, and (102866) 1999 WA5." *Icarus* **158**, 379-388.

Fauerbach, M.; Bennett, T.; Marks, S.A. (2007). "Lightcurve Results for 81 Terpsichore, 242 Kriemhild 503 Evelyn, 522 Helga, and 578 Happelia." *Minor Planet Bulletin* **34**, 57-58.

Ferrero, A. (2020). "Photometric Lightcurves of Eight Main-belt Asteroids." *Minor Planet Bulletin* **47**, 172-174.

Garcerán, A. C., Macias, A. A., Mansego, E. A., Rodriguez, P. B., & de Haro, J. L. (2015). "Lightcurve Analysis of Six Asteroids." *Minor Planet Bulletin*, **42(4)**, 235-237.

Hanuš, J.; Ďurech, J.; Brož, M.; Warner, B.D.; Pilcher, F.; et al., (2011). "A study of asteroid pole-latitude distribution based on an extended set of shape models derived by the lightcurve inversion method." *Astronomy & Astrophysics* **530**, A134.

Harris, A.W.; Young, J.W.; Scaltriti, F.; Zappala, V. (1984). "Lightcurves and phase relations of the asteroids 82 Alkmene and 444 Gyptis." *Icarus* **57**, 251-258.

Mazzone, F.; Colazo, C.; Mina, F.; Melia, R.; Spagnotto, J.; Bernal, A. (2014). "Collaborative asteroid photometry and lightcurve analysis at observatories OAEGG, OAC, EABA AND OAS." *Minor Planet Bulletin* **41**, 17-18

Melton, E.; Carver, S.; Harris, A.; Karnemaat, R.; Klaasse, M.; Ditteon, R. (2012). "Asteroid Lightcurve Analysis at the Oakley Southern Sky Observatory: 2011 November-December." *Minor Planet Bulletin*, **39(3),** 131-133.

Pilcher, F.; Martinez, L. (2015). "Rotation Period Determination for 318 Magdalena and 335 Roberta." *Minor Planet Bulletin **42***, 239.

Pilcher, F. (2019). "New Lightcurves of 153 Hilda, 293 Brasillia, and 318 Magdalena." *Minor Planet Bulletin* **46**, 130-131.

Pilcher, F. (2020). "Lightcurves and Rotation Periods of 10 Hygiea, 47 Aglaja, 455 Bruchsalia, 463 Lola, and 576 Emanuela." *MinorPlanetBulletin* **47**, 133-135.

Warner, B.D.; Harris, A.W.; Pravec, P. (2009) "The asteroid lightcurve database." *Icarus* **202**, 134-146. Updated 2021 June 7. *http://www.minorplanet.info/lightcurvedatabase.html*

LIGHTCURVE ANALYSIS FOR THIRTEEN MINOR PLANETS

Tom Polakis
Command Module Observatory
121 W. Alameda Dr.
Tempe, AZ 85282
tpolakis@cox.net

(Received: 2021 June 18)

Photometric measurements were made for 13 main-belt asteroids, based on CCD observations made from 2021 March through 2021 May. Phased lightcurves were created for nine asteroids, while four did not yield a period solution. All the data have been submitted to the ALCDEF database.

CCD photometric observations of 13 main-belt asteroids were performed at Command Module Observatory (MPC V02) in Tempe, AZ. Images were taken using a 0.32-m f/6.7 Modified Dall-Kirkham telescope, SBIG STXL-6303 CCD camera, and a 'clear' glass filter. Exposure time for all the images was 2 minutes. The image scale after 2×2 binning was 1.76 arcsec/pixel. Table I shows the observing circumstances and results. All of the images for these asteroids were obtained between 2021 March and 2021 May.

Images were calibrated using a dozen bias, dark, and flat frames. Flat-field images were made using an electroluminescent panel. Image calibration and alignment was performed using *MaxIm DL* software.

The data reduction and period analysis were done using *MPO Canopus* (Warner, 2020). The 45′×30′ field of the CCD typically enables the use of the same field center for three consecutive nights. In these fields, the asteroid and three to five comparison stars were measured. Comparison stars were selected with colors within the range of 0.5 < B-V < 0.95 to correspond with color ranges of asteroids. In order to reduce the internal scatter in the data, the brightest stars of appropriate color that had peak ADU counts below the range where chip response becomes nonlinear were selected. MPO Canopus plots instrumental vs. catalog magnitudes for solar-colored stars, which is useful for selecting comp stars of suitable color and brightness.

Since the sensitivity of the KAF-6303 chip peaks in the red, the clear-filtered images were reduced to Sloan r′ to minimize error with respect to a color term. Comparison star magnitudes were obtained from the ATLAS catalog (Tonry et al., 2018), which is incorporated directly into *MPO Canopus*. The ATLAS catalog derives Sloan *griz* magnitudes using a number of available catalogs. The consistency of the ATLAS comp star magnitudes and color-indices allowed the separate nightly runs to be linked often with no zero-point offset required or shifts of only a few hundredths of a magnitude in a series.

A 9-pixel (16 arcsec) diameter measuring aperture was used for asteroids and comp stars. It was typically necessary to employ star subtraction to remove contamination by field stars. For the asteroids described here, I note the RMS scatter on the phased lightcurves, which gives an indication of the overall data quality including errors from the calibration of the frames, measurement of the comp stars, the asteroid itself, and the period-fit. Period determination was done using the *MPO Canopus* Fourier-type FALC fitting method (cf. Harris et al., 1989). Phased lightcurves show the maximum at phase zero. Magnitudes in these plots are apparent and scaled by *MPO Canopus* to the first night. In cases where rotation periods could not be determined, raw lightcurves are presented, with "Raw" appearing in the upper right-hand corner of the plots.

Most asteroids were selected from the CALL website (Warner, 2011) In this set of observations, 3 of the 13 asteroids had no previous period analysis, 2 had U = 1, 2 had U=2, and the remainder had U = 3. The Asteroid Lightcurve Database (LCDB; Warner et al., 2009) was consulted to locate previously published results. All the new data for these asteroids can be found in the ALCDEF database.

363 Padua was discovered by Auguste Charlois at Nice in 1893. Koff (2006) computed a rotational period of 8.401 ± 0.001 h, and Pál et al. (2020) shows 8.40077 ± 0.00005 h. A total of 363 images were gathered over the course of three nights, yielding a period of 8.413 ± 0.004 h, agreeing with published values. The lightcurve has an amplitude of 0.08 mag. with an RMS error of 0.010 mag.

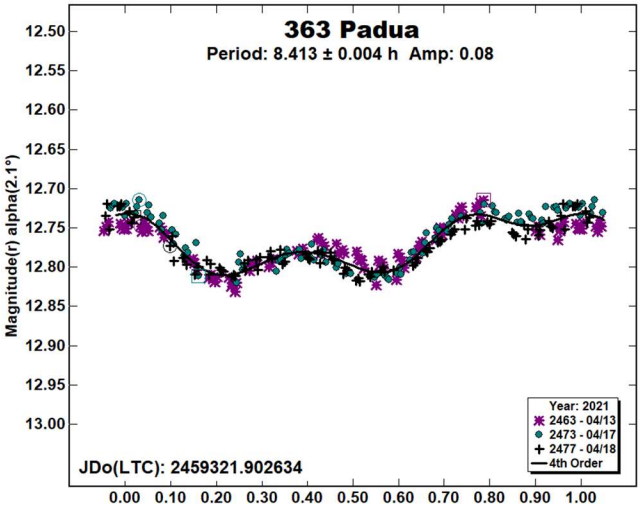

412 Elisabetha. This outer main-belt asteroid was discovered at Heidelberg in 1896 by Max Wolf. Two concurring period solutions are Cooney and Robinson (2002): 19.67 ± 0.1 h and Stephens (2012), 19.635 ± 0.005 h. Pál (2020) derived a period of 39.3269 ± 0.0005 h. During three nights, 323 images were taken, resulting in a period of 19.60 ± 0.06 h, with an amplitude of 0.09 ± 0.008 mag. This result agrees with Cooney's and Stephens's solutions.

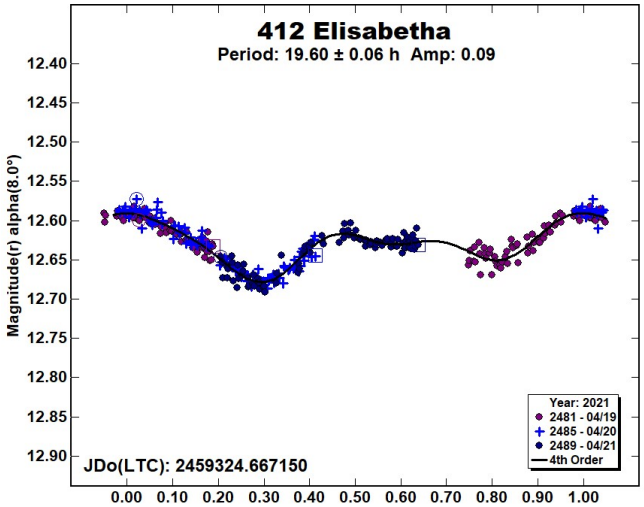

Number	Name	yy/mm/dd	Phase	L_{PAB}	B_{PAB}	Period(h)	P.E.	Amp	A.E.	Grp
363	Padua	21/04/13-04/18	2.1,3.1	202	5	8.413	0.004	0.08	0.01	MB-O
412	Elisabetha	21/04/19-04/21	8.0,7.9	210	17	19.60	0.06	0.09	0.01	MB-O
536	Merapi	21/04/19-04/21	6.7,7.1	193	16	8.806	0.005	0.19	0.01	MB-O
563	Suleika	21/04/13-04/18	*4.2,4.2	205	11	5.629	0.001	0.16	0.01	MB-O
820	Adriana	21/03/17-03/22	2.6,4.0	172	6	12.42	0.01	0.39	0.03	MB-O
1390	Abastumani	21/03/20-03/28	7.1,8.7	164	16	26.49	0.07	0.13	0.02	MB-O
1458	Mineura	21/03/17-04/26	*1.3,15.8	179	0	930.5	3.6	0.68	0.06	EUN
2326	Tololo	21/03/30-04/01	3.8,4.1	188	10	9.60	0.05	0.11	0.05	MB-O
2521	Heidi	21/03/05-03/07	4.4,4.5	165	-9	--	--	--	--	MB-O
2777	Shukshin	21/03/17-05/01	4.8,22.4	171	4	1008.6	3.4	0.75	0.08	MB-I
3275	Oberndorfer	21/03/30-04/01	5.8,6.4	185	8	--	--	--	--	MB-I
4133	Heureka	21/03/05-03/07	2.9,3.5	163	-5	--	--	--	--	EUN
4238	Audrey	21/03/05-03/06	1.6,1.1	167	1	--	--	--	--	MB-I

Table I. Observing circumstances and results. The phase angle is given for the first and last date. If preceded by an asterisk, the phase angle reached an extrema during the period. L_{PAB} and B_{PAB} are the approximate phase angle bisector longitude/latitude at mid-date range (see Harris et al., 1984). Grp is the asteroid family/group (Warner et al., 2009).

536 Merapi was discovered in Washington by George Henry Peters in 1904. Several consistent period solutions appear in the LCDB: Koff (2000), 8.78 ± 0.01 h; Ditteon and Hawkins (2007), 8.209 ± 0.008 h; and Behrend (2020web), 8.791 ± 0.001 h. A total of 277 data points were acquired in three nights, and the resulting period solution is 8.806 ± 0.005 h, which agrees with previous assessments. The amplitude and RMS error on the fit are 0.19 mag and 0.012 mag.

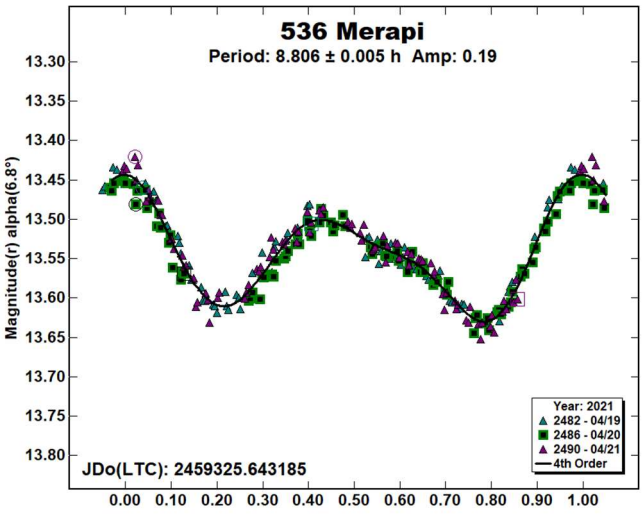

563 Suleika. This outer main-belt asteroid in a highly eccentric orbit was discovered by Paul Gotz at Heidelberg in 1905. The LCDB shows six similar period solutions. Two of the most recent are Ditteon and Hawkins (2007), 5.628 ± 0.002 h and Franco et al. (2020), 5.6656 ± 0.0004 h. During three nights, 270 images were taken. A 6th order fit produced a period solution of 5.629 ± 0.001 h, and an amplitude of 0.16 ± 0.010 mag.

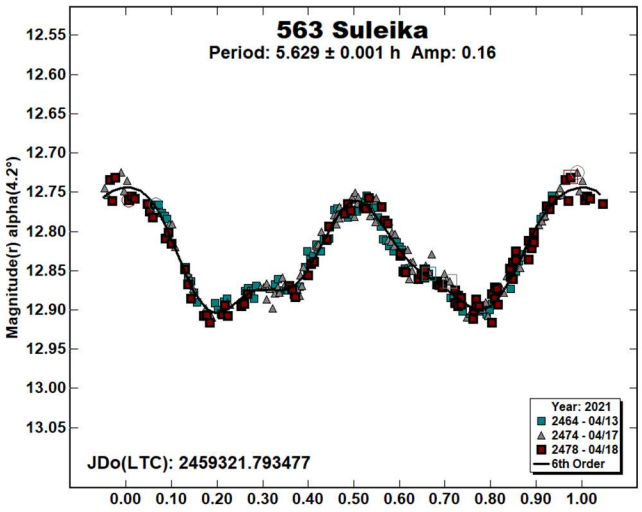

820 Adriana, discovered in 1916, is another of Max Wolf's discoveries at Heidelberg. Only one rotational period appears in the LCDB, that of Ditteon et al. (2018), who computed 6.527 ± 0.006 h. During four nights, 272 images were gathered, producing a period solution of 12.42 ± 0.01 h, disagreeing with Ditteon's result. The amplitude of the lightcurve is 0.39 ± 0.034 mag.

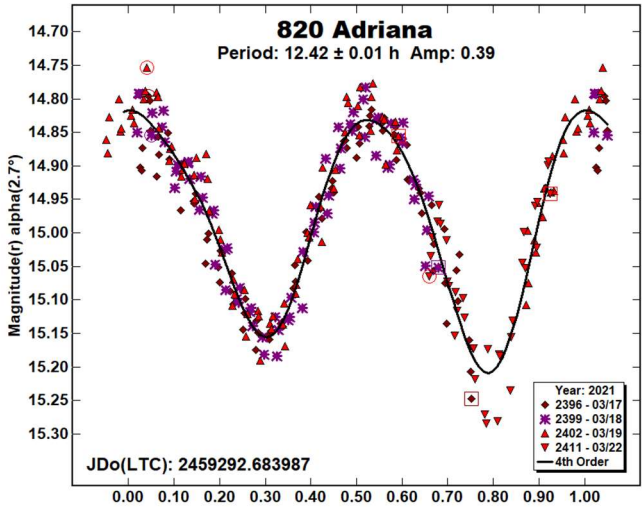

1390 Abastumani. Grigory Shajn discovered this outer main-belt asteroid in an inclined orbit at Simeis in 1935. Gross (2003) published a period of 17.100 ± 0.005 h, and Durech et al. (2018) calculated 13.16482 ± 0.00002 h. Over the course of six nights, 502 images were obtained, yielding a synodic period of 26.49 ± 0.07 h, which is roughly double Durech's period. The amplitude is 0.13 mag., and the RMS error on the fit is 0.022 mag.

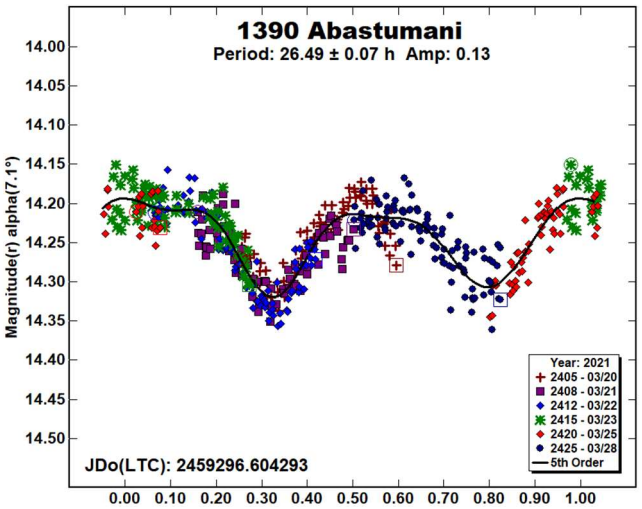

1458 Mineura is a member of the Eunomia family. It was discovered by Fernand Rigaux at Uccle in 1937. The only entry in the LCDB is that of Behrend (2005web), who shows a period estimate of 36 h. The slow rotator required 37 nights of observation to cover a single rotation, during which 874 images were obtained. The period is 930.5 ± 3.6 h. The amplitude is 0.68 mag., with an RMS error on the fit of 0.059 mag.

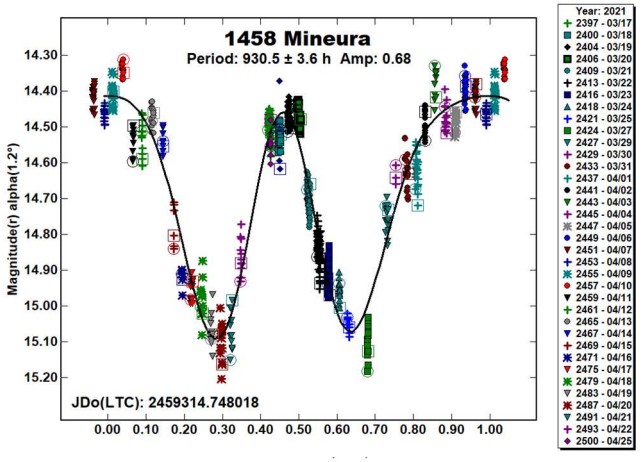

2326 Tololo. This outer main-belt minor planet was discovered by Goethe Link at Brooklyn in 1965. Percy (2019) published a period of 9.488 ± 0.001 h, and Polakis (2020) computed 9.49 ± 0.05 h. The asteroid was observed for three nights, and 237 images were taken. The best period solution appears at of 9.60 ± 0.05 h. While the period matches previous values, the fit is poor: the RMS error of 0.047 mag is high relative to the amplitude of 0.11 mag.

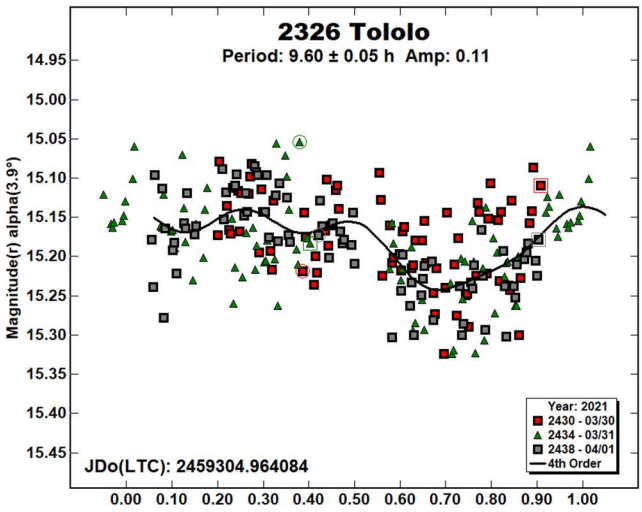

2521 Heidi. Paul Wild made this discovery at Zimmerwald in 1979. The only period estimate is >12 h, by Behrend (2004web). The lightcurve remained flat after three nights, during which 241 images were taken, and no period solution was derived. Only the raw lightcurve is provided. The very slow increase in brightness indicates that it may be a slow rotator.

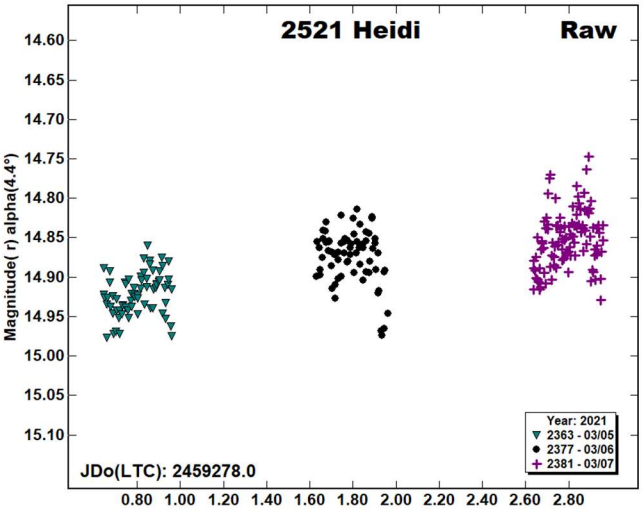

2777 Shukshin is an inner main-belt asteroid, discovered by Nikolai Chernykh in in 1979 at Nauchnyj. No periods appear for it in the LCDB. This is another slowly rotating body, and it required 42 nights of observations, during which 809 images were taken. The rotational period is 1008.6 ± 3.4h. The amplitude is 0.75 ± 0.079 mag.

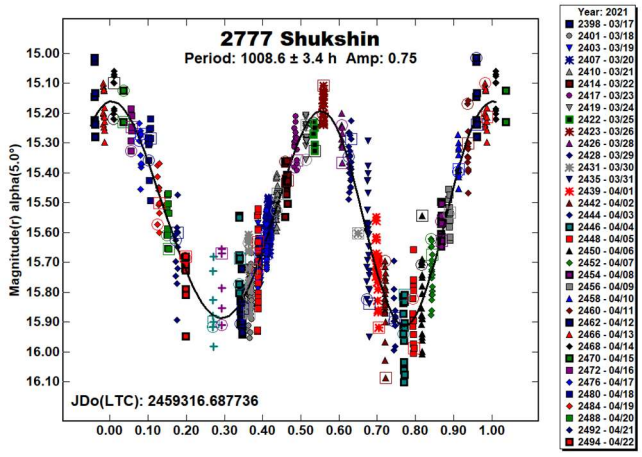

3275 Oberndorfer was discovered by Edward Bowell at Lowell in 1982. Pál (2020) computed a period of 9.23645 ± 0.00005 h. No period solutions were found after 236 images were taken in three nights. The raw lightcurve is provided.

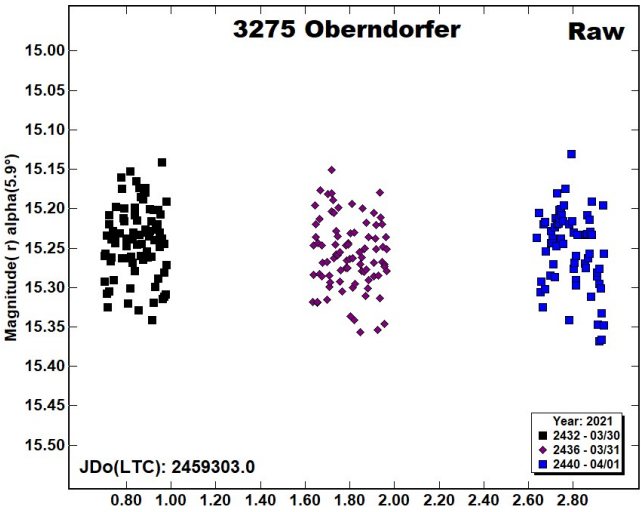

4133 Heureka. Liisi Oterma discovered this Eunomia-family asteroid from Turku in 1942. There are no published period solutions for it. Again, the lightcurve was flat during three nights, so only a raw lightcurve is provided.

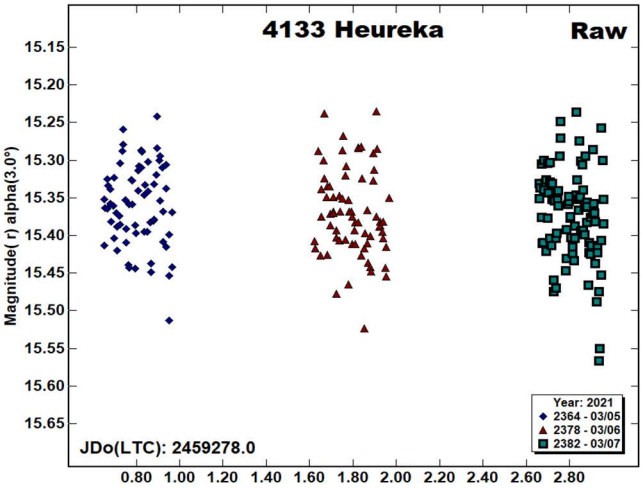

4238 Audrey was discovered in 1980 by Anton Mrkos at Klet. The LCDB shows no period solutions. A total of 150 images were taken during two nights. Again, no period solution was found.

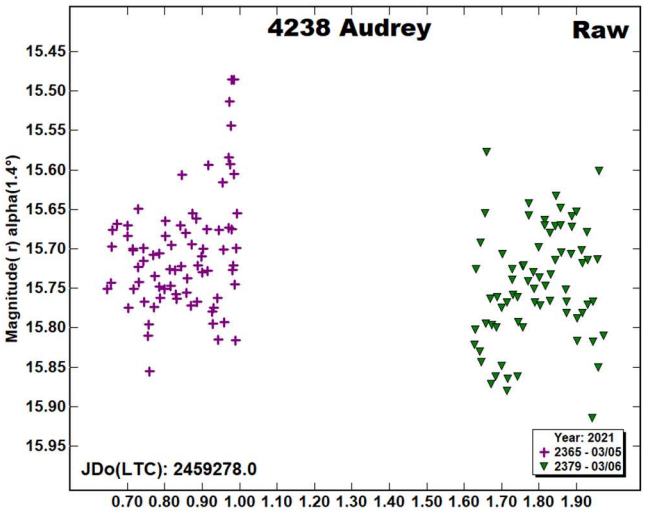

Acknowledgements

The author would like to express his gratitude to Brian Skiff for his indispensable mentoring in data acquisition and reduction. Thanks also go out to Brian Warner for support of his *MPO Canopus* software package.

References

Behrend, R. (2004web, 2005web, 2020web). Observatoire de Geneve web site. *http://obswww.unige.ch/~behrend/page_cou.html*

Cooney, W.R.; Robinson, L. (2002). "Rotation Periods and Light Curves of Minor Planets (412) Elisabetha (547) Praxedis, and (7564) 1988 CA." *Minor Planet Bull*. **29**, 78-79.

Ditteon, R.; Hawkins, S. (2007). "Asteroid Lightcurve Analysis at the Oakley Observatory - October-November 2006." *Minor Planet Bull.* **34**, 59-64.

Ditteon, R.; Black, S.; Masner, Z.; Osborne, J.; Trent, L. (2018). "Lightcurve Analysis of Minor Planets Observed at the Oakley Southern Sky Observatory: 2017 August-September." *Minor Planet Bull*. **45**, 338-340.

Durech, J.; Hanus, J.; Ali-Lagoa, V. (2018). "Asteroid models reconstructed from the Lowell Photometric Database and WISE data." *Astron. Astrophys*. **617**, A57.

Franco, L.; Marchini, A.; Scarfi, G.; Bacci, P.; Galli, G.; Baj, G.; Papini, R.; Marino, G.; Banfi, M.; Salvaggio, F.; Bacci, R.; Tinelli, L.; Mortari, F.; Foylan, M. (2020). "Collaborative Asteroid Photometry from UAI: 2019 October-December." *Minor Planet Bull*. **47**, 144-147.

Gross, J. (2003). "Sonoran Skies Observatory lightcurve results for asteroids 1054, 1390, 1813 1838, 2988, 3167, 4448, and 5262." *Minor Planet Bull*. **30**, 44-46.

Harris, A.W.; Young, J.W.; Scaltriti, F.; Zappala, V. (1984). "Lightcurves and phase relations of the asteroids 82 Alkmene and 444 Gyptis." *Icarus* **57**, 251-258.

Harris, A.W.; Young, J.W.; Bowell, E.; Martin, L.J.; Millis, R.L.; Poutanen, M.; Scaltriti, F.; Zappala, V.; Schober, H.J.; Debehogne, H.; Zeigler, K.W. (1989). "Photoelectric Observations of Asteroids 3, 24, 60, 261, and 863." *Icarus* **77**, 171-186.

Koff, R.A. (2000). "Rotation Periods and Lightcurves of 536 Merapi and 760 Massinga." *Minor Planet Bull*. **27**, 26-27.

Koff, R.A. (2006). "Lightcurves of asteroids 141 Lumen, 259 Alatheia, 363 Padua, 455 Bruchsalia 514 Armida, 524 Fidelio, and 1139 Atami." *Minor Planet Bull*. **33**, 31-33.

Pál, A.; Szakáts, R.; Kiss, C.; Bódi, A.; Bognár, Z.; Kalup, C.; Kiss, L.L.; Marton, G.; Molnár, L.; Plachy, E.; Sárneczky, K.; Szabó, G.M.; Szabó, R. (2020). "Solar System Objects Observed with TESS – First Data Release: Bright Main-belt and Trojan Asteroids from the Souther Survey." *Ap. J. Suppl Ser*. **247**, id. 26.

Percy, S.C. (2019). "Rotation Period for 2326 Tololo." *Minor Planet Bull*. **46**, 13-14.

Polakis, T. (2020). "Photometric Observations of Thirty Minor Planets." *Minor Planet Bull*. **47**, 177-186.

Stephens, R.D. (2012). "Asteroids Observed from Santana, CS3 and GMARS Observatories: 2012 April - June." *Minor Planet Bull*. **39**, 226-228.

Tonry, J.L.; Denneau, L.; Flewelling, H.; Heinze, A.N.; Onken, C.A.; Smartt, S.J.; Stalder, B.; Weiland, H.J.; Wolf, C. (2018). "The ATLAS All-Sky Stellar Reference Catalog." *Ap. J.* **867**, A105.

Warner, B.D.; Harris, A.W.; Pravec, P. (2009). "The Asteroid Lightcurve Database." *Icarus* **202**, 134-146. Updated 2020 Aug. *http://www.minorplanet.info/lightcurvedatabase.html*

Warner, B.D. (2011). Collaborative Asteroid Lightcurve Link website. *http://www.minorplanet.info/call.html*

Warner. B.D. (2020). MPO Canopus software. *http://bdwpublishing.com*

LIGHTCURVE ANALYSIS OF L4 AND L5 TROJAN ASTEROIDS AT THE CENTER FOR SOLAR SYSTEM STUDIES: 2021 APRIL TO JUNE

Robert D. Stephens
Center for Solar System Studies (CS3) / MoreData!
11355 Mount Johnson Ct., Rancho Cucamonga, CA 91737 USA
rstephens@foxandstephens.com

Daniel R. Coley
Center for Solar System Studies
Corona, CA

Brian D. Warner
Center for Solar System Studies (CS3) / MoreData!
Eaton, CO

(Received: 2021 July 13, Revised: 2021 August 22)

Lightcurves for two L5 Jovian Trojan asteroids were obtained at the Center for Solar System Studies (CS3) from 2021 April to June. In addition, recovered data from 2017 to 2019 allowed finding nine previously unreported periods and restating three previously reported Trojan rotational periods.

For several years, the Center for Solar System Studies (CS3, MPC U81) has been conducting a study of Jovian Trojan asteroids. This paper reports CCD photometric observations of two Trojan asteroids from the L_5 (Trojan) Lagrange point from 2021. In addition, a substantial dataset was recovered with unpublished observations from both the L_4 and L_5 Lagrange points from 2017 to 2019. That recovered dataset also allowed us to reevaluate previous published results for (11395) 1998 XN77 for 2015, 2016, and 2017.

Table I lists the telescopes and CCD cameras that were used to make the observations. Images were unbinned with no filter and had master flats and darks applied. The exposures depended upon various factors including magnitude of the target, sky motion, and Moon illumination.

Telescope	Camera
0.40-m f/10 Schmidt-Cass	FLI Proline 1001E
0.40-m f/10 Schmidt-Cass	Fli Microline 1001E
0.35-m f/10 Schmidt-Cass	Fli Microline 1001E

Table I. List of telescopes and CCD cameras used at CS3.

Image processing, measurement, and period analysis were done using *MPO Canopus* (Bdw Publishing), which incorporates the Fourier analysis algorithm (FALC) developed by Harris (Harris et al., 1989). The Comp Star Selector feature in *MPO Canopus* was used to limit the comparison stars to near solar color. Night-to-night calibration was done using field stars from the ATLAS catalog (Tonry et al., 2018), which has Sloan *griz* magnitudes that were derived from the GAIA and Pan-STARR catalogs and are the "native" magnitudes of the catalog.

Unless otherwise indicated, the Y-axis of lightcurves gives ATLAS SR "sky" (catalog) magnitudes. Some of the older recovered datasets used Johnson V or R (catalog) magnitudes. During period analysis, the magnitudes were normalized to the phase angle and value for *G* given in the parentheses. The X-axis rotational phase ranges from –0.05 to 1.05.

The amplitude indicated in the plots (e.g., Amp. 0.23) is the amplitude of the Fourier model curve and not necessarily the adopted amplitude of the lightcurve.

For brevity, only some of the previously reported rotational periods may be referenced. A complete list is available at the lightcurve database (LCDB; Warner et al., 2009).

884 Priamus. Mottola et al. (2011) reported two periods for this L_5 Trojan. Stephens (2017, and references therein) also observed it four times in the past, each time finding a period near 6.86 h. The period from the 2017 recovered dataset is in good agreement with the past results.

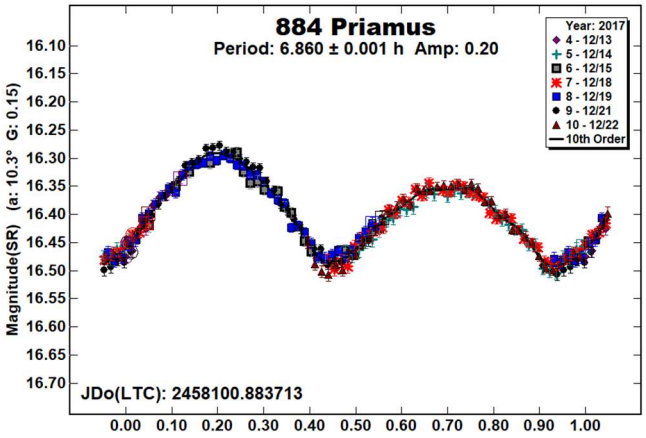

2895 Memnon. Stephens and Warner (2020a, and references therein) obtained rotational periods for this Trojan five times in the past, each time finding a period near 7.52 h. Two recovered datasets, one from 2019 and the other obtained a month before the previous 2020 data, produced periods that are in good agreement with the prior results.

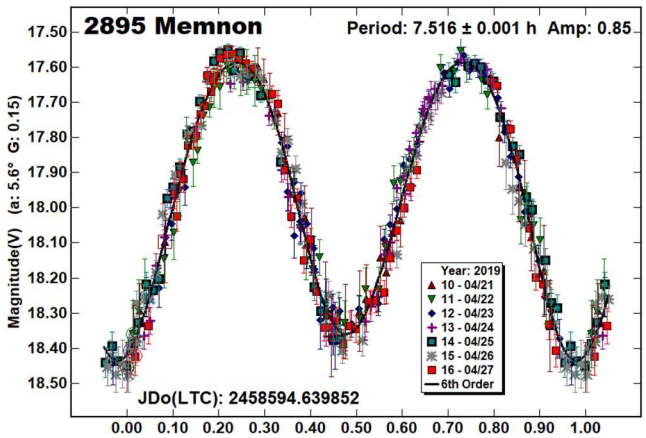

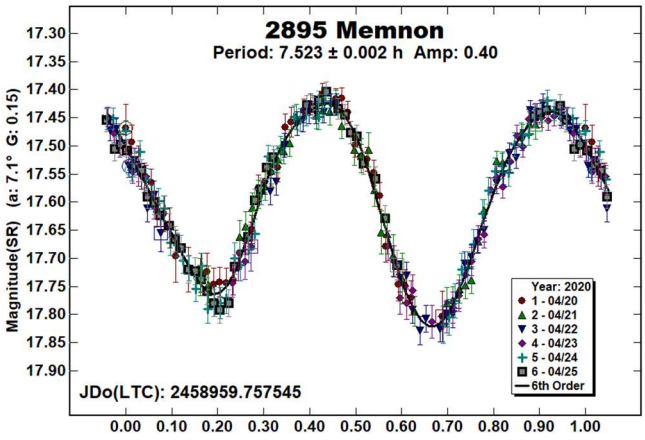

3063 Makhaon. Stephens and Warner (2020b, and references within) observed this L_4 Trojan three times in the past. Mottola et al. (2011) also observed it twice. The results using the recovered datasets from 2018 and 2019 are in good agreement with those prior findings.

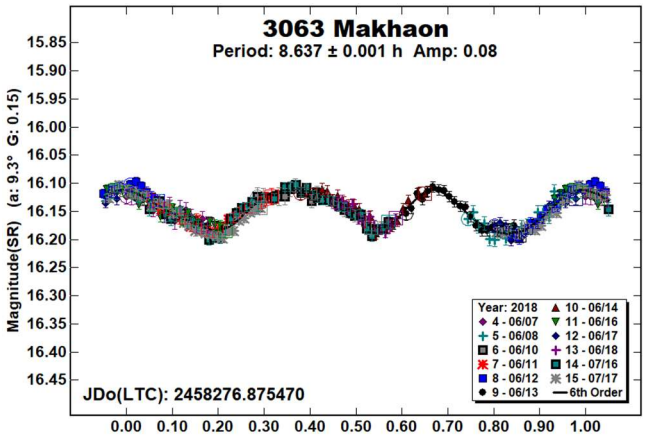

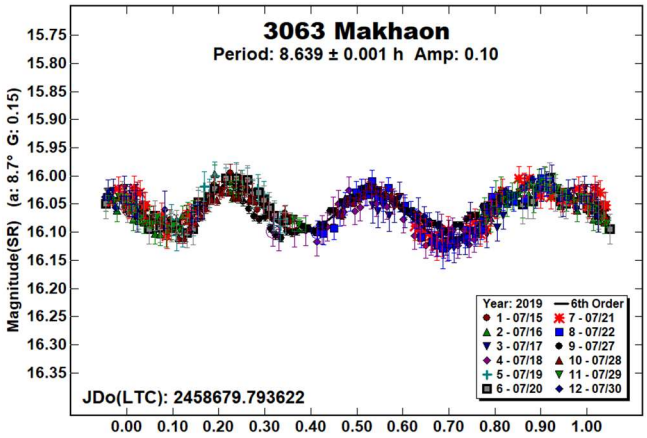

3317 Paris. This L_5 Trojan has been observed many times in the past (Mottola et al., 2011; Stephens and Warner, 2020a, and references therein). All of these previous periods were near 7.08 h. We recovered datasets from 2017 and 2020 and observed it again in 2021 May. The results from these three datasets are in good agreement with the prior results.

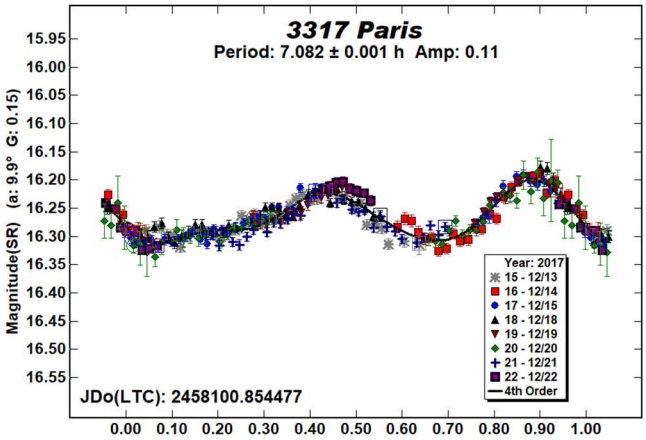

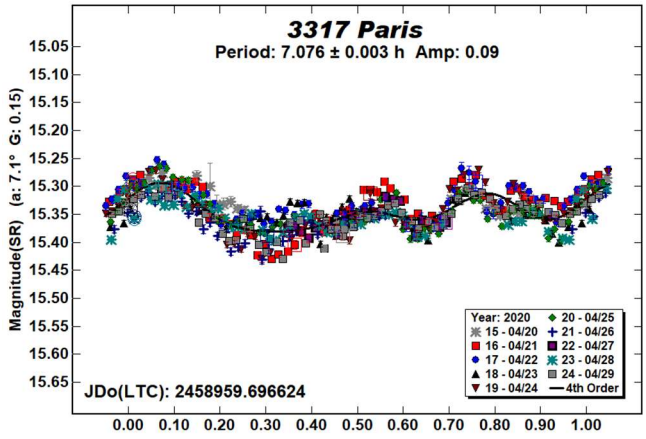

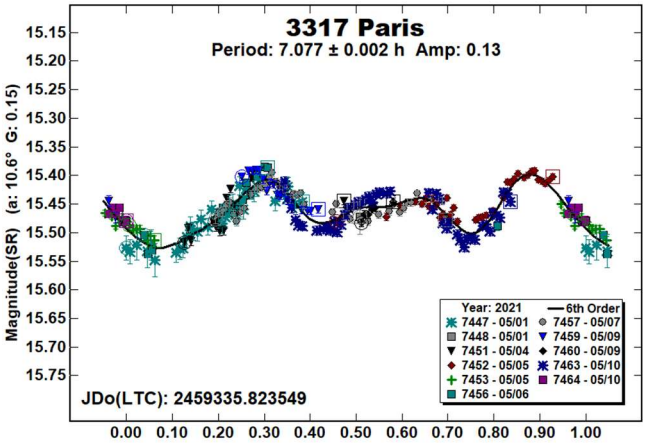

4708 Polydoros. Stephens and Warner (2018, and references therein) observed Polydoros four times in the past finding a common period near 7.5 h for all of the datasets. Using data from the TESS spacecraft, Pál et al. (2020) found a period of 7.51411 h, The results using recovered data from 2017 are in good agreement with the prior results.

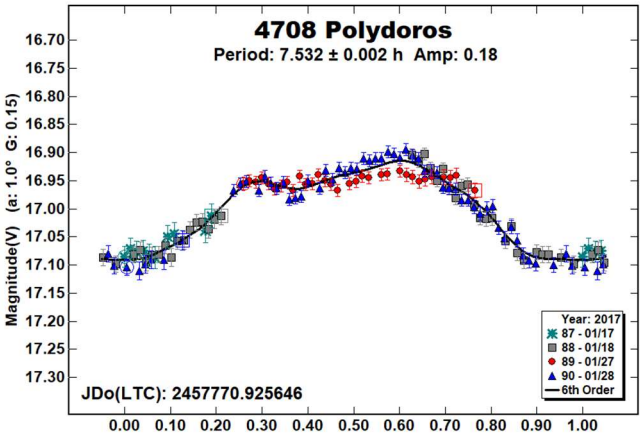

(11395) 1998 XN77. Determining a rotational period for this L_4 Trojan has always been difficult due to its low amplitude. It has been observed five times in the past, with the amplitude never exceeding 0.14 mag. Mottola et al. (2011) observed this Trojan in 2009 and 2010, finding periods of 13.70 h and 13.696 h, respectively. Stephens et al. (2016) and Stephens and Warner (2017) observed it three times. Our initial analysis found periods near 17.9 h with low amplitude asymmetric lightcurves.

A recovered dataset from 2019 had a 13.704 h period, ruled out the longer 17.9 h period, and confirmed the earlier Mottola rotational periods. We corrected some zero-point adjustments and rephase the 2015, 2016, and 2017 data to this period.

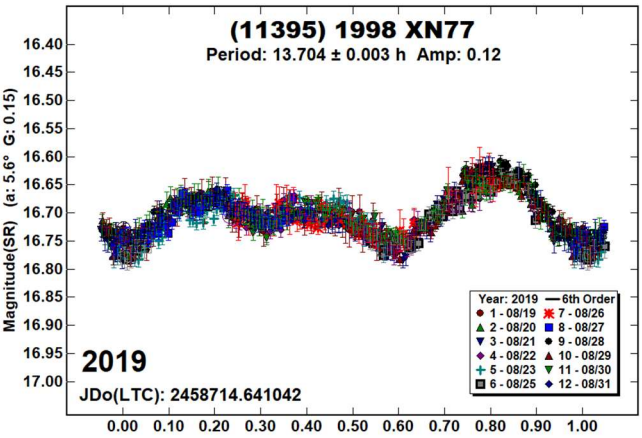

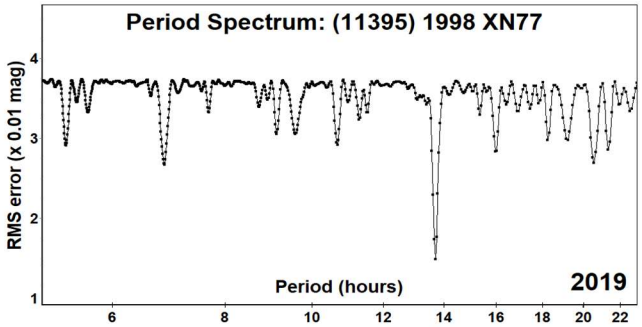

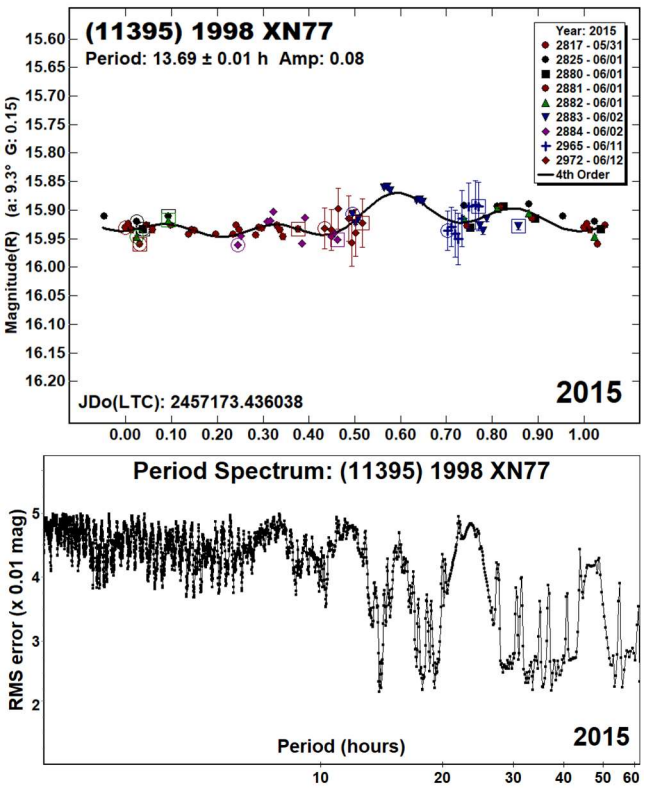

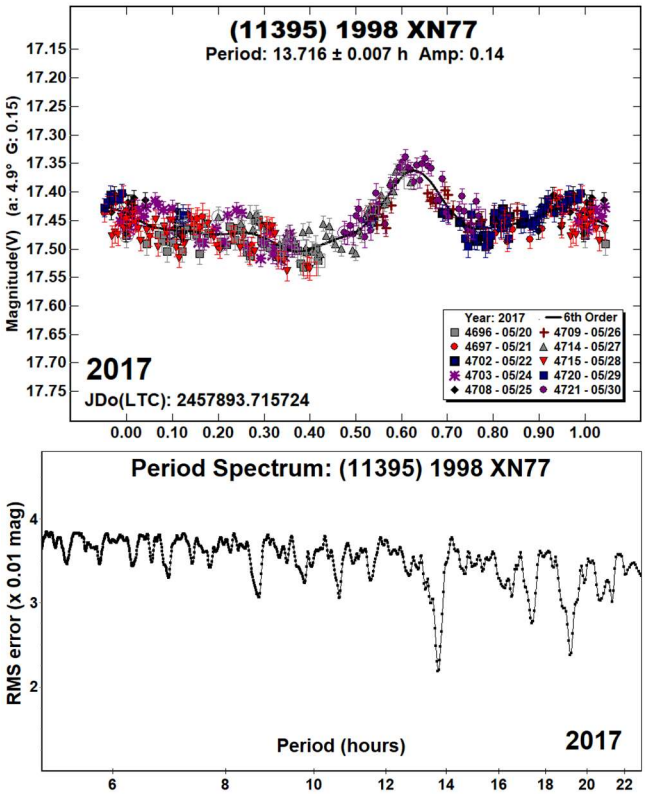

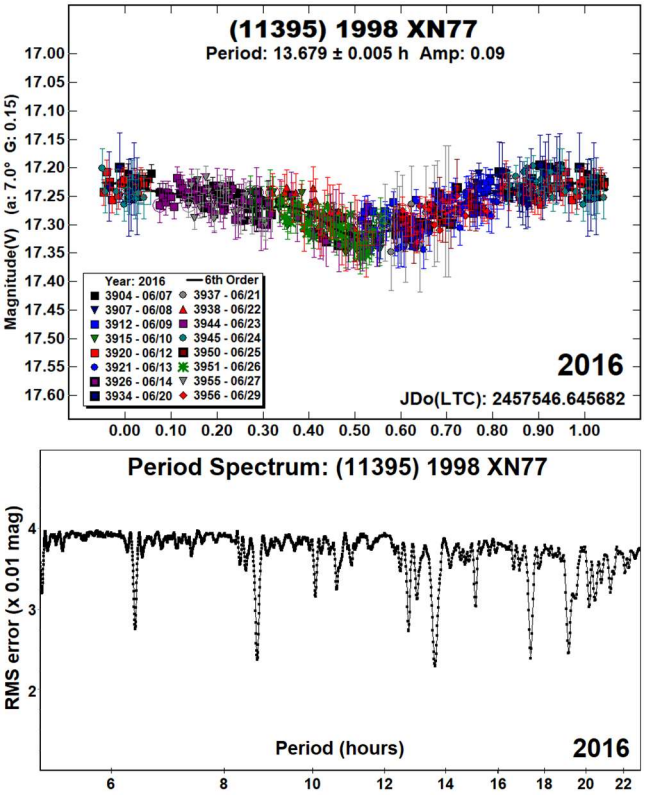

12444 Prothoon. This L_5 Trojan has been observed twice in the past (French et al., 2012; Stephens and Warner 2020a). Our results from 2021 are in good agreement with those findings. Using data from the TESS spacecraft, Pál et al. (2020) found a period of 23.1005 h, a 2:3 alias of our period. The period spectra for all three of our dense datasets show periods near 23 h. However, the 2011 lightcurve rephased to approximately 23 h has a bad fit and the 2020 and 2021 rephased lightcurves have an unlikely shape with the extrema being only 0.3 phase apart. This causes us to reject 23 h as a plausible period.

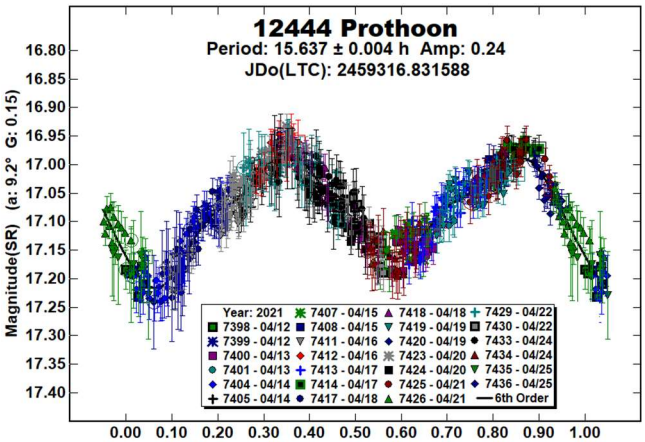

Number	Name	yy/mm/dd	Phase	L_{PAB}	B_{PAB}	Period(h)	P.E.	Amp	A.E.
884	Priamus	17/12/13-12/22	10.3,10.0	159	-5	6.860	0.001	0.20	0.02
2895	Memnon	19/04/21-04/27	5.6,5.7	203	29	7.516	0.001	0.85	0.02
2895	Memnon	20/04/20-04/25	7.1,6.7	238	29	7.523	0.002	0.40	0.01
3063	Makhaon	18/06/07-07/17	9.3,3.8	313	5	8.637	0.001	0.08	0.01
3063	Makhaon	19/07/15-07/30	8.7,6.9	342	10	8.639	0.001	0.10	0.01
3317	Paris	17/12/13-12/22	9.9,9.5	155	8	7.082	0.001	0.11	0.01
3317	Paris	20/04/20-04/29	7.1,6.8	222	31	7.076	0.003	0.09	0.01
3317	Paris	21/05/01-05/10	10.6,9.6	268	25	7.077	0.002	0.13	0.02
4708	Polydoros	17/01/17-01/28	*0.9,1.7	121	-3	7.532	0.002	0.18	0.01
11395	1998 XN77	15/05/31-06/12	9.3,10.2	194	-7	ʳ13.69	0.01	0.08	0.01
11395	1998 XN77	16/06/07-06/29	7.0,9.7	222	6	ʳ13.679	0.005	0.09	0.01
11395	1998 XN77	17/05/20-05/30	4.9,4.0	254	18	ʳ13.716	0.007	0.14	0.02
11395	1998 XN77	19/08/19-08/31	*5.6,5.4	333	24	13.704	0.003	0.12	0.01
12444	Prothoon	21/04/12-04/25	9.2,7.5	247	18	15.637	0.004	0.24	0.02

Table II. Observing circumstances and results. ʳRestated previous period. The phase angle is given for the first and last dates. If preceded by an asterisk, the phase angle reached an extremum during the period. L_{PAB} and B_{PAB} are the approximate phase angle bisector longitude/latitude at mid-date range (see Harris et al., 1984).

Acknowledgements

Observations at CS3 and continued support of the asteroid lightcurve database (LCDB; Warner et al., 2009) are supported by NASA grant 80NSSC18K0851. This work includes data from the Asteroid Terrestrial-impact Last Alert System (ATLAS) project. ATLAS is primarily funded to search for near earth asteroids through NASA grants NN12AR55G, 80NSSC18K0284, and 80NSSC18K1575; byproducts of the NEO search include images and catalogs from the survey area. The ATLAS science products have been made possible through the contributions of the University of Hawaii Institute for Astronomy, the Queen's University Belfast, the Space Telescope Science Institute, and the South African Astronomical Observatory. The purchase of a FLI-1001E CCD camera was made possible by a 2013 Gene Shoemaker NEO Grant from the Planetary Society.

References

French, L.M.; Stephens, R.D.; Coley, D.R.; Megna, R.; Wasserman, L.H. (2012). "Photometry of 17 Jovian Trojan Asteroids." *Minor Planet Bull.* **39**, 183-187.

Harris, A.W.; Young, J.W.; Scaltriti, F.; Zappala, V. (1984). "Lightcurves and phase relations of the asteroids 82 Alkmene and 444 Gyptis." *Icarus* **57**, 251-258.

Harris, A.W.; Young, J.W.; Bowell, E.; Martin, L.J.; Millis, R.L.; Poutanen, M.; Scaltriti, F.; Zappala, V.; Schober, H.J.; Debehogne, H.; Zeigler, K.W. (1989). "Photoelectric Observations of Asteroids 3, 24, 60, 261, and 863." *Icarus* **77**, 171-186.

Mottola, S.; Di Martino, M.; Anders, E.; Gonano-Beurer, M.; Carbognani, A.; Carsenty, U.; Hahn, G.; Schober, H.-J.; Lahulla, F.; Delbò, M.; Lagerskvist, C.-I. (2011). "Rotational Properties of Jupiter Trojans. I. Light Curves of 80 Objects." *Astron. J.* **141**, A170.

Pál, A.; Szakáts, R; Kiss, C.; Bódi, A.; Bognár, Z.; Kalup, C.; Kiss, L.; Marton, G.; Molnár, L.; Plachy, E.; Sárneczky, K.; Szabó, G.; Szabó, R. (2020). "Solar System Objects Observed with TESS - First Data Release: Bright Main-belt and Trojan Asteroids from the Southern Survey." *Astron. J.* **247**, id 26.

Stephens, R.D.; Coley, D.R.; Warner, B.D.; French, L.M. (2016). "Lightcurves of Jovian Trojan Asteroids from the Center for Solar System Studies: L4 Greek Camp and Spies." *Minor Planet Bull*. **43**, 323-331.

Stephens, R.D. (2017). "Lightcurve Analysis of Trojan Asteroids at the Center for Solar System Studies 2016 October - December." *Minor Planet Bull.* **44**, 123-125.

Stephens, R.D.; Warner, B.D., (2017). "Lightcurve Analysis of L4 Trojan Asteroids at the Center for Solar System Studies 2017 April - June." *Minor Planet Bull*. **44**, 312-316.

Stephens, R.D.; Warner, B.D. (2018). "Lightcurve Analysis of L5 Trojan Asteroids at the Center for Solar System Studies: 2018 January to March." *Minor Planet Bul.* **45**, 301-304.

Stephens, R.D.; Warner, B.D. (2020a). "Lightcurve Analysis of L5 Trojan Asteroids at the Center for Solar System Studies: 2020 April to June." *Minor Planet Bull*. **47**, 285-289.

Stephens, R.D.; Warner, B.D. (2020b). "Lightcurve Analysis of L4 Trojan Asteroids at the Center for Solar System Studies: 2020 October to December." *Minor Planet Bull*. **48**, 167-170.

Tonry, J.L.; Denneau, L.; Flewelling, H.; Heinze, A.N.; Onken, C.A.; Smartt, S.J.; Stalder, B.; Weiland, H.J.; Wolf, C. (2018). "The ATLAS All-Sky Stellar Reference Catalog." *Ap. J.* **867**, A105.

Warner, B.D.; Harris, A.W.; Pravec, P. (2009). "The Asteroid Lightcurve Database." *Icarus* **202**, 134-146. Updated 2020 Oct. *http://www.minorplanet.info/lightcurvedatabase.html*

CAVEAT EMPTOR: SPURIOUS SPIN VECTORS FROM INCORRECT SIDEREAL PERIODS

Stephen M. Slivan
Massachusetts Institute of Technology,
Dept. of Earth, Atmospheric, and Planetary Sciences
77 Mass. Ave. Rm. 54-410, Cambridge, MA 02139
slivan@mit.edu

(Received: 2021 June 16, Revised: 2021 July 28)

Spin vector and shape solutions are among the most sophisticated and nuanced analyses that might be undertaken by lightcurve observers who compile measurements from multiple apparitions. Unambiguously determining the correct sidereal period before attempting convex inversion is key, because an incorrect period leads naturally to a spurious spin vector solution. A specific case study for (1443) Ruppina is examined here, with advice on how to recognize an incorrect sidereal period and avoid proceeding with a convex inversion analysis that will be spurious.

Introduction

Convex inversion is a powerful tool for modeling asteroid shapes from lightcurves, but care must be taken to use it correctly. Its design as a nonlinear iterative algorithm (Kaasalainen et al., 2001) requires that initial values be supplied for several parameters including the sidereal rotation period, which the algorithm will be unable to correct if the value is systematically wrong. Instead, it will use the many degrees of freedom at its disposal to do its powerful best and deliver a solution based on the faulty input values, yielding results which might appear to be reasonable despite in fact being spurious. Similarly, quietly wrong outcomes are possible if the available epoch information is not sufficient to distinguish the correct sidereal period. A series of articles in the *Minor Planet Bulletin* (Slivan, 2012; 2013; 2014) discusses the issues related to counting rotations across a lightcurve data set spanning multiple apparitions, and presents information to help manage ambiguity and avoid incorrect determinations of sidereal periods.

A published analysis for asteroid (1443) Ruppina by Stephens and Warner (2020), hereafter "S&W20," provides an instructive case study. The authors observed lightcurves of Ruppina during its 2020 apparition, and combined it with lightcurves from one prior apparition (Stephens, 2018) plus "sparse data" to report a sidereal rotation period result of 5.87929 h. They also reported a corresponding spin vector solution obtained using convex inversion, with one retrograde pole at (120°; –15°) and inconsistent locations given for the symmetric retrograde pole—the text on p. 276 says (295°;–22°) but the Fig. 4 on p. 277 says (300°;–15°). (Note that in the article, figure numbers 1 through 6 are each assigned to two different figures.).

The information in the S&W20 Fig. 1 on p. 277 and accompanying text, suggests that the initial value for the sidereal period was selected based on a statistical approach of identifying a global minimum in a noise spectrum. However, the model used as the basis for the calculations is neither identified nor explained for the reader, and despite including only two published lightcurves, no basis is discussed for confidence that the approach identified the correct sidereal period and merited subsequent spin vector determination. There are other indications in the article that warrant caution, mainly that the graphs of selected lightcurve fits presented as the S&W20 Fig. 5/6 on p. 277 show that, contrary to the caption, the model lightcurves are not "very close on all occasions"—both graphs show systematic mismatches in the shapes of the fitted model lightcurve minima, near phase 0.6 in 2017 and near phase 0.2 in 2020, that appear to be corroborated by the composited lightcurves' graphs in their original publications (Stephens, 2018, p. 51; Stephens and Warner, 2020, p. 276). Also, with regard to the identification of a preferred solution from the symmetric pair of poles, Earth-based lightcurves cannot resolve the ambiguity for Ruppina because of its low orbit inclination of only 2 degrees; thus, a solution that statistically significantly favors one region over the other would be suspect.

Considering especially the limited data upon which the solution is based, a first place to check for a problem is the sidereal period. Slivan (2013) has already detailed for lightcurve observers how to calculate a comprehensive set of sidereal period ranges that are consistent with a set of lightcurve epochs, a calculation which will be used here to test whether the sidereal period solution is consistent with epochs from the four apparitions from which lightcurves have previously been published. The first step is to identify appropriate upper and lower bounds on the sidereal rotation period informed by the best constraint on the synodic rotation period, as illustrated here for Ruppina.

Synodic constraints on sidereal period

For Ruppina the synodic period is very secure as there had already been published four independent determinations, all of which agree (Neugent and Slivan, 2008; Arredondo et al., 2014; Stephens, 2018; Stephens and Warner, 2020). The statistically optimal combination of the measurements is the mean of the individual values weighted by the inverse squares of their errors, yielding 5.8800 ± 0.0006 h. (Note that there is a typographic error in Stephens (2018), p. 51, col. 2, line 3, where the period should read "5.88 h".) However, a subtlety arises from the individual periods' errors having been rounded to a single significant digit—each of the 0.001-h errors could represent unrounded values of up to 0.0015 h, which would underreport the magnitude of the error by up to one-third of its value. In the context of particular priority to not underestimate the allowed range of periods, the possible effect of such rounding is accounted for here by increasing the error of the weighted mean proportionally to ± 0.0009 h.

This one-sigma error corresponds to a confidence interval of about 68%. Adopting 2.5σ to use a more inclusive confidence interval of about 99% as the estimated bounds on the sidereal period yields the range 5.8777 to 5.8823 h.

A remaining consideration is the systematic difference between the sidereal period and the synodic period. For a main-belt object such as Ruppina this difference is too small to distinguish during a single apparition, but for completeness let us consider here what the effect of changing viewing aspect on the measured synodic period actually is. Ephemeris calculations using JPL HORIZONS indicate that for Ruppina the maximum rate of change in phase angle bisector (PAB) longitude is about 0.00088°/h which occurs near oppositions in February or March. This rate corresponds to a maximum possible apparent period change of 0.000084 h per rotation, which can be accounted for here by expanding the bounded interval by only another 0.0001 h at both ends. Thus, the corresponding constraint on the sidereal period for Ruppina, based on the ~99% confidence interval, is 5.8776 to 5.8824 h.

The span of the S&W20 Fig. 1 graph on p. 277 is more than 50 times wider than the synodic constraint, which compresses the bounded range into just over a millimeter, and renders unreadable the only part of the graph that is pertinent to determining the sidereal period. A constructive suggestion for an informative presentation instead would be to illustrate in detail the behavior of the chi-square values within the bounded range, accompanied by context information documenting the model used to calculate the values plotted on the graph.

Published data rule out the reported sidereal period

With the synodic constraint as an input, the "sieve algorithm" of Slivan (2013) is used here to identify the ranges of sidereal periods allowed by the epochs of the already-published lightcurves of Ruppina (Table I). The estimated epoch measurement errors used are 15 min, which is 1.5× the maximum observed asymmetry of the timing of the extrema in the composite lightcurves. A graphical presentation of the results (Fig. 1) shows more than one allowed range for the sidereal period, indicating that these epochs are not sufficient to unambiguously count rotations. Nevertheless, they are sufficient to show that the reported period solution falls outside all of the allowed ranges, thus ruling it out as not consistent with the published lightcurves.

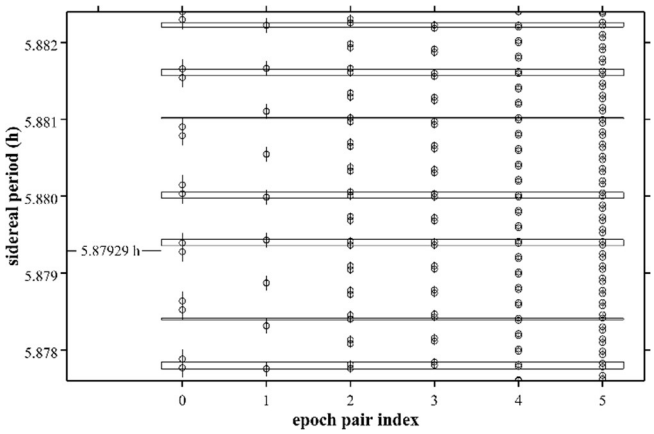

Figure 1: Ranges of possible sidereal rotation periods of (1443) Ruppina allowed by the epochs in Table I, within the synodic constraint 5.8776 to 5.8824 h. Each horizontal coordinate index corresponds to the time interval between a pair of epochs as detailed in Table II, ordered with longer intervals to the right. Open circles and vertical bars represent sidereal periods and period ranges, respectively, calculated from every possible number of rotations that could elapse during the interval. Thin horizontal rectangles identify the ranges of periods that are allowed by all six time intervals. Also marked is the period solution of S&W20, which is not within any of the allowed ranges.

Comparing the sidereal period and poles with a solution based on sufficient data

A key implication of the nonlinear nature of convex inversion is that a small systematic error in the sidereal period can easily produce a huge systematic error in the pole. In the context of the present case study, it would be instructive to be able to also demonstrate here how much of a difference using this incorrect sidereal period actually made in the pole location result reported.

As shown above, epochs from the previously published lightcurves available for Ruppina do not resolve the correct sidereal period for such a demonstration. However, additional lightcurves being reported in a companion paper (Slivan, 2021; this issue) make the needed solution possible—the expanded data set satisfies the criteria of Slivan (2012; 2013; 2014) to unambiguously count rotations and determine a secure sidereal period suitable for spin vector solution, specifically avoiding relying on a statistical noise spectrum. As is fully reported with the additional lightcurves, the analysis determines a sidereal period of 5.87941 h and a symmetric pair of prograde poles near (160°;+79°) and (358°;+79°). That solution based on data from five apparitions predates lightcurves from the 2020 apparition but is consistent with those data; including them in the analysis as a sixth apparition (Fig. 2) leaves the sidereal period unchanged and nudges the pole location by less than one degree of arc.

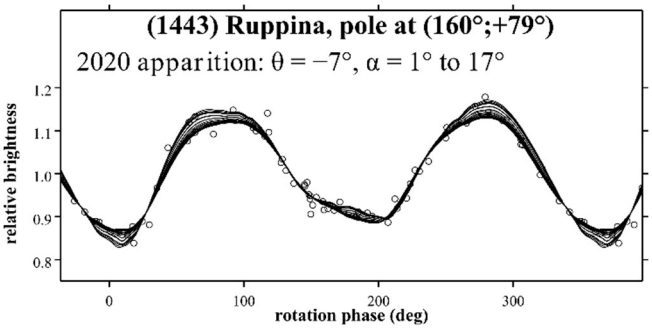

Figure 2: Lightcurve model fits to the same ATLAS-MLO data from 2020 identified in the caption for Table I, as brightness vs. sidereal rotation phase for the P_1 solution of (1443) Ruppina reported by Slivan (2021; this issue), formatted identically to Fig. 4 in that same paper for easy comparison. Open circles represent observed brightnesses; solid curves represent the model. Changes in the lightcurve shape during the course of the observations appear as non-overlapping model curves. θ is the sub-PAB latitude and α is the included range of solar phase angles.

Fig. 2 also permits a visual consistency check of relative amplitudes expected for the pole positions from the two analyses, as a function of the asterocentric latitudes θ of the phase angle bisectors ("sub-PAB latitudes"). For the pole at (160°;+79°) the viewing geometry remains always close to equatorial, predicting that the lightcurves will all exhibit similar amplitudes as has been observed (Slivan, 2021, Fig. 4; this issue). In contrast, for a pole solution at (120°;–15°) the viewing aspect in 2020 at θ = +13° would be similar to equatorial, but the aspect in 2014 at θ = –60° would be more than 45 degrees farther from equatorial and closer to pole-on, predicting a significantly smaller relative amplitude in 2014 that is not consistent with the observations.

Note that while the sidereal periods of the two analyses differ by only 0.00012 h, that small error in the period produced a pole location error of more than 90 degrees of arc; in other words, the spurious pole solutions are not even approximately correct. It demonstrates the importance of understanding that a wrong sidereal period is a systematic error rather than a statistical error, and also shows clearly how insidiously wrong a spurious solution can be as it is effectively a random result.

Conclusion

When using convex inversion to model spins and shapes from lightcurves, supplying the correct sidereal period is required in order to have confidence in the results, even to qualify them as 'preliminary' or as 'possible.' The need for sufficient epoch information and proper attention to its analysis remains unchanged whether using dense published lightcurves or sparse data from surveys:

Precept 1: Don't underestimate the effort—the sidereal period is a full-fledged science result on its own requiring and deserving due respect.

Precept 2: Don't underestimate the importance—markedly wrong spin vectors result from even slightly wrong sidereal periods.

UT epoch	PAB λ,β(°)
2007 Nov 07 0.99 h	68.6 −2.2
2014 Feb 23 1.08 h	146.8 −1.1
2017 Sep 05 0.68 h	56.3 −1.6
2020 Apr 16 1.75 h	222.7 +1.7

Table I: Summary of (1443) Ruppina lightcurve epochs, in each case locating a maximum from the second harmonic of a Fourier series model that was fit to lightcurves. The 2007 and 2014 epochs are measured from the observations reported by Neugent and Slivan (2007) and by Arredondo et al. (2014), respectively. The 2017 epoch is measured from the observations reported by Slivan (2021; this issue) composited to the same date as the lightcurves of Stephens (2018, p. 51). The 2020 epoch is measured from ATLAS-MLO survey (Tonry et al., 2018) *o*-band photometry recorded between the stationary points of the 2020 apparition, retrieved from the MPC Orbits/Observations Database and composited to the same date as the lightcurves of Stephens and Warner (2020, p. 276). λ,β are J2000 ecliptic longitude and latitude of the phase angle bisector (PAB).

Epoch pair index	Interval (d)	Interval (app.)	Epochs source apparitions
0	954.0	2	2017, 2020
1	1290.0	3	2014, 2017
2	2244.0	5	2014, 2020
3	2300.0	5	2007, 2014
4	3590.0	8	2007, 2017
5	4544.0	10	2007, 2020

Table II: Time intervals between the epochs given in Table I, used to identify the ranges of sidereal periods allowed by the already-published lightcurves of (1443) Ruppina. Columns are: the epoch pair index label used in Fig. 1, the interval length rounded to 0.1 d, the corresponding integer count of elapsed apparitions, and identification of the apparitions from which the defining epochs were measured.

Acknowledgements

I thank Dr. Richard Binzel for suggestions that improved this paper. This work has made use of data and services provided by the International Astronomical Union's Minor Planet Center; specifically, the brightnesses accompanying astrometry from the Asteroid Terrestrial-impact Last Alert System (ATLAS) survey observing program.

References

Arredondo, A.; Hartt, A.; Yazdi, S.K. (2014). "Rotation Periods and *R* Magnitudes of Three Koronis Family Members." *Minor Planet Bull.* **41**, 252-254.

Kaasalainen, M.; Torppa, J.; Muinonen, K. (2001). "Optimization methods for asteroid lightcurve inversion. II. The complete inverse problem." *Icarus* **153**, 37-51.

Neugent, K.F.; Slivan, S.M. (2008). "Rotation Periods and *H* Magnitudes of Two Koronis Family Members." *Minor Planet Bull.* **35**, 116-118.

Slivan, S.M. (2012). "Epoch Data in Sidereal Period Determination. I. Initial Constraint from Closest Epochs." *Minor Planet Bull.* **39**, 204-206.

Slivan, S.M. (2013). "Epoch Data in Sidereal Period Determination. II. Combining Epochs from Different Apparitions." *Minor Planet Bull.* **40**, 45-48.

Slivan, S.M. (2014). "Sidereal Photometric Astrometry as Efficient Initial Search for Spin Vector." *Minor Planet Bull.* **41**, 282-284.

Slivan, S.M. (2021). "Lightcurves, Sidereal Rotation Period, Spin Pole, and Convex Model Shape of Koronis Family Asteroid (1443) Ruppina." *Minor Planet Bull.* **48**, 331-334.

Stephens, R.D. (2018). "Asteroids Observed from CS3: 2017 July-September." *Minor Planet Bull.* **45**, 50-54.

Stephens, R.D.; Warner, B.D. (2020). "Main-Belt Asteroids Observed from CS3: 2020 April to June." *Minor Planet Bull.* **47**, 275-284.

Tonry, J.L.; Denneau, L.; Heinze, A.N.; Stalder, B.; Smith, K.W.; Smartt, S.J.; Stubbs, C.W.; Weiland, H.J.; Rest, A. (2018). "ATLAS: A High-cadence All-sky Survey System." *PASP* **130**, 064505.

LIGHTCURVE PHOTOMETRY OPPORTUNITIES: 2021 OCTOBER-DECEMBER

Brian D. Warner
Center for Solar System Studies / MoreData!
446 Sycamore Ave.
Eaton, CO 80615 USA
brian@MinorPlanetObserver.com

Alan W. Harris
MoreData!
La Cañada, CA 91011-3364 USA

Josef Ďurech
Astronomical Institute
Charles University
18000 Prague, CZECH REPUBLIC
durech@sirrah.troja.mff.cuni.cz

Lance A.M. Benner
Jet Propulsion Laboratory
Pasadena, CA 91109-8099 USA
lance.benner@jpl.nasa.gov

We present lists of asteroid photometry opportunities for objects reaching a favorable apparition and have no or poorly-defined lightcurve parameters. Additional data on these objects will help with shape and spin axis modeling using lightcurve inversion. We have changed the presentation of the "Radar-Optical Opportunities" section to include a list of potential radar targets as well as some that are in critical need of astrometric data and, if found, might also be targets for radar. These can have ephemeris errors on the order of tens to thousands of arcseconds and, despite the current surveys, have not been observed for several years. This makes them a double challenge: first to be found and, second, to determine astrometric positions and photometric properties.

We present several lists of asteroids that are prime targets for photometry and/or astrometry during the period 2021 October-December. The "Radar-Optical Opportunities" section has a new format that provides an expanded list of potential targets and no longer gives geocentric ephemerides.

In the first three sets of tables, "Dec" is the declination and "U" is the quality code of the lightcurve. See the latest asteroid lightcurve data base (LCDB from here on; Warner et al., 2009) documentation for an explanation of the U code:

http://www.minorplanet.info/lightcurvedatabase.html

The ephemeris generator on the CALL web site allows creating custom lists for objects reaching V ≤ 18.0 during any month in the current year and up to five years in the future, e.g., limiting the results by magnitude and declination, family, and more.

http://www.minorplanet.info/PHP/call_OppLCDBQuery.php

We refer you to past articles, e.g., Warner et al. (2021) for more detailed discussions about the individual lists and points of advice regarding observations for objects in each list.

Once you've obtained and analyzed your data, it's important to publish your results. Papers appearing in the *Minor Planet Bulletin* are indexed in the Astrophysical Data System (ADS) and so can be referenced by others in subsequent papers. It's also important to make the data available at least on a personal website or upon request. We urge you to consider submitting your raw data to the ALCDEF database. This can be accessed for uploading and downloading data at

http://www.alcdef.org

The database contains more than 3.9 million observations for 15,000+ objects, making it one of the more useful sources for raw asteroid *time-series* lightcurve data.

Lightcurve/Photometry Opportunities

Objects with U = 3– or 3 are excluded from this list since they will likely appear in the list for shape and spin axis modeling. Those asteroids rated U = 1 should be given higher priority over those rated U = 2 or 2+, but not necessarily over those with no period. On the other hand, d*o not overlook asteroids with* U = 2/2+ *on the assumption that the period is sufficiently established.* Regardless, do not let the existing period influence your analysis since even highly-rated result have been proven wrong at times. Note that the lightcurve amplitude in the tables could be more or less than what's given. Use the listing only as a guide.

An entry in bold italics is a near-Earth asteroid (NEA).

		Brightest			LCDB Data		
Number	Name	Date	Mag	Dec	Period	Amp	U
7328	Casanova	10 01.3	15.4	+7	9.122	0.31	2
7825	1991 TL1	10 01.4	15.4	+8	>10	0.05	2
6946	1980 RX1	10 01.8	15.2	-3	15.104	0.18	2
2972	Niilo	10 04.3	14.5	+5	8.592	0.12	2
5058	Tarrega	10 05.4	15.1	-10	4.983	0.57	2
666	Desdemona	10 06.4	12.5	+10	14.607	0.06-0.22	2+
6200	Hachinohe	10 06.5	14.9	-7	78.327	0.41	2
39317	2001 UU168	10 06.5	15.4	+13	86.895	0.73-0.75	2
3461	Mandelshtam	10 06.8	15.4	+1	2.848	0.20	2
5714	Krasinsky	10 06.9	15.1	+5	18.184	0.45	2
5093	Svirelia	10 10.6	15.3	+13	2.809	0.24	2
16009	1999 CM8	10 10.6	14.4	-4	16.7	0.54-0.65	2+
3277	Aaronson	10 11.5	14.6	-6	9.8	0.14	2+
1007	Pawlowia	10 14.8	14.2	+12	121	0.51	2
6083	Janeirabloom	10 18.6	15.5	+8	10.151	0.23	2
40717	1999 SC2	10 20.1	15.0	+10	3.436	0.11-0.22	2
995	Sternberga	10 20.8	12.8	+16	14.612	0.06-0.20	2+
6706	1988 VD3	10 21.3	15.2	+13	27.021	0.05	1
957	Camelia	10 23.5	13.8	+20	150	0.30	1+
4023	Jarnik	10 23.5	15.3	+13	4.776	0.27	2
9755	1990 RR2	10 26.5	15.5	+9	4.774	0.37	2
1913	Sekanina	10 27.4	15.0	+14	13.97	0.30-0.31	2+
2743	Chengdu	10 29.3	14.9	+26	8.321	0.45	2
2970	Pestalozzi	11 02.1	15.5	+32	126.942	0.66	2
846	Lipperta	11 07.7	13.5	+17	1641	0.30	2
87024	***2000 JS66***	***11 11.3***	***15.5***	***+21***	***27.6***	***1.52***	***2***
1781	Van Biesbroeck	11 11.8	15.0	+19	6.385	0.45	2
6854	Georgewest	11 16.2	15.2	+17	3.64	0.66	2
4086	Podalirius	11 19.0	15.5	+20	10.43	0.08-0.16	2+
6887	Hasuo	11 24.4	15.0	+23	2.752	0.18	2
2837	Griboedov	11 25.0	15.4	+21	3.95		2
6659	Pietsch	11 25.1	15.4	+23	12.985	0.31-0.44	2
4214	Veralynn	11 26.3	15.3	+26	7.6	0.35	2-
1720	Niels	11 27.4	14.3	+20	250.9	0.61	2
6838	Okuda	11 29.0	14.8	+22	8.983	0.14-0.34	2+
6242	1990 OJ2	11 29.2	15.3	+21	5.475		2
6314	Reigber	12 05.5	15.3	+18	96.446		2
4660	Nereus	12 07.9	12.5	+69	15.1	0.6- 0.8	2
3550	Link	12 12.0	14.7	+23	12.371	0.21	2
163899	2003 SD220	12 13.2	13.8	+55	285	1.39- 2.5	2+
1450	Raimonda	12 14.0	14.5	+24	12.66	0.57	2
1091	Spiraea	12 18.6	15.2	+24	7.01	0.03	1+
2906	Caltech	12 20.3	14.4	+27	12.994	0.16-0.27	2+
4276	Clifford	12 24.3	15.5	+40	3.239	0.09	2
6662	1993 BP13	12 24.7	15.0	+22	>24	0.94	1
2336	Xinjiang	12 25.1	15.4	+24	37.299	0.12	2
7430	Kogure	12 30.0	14.4	+24	335.9	0.57	2

Low Phase Angle Opportunities

The Low Phase Angle list includes asteroids that reach very low phase angles ($\alpha < 1°$). The "α" column is the minimum solar phase angle for the asteroid. Getting accurate, calibrated measurements (usually V band) at or very near the day of opposition can provide important information for those studying the "opposition effect." Use the on-line query form for the LCDB to get more details about a specific asteroid.

http://www.minorplanet.info/PHP/call_OppLCDBQuery.php

You will have the best chance of success working objects with low amplitude and periods that allow covering at least half a cycle every night. Objects with large amplitudes and/or long periods are much more difficult for phase angle studies since, for proper analysis, the data must be reduced to the average magnitude of the asteroid for each night. This reduction requires that you determine the period and the amplitude of the lightcurve; for long period objects that can be difficult. Refer to Harris et al. (1989) for the details of the analysis procedure.

As an aside, it is arguably better for physical interpretation (e.g., *G* value versus albedo) to use the maximum light rather than mean level to find the phase slope parameter (*G*). This better models the behavior of a spherical object of the same albedo, but it can produce significantly different values for both *H* and *G* versus using average light, which is the method used for values listed by the Minor Planet Center. Using and reporting the results of both methods can provide additional insights into the physical properties of an asteroid.

The International Astronomical Union (IAU) has adopted a new system, H-G_{12}, introduced by Muinonen et al. (2010). It will be some years before H-G_{12} becomes widely used, and hopefully not until a discontinuity flaw in the G_{12} function has been fixed. This discontinuity results in false "clusters" or "holes" in the solution density and makes it impossible to draw accurate conclusions.

We strongly encourage obtaining data as close to 0° as possible, then every 1-2° out to 7°, below which the curve tends to be non-linear due to the opposition effect. From 7° out to about 30°, observations at 3-6° intervals should be sufficient. Coverage beyond about 50° is not generally helpful since the H-G system is best defined with data from 0-30°.

It's important to emphasize that all observations should (must) be made using high-quality catalogs to set the comparison star magnitudes. These include ATLAS, Pan-STARRS, SkyMapper, and GAIA2. Catalogs such as CMC-15, APASS, or the MPOSC from *MPO Canopus* should not be used due to significant systematic errors.

Also important is that that there are sufficient data from each observing run such that their location can be found on a combined, phased lightcurve derived from two or more nights obtained *near the same phase angle.* This is so that the lightcurve amplitude isn't significantly different. If necessary, the magnitudes for the given run should be adjusted so that they correspond to mid-light of the combined lightcurve. This goes back to the H-G system being based on average, not maximum or minimum light.

For this table, the asteroid magnitudes are brighter than in others. This is because higher precision is required for this work and the asteroid may be a full magnitude or fainter when it reaches phase angles out to 20-30°.

Num	Name	Date	α	V	Dec	Period	Amp	U
359	Georgia	10 01.6	0.26	11.8	+04	5.537	0.16 0.54	3
4856	Seaborg	10 03.0	0.04	15.0	+04	15.853	0.41	3
2972	Niilo	10 04.4	0.37	14.5	+05	8.592	0.12	2
312	Pierretta	10 04.6	0.46	12.4	+06	10.282	0.32	3
2004	Lexell	10 04.8	0.32	14.6	+05	5.443	0.42-0.51	3
1508	Kemi	10 06.0	0.54	14.7	+04	9.196	0.25-0.55	3
551	Ortrud	10 07.2	0.10	13.2	+06	17.416	0.14-0.19	3
1008	La Paz	10 07.2	0.53	14.4	+04	8.998	0.14-0.19	3
1848	Delvaux	10 08.1	0.53	14.7	+07	3.637	0.57-0.69	3
3673	Levy	10 10.2	0.47	14.5	+08	2.688	0.13	3
310	Margarita	10 11.7	0.78	14.3	+09	12.070	0.14-0.37	3
1143	Odysseus	10 11.7	0.30	15.0	+09	10.114	0.15-0.22	3
377	Campania	10 13.9	0.74	12.0	+10	11.664	0.14-0.27	3
279	Thule	10 16.5	0.55	14.3	+07	23.896	0.02-0.10	3
40717	1999 SC2	10 20.1	0.41	15.0	+10	3.436	0.22	2
454	Mathesis	10 23.0	0.15	13.1	+11	8.378	0.20-0.37	3
1447	Utra	10 23.0	0.32	14.7	+11	257.	0.63	2
460	Scania	10 23.6	0.31	13.6	+11	9.55	0.05	2-
223	Rosa	10 24.9	0.27	13.8	+11	20.283	0.06-0.13	3
1518	Rovaniemi	10 26.0	0.60	13.9	+13	5.249	0.25-0.26	3
1082	Pirola	10 26.2	0.94	14.0	+10	15.853	0.53-0.62	3
461	Saskia	10 26.4	0.64	14.4	+11	7.348	0.25-0.36	3
614	Pia	10 26.9	0.32	13.8	+13	4.572	0.21-0.42	3
1913	Sekanina	10 27.4	0.55	14.9	+14	13.97	0.30-0.31	2+
2379	Heiskanen	10 30.0	0.25	14.2	+13	3.76	0.17-0.23	3
151	Abundantia	11 05.0	0.26	12.5	+16	9.864	0.15-0.20	3
2193	Jackson	11 07.4	0.76	15.0	+19	4.754	0.23-0.24	3
846	Lipperta	11 07.7	0.18	13.5	+17	1641.	0.30	2
9513	1971 UN	11 08.0	0.97	15.7	+19			
907	Rhoda	11 09.7	0.94	13.1	+19	22.44	0.08-0.16	3-
3396	Muazzez	11 10.5	0.75	15.0	+19			
981	Martina	11 11.2	0.11	14.3	+18	11.267	0.15-0.24	2
494	Virtus	11 13.9	0.75	13.4	+20	5.57	0.03-0.12	2+
435	Ella	11 15.9	0.75	12.7	+20	4.623	0.30-0.38	3
1199	Geldonia	11 19.0	0.09	14.2	+19	28.3	0.11	2-
311	Claudia	11 22.0	0.61	13.8	+18	7.532	0.16-0.89	3
2828	Iku-Turso	11 22.9	0.72	14.9	+19		0.60	
1911	Schubart	11 26.0	0.44	14.7	+22	11.915	0.11-0.22	2
1720	Niels	11 27.4	0.67	14.3	+20	9.976	0.15	1
396	Aeolia	11 27.5	0.17	14.3	+21	14.353	0.36	3
322	Phaeo	11 27.8	0.74	11.7	+23	17.584	0.13-0.20	3
1289	Kutaissi	11 28.9	0.66	14.5	+19	3.60	0.20-0.42	3
6838	Okuda	11 29.0	0.28	14.8	+22	8.983	0.14	2+
2571	Geisei	12 02.1	0.14	14.8	+22	7.823	0.50	3-
197	Arete	12 04.1	0.83	13.0	+20	6.608	0.10-0.16	3
1801	Titicaca	12 04.1	0.60	14.8	+20	3.211	0.50	3
106	Dione	12 05.4	0.50	11.1	+24	16.210	0.08-0.18	3
514	Armida	12 06.1	0.49	13.2	+24	21.851	0.16-0.27	3
1001	Gaussia	12 07.6	0.35	13.4	+24	20.99	0.11-0.16	3
586	Thekla	12 08.0	0.39	13.2	+22	13.670	0.24-0.30	3
42	Isis	12 09.1	0.68	10.7	+21	13.590	0.14-0.32	3
1666	van Gent	12 09.5	0.31	14.6	+23	4.165	0.23-0.42	3
857	Glasenappia	12 12.0	0.21	14.0	+23	8.20	0.27-0.92	3
3550	Link	12 12.0	0.21	14.7	+23	12.371	0.21	2
	2019 CT11	12 12.9	0.42	14.2	+24			
1517	Beograd	12 13.3	0.85	14.9	+26	6.943	0.18-0.23	2
1450	Raimonda	12 13.9	0.50	14.4	+24	12.66	0.57	2
936	Kunigunde	12 14.0	0.33	15.0	+24	8.80	0.25	2
270	Anahita	12 17.1	0.34	11.2	+23	15.06	0.25-0.32	3
1817	Katanga	12 21.6	0.31	14.4	+24	8.481	0.22-0.42	3
6662	1993 BP13	12 24.7	0.65	15.0	+22	>24.	0.94	1
517	Edith	12 29.1	0.14	12.8	+23	9.275	0.08-0.18	3
1075	Helina	12 29.2	0.33	14.4	+22	44.9	0.64-0.91	3-
580	Selene	12 29.3	0.13	14.1	+23	9.47	0.27	3-
7430	Kogure	12 30.0	0.27	14.3	+24			
550	Senta	12 31.0	0.74	13.3	+21	20.555	0.3 0.41	3

Shape/Spin Modeling Opportunities

Those doing work for modeling should contact Josef Ďurech at the email address above. If looking to add lightcurves for objects with existing models, visit the Database of Asteroid Models from Inversion Techniques (DAMIT) web site

https://astro.troja.mff.cuni.cz/projects/damit/

Additional lightcurves could lead to the asteroid being added to or improving one in DAMIT, thus increasing the total number of asteroids with spin axis and shape models.

Included in the list below are objects that:

1. Are rated U = 3– or 3 in the LCDB
2. Do not have reported pole in the LCDB Summary table
3. Have at least three entries in the Details table of the LCDB where the lightcurve is rated U ≥ 2.

The caveat for condition #3 is that no check was made to see if the lightcurves are from the same apparition or if the phase angle bisector longitudes differ significantly from the upcoming apparition. The last check is often not possible because the LCDB does not list the approximate date of observations for all details records. Including that information is an on-going project.

Favorable apparitions are in bold text. NEAs are in italics.

		Brightest			LCDB Data		
Num	Name	Date	Mag	Dec	Period	Amp	U
891	Gunhild	10 01.5	14.1	-16	11.892	0.18-0.37	3-
359	**Georgia**	**10 01.6**	**11.8**	**+4**	**5.537**	**0.14-0.54**	**3**
1830	Pogson	10 03.7	15.0	+0	2.57	0.07-0.18	3
2209	Tianjin	10 05.6	14.7	+2	9.47	0.41-0.42	3
551	Ortrud	10 07.2	13.2	+6	17.416	0.14-0.19	3
100	Hekate	10 10.5	11.5	-2	27.066	0.11-0.23	3
764	Gedania	10 11.9	13.9	+19	24.968	0.01-0.35	3-
2535	Hameenlinna	10 12.0	14.9	+5	3.231	0.07-0.11	3
111	Ate	10 12.5	11.6	+14	22.072	0.08-0.18	3
701	Oriola	10 16.1	13.6	+15	9.09	0.20-0.37	3
788	Hohensteina	10 16.7	13.7	+1	37.137	0.10-0.18	3
259	Aletheia	10 21.1	12.8	-1	8.143	0.09-0.12	3
1577	**Reiss**	**10 23.1**	**14.3**	**+3**	**4.505**	**0.12-0.20**	**3**
901	Brunsia	10 25.0	13.1	+18	3.136	0.09-0.28	3
169	Zelia	10 25.5	11.9	+18	14.537	0.13-0.17	3
911	Agamemnon	10 31.3	14.8	+36	6.592	0.04-0.29	3
6249	**Jennifer**	**10 31.3**	**13.6**	**+20**	**4.957**	**0.06-0.49**	**3**
4223	Shikoku	11 01.0	14.8	+25	9.137	0.12-0.19	3
2162	**Anhui**	**11 03.3**	**14.5**	**+9**	**8.105**	**0.14-0.18**	**3**
4935	**Maslachkova**	**11 04.3**	**14.9**	**+4**	**2.902**	**0.23**	**3**
626	Notburga	11 09.2	12.1	+62	19.353	0.10-0.21	3
907	**Rhoda**	**11 09.9**	**13.1**	**+19**	**22.44**	**0.06-0.16**	**3-**
577	Rhea	11 10.2	13.9	+25	12.249	0.19-0.24	3-
796	**Sarita**	**11 11.0**	**11.1**	**+31**	**8.175**	**0.27-0.33**	**3**
1146	Biarmia	11 11.5	14.8	+11	5.47	0.14-0.32	3
5143	Heracles	11 11.5	14.2	+37	2.706	0.05-0.22	3
159857	**2004 LJ1**	**11 12.9**	**14.3**	**+6**	**2.725**	**0.15-0.59**	**3**
613	Ginevra	11 14.5	13.5	+28	12.906	0.12-0.20	3
3361	**Orpheus**	**11 15.6**	**14.3**	**-32**	**3.533**	**0.17-0.32**	**3**
535	Montague	11 17.5	12.7	+14	10.248	0.18-0.25	3
2460	Mitlincoln	11 19.4	14.7	+13	3.007	0.03-0.20	3
1096	Reunerta	11 20.4	13.9	+14	13.036	0.20-0.39	3
1717	Arlon	11 20.6	14.2	+31	5.148	0.06-0.12	3
2323	Zverev	11 20.7	14.9	+25	3.921	0.28-0.39	3
3687	Dzus	11 23.3	14.9	+13	58.12	0.06-0.15	3-
530	Turandot	11 24.6	13.8	+10	19.96	0.10-0.17	3-
1346	Gotha	11 24.8	14.2	-3	2.641	0.10-0.16	3-
288	Glauke	11 25.1	14.2	+15	1170	0.36- 0.9	3
833	Monica	11 26.0	15.0	+35	12.09	0.11-0.21	3
3425	Hurukawa	11 27.3	14.9	+31	24.84	0.17-0.47	3-
1093	Freda	11 27.6	13.8	+28	19.67	0.06-0.21	3
1189	Terentia	12 01.6	13.7	+29	19.308	0.32-0.38	3
3447	Burckhalter	12 01.9	14.9	+58	59.8	0.30-0.39	3
978	Aidamina	12 03.2	14.0	+3	10.099	0.09-0.24	3
197	Arete	12 03.9	13.1	+20	6.608	0.10-0.16	3
1888	Zu Chong-Zhi	12 04.1	14.2	+21	11.053	0.28-0.56	3
308	Polyxo	12 05.0	11.9	+16	12.029	0.08-0.15	3-
514	Armida	12 06.0	13.2	+24	21.851	0.16-0.27	3
1394	Algoa	12 07.8	14.9	+18	2.768	0.20-0.21	3
586	**Thekla**	**12 08.0**	**13.2**	**+22**	**13.67**	**0.24-0.30**	**3**
2577	Litva	12 15.2	14.9	-26	2.813	0.14-0.36	3
467	Laura	12 20.9	14.5	+32	70.63	0.13-0.15	3
1817	Katanga	12 21.7	14.4	+24	8.481	0.22-0.30	3
301	Bavaria	12 27.4	14.3	+18	12.253	0.25-0.31	3
126	Velleda	12 28.9	12.3	+28	5.367	0.07-0.22	3

Radar-Optical Opportunities

Table I below gives a list of near-Earth asteroids reaching maximum brightness for the current quarter-year based on calculations by Warner. We have switched to this presentation in lieu of ephemerides for chosen objects for several reasons.

The most important among them is that for some objects, those marked "Astrometry needed," the last observations may have been many years ago and so the ephemeris uncertainties may be extremely large. A case in point, and what prompted the change, is 2016 XG1. Our positions and magnitudes for 2021 November were similar to those from the Minor Planet Center. However, the JPL Horizons ephemeris showed the asteroid almost 3 magnitudes fainter and a difference of many hours in Right Ascension.

Another reason is that the previous ephemeris listings were for geocentric positions. For close-approach apparitions, the offsets between those and topocentric (those from a given location on the Earth's surface) could be significant and, furthermore, the orbital elements may have been updated since our ephemerides were generated, resulting in significant changes in positions and/or magnitudes.

The initial list started with one generated by the planning tool at

http://www.minorplanet.info/PHP/call_OppLCDBQuery.php

where the search was limited to only near-Earth asteroids at V ≤ 18 during the quarter.

The list was then filtered to include objects that might be targets for the Goldstone radar facility or, if it were still operational, the Arecibo radar. This was based on the calculated radar SNR using

http://www.naic.edu/~eriverav/scripts/index.php

and assuming a rotation period of 4 hours (2 hours if $D \leq 200$ m) if a period was not given in the asteroid lightcurve database (LCDB; Warner et al., 2009). The SNR values are estimates only and assume that the radar is fully functional.

If an asteroid was on the list but failed the SNR test, we checked if it might be a suitable target for radar and/or photometry sometime through 2050. If so, it was kept on the list to encourage physical and astrometric observations during the current apparition.

The final step was to cross-reference our list with that found on the Goldstone planned targets schedule at

http://echo.jpl.nasa.gov/asteroids/goldstone_asteroid_schedule.html

It's important to note that the final list in Table I is based on *known* targets and orbital elements when it was prepared. It is common for newly discovered objects to move into, out of, or up the list and become radar targets on short notice. We recommend that you keep up with the latest discoveries by using the Minor Planet Center observing tools.

In particular, monitor NEAs and be flexible with your observing program. In some cases, you may have only 1-3 days when the asteroid is within reach of your equipment. Be sure to keep in touch with the radar team (through Benner's email or their Facebook or Twitter accounts) if you get data. The team may not always be observing the target but your initial results may change their plans. In all cases, your efforts are greatly appreciated.

For observation planning, use these two sites

MPC: *http://www.minorplanetcenter.net/iau/MPEph/MPEph.html*
JPL: *http://ssd.jpl.nasa.gov/?horizons*

It's good to cross-check the ephemerides from the two sites just in case there is a situation such as that with 2016 XG1 mentioned above.

About YORP Acceleration

Near-Earth asteroids are particularly sensitive to YORP acceleration. YORP (Yarkovsky–O'Keefe–Radzievskii–Paddack; Rubincam, 2000) is the asymmetric thermal re-radiation of sunlight that can cause an asteroid's rotation period to increase or decrease. High precision lightcurves at multiple apparitions can be used to model the asteroid's *sidereal* rotation period and see if it's changing.

It usually takes four apparitions to have sufficient data to determine if the asteroid rotation rate is changing under the influence of YORP. This is why observing an asteroid that already has a well-known period remains a valuable use of telescope time. It is even more so when considering the BYORP (binary-YORP) effect among binary asteroids that has stabilized the spin so that acceleration of the primary body is not the same as if it would be if there were no satellite.

The Quarterly Target List Table

The Table I columns are

Num	Asteroid number, if any.
Name	Name assigned by the MPC.
H	Absolute magnitude from MPCOrb.
Dia	Diameter (km) assuming $p_V = 0.2$.
Date	Date (mm dd.d) of brightest magnitude.
V	Approximate V magnitude at brightest.
Dec	Approximate declination at brightest.
Period	Synodic rotation period from summary line in the LCDB summary table.
Amp	Amplitude range (or single value) of reported lightcurves.
U	LCDB U (solution quality) from 1 (probably wrong) to 3 (secure).
A	Approximate SNR for Arecibo (if operational and at full power).
G	Approximate SNR for Goldstone radar at full power.
Notes	Comments about the object.

Rows in bold were listed on the Goldstone scheduling page.

"PHA" is a potentially hazardous asteroid. "Requested" in the notes field indicates that astrometry and/or photometry were requested to support Goldstone observations. "Astrometry needed" is given for those objects that were last observed several years ago and for which ephemerides uncertainties given by the MPC can be in the tens to thousands of arcseconds.

The sources for the rotation period are given in the Notes column. If none are qualified with a specific period, then the periods from multiple sources were in general agreement.

Higher priority should be given to those where the current apparition is the last one V ≤ 18 through 2050 or several years to come.

References

Aznar, A.M.; Predatu, M.; Vaduvescu, O.; Oey, J. (2018). "EURONEAR - First light curves and Physical Properties of Near Earth Asteroids." arXiv:1801.09420. *Romanian J. Phys.* **62**, 904.

Benner, L.A.M.; Nolan, M.C.; Ostro, S.J.; Giorgini, J.D.; Margot, J.-L. (2001). "1998 ST_27." *IAUC* **7730**.

Birtwhistle, P. (2011). "Lightcurves for Five Close Approach Asteroids." *Minor Planet Bull*. **38**, 104-106.

Brozovic, M.; Ostro, S.J.; Benner, L.A.M.; Giorgini, J.D.; Jurgens, R.F.; Rose, R.; Nolan, M.C.; Hine, A.A.; Magri, C.; Scheeres, D.J.; Margot, J.-L. (2009). "Asteroid 4660 Nereus, a prime space mission target." *Icarus* **201**, 153-166.

Galad, A.; Pravec, P.; Kusnirak, P.; Gajdos, S.; Kornos, L.; Vilagi, J. (2005). "Joint Lightcurve Observations of 10 Near-Earth Asteroids from Modra and Ondrejov." *Earth, Moon, and Planets* **97**, 147-163.

Gandolfi, D.; Cigna, M.; Fulvio, D.; Blanco, C. (2009). "CCD and photon-counting photometric observations of asteroids carried out at Padova and Catania observatories." *Planet. Space Sci.* **57**, 1-9.

Harris, A.W.; Young, J.W.; Bowell, E.; Martin, L.J.; Millis, R.L.; Poutanen, M.; Scaltriti, F.; Zappala, V.; Schober, H.J.; Debehogne, H.; Zeigler, K.W. (1989). "Photoelectric Observations of Asteroids 3, 24, 60, 261, and 863." *Icarus* **77**, 171-186.

Ishibashi, Y.; Abe, M.; Takagi, Y. (2000). "Lightcurve of asteroid Nereus." *Adv. Space Res*. **25**, 277-280.

Muinonen, K.; Belskaya, I.N.; Cellino, A.; Delbò, M.; Levasseur-Regourd, A.-C.; Penttilä, A.; Tedesco, E.F. (2010). "A three-parameter magnitude phase function for asteroids." *Icarus* **209**, 542-555.

Pravec, P.; Wolf, M.; Sarounova, L. (1998web; 2004web; 2011web; 2019web). *http://www.asu.cas.cz/~ppravec/neo.htm*

Rubincam, D.P. (2000). "Radiative Spin-up and Spin-down of Small Asteroids." *Icarus* **148**, 2-11.

Skiff, B.A.; McLelland, K.P.; Sanborn, J.J.; Pravec, P.; Koehn, B.W. (2019). "Lowell Observatory Near-Earth Asteroid Photometric Survey (NEAPS): Paper 3." *Minor Planet Bull*. **46**, 238-265.

Vaduvescu, O.; Macias, A.; Tudor, V.; Predatu, M.; Galád, A.; Gajdos, S.; Vilagi, J.; Stevance, H.F.; Errmann, R.; Unda-Sanzana, E.; Char, F.; Peixinho, N.; Popescu, M.; Sonka, A.; Cornea, R.; Suciu, O.; Toma, R.; Santos-Sanz, P.; Sota, A.; Licandro, J.; Serra-Ricart, M.; Morate, D.; Mocnik, T.; Diaz-Alfaro, M.; Lopez-Martinez, F.; McCormac, J.; Humphries, N. (2017). "The EURONEAR Lightcurve Survey of Near-Earth Asteroids." *Earth, Moon, and Planets* **120**, 41-100.

Warner, B.D. (2015). "Near-Earth Asteroid Lightcurve Analysis at CS3-Palmer Divide Station: 2014 June-October." *Minor Planet Bull*. **42**, 41-53.

Warner, B.D. (2016). "Near-Earth Asteroid Lightcurve Analysis at CS3-Palmer Divide Station: 2015 October-December." *Minor Planet Bull*. **43**, 143-154.

Warner, B.D.; Stephens, R.D. (2019). "Near-Earth Asteroid Lightcurve Analysis at the Center for Solar System Studies: 2018 September-December." *Minor Planet Bull*. **46**, 144-152.

Num	Name	H	Dia	Date	V	Dec	Period (h)	Amp	U	A	G	Notes
363027	1998 ST27*	19.5	0.375	10 01.1	17.7	22	3	0.1	2			Next: 2024 Oct; V ~12.9. Binary and period from Benner et al. (2001).
312070	2007 TA19*	19.4	0.391	10 01.2	17.6	-14						Next: 2034 Oct; V ~ 17.7.
	2014 TM*	26.2	0.017	10 02.6	17.6	22				585	165	
	2017 TS3*	**22.1**	**0.114**	**10 28.4**	**17.5**	**70**				**65**	**18**	**Astrometry/photometry requested.**
7341	1991 VK	16.8	1.273	10 30.9	16.3	17	4.2096	0.21 0.7	3	20	5	Next: 2022/02; V ~ 14.8. Pravec et al. (1998web), Vaduvescu et al. (2017), and Warner (2016) are all from 2016 or earlier.
	2019 XS*	23.7	0.053	11 10.0	14.5	-1				3220	920	SNR for 0.01 au; min distance is 0.004 au.
87024	2000 JS66*	18.6	0.561	11 11.3	15.5	21	27.6	1.52	2	19	5	Pravec et al. (2004web). Next: 2038/10; V ~ 16.1.
	2004 UE*	**21**	**0.188**	**11 12.1**	**16.0**	**-21**	**5.6**	**0.98**	**2+**	**580**	**165**	**PHA. Astrometry/photometry requested.** Gandolfi et al. (2009).
159857	2004 LJ1*	15.4	2.438	11 12.9	14.3	6	2.7247	0.15 0.59	3	40	10	2038/11; V ~ 8.1. Galad et al., (2005); Warner (2015).
	2017 WP*	23.1	0.072	11 15.1	17.6	-9				58	16	Astrometry needed.
138852	2000 WN10	20.2	0.274	11 15.2	17.9	-32	4.4622	0.38 0.44	3	2		Dates/Dec about same every year through 2050. Pravec et al. (2011web);
3361	**Orpheus***	**19.0**	**0.464**	**11 15.6**	**14.3**	**-32**	**3.5327**	**0.17 0.32**	**3**	**935**	**265**	**PHA. Photometry requested. NHATS.** Pravec et al. (2019web); Skiff et al. (2019).
	2010 VK139*	**23.7**	**0.053**	**11 15.7**	**17.1**	**13**	**0.0299522**	**0.5**	**3**	**90**	**25**	**Astrometry/photometry requested.** Birtwhistle (2011).
	2015 FF37*	18.7	0.540	11 19.2	17.2	62				45	10	Last observed: 2019; Astrometry needed.
374855	2006 VQ13*	20.0	0.297	11 19.6	17.6	2				6	2	Last at V <18 though 2050.
	2009 WB105*	23.5	0.061	11 25.0	16.9	22				30	10	Circumstances repeat about every 3 years.
	2017 KM27*	22.8	0.083	11 25.5	16.2	55				1890	540	Last at V < 18 through 2050.
152742	1998 XE12*	19.1	0.450	11 25.5	17.5	72				2		Next: 2024/01; V ~ 17.1.
	2007 TC23*	20.5	0.236	11 26.0	17.7	20				2		Astrometry needed. Last V < 18 through 2050.
	2002 TP69*	21.9	0.124	11 26.1	16.7	1				30	8	Last observed 2003. Last V < 18 through 2050.
516396	2000 WY28*	20.1	0.283	11 26.1	17.2	26				1		Astrometry needed. Last V < 18 through 2050.
531914	2013 BW76*	18.5	0.593	12 01.0	18.0	-14				3		Next: 2024/11; V ~ 17.4.
	1994 WR12*	22.3	0.104	12 02.2	16.8	46				60	15	Next: 2046/11; V ~ 14.0.
4660	**Nereus***	**18.3**	**0.647**	**12 07.9**	**12.5**	**69**	**15.1**	**0.6 0.8**	**2**	**15100**	**4300**	**Photometry desirable. NHATS.** Ishibashi et al. (2000); Brozovic et al. (2009).
518678	**2008 UZ94***	**17.4**	**0.984**	**12 08.1**	**15.1**	**-51**				**610**	**175**	**PHA. Astrometry/photometry requested.**
480883	2001 YE4*	20.7	0.215	12 10.1	17.2	75				14	4	Last observed 2017; Next: 2026/12; V ~ 17.5.
163899	**2003 SD220***	**17.7**	**0.873**	**12 13.2**	**13.8**	**55**	**285**	**1.39 2.5**	**2+**	**29600**	**8500**	**PHA. Photometry requested. NHATS.** Warner (2016); Aznar et al. (2018, 173.4 h); Skiff et al. (2019, 280 h); Warner and Stephens (2019, 125 h).
363505	2003 UC20*	18.4	0.621	12 19.1	17.6	-21	29.6	0.88	2+	16	4	Last observed 2017; Next 2023/11; V ~ 14.2. Pravec et al. (2019web).
	2018 AH*	22.5	0.093	12 30.4	18.0	-5				150	40	Last observed 2018; Astrometry needed.

Table I. A list of near-Earth asteroids reaching brightest in the fourth quarter of 2021. * Favorable apparition. PHA: potentially hazardous asteroid. NHATS: Near-Earth Object Human Space Flight Accessible Targets Study.

The diameters (Dia column) are kilometers and based on an assumed albedo of 0.20. The date, V, and Dec columns give, respectively, the mm/dd.d, approximate magnitude, and declination when the asteroid is brightest. The Amp column gives the single or range of amplitudes. The A and G columns are, respectively, the approximate SNRs for an assumed full-power Arecibo (not operational) and Goldstone radars. The references in the Notes column are those for the reported periods and amplitudes.

Warner, B.D.; Harris, A.W.; Pravec, P. (2009). "The asteroid lightcurve database." *Icarus* **202**, 134-146.

Warner, B.D.; Harris, A.W.; Durech, J.; Benner, L.A.M. (2021). "Lightcurve Photometry Opportunities: 2021 January-March." *Minor Planet Bull.* **48**, 89-97.

INDEX TO VOLUME 48

Franco, L.; Marchini, A.; Cavaglioni, L.; Papini, R.; Privitera, C.A.; Baj, G.;Galli, G.; Scarfi, G.; Aceti, P.; Banfi, M.; Bacci, P.; Maestripieri, M.; Mannucci, M.; Montigiani, N.; Tinelli, L.; Mortari, F. "Collaborative Asteroid Photometry from UAI: 2021 January-March" 219-222.

Franco, L.; Marchini, A.; Iozzi, M.; Scarfi, G.; Montigiani, N.; Mannucci, M.; Aceti, P.; Banfi, M.; Mortari, F.; Galli, G.; Bacci, P.; Maestripieri, M.; Valvasori, A.; Guido, E. "Collaborative Asteroid Photometry from UAI: 2021 April - June" 372-374.

Franco, L.; Marchini, A.; Papini, R.; Baj, G.; Scarfi, G.; Mortari, F.; Aceti, P.; Schmidt, R.E.; Koff, R.A "Spin-Shape Model for 374 Burgundia" 316-318.

Guido, E.; Catapano, A.; Noschese, A.; Vecchione, A. "Rotational Period and Lightcurve Determination of 2020 UQ6: A Super Fast Rotator" 105-106.

Loera-González, P.; Olguín, L.; Saucedo-Morales, J.; Núñez-López, R.; Domínguez-González, R. "Lightcurve Based Rotational Period for Asteroids 1995 WZ41 and 99942 Apophis" 203-204.

Marchini, A.; Papini, R.; Deldem, M.; Behrend, R. "Rotation Period Determination for Asteroid 2409 Chapman" 1-2.

Marchini, A.; Papini, R.; Baj, G.; Galli, G.; Bacci, P.; Franco, L. "Photometric Analysis and Rotation Period Determination of the Potentially Hazardous Asteroid 2020 WU5" 104-105.

Marchini, A.; Papini, R.; Scarfi, G. "Photometric Analysis and Rotation Period Determination for Asteroids 5445 Williwaw, (8823) 1987 WS3 and (26568) 2000 ET49" 110-112.

Marchini, A.; Cavaglioni, L.; Privitera, C.A.; Papini, R.; Salvaggio, F. "Rotation Period Determination for Asteroids 2243 Lonnrot, (10859) 1995 GJ7, (18640) 1998 EF9 and (49483) 1999 BP13" 206-208.

Marchini, A.; Cavaglioni, L.; Privitera, C.A.; Papini, R.; Salvaggio, F. "Rotation Period Determination for (13832) 1999 XR13" 330.

Mieczkowska, I.; Marciniak, A.; Hirsch, R.; Kamiński, K.; Kamińska, M.K.; Polińska, M.; Oszkiewicz, D.; Sobkowiak, K.; Wróblewski, R.; Żukowski, K. "Serendipitous Asteroids" 352-357.

Newcomb, S.D.; Fieber-Beyer, S.K. "Photometric Observations of (68347) 2001 KB67, (494999) 2010 JU39, and (455432) 2003 RP8" 223-224.

Noschese, A.; Vecchione, A. "Rotational Period and Lightcurve Determination of 3390 Demanet and (18640) 1998 EF9" 205-206.

Noschese, A.; Catapano, A.; Mollica, M.; Vecchione, A. "Rotational Periods and Lightcurve Determination of 6259 Maillol, 6792 Akiyamatakashi and 85275 (1994 LY)" 11-12.

Noschese, A.; Ruocco, N.; Catapano, A.; Mollica, M.; Vecchione, A. "Rotational Period and Lightcurve Determination of 4625 Shchedrin, (8823) 1987 WS3, (15010) 1998 QL92, (19755) 2000 EH34, and 21082 Araimasaru" 147-149.

Odden, C.E.; Cahill, C.; Darling, V.; Ellsweig, E.; Mao, T.; Wang, K.; Xie, Y.; Zhou, J. "Lightcurve Analysis of Asteroids (21242) 1995 WZ41 and (44896) 1999 VB12" 201-203.

Odden, C.; Bingham, L.; Cordover, S.; Darling, V.; DiNatale, A.; Hsieh, G.; Kusaka, R.; Lin. J.; Mao, T.; Marquis, K.; Merove, P.; Mittal, T.; Yarynich, O. "Lightcurve Analysis of Asteroids 1228 Scabiosa and 12016 Green" 370-371.

Owings. L.E. "Lightcurve Analysis of Ten Asteroids" 236-238.

Pilcher, F. "Lightcurves and Rotation Periods of 49 Pales, 383 Janina, and 764 Gedania" 5-6.

Pilcher, F. "Minor Planets at Unusually Favorable Elongations in 2021" 83-85.

Pilcher, F. "Lightcurves and Rotation Periods of 67 Asia, 74 Galatea, 356 Liguria, 570 Kythera, 581 Tauntonia, 589 Croatia and 605 Juvisia" 132-135.

Pilcher, F. "Call for Observations" 170.

Pilcher, F. "Lightcurves and Rotation Periods of 47 Aglaja, 504 Cora, 527 Euryanthe, 593 Titania, and 594 Mireille" 217-218.

Pilcher, F. "General Report of Position Observations by the ALPO Minor Planets Section for the Year 2020" 309-312.

Pilcher, F. "Lightcurves and Rotation Periods of 420 Bertholda, 664 Judith, and 2779 Mary" 360-361.

Pilcher, F.; Benishek, V. "Lightcurve and Rotation Period of the Tumbling Asteroid 1513 Matra" 209.

Pilcher, F.; Benishek, V.; Bonamico, R.; Ferrero, A.; Kemp, J.; Odden, C.E.; Papini, R. "Lightcurve and Rotation Period of 426 Hippo" 4-5.

Pilcher, F.; Franco, L.; Marchini, A.; Oey, J. "357 Ninina and 748 Simeisa - Two Asteroids with Earth Commensurate Rotation Periods" 233-235.

Polakis, T. "Photometric Observations of Seven Minor Planets" 23-25.

Polakis, T. "Photometric Observations of Eight Minor Planets for Shape Modeling" 144-147.

Polakis, T. "Period Determinations for Seventeen Minor Planets" 158-163.

Polakis, T. "Period Determinations for Twenty Minor Planets" 239-245.

Polakis, T.; Stephens, R.D. "1803 Zwicky a Confirmed Binary Asteroid" 272-273.

Polakis, T. "Lightcurve Analysis for Thirteen Minor Planets" 394-398.

Romanishin, W. "Lightcurves of Three Hildas" 15-16.

Romanishin, W. "Using Pan-STARRS Data to Calibrate Red Lightcurve Images" 86-87.

Romanishin, W. "The Elusive Period of the Hilda 1269 Rollandia" 102-103.

Salthouse, A. "Visual Observation of 3000+ Minor Planets" 113-114.

Sani, I.A.; Offor, P.; Njoku-Achu, N.; Okere, R.; Onyeuwaoma, N.; Obi, I.; Ofodum, C.; Okere, B. "Lightcurve Photometry of Asteroid (15989) 1998 XK39" 327-328.Scardella, M.; Badoni, F.; Tomassini, A.; Pierri, F. "Rotational Period Determination of 1526 Mikkeli" 109.

Silvan, S.M. "Lightcurves, Sidereal Rotation Period, Spin Pole, and Convex Model Shape of Koronis Family Member (1443) Ruppina" 331-334.

Silvan, S.M. "*Caveat Emptor*: Spurious Spin Vectors from Incorrect Sidereal Periods" 403-405.

Slivan, S.M.; Wilkin, F.P. "Rotation Period of Koronis Family Member (1442) Corvina" 211-212.

Slivan, S.M.; McLellan-Cassivi, C.; Shishido, R.; Wang, N. "Rotation Period of Koronis Family Member 1840 Hus" 112-113.

Sioulas, N. "Rotation Period Determination for 665 Sabine" 99.

Sonka, A.B.; Turcu, V.; Nedelcu, A.; Birlan, M.; Moldovan, D. "Fast Rotator Minor Planet 2020 UA from Cluj and Berthelot Observatory" 100-101.

Stephens, R.D.; Warner, B.D. "Lightcurve Analysis of L4 Trojan Asteroids at the Center for Solar System Studies:"
2020 July to September 13-15.
2020 October to December 167-170.

Stephens, R.D.; Coley, D.R.; Warner, B.D. "Lightcurve Analysis of L4 Trojan Asteroids at the Center for Solar System Studies:
2021 April to June 398-402.

Stephens, R.D.; Warner, B.D. "Main-Belt Asteroids Observed from CS3:"
2020 July to September 56-69.
2020 October to December 150-158.

Stephens, R.D.; Coley, D.R.; Warner, B.D. "Main-Belt Asteroids Observed from CS3:"
2021 January to March 246-267.
2021 April to May 380-387.

Teer, A.; Montgomery, K. "Determining Lightcurves and Rotational Periods of Four Main Belt Asteroids" 366-367.

Thomas, N.B.; Lopez, P.R. "Observations of 148 Gallia" 328-329.

Warner, B.D. "Asteroid-Deepsky Appulses in 2021" 88.

Warner, B.D.; Harris, A.W. "All in the Family: Upcoming Changes in the LCDB" 313-315.

Warner, B.D.; Stephens, R.D. "Lightcurve Analysis of Hilda Asteroids at the Center for Solar System Studies:"
2020 August - September 17-19.
2020 October - December 164-165.

Warner, B.D.; Stephens, R.D.; Coley, D.R. "Lightcurve Analysis of Hilda Asteroids at the Center for Solar System Studies:"
2021 January - March 303-308.
2021 February - March 334-336.

Warner, B.D.; Stephens, R.D. "Near-Earth Asteroid Lightcurve Analysis at the Center for Solar System Studies:"
2020 July - September 30-39.
2020 September - 2021 January 170-179.
2021 January - March 294-302.
2021 March - April 337-340.

Warner, B.D.; Stephens, R.D.; Harris, A.W. "On Confirmed and Suspected Binary Asteroids Observed at the Center for Solar System Studies" 40-49.

Warner, B.D.; Stephens, R.D.; Harris, A.W. "On Confirmed and Suspected Binary Asteroids Observed at the Center for Solar System Studies" 187-193.

Warner, B.D.; Stephens, R.D.; Coley, D.R. "On Confirmed and Suspected Binary Asteroids Observed at the Center for Solar System Studies" 274-280.

Warner, B.D.; Stephens, R.D.; Coley, D.R. "On Confirmed and Suspected Binary Asteroids Observed at the Center for Solar System Studies" 358-360.

Warner, B.D.; Harris, A.W.; Ďurech, J.; Benner, L.A.M. "Lightcurve Photometry Opportunities:"
2021 January - March 89-97.
2021 April - June 194-198.
2021 July - September 318-323.
2021 October - December 406-410.

Zeigler, K. "CCD Photometric Observations of Asteroids 4493 Naitomitsu, (21242) 1995 WZ41, (68130) 2001 AO17, and (183230) 2002 TC58" 123-124.

Zeigler, K. "CCD Photometric Observations of Asteroids 2984 Chaucer, (26206) 1997 PJ4, (87035) 2000 KE2, and 2015 NU13" 368-369.

IN THIS ISSUE

This list gives those asteroids in this issue for which physical observations (excluding astrometric only) were made. This includes lightcurves, color index, and H-G determinations, etc. In some cases, no specific results are reported due to a lack of or poor-quality data. The page number is for the first page of the paper mentioning the asteroid. EP is the "go to page" value in the electronic version.

Number	Name	EP	Page	Number	Name	EP	Page
34	Circe	26	352	486	Cremona	49	375
81	Terpsichore	46	372	486	Cremona	63	391
148	Gallia	2	328	503	Evelyn	63	391
153	Hilda	37	363	527	Euryanthe	49	375
318	Magdalena	63	391	535	Montague	26	352
323	Brucia	54	380	536	Merapi	66	394
329	Svea	49	375	563	Suleika	46	372
357	Ninina	37	363	563	Suleika	66	394
363	Padua	46	372	664	Judith	34	360
363	Padua	66	394	664	Judith	49	375
366	Vincentina	37	363	664	Judith	63	391
412	Elisabetha	66	394	709	Fringilla	37	363
420	Bertholda	34	360	739	Mandeville	37	363
455	Bruchsalia	63	391	755	Quintilla	36	362

Number	Name	EP	Page	Number	Name	EP	Page	Number	Name	EP	Page
755	Quintilla	60	388	3478	Fanale	26	352	15375	Laetitiafoglia	26	352
820	Adriana	66	394	3523	Arina	60	388	15989	1998 XK39	1	327
884	Priamus	70	398	3717	Thorenia	40	366	17431	Sainte-Colombe	26	352
909	Ulla	46	372	3760	Poutanen	46	372	18418	Ujibe	60	388
929	Algunde	46	372	3955	Bruckner	26	352	18434	Mikesandras	54	380
1038	Tuckia	8	334	4004	List'ev	26	352	18503	1996 PY4	32	358
1048	Feodosia	46	372	4107	Rufino	49	375	26206	1997 PJ4	42	368
1056	Azalea	49	375	4133	Heureka	66	394	29032	2059 T-1	40	366
1106	Cydonia	54	380	4238	Audrey	66	394	30958	1994 TV3	54	380
1118	Hanskya	49	375	4700	Carusi	40	366	31146	1997 UV3	26	352
1132	Hollandia	37	363	4708	Polydoros	70	398	33785	1999 RD192	26	352
1228	Scabiosa	44	370	5182	Bray	60	388	37870	1998 FJ23	26	352
1257	Mora	54	380	5189	1990 UQ	11	337	53134	1999 BG1	54	380
1390	Abastumani	66	394	5245	Maslyakov	26	352	66846	Frankllederer	54	380
1413	Roucarie	54	380	5401	Minamioda	60	388	69695	1998 HL36	26	352
1428	Mobassa	49	375	5405	Neverland	60	388	80366	1999 XA142	54	380
1443	Ruppina	5	331	5551	Glikson	49	375	87035	2000 KE2	42	368
1443	Ruppina	75	403	6009	Yuzuruyoshii	32	358	142464	2002 TC9	11	337
1458	Mineura	66	394	6353	Semper	26	352	163799	2003 RQ69	26	352
1504	Lappeenranta	49	375	6520	Sugawa	26	352	271480	2004 FX31	11	337
1886	Lowell	49	375	6600	Qwerty	26	352		2012 XE54	19	345
2261	Keeler	49	375	7052	Octaviabutler	26	352		2015 NU13	42	368
2326	Tololo	66	394	7288	1991 FE1	60	388		2015 HO116	15	341
2394	Nadeev	40	366	7327	Crawford	26	352		2018 CB	19	345
2521	Heidi	66	394	7792	1995 WZ3	54	380		2018 GE3	19	345
2549	Baker	26	352	8361	1990 JN1	26	352		2020 KK7	19	345
2699	Kalinin	60	388	10177	Ellison	54	380		2021 FH	19	345
2777	Shukshin	66	394	11395	1998 XN77	70	398		2021 HN	15	341
2779	Mary	34	360	12016	Green	44	370		2021 HN	19	345
2875	Lagerkvist	26	352	12444	Prothoon	70	398		2021 KN2	15	341
2895	Memnon	70	398	12923	Zephyr	11	337		2021 HC3	15	341
2984	Chaucer	42	368	13374	1998 VT10	26	352		2021 JR3	15	341
3063	Makhaon	70	398	13832	1999 XR13	4	330		2021 JB6	15	341
3275	Oberndorfer	66	394	14381	1990 CE	26	352		2021 GQ10	19	345
3317	Paris	70	398	14411	Clerambault	26	352		2021 GG11	15	341
3385	Bronnina	46	372	14653	1998 YV11	54	380				

THE MINOR PLANET BULLETIN (ISSN 1052-8091) is the quarterly journal of the Minor Planets Section of the Association of Lunar and Planetary Observers (ALPO, http://www.alpo-astronomy.org). Current and most recent issues of the *MPB* are available on line, free of charge from:

https://mpbulletin.org/

The Minor Planets Section is directed by its Coordinator, Prof. Frederick Pilcher, 4438 Organ Mesa Loop, Las Cruces, NM 88011 USA (fpilcher35@gmail.com). Dr. Alan W. Harris (MoreData! Inc.; harrisaw@colorado.edu), and Dr. Petr Pravec (Ondrejov Observatory; ppravec@asu.cas.cz) serve as Scientific Advisors. The Asteroid Photometry Coordinator is Brian D. Warner (Center for Solar System Studies), Palmer Divide Observatory, 446 Sycamore Ave., Eaton, CO 80615 USA (brian@MinorPlanetObserver.com).

The Minor Planet Bulletin is edited by Professor Richard P. Binzel, MIT 54-410, 77 Massachusetts Ave, Cambridge, MA 02139 USA (rpb@mit.edu). Brian D. Warner (address above) is Associate Editor, and Dr. David Polishook, Department of Earth and Planetary Sciences, Weizmann Institute of Science (david.polishook@weizmann.ac.il) is Assistant Editor. The *MPB* is produced by Dr. Pedro A. Valdés Sada (psada2@ix.netcom.com). The MPB is distributed by Dr. Melissa Hayes-Gehrke. Direct all subscriptions, contributions, address changes, etc. to:

Dr. Melissa Hayes-Gehrke
UMD Astronomy Department
1113 PSC Bldg 415
College Park, MD 20742 USA
(mhayesge@umd.edu)

Effective with Volume 38, the *Minor Planet Bulletin* is a limited print journal, where print subscriptions are available only to libraries and major institutions for long-term archival purposes. In addition to the free electronic download of the *MPB* noted above, electronic retrieval of all *Minor Planet Bulletin* articles (back to Volume 1, Issue Number 1) is available through the Astrophysical Data System:

http://www.adsabs.harvard.edu/

Authors should submit their manuscripts by electronic mail (rpb@mit.edu). Author instructions and a Microsoft Word template document are available at the web page given above. All materials must arrive by the deadline for each issue. Visual photometry observations, positional observations, any type of observation not covered above, and general information requests should be sent to the Coordinator.

* * * * *

The deadline for the next issue (49-1) is October 15, 2021. The deadline for issue 49-2 is January 15, 2022.